Transcriptional States and microRNA Regulation of Adult Neural Stem Cells

Annina Maria Fiorella di Primavera DeLeo

Submitted in partial fulfillment of the

requirements for the degree of

Doctor of Philosophy

under the Executive Committee

of the Graduate School of Arts and Sciences

COLUMBIA UNIVERSITY

2015

Abstract

Transcriptional States and microRNA Regulation of Adult Neural Stem Cells

Annina Maria Fiorella di Primavera DeLeo

Adult neural stem cells are specialized astrocytes that generate neurons in restricted regions of the mammalian brain. The largest neurogenic region is the ventricular-subventricular zone, which lines the lateral ventricles and generates olfactory bulb neurons. Stem cell astrocytes give rise to new neurons in both homeostatic and regenerative conditions, suggesting that they can potentially be harnessed for regenerating the brain after injury, stroke, or neurodegenerative disease. Previous work has shown that stem cell astrocytes exist in both quiescent and activated states, but due to a lack of markers, it was not feasible to purify them. Using a novel fluorescence activated cell sorting (FACS) strategy that allows quiescent neural stem cells (qNSCs) and activated neural stem cells (aNSCs) to be purified for the first time, we performed transcriptome profiling to illuminate the molecular pathways active in each population. This analysis revealed that qNSCs are enriched in signaling pathways, especially G-protein coupled receptors, as well as for adhesion molecules, which facilitate interactions with the niche. qNSCs and aNSCs utilize different metabolic pathways. qNSCs are enriched for lipid and glycolytic metabolism, while aNSCs are enriched for DNA, RNA, and protein metabolism. Many receptors and ligands are reciprocally distributed between qNSCs and aNSCs, suggesting that they may regulate each other. Finally, comparison of the transcriptomes of qNSCs and aNSCs with their counterparts in

other organs revealed that pathways underlying stem cell quiescence are shared across diverse tissues.

A key step in recruiting adult neural stem cells for brain repair is to define the molecular pathways regulating their switch from a quiescent to an activated state. MicroRNAs are small non-coding RNAs that simultaneously target hundreds of mRNAs for degradation and translational repression. MicroRNAs have been implicated in stem cell self-renewal and differentiation. However, their role in adult neural stem cell activation is unknown. We performed miRNA profiling of FACS-purified quiescent and activated adult neural stem cells to define their miRNA signatures.

Bioinformatic analysis identified the miR-17~92 cluster as highly upregulated in activated (actively dividing) stem cells in comparison to their quiescent counterparts. Conditional deletion of the miR-17~92 cluster in FACS purified neural stem cells *in vitro* reduced adult neural stem cell activation, proliferation, and self-renewal. In addition, miR-17~92 deletion led to a selective decrease in neuronal differentiation. Using an *in vivo* conditional deletion model, we showed that loss of miR-17~92 led to an increase in the proportion of $GFAP^+$ cells and decrease in $MCM2^+$ cells, as well as decreased neurogenesis. Finally, I identify Sphingosine 1 phosphate receptor 1 (S1pr1) as a computationally predicted target of the miR-17~92 cluster. S1pr1 is highly enriched in quiescent neural stem cells. Treatment of quiescent neural stem cells with S1P, the ligand for S1PR1, reduced their activation and proliferation. *In vivo* deletion of miR-17~92 lead to an increase in $S1PR1^+$ cells, even among $MCM2^+$ cells. Together, these data reveal that the miR-17~92 cluster is a key regulator of adult neural stem cell activation from the quiescent state and subsequent proliferation.

Table of Contents

List of Figures

List of Tables

Acknowledgements
Joshua Parks, for his ability to fix almost everything in Microsoft Word, and for helping me say what I mean;

Dr. Paolo Codega, my post-doc, for teaching me;

Dr. Violeta Silva-Vargas, mi hermana del alma;

Alex Paul for always listening to my ideas;

Especially to Fabrizio Favaloro for his direct involvement in the luciferase part of this project, and for helping me to clarify my ideas on microRNAs;

and especially Dr. Jun-An Chen for giving me all of the miR 17~92 mice for this project and getting me started on the miR portion of this thesis;

Other members of the Doetsch, Kohwi, and Wichterle labs for being generous with their time, ideas, reagents and friendship;

Friends working on 14th floor of the Physicians and Surgeons building for their support, empathy, and unflagging encouragement;

Drs. Ron Liem, Patrice Spitalnik, Steven Spitalnik, Joshua Wiley, James Noble, and Oren Levy for their introduction into the clinical aspects of working in the brain, mentorship, and financial support of this project via the Med into Grad program;

The Herbert Irving Cancer Center Flow Cytometry Core, especially Sandra Tetteh, Kristie Gordon, and Carl Constant for training and cell sorting which were essential to this project;

Zaia Sivo for her administrative and personal support;

My thesis committee, Drs. James Goldman, Alla Grishok, and Hynek Wichterle for their invaluable insights;

and Dr. Fiona Doetsch for believing in me and taking me into her lab in the first place, as well as her outstanding mentorship and guidance over the course of this degree, and amazing source of inspiration.

Dedication

To my grandparents and great-grandparents who laid the foundation, my parents who encouraged the walls into being, and to my Joshua, who helped me make the roof, and all the stories in-between.

Chapter 1 Introduction

Stem Cells

Stem cells are defined by two cardinal properties; the ability to self-renew, that is to give rise to another cell that is identical to itself, and the ability to differentiate into diverse cell types. Stem cells broadly fall into two categories; embryonic stem cells, which are pluripotent and give rise to all organs and tissues, and adult stem cells, which are multi or even unipotent, and responsible for the maintenance of organs and tissues over the lifetime of an organism. These adult stem cells are thought to be active during organ homeostasis, but can also act as a reservoir for replenishing cells during a crisis in the organ, such as injury.

The location of adult stem cells within a given tissue is thought to play an important role in the regulation of their behavior. These specialized stem cell locations are known as "niches" and often contain other types of specialized support cells and secreted factors, which may signal the cells to remain quiescent, to divide, or to leave the niche (reviewed in Li & Clevers, 2010).

A Brief History of Adult Neurogenesis

In 1897, Schaper proposed that a reserve of "indifferent cells" would exist postnatally and, "play an important role in in regenerative processes within the central nervous system" (Schaper, 1897). Indeed, dividing cells within what would later be identified as the ventricular-subventricular zone (V-SVZ), adjacent to the lateral ventricles, were first discovered by Ezra Allen in adult albino rats in 1912 (Allen, 1912). These studies were confirmed by other researchers, some of whom proposed that immature cells might divide and become neurons (reviewed and further confirmed in Globus & Kuhlenbeck, 1944). Despite these studies, it was long believed that the adult brain was a static entity incapable of new neuron formation because no signs of mitosis were convincingly shown in neurons. This led the eminent neuroscientist

Santiago Ramon y Cajal to declare that, "nervous restoration is a purely expansional act, in which the cell body never participates" and that, "Everything may die, nothing may be regenerated" (Cajal & May, 1991; Kershman, 1938). Although we now know that neurons themselves do not divide, the formation of new neurons via adult neurogenesis would not be shown definitively until Joseph Altman's seminal studies with audioradiographic $[H]^3$-thymidine in 1962, 1963, and 1965. These studies showed that neurons in the adult had incorporated radiolabeled thymidine, indicating that they had arisen from progenitors dividing at the time of thymidine treatment (Altman, 1962a; Altman, 1962b; Altman, 1963; Altman & Chorover, 1963; Altman & Das, 1965). Since then, dividing cells capable of neurogenesis have been found in the adult brain of many species, including cats, dogs, songbirds, monkeys, and humans (reviewed in Altman, 1969 and Sanai et al., 2011). In 1965 and 1966, it was determined that these immature thymidine incorporating cells were capable of forming new neurons that integrated into the hippocampus (Altman & Das, 1965), as well as the olfactory bulb (OB), cerebellum, and cochlear nucleus (Altman & Das, 1966). The exact identity of the progenitor cells for these regions in mammals was unknown until 1999, when the V-SVZ cells capable of giving rise to immature neuronal precursors were found to be glial fibrillary acidic protein ($GFAP^+$) positive stem cell astrocytes (Doetsch et al., 1999a), and were confirmed to give rise to OB neurons (Doetsch, et al., 1999b). Soon after these discoveries, $GFAP^+$ cells were shown to be the stem cells for the subgranular zone (SGZ) of the hippocampus (Seri et al., 2001).

Adult Neural Stem Cells and Their Progeny

We now know that in mammals, adult neural stem cells (NSCs) exhibit features of astrocytes and exist in two major reservoirs; the V-SVZ and the subgranular zone (SGZ) in the hippocampal formation. In both areas, the stem cells have radial morphology and are in fact

derived from embryonic radial glial progenitors (reviewed in Kriegstein & Alvarez-Buylla, 2009). This resemblance has earned them the moniker "stem-cell astrocytes" and indeed they express GFAP and the Glutamate Aspartate Transporter (GLAST, also called Slc1a3 or EAAT1) much as radial glia and astrocytes do (Doetsch et al., 1997, radial glial and astrocyte marker expression reviewed in Kriegstein & Alvarez-Buylla, 2009). In both regions, adult neural stem cells contact blood vessels and go on to form mature neurons that migrate away from their niche. While the progeny of stem cells from the V-SVZ travel several millimeters to their maturation site in the OB, in the SGZ, the progeny migrate only a few cell layers to the adjacent granule cell layer of the dentate gyrus (Lois & Alvarez-Buylla, 1994, reviewed in Montalbán-Loro, 2015).

The stem cells within the V-SVZ reside within the first few cell layers adjacent to the lateral ventricles. The layer immediately adjacent to the ventricle consists mostly of ependymal cells, which are large, cuboidal, and multi-ciliated. Ependymal cells use their cilia to maintain the flow of cerebrospinal fluid (CSF) throughout the ventricular system (Yamadori & Nara, 1979). V-SVZ stem cells contact the CSF at the center of ependymal cell pinwheels (Mirzadeh et al., 2008).

GFAP-positive stem cells are largely quiescent. Once activated, they upregulate epidermal growth factor receptor (EGFR) (Doetsch et al., 2002; Pastrana et al, 2009), and divide to form transit amplifying cells. Stem cells can divide symmetrically or asymmetrically depending on context. Although V-SVZ neural stem cells undergo asymmetric division *in vitro*, their precise mode of division *in vivo* is still unknown (Costa et al., 2011; Doetsch et al., 1999b; Figure 1.1).

Transit amplifying cells (TACs) make up the bulk of proliferating cells in the V-SVZ (Doetsch et al., 1997; Ponti et al., 2013). Their divisions are mostly symmetrical, thereby expanding the pool of progenitors (Costa et al., 2011; Doetsch et al., 1997). Unlike their quiescent and activated stem cell forbearers, TACs have lost expression of GFAP, but retain that of EGFR. Additionally, they express the transcription factors Ascl1 and Dlx2 (Parras et al., 2004; Kim et al., 2011; Doetsch et al., 2002; Figure 1.1).

Neuroblasts arise after TACs have undergone several rounds of divisions. Interestingly, Costa et al. found that transit amplifying cells increase their cell cycle length as they become neuroblasts, as compared to the divisions that give rise to more transit amplifying cells. Neuroblasts can be further characterized by their migratory behavior and expression of Doublecortin (DCX) (Gleeson et al., 1999; Nacher et al., 2001; Garcia et al., 2004), CD24 (Calaora et al., 1996) and TuJ1 (also called Beta-III tubulin, Doetsch et al., 1997), as well as continued expression of Dlx2 (Doetsch et al., 2002). *In vivo*, neuroblasts form chains in the V-SVZ and migrate towards the OB along a specific pathway called the rostral migratory stream (RMS) (Altman, 1969; Doetsch et al., 1997; Figure 1.1).

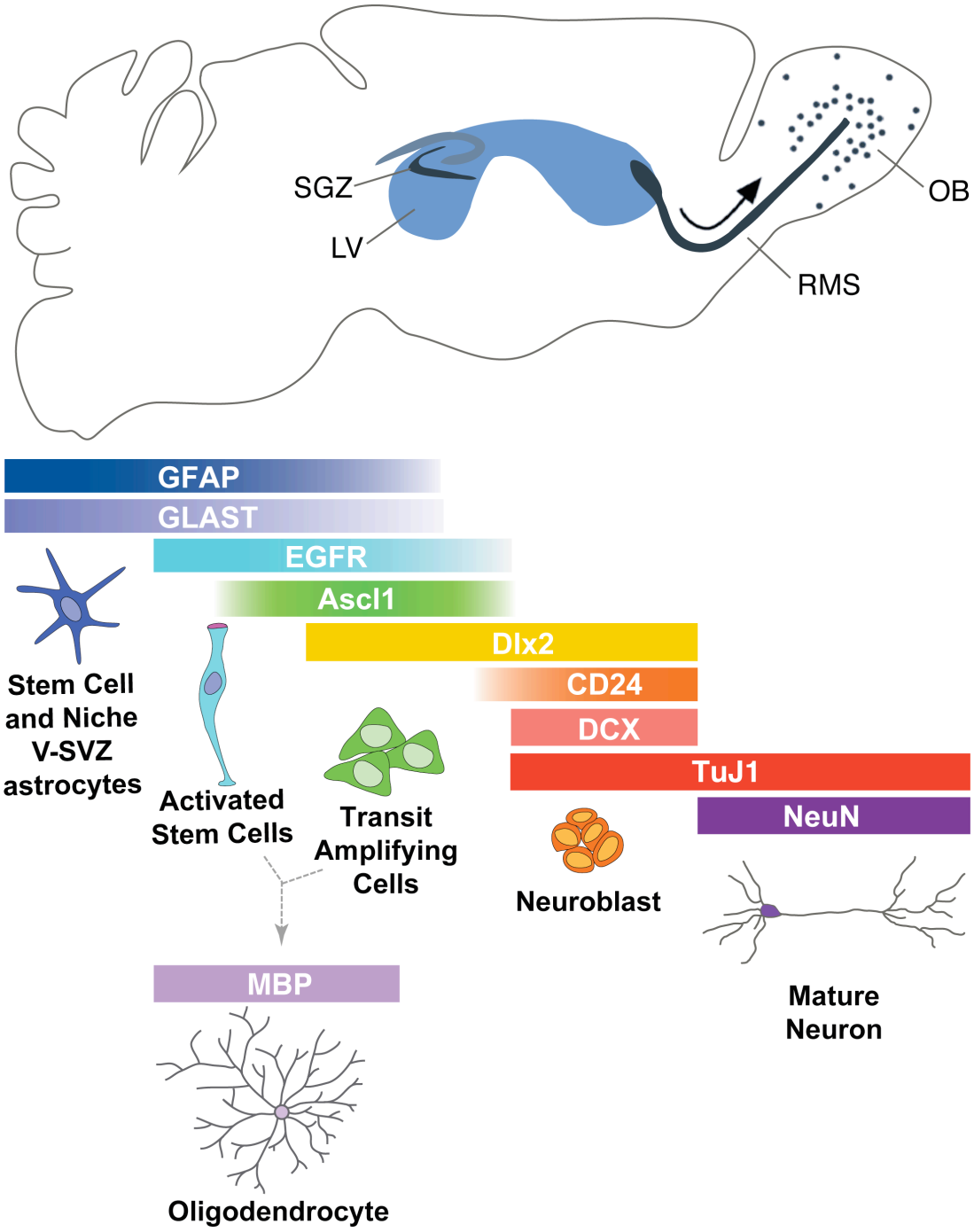

Figure 1.1 The adult V-SVZ stem cell lineage and markers.

(Top) Sagittal view of the adult murine brain. The V-SVZ lies adjacent to the lateral ventricles (LV, blue). (Middle and Bottom) Markers of V-SVZ cells and their progeny. Within the V-SVZ stem cells are GFAP$^+$ and GLAST$^+$ astrocytes. Activated adult neural stem cells express GFAP, GLAST, and EGFR (light blue bar). aNSCs also express Ascl1 (green). Transit amplifying cells express EGFR, Ascl1, and Dlx2 (yellow). Transit amplifying cells give rise to neuroblasts, which are CD24 (orange bar), DCX (tangerine bar), and TuJ1 (red bar) positive. Neuroblasts leave the V-SVZ and traverse the rostral migratory stream (RMS) into the olfactory bulb (OB). Mature OB neurons express TuJ1 and NeuN. Some aNSCs and TACs are capable of forming MBP$^+$ (lilac bar) oligodendrocytes.

In the OB, newly generated neurons, which are TuJ1 positive (Parras et al., 2004), exit the RMS and turn radially to migrate to different layers. For these cells, navigating from the inner to the outer cortex of the OB can take at least 6 days (Altman, 1969; Lois & Alvarez-Buylla, 1994). Within the OB, newly generated neurons generally become granule cells, which reside in the granule cell layer. A small number of the newly generated neurons become periglomerular cells, which reside in the glomerular layer. Mature, NeuN positive (Neuronal Nuclei, or Rbfox3, Mullen et al., 1992) olfactory bulb interneurons are largely GABAergic and inhibitory, outnumbering the primary mitral and tufted neurons of the OB by 50 or 100 to 1 (reviewed in Sakamoto et al., 2014a). Periglomerular cells can be further differentiated by their expression of tyrosine hydroxylase (TH), Calbindin (CalB), or Calretinin (CalR) (Reviewed in Merkle et al., 2014; Sakamoto et al., 2014a). Some granule cells express Calretinin as well. Due to a lack of markers that can distinguish between the different OB interneuron subtypes, granule cells are usually sub-categorized by what layer their cell body resides in (i.e. the superficial, intermediate or deep layer) (reviewed in Merkle et al., 2014). Recently, additional adult-derived OB neuronal subtypes in the external plexiform layer, mitral layer, and internal plexiform layer have been identified (Merkle et al., 2014). More and more studies are unveiling the connection between stem cell location within the V-SVZ, expression of certain transcription factors, and mature olfactory bulb interneuron subtype and location (reviewed in Lim & Alvarez-Buylla, 2014).

Strikingly, only 50% of the neurons that reach the olfactory bulb will be integrated into existing circuits, and less than 10% of neurons formed in rats during young adulthood survive for more than 21 months (Imayoshi et al., 2008; Kaplan et al., 1985). In conjunction with the expression of apoptotic markers in the OB and the static volume of this structure, this low

survival rate is thought to indicate turnover of OB neurons (Petreanu & Alvarez-Buylla, 2002; Sakamoto et al., 2014a). The normal function of these newly formed interneurons is to modulate the activity of mitral and tufted cells, thereby optimizing olfactory information processing by reducing overlapping odor signals to the brain (Gheusi et al., 2000; reviewed in Sakamoto et al., 2014a). The continual replacement of OB neurons is also important for modification of odor-related memory as well as the value assigned to it, as ablation of adult neurogenesis impairs the ability to discriminate between new odors in rodents (Sakamoto et al., 2014a).

Adult V-SVZ stem cells do not only give rise to neurons. In fact, some adult neural stem cells and a small subset of TACs express the transcription factor Olig2 and go on to form immature oligodendrocytes that are O4-antigen positive (Reynolds & Hardy, 1997; Marshall et al., 2005; Menn et al., 2006), followed by myelin basic protein (MBP) expressing mature oligodendrocytes (Nait-Oumesmar et al., 1999; Figure 1.1)

V-SVZ $GFAP^+$ stem cells are also present in adult humans, where they are largely quiescent (Sanai et al., 2004; Sanai et al., 2011; Van Den Berge et al., 2010). Unlike in rodents, olfactory bulb neurogenesis in humans ends in infancy, and there is very little turnover of neurons over the lifetime of an individual (Sanai et al., 2011; W. Wang et al., 2011; Bergmann et al., 2012). Recent evidence using carbon dating suggests that new neurons may be added to the striatum, and that the formation of striatal interneurons is reduced in Huntington's disease (Sanai et al., 2011; Ernst et al., 2014; reviewed in Sakamoto et al., 2014b).

Quiescence and Activation are Important for Stem Cell Function

It is becoming increasingly apparent that quiescent (non-dividing) and activated (actively dividing) stem cells coexist in many adult stem cell niches (Li & Clevers, 2010). Stem cell quiescence and activation play an essential role in many organs, underlying tissue maintenance, regeneration, function, plasticity, aging, and disease. For example, in homeostatic conditions, a small amount of the cells that make up a tissue or organ may be dying and replaced at a steady rate. Under these conditions, most stem cells will be in a quiescent state, while a few are activated in order to replace the cells that have died. In the case of injury, the balance may switch such that the majority of stem cells are in an activated state to compensate for the large number of cells lost in an injury.

It is currently unknown if the same pool of stem cells is responsible for both tissue homeostasis and regeneration, or if there are separate pools of stem cells for each process. Importantly, maintaining the balance between quiescence and activation is essential to sustaining homeostasis. Without such balancing mechanisms, an excess of cells might remain in a quiescent or activated state, preventing homeostasis and appropriate injury response. Furthermore, an excess of divisions increases the chance of mutation occurring. Increased chance of mutagenesis, in combination with excess proliferating cells, could lead to cancer.

Quiescent stem cells dynamically integrate extrinsic and intrinsic signals to either actively maintain their dormant state or become proliferative and give rise to differentiated progeny (Cheung & Rando, 2013). The signals maintaining and potentially regulating transitions between quiescent and active stem cell states are only beginning to be understood. Recent findings suggest that quiescent and activated states are differentially regulated at multiple levels including adhesion, transcriptional regulators, diffusible signals, and cell-cell contact. In the

adult V-SVZ, interaction with extracellular matrix proteins such as β1 integrin, Ncam1, or Vcam1 prevents adult neural stem cells from dividing and migrating (Kazanis et al., 2010; Porlan et al., 2014; Kokovay et al., 2012). Cell-cell signaling involving Notch1 promotes activation (Basak et al., 2012). Diffusible signals such as neurotransmitters or epidermal growth factor (EGF) also promote proliferation (Young et al., 2011; Alfonso et al., 2012; Doetsch et al., 2002). More recently, diffusible signals have also been show to play a role in quiescence, as in the case of endothelial-derived NT-3 (Delgado et al., 2014).

Quiescent and activated neural stem cells are also likely to have distinct transcriptional programs through differentia expression of transcription factors. For example, p21 has been shown to prevent NSC division by upregulating the transcription factor Sox2 (Marqués-Torrejón et al., 2013) and suppressing Bmp2 (Porlan et al., 2013). Interestingly, other components of the Notch signaling pathway have also been implicated in maintaining quiescence; notch effector Hes5 expression is linked to quiescent cells, while Dll1, a Notch ligand, is expressed in activated NSCs, and signals neighboring cells to be quiescent through Notch receptors expressed there (Giachino et al., 2014; Kawaguchi et al., 2013).

Understanding how stem cell astrocytes become activated is important to eventually harnessing the regenerative power of stem cells for treating brain injury and neurodegenerative diseases. Conversely, stem cells are thought to be the source of some brain tumors (reviewed in Reya et al., 2001; Sanai et al., 2005; Nicolis, 2007) and understanding what maintains their quiescence will be important to combating cancer. Thus, a key step in recruiting adult neural stem cells for brain repair or treating cancers is to define the molecular pathways regulating their switch from a quiescent to an activated state.

Approaches for Studying Stem Cells

In order to explore the biology of adult stem cells, it is key to be able to identify them *in vivo*, to be able to trace the progeny they give rise to, and to be able to isolate them prospectively from their niche to study their properties. Below, I briefly outline approaches I have used in my thesis.

Sphere Forming Assays

Neurospheres have been widely used as a retrospective assay to identify neural stem cells, as they allow one to test if a cell can self-renew and is multipotent. In the neurosphere assay, cells are plated at clonal density in non-adherent conditions in the presence of growth factors. If the cells are actively dividing, they give rise to spheres. The efficiency of sphere formation can be used to assess activation, while size of spheres can give a rough idea of proliferative ability. Passaging of spheres to form secondary spheres can be used to assess self-renewal capacity. Subsequent plating of these cells on adherent substrates without mitogens can give an idea of the cells' ability to differentiate into mature cell types. However, several recent studies have shown that in addition to stem cells, other proliferative populations can give rise to neurospheres (reviewed in Pastrana et al., 2011). Therefore, the neurosphere assay cannot be used as a measure of *in vivo* stem cell identity.

Fluorescence-Activated Cell Sorting

Fluorescence-activated cell sorting (FACS) is a specialized type of flow cytometry that allows sub-populations of live cells to be purified based on their expression of markers that have been tagged with fluorescent molecules (Herzenberg et al., 2002). This method was originally used to sort lymphocytes (Julius et al., 1972), and has since been widely applied to understanding the subpopulations of cells within other tissues and tumors, as well as to assess cell cycle or

survival status. This method has been especially useful for prospectively isolating stem cells, in both quiescent and activated states, from other tissues.

More recently, FACS approaches have been applied to the brain to isolate stem cells from their *in vivo* niches using cell surface markers or transgenic reporter mice (Morrison et al., 1999; Uchida et al., 2000; Capela & Temple, 2002; Lim et al., 2006; Doetsch et al., 2002; Barraud et al., 2005; Kawaguchi et al., 2001; Ciccolini et al., 2005). However, most of these methods fail to uniquely isolate stem cells, as the markers used are too widely expressed.

A major limitation in the adult neural stem cell field has been the lack of markers that allow mature astrocytes to be distinguished from stem cell astrocytes. GFAP::GFP mice, in which green fluorescent protein (GFP) is expressed under the GFAP promoter, are a powerful tool that allow the isolation of GFAP-expressing cells. By combining different surface markers and FACS with GFAP::GFP mice, it is now possible to prospectively isolate V-SVZ stem cells. A combination of EGF ligand and CD24 allows the simultaneously isolation of activated NSCs and their progeny (Pastrana et al., 2009). Another marker that has been used is CD133 (Prominin). In the adult, CD133 is highly expressed by ependymal cells (Coskun et al., 2008), as well as by a subset of V-SVZ astrocytes (Mirzadeh et al., 2008; Beckervordersandforth et al., 2010). Transcriptome analysis of FACS purified $CD133^{+}GFAP::GFP^{+}$ cells, as compared to ependymal cells and other brain astrocytes, was proposed to define a neural stem cell signature (Beckervordersandforth et al., 2010). However, this strategy did not differentiate between quiescent and activated neural stem cell populations.

Lineage Tracing

Lineage tracing is generally defined as marking a single cell or population such that, "the mark is transmitted to the [labeled] cell's progeny, resulting in a set of labeled clones"

(Kretzschmar & Watt, 2012). To identify stem cell populations *in vivo,* lineage tracing approaches often use conditional expression of the Cre recombinase protein under a promoter of interest that causes deletion of a floxed stop cassette and subsequent expression of a reporter gene, such as GFP, Tomato, or Lac-Z, thereby permanently marking the cell and its progeny. This approach allows the fate of the marked cells to be followed and to determine whether they self-renew or differentiate, the two cardinal properties of stem cells. This approach can also be used to delete genes of interest to define their functional roles.

microRNAs: Biogenesis and Mode of Action

MicroRNAs (miRNAs or miRs) are a subset of non-coding RNAs (ncRNAs) that are emerging as key post-transcriptional regulators. miRs are conserved in animals, plants, single-celled eukaryotes, and have even been observed in viruses (reviewed in Stroynowska-Czerwinska et al., 2014). miRs are endogenously transcribed in the nucleus and are located in both intronic and intergenic regions. Transcripts may contain one or many miRs, the latter of which is called a "microRNA cluster". Each miR generally has a hairpin or stem-loop secondary structure within a larger transcript, which collectively is known as a "Pri-miR". These hairpins are cleaved from the rest of the transcript by Drosha and DGCR8 (DiGeorge syndrome critical region 8) and, once freed, are called "Pre-miRs". The Pre-miRs are transported into the cytoplasm by Exportin 5 where they are loaded into the protein Dicer in complex with TRBP (TAR RNA binding protein 2), where the loop is cleaved from the stem, resulting in a ~22 bp duplex. This duplex is then loaded onto Argonaut 2 (Ago2), to form the RNA-initiated silencing complex (RISC). In RISC, the RNA duplex is unwound and a single mature miR strand kept for guiding RISC to target mRNAs, while the passenger strand is degraded. An overview of the main pathway for microRNA biogenesis is provided in Figure 1.2.

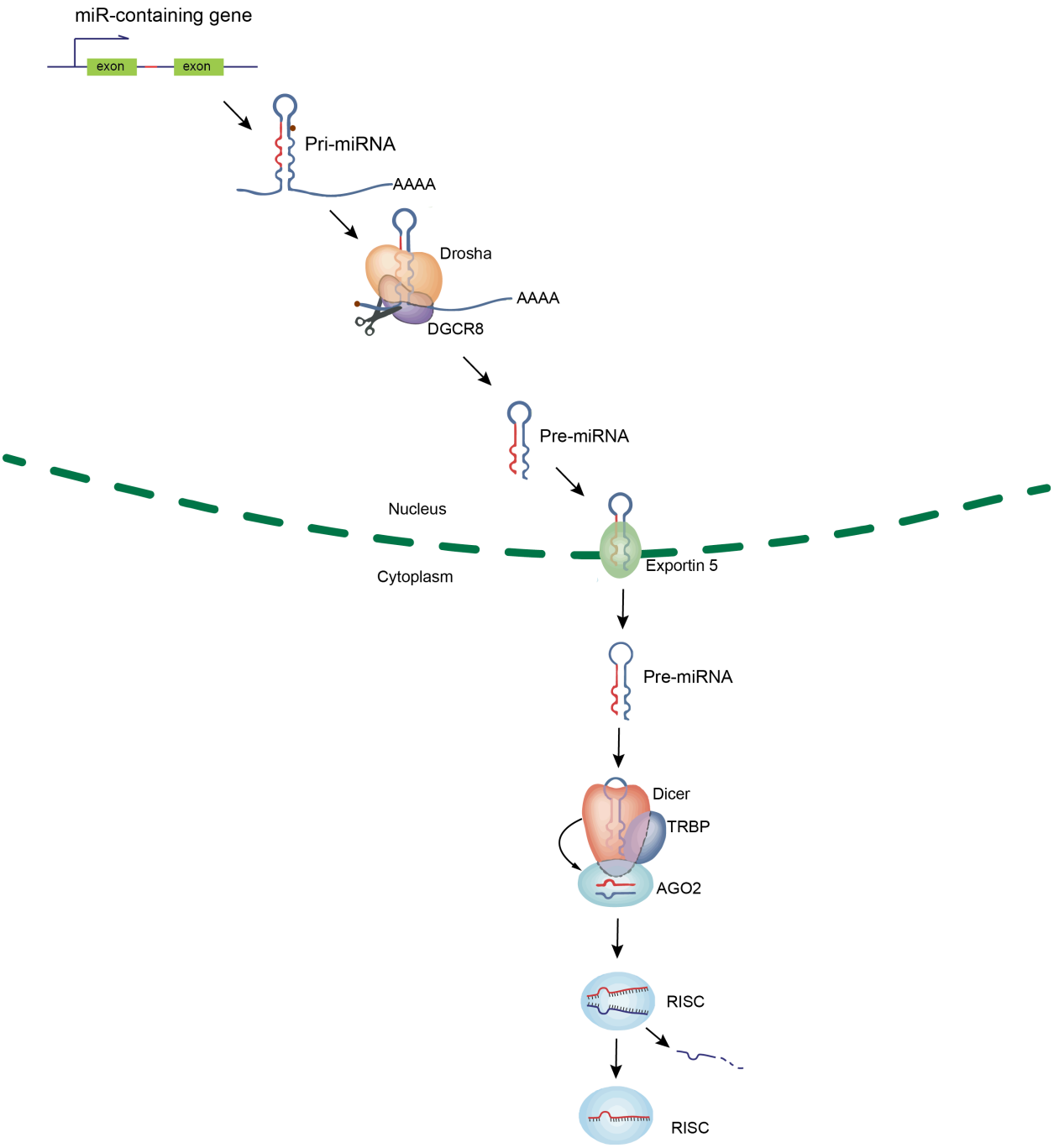

Figure 1.2 Overview of the primary pathway of miRNA biogenesis

miRs are often transcribed from within the intronic regions of genes or from intergenic regions as hairpin structures called Pri-miRNA. Drosha and DGCR8 cleave the hairpin from the rest of the transcript to make a Pre-miRNA. The Pre-miRNA is loaded into Exportin 5 and transported to the cytoplasm. Here, the proteins Dicer and TRBP cleave the loop of the hairpin to leave an RNA duplex, which is loaded into AGO2. AGO2 then joins the RIS-Complex, where the duplex is unwound, and only the mature miR is retained for later targeting of RISC to mRNAs. Adapted from Li and Rana 2014 and He and Hannon 2004.

miRNAs use nucleotide positions 2 through 6 or 8, also known as the "seed sequence", to guide RISC to mRNA targets. In mammals, miRs largely act through imperfect base pairing between the seed sequence and the 3' untranslated region (UTR) of an mRNA. This base-paring causes deadenylation of the polyA tail via recruitment of exonuclease, followed by decapping of the mRNA by mRNA-decapping enzyme 1 or 2 (DCP1/2) (Figure 1.3, reviewed in Brümmer & Hausser, 2014; Li & Rana, 2014). Imperfect binding of the seed sequence to the coding region of mRNAs causes translational inhibition without affecting measurable mRNA abundance, although the exact mechanism of this process is not well understood (Figure 1.3, reviewed in Brümmer & Hausser, 2014; Wilczynska & Bushell, 2014). In other organisms, perfect seed sequence to mRNA binding has been observed, and results in mRNA degradation via the catalytic action of Ago2. However, this form of miR-mediated regulation is thought to occur only rarely in animals (reviewed in Jonas & Izaurralde, 2015).

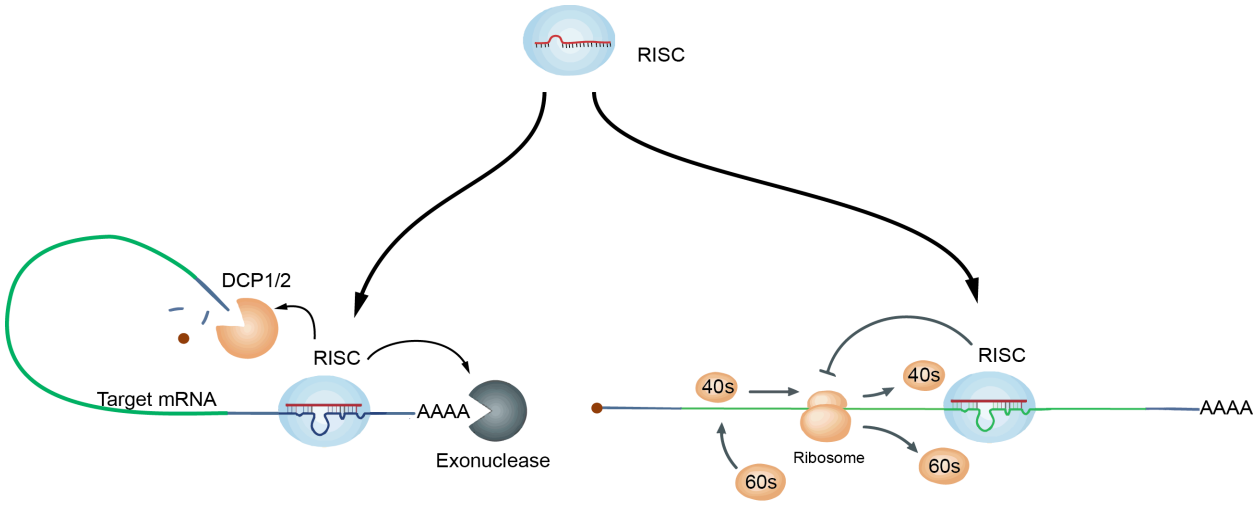

Figure 1.3 Post-transcriptional regulation by miRNAs

(Left) Imperfect binding of miRs within the 3' UTR of an mRNA target (navy line) results in deadenylation of the poly-A tail, followed by decapping (red circle) by DCP1/2 and 5' → 3' digestion. (Right) miRNA binding within the coding region (green) of a target mRNA results in translation inhibition, which does not result in mRNA degradation. Figure modified from Li and Rana, 2014 and He and Hannon, 2004.

As the microRNA seed sequence is short in length and, especially in mammals, often acts with imperfect base-pairing, miRs have the potential to regulate hundreds of mRNAs simultaneously (reviewed in Jonas & Izaurralde, 2015; Brümmer & Hausser, 2014; He & Hannon, 2004). Additionally, because miRs act to suppress translation from mRNAs, the functional output of their regulatory action is highly dependent on the mRNAs expressed in a given cell (reviewed in Ha, 2011).

microRNA Function in Stem Cells

microRNAs are gaining wide acceptance as essential regulators of normal stem cell and progenitor function in many tissues, although most of the work so far has focused on the microRNA regulation of the proliferation-differentiation axis (Gangaraju & Lin, 2009). For example, miR-363 maintains adipose stem cells (called adipose tissue-derived stromal cells) in a multipotent state, and must be downregulated in order for these cells to differentiate (Chen et al., 2014). Likewise, in osteoblasts, miR-125b maintains a proliferative progenitor state and is downregulated upon differentiation (Mizuno et al., 2008), as is miR-155 in the hematopoietic system (Georgantas et al., 2007). miR-203 acts in the opposite manner in the skin, where its expression prohibits proliferation and promotes differentiation (Yi et al., 2008). miRs have recently been linked with stem cell quiescence; in muscle stem cells, global loss of miR function causes them to become activated. Furthermore, miR-489 expression was found to be sufficient to mediate the quiescent state of muscle stem cells (Cheung et al., 2013).

microRNA Function in Neural Stem Cells, Their Progeny, and Brain Tumors

microRNAs are essential for normal brain development; Ago2-deficient mice fail to have full neural tube closure, and exhibit forebrain mis-patterning (Liu et al., 2004). Selective loss of Dicer under various brain specific promoters causes mice to have smaller cortices and abnormal

neuronal maturation, and caused hippocampal stem cells to fail to proliferate and differentiate (Hébert et al., 2010; reviewed in Sun & Shi, 2015; Bian & Sun, 2011). Additionally, deletion of Dicer from postnatal astrocytes caused a rapid neurological decline, and death 4-5 weeks after deletion (Tao et al., 2011). Several miRs have been implicated in proliferation and differentiation of neural stem cells and progenitors. In terms of specific microRNAs, miR-184 keeps cells in an NSC/progenitor state where cells are actively cycling but do not differentiate (Liu et al., 2010). miR-137 is expressed in the V-SVZ, where it functions to reduce cell cycling and increase neural differentiation (Silber et al., 2008). let-7b, one of the first microRNAs discovered in *C. elegans*, also promotes cell cycle exit and differentiation in perinatal neural stem cells (Zhao et al., 2010). miR-9 acts in a similar manner to let-7b in these cells, perhaps because they both target the transcription factor *Nr2e1 (Tlx)* (Zhao et al., 2009; Zhao et al., 2010). miR-124 is the most abundant microRNA in the brain and is highly expressed in neurons (reviewed in Shi et al., 2010, Cheng et al., 2009). miR-124 is also expressed by V-SVZ-generated neuroblasts and promotes the timing of lineage progression via repression of the transcription factor *Sox9* (Cheng et al., 2009). However, functions of miRs at the earliest stages of the V-SVZ lineage have not been described.

miRs are also misexpressed in disease states, most notably and widely in cancers. Glioblastoma multiforme (GBM) has strong upregulation of miR-221, while miR-128 and miR-7, both of which target EGFR, are often downregulated in these tumors (reviewed in Garg et al., 2013; Mira et al., 2010). miR-363 expression is high in GBMs, and promotes tumor migration and survival (reviewed in Garg et al., 2013). miR-25 expression is also high in pediatric high-grade gliomas and seems to have a similar function to miR-363 (reviewed in Garg et al., 2013). Interestingly, in the context of GBMs, miR-124 and miR-137 can act as tumor suppressors as

they are able to induce cell cycle arrest and differentiation, which explains their low expression in many of these malignancies (reviewed in Garg et al., 2013; Mira et al., 2010). miR-124 likely also exhibits low expression in medulloblastomas for the same reason (reviewed in Garg et al., 2013). Recent studies have further implicated misexpression of miRs in neurological and neurodegenerative disorders, including Schizophrenia, Alzheimer's disease, and Huntington's Disease (reviewed in Bian et al., 2013).

The miR-17~92 Cluster and The Brain

The miR-17~92 cluster was first identified as an oncomiR, as it stimulates proliferation and cell survival in tumors (He et al., 2005) including secondary glioblastoma, pediatric high grade glioma, neuroblastomas, and medulloblastomas (Ernst et al., 2010; Malzkorn et al., 2010; reviewed in Garg et al., 2013). However, this cluster also plays an essential role in development. Homozygous deletion of the miR-17~92 cluster in the embryo results in death at P0 because the neonates have extensively underdeveloped hearts and lungs (Ventura et al., 2008). Notably, deletion of only one copy of the 17~92 cluster resulted in pups that were viable and fertile, but only 60% the size of wild-type littermates (Ventura et al., 2008).

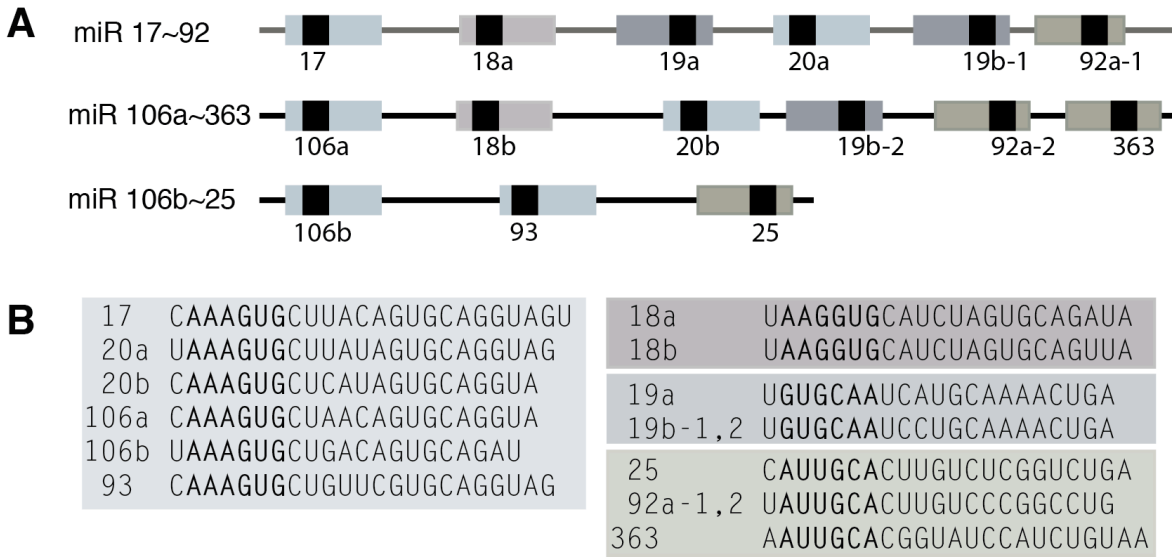

Figure 1.4 The miR-17~92 cluster, its paralogs and seed sequence family members

(A) The polycistronic miR-17~92 cluster shares overall ordering of miRs with its homologs, the miR-106a~363 and miR-106b~25 clusters. (B) The individual miRs from these clusters can be grouped into family based on sequence homology, although the rest of their mature forms show homology as well.

Interestingly, the miR-17~92 cluster has two paralogs, the miR-106a~363 cluster and the miR-106b~25 cluster (Figure 1.4). These clusters are thought to have arisen through a duplication event as the individual miRs within the clusters share sequence homology with those in the miR-17~92 cluster, and the overall ordering of the miRs within each cluster are strikingly similar. However, the additional clusters are not essential for normal development; homozygous deletion of either the miR-106a~363 or miR-106b~25 clusters resulted in normal pups (Ventura et al., 2008). Intriguingly, deletion of both miR-17~92 and miR-106b~25 increased the severity of defects as opposed to when miR-17~92 alone was deleted. This suggests that miR-106b~25 may have redundant functions to miR-17~92 (Ventura et al., 2008). Recent work has shown the miR-106b~25 cluster to be important for proliferation, self-renewal, and neurogenesis of cultured neural progenitors from the forebrain of adult mice (Brett et al., 2011).

Since the 2008 Ventura study, miR-17~92 has been shown to have diverse roles in many tissues where it promotes proliferation, cell survival, and angiogenesis, and inhibits differentiation, both during development and in cancers (Reviewed in Olive et al., 2010; Mogilyansky & Rigoutsos, 2013). The function of the miR-17~92 cluster in the central nervous system has begun to be uncovered as well. A minor product of the miR-17~92 cluster is needed for normal spinal cord motor neuron patterning (Chen et al., 2011), while the whole cluster promotes survival of limb-innervating motor neurons (Tung et al., 2015). miR-17 and 20a have been shown to downregulate pro-neuronal differentiation genes in the SH-SY5Y cell line (Beveridge et al., 2009). The miR-17~92 cluster is also important for maintaining NSC proliferation in the embryonic cortex (Bian et al., 2013; Mao et al., 2014). Furthermore, this cluster is important to maintaining embryonic neurogenesis and must be downregulated for gliogenesis to occur in engineered multipotent neural stem cells (Naka-Kaneda et al., 2014). Expression of miR-17~92 is elevated in neural progenitors following a model of stroke (Liu et al., 2013). In humans, the second ever miRNA-based disease was recently identified: a subset of patients with Feingold syndrome, in which patients present with microcephaly, short stature, digital abnormalities, and varying degrees of learning disabilities, have been found to harbor a hemizygous deletion of the miR-17~92 cluster (de Pontual et al., 2011), further highlighting the need to better understand the role of this cluster in normal development and disease.

Sphingosine 1 Phosphate Receptor 1 Function

Sphingosine 1 phosphate receptor 1 (S1pr1) is the first of five known receptors for the ligand sphingosine 1 phosphate (S1P), and is a computationally predicted target of the miR-17~92 cluster. Of the five S1P receptors, S1pr1 is the only one for which homozygous deletion is embryonic lethal. In homozygously deleted mice, the lack of S1PR1 results in death between

e12.5-14.5, as, despite having formed a normal vascular network, there is a defect in the vascular barrier. Especially on major vessels, there is a lack of coverage by pericytes and vascular smooth muscle cells (reviewed in Blaho & Hla, 2014). In fact, a major role of S1PR1 is helping cells to migrate towards concentrated areas of S1P. This ability is necessary for hematopoietic stem cells to egress from the lymph nodes and bone marrow (reviewed in Chun & Hartung, 2010; Blaho & Hla, 2014). S1PR1-mediated migration is also needed for neural precursors to reach S1P-rich sites of injury in the spinal cord (Kimura et al., 2006). S1PR1 is very important for normal angiogenesis postnatally; inhibition of S1PR1 signaling from P8 retinas leads to increased endothelial sprouting and ectopic vessel branches, whereas signaling though S1PR1 prohibits angiogenic sprouting and promotes cell-cell adhesion (Gaengel et al., 2012).

In the human brain, S1PR1 staining is present at the V-SVZ. S1PR1-positive cells exhibit similar staining patterns to those positive for GFAP and Aquaporin4 (AQP4) (Nishimura et al., 2010; Akiyama et al., 2008). Together, these data suggest that S1PR1 may also play an important role in the stem cells of the human brain.

In this thesis, I describe the transcriptional states of FACS purified qNSCs and aNSCs, as well as a key role for miRNA regulation of aNSCs. First, I shed light on the regulatory, metabolic, and signaling pathways active in each stem cell type in Chapter 2. Then, I compare the quiescent and activated stem cell transcriptomes to their counterparts in other tissues. In Chapter 3, I show that the miR-17~92 cluster is greatly enriched in aNSCs over qNSCs in the V-SVZ. I next present data on the functional role of this cluster. Finally, I show that S1PR1 is a miR-17~92 target in adult neural stem cells in Chapter 4.

These studies provide the first transcriptome-based insight into quiescent adult neural stem cells, and highlight a role for miR-based regulation of activated neural stem cells, a potential target of which mediates adult neural stem cell quiescence.

Chapter 2 Transcriptional states of Quiescent and Activated stem cell states

The data in this chapter are largely published in Codega et al., 2014 which is included in the Appendix. Erika Pastrana, Paolo Codega, and Violeta Silva-Vargas developed the FACS purification strategy. Paolo Codega and Annina DeLeo performed FACS purification of cells for qPCR and microarrays. Annina DeLeo performed RNA extraction and cDNA synthesis for qPCR and microarrays. Annina DeLeo performed all bioinformatic analysis. Alex Paul performed the small molecule screen. Annina DeLeo and Alex Paul performed qPCR.

Introduction

Quiescent and actively dividing (activated) stem cells coexist in adult stem cell niches (Li & Clevers, 2010). Stem cell quiescence and activation play an essential role in many organs, underlying tissue maintenance, regeneration, function, plasticity, aging, and disease.

Currently, little is understood about the molecular differences driving the biology of quiescent and activated stem cells. The main difficulty lies in identifying and prospectively purifying stem cells, especially the quiescent subpopulations, from their *in vivo* niches. In this chapter, I briefly outline a fluorescence-activated cell sorting (FACS) strategy developed by the Doetsch laboratory that allows qNSCs and aNSCs to be purified for the first time from the adult brain, and describe the functional properties of each population (Codega et al., 2014). I took advantage of this FACS approach to perform transcriptional profiling of freshly isolated qNSCs and aNSCs so as to illuminate their molecular regulation, marker expression, and important pathways, as well as to determine whether they shared features with quiescent and activated stem cells in other organs.

Results

FACS Purification and Functional Properties of qNSCs and aNSCs

Previous work in the Doetsch lab developed a simple strategy to simultaneously isolate activated stem cells (GFAP::GFP$^+$EGFR$^+$), transit-amplifying cells (TACs, EGFR$^+$), and neuroblasts (CD24$^+$) from the V-SVZ by combining EGF-A647 and CD24 immunostaining with GFAP::GFP mice (Pastrana et al., 2009). CD133 is highly expressed by the ependymal cells (Coskun et al., 2008), while a subset of GFAP$^+$ astrocytes contacting the ventricle also express CD133 (Mirzadeh et al., 2008; Beckervordersandforth et al., 2010). By including CD133 in the above sorting strategy, we are able to distinguish and isolate two CD133$^+$ stem cell astrocyte populations, which, based on the functional data described below, correspond to qNSCs (GFAP::GFP$^+$CD133$^+$) and aNSCs (GFAP::GFP$^+$CD133$^+$EGFR$^+$) (Figure 2.1). The remaining GFAP::GFP$^+$-only cells comprise niche and other astrocytes (Figure 2.1).

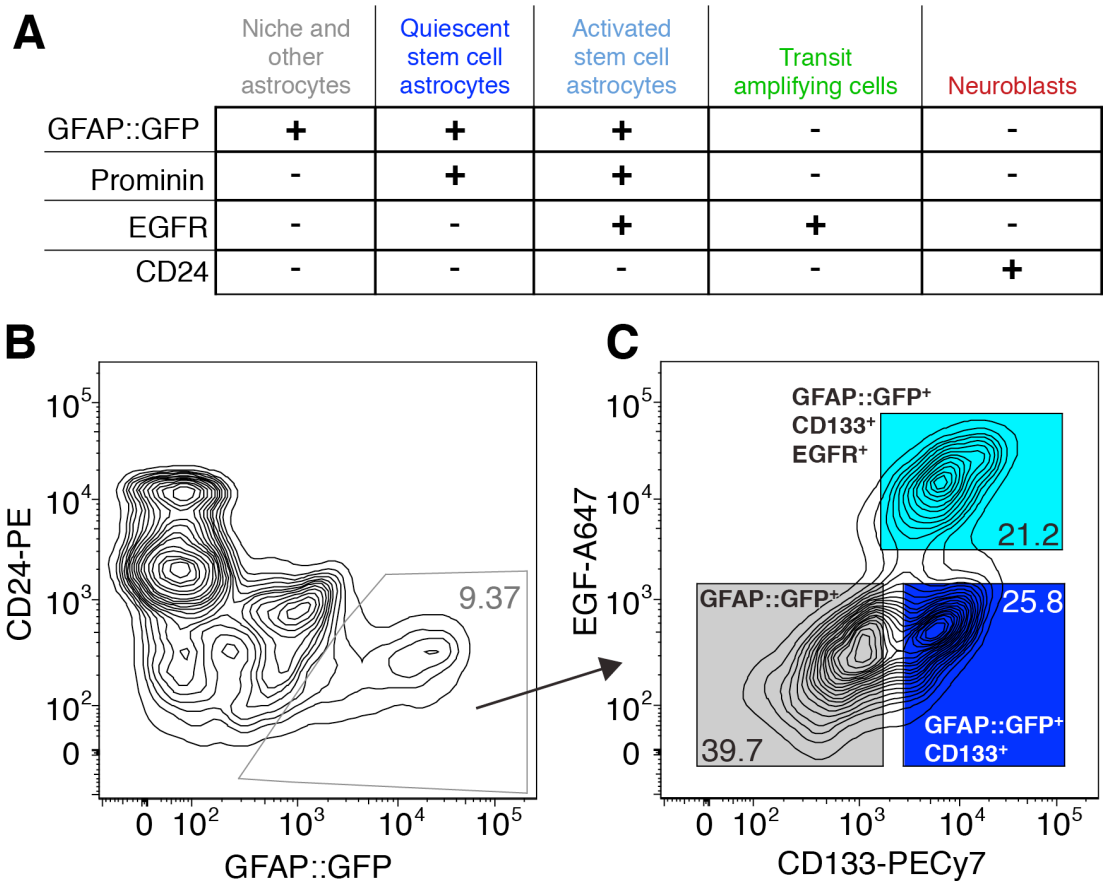

Figure 2.1 FACS purification strategy using CD133

(A) Table of markers used to identify and FACS-purify V-SVZ cells and their progeny. (B and C) Representative FACS plots showing gating strategy. In (B), the gate used to select GFAP::GFP+CD24- cells, which are then gated on EGF-A647 and CD133-PE-Cy7. In (C), three populations are clearly defined: GFAP::GFP+ (gray), GFAP::GFP+CD133+ (qNSCs, blue), and GFAP::GFP+ CD133+EGFR+ (aNSCs, cyan). For both (B) and (C) percentages of cells corresponding to each gate are included.

Functional studies on the FACS-purified populations showed that the qNSC population was slowly dividing, resistant to anti-mitotic drug treatment, and lacked expression of MCM2 and Ki67, intrinsic markers of cell division (figure 2.2). In contrast, the aNSC population was rapidly dividing, killed by anti-mitotic treatment, and highly enriched in MCM2 and Ki67 expression (Figure 2.2B, green line, Codega et al., 2014). Importantly, qNSCs only very rarely gave rise to colonies *in vitro*, and gave rise to neurons *in vivo* with delayed kinetics as compared

to aNSCs, which were highly enriched in colony formation, and rapidly formed neurons *in vivo* (Figure 2.2B, cyan and purple lines). Notably, qNSCs also lacked Nestin expression, but upregulated both Nestin and EGFR upon activation (Figure 2.2A, green and cyan bars respectively). The ability to purify qNSCs and aNSCs directly from their *in vivo* niche opens up many avenues to further explore their functional and molecular properties. In the next section, I describe my findings on the transcriptional profiles of qNSCs and aNSCs from the adult V-SVZ.

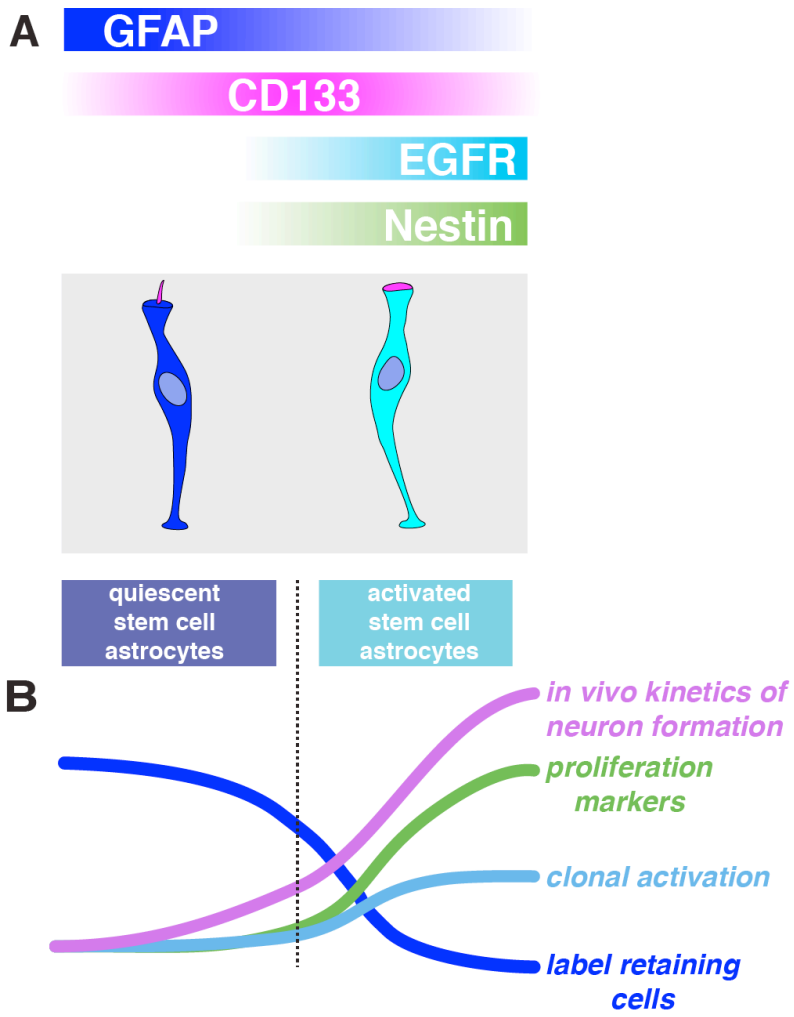

Figure 2.2 Markers and functional properties of qNSCs and aNSCs

(A) Distribution of selected markers in adult V-SVZ stem cells. (B) Functional properties of qNSCs and aNSCs.

Bioinformatic Analysis of Purified qNSCs and aNSCs Reveals Distinct Molecular Signatures

To define the transcriptomes of qNSCs and aNSCs, I FACS purified both populations as described above. Total RNA was isolated, cDNA amplified, labeled, and hybridized to Affymetrix MOE430.2 chips. The data was then normalized and analyzed using the Genespring GX 11 software suite.

Differential expression analysis revealed that a few thousand genes were uniquely and significantly enriched in each population (Figure 2.3A, 2312 probes enriched in qNSCs, 1503 in aNSCs, corrected p-value less than 0.05 by Benjamini-Hochberg multiple testing correction, complete list in Table S1). To understand the functional properties of these differentially expressed genes, I analyzed their associated Gene Ontologies (GO). Gene Ontology is an ever-growing database used to categorize genes and their proteins by their known biological process, molecular function, or presence in a particular sub-cellular compartment or component (Ashburner et al., 2000). I focused my analysis on the biological process categories of the differentially expressed genes to understand the molecular underpinnings for the behavior differences observed between quiescent and activated NS. Gene Ontologies with a p-value less than 0.05 were considered.

In accordance with their actively cycling status, most of the categories found for aNSC-enriched genes were related to cycle and division. aNSCs show a concordant increase in the number of genes involved in cellular metabolic processes over qNSCs (Figure 2.3B and C, light orange wedges). In contrast, qNSCs were enriched for the GO categories of cell communication and response to stimulus, suggesting that either they are poised for activation and are awaiting crucial “activation” signals, or that quiescence is actively maintained via signaling from the

niche (Figure 2.3B; full categories can be found in Table S2). qNSCs also show enrichment in genes involved in cell adhesion, further underscoring the dynamic regulation of the quiescent state via interaction with the microenvironment.

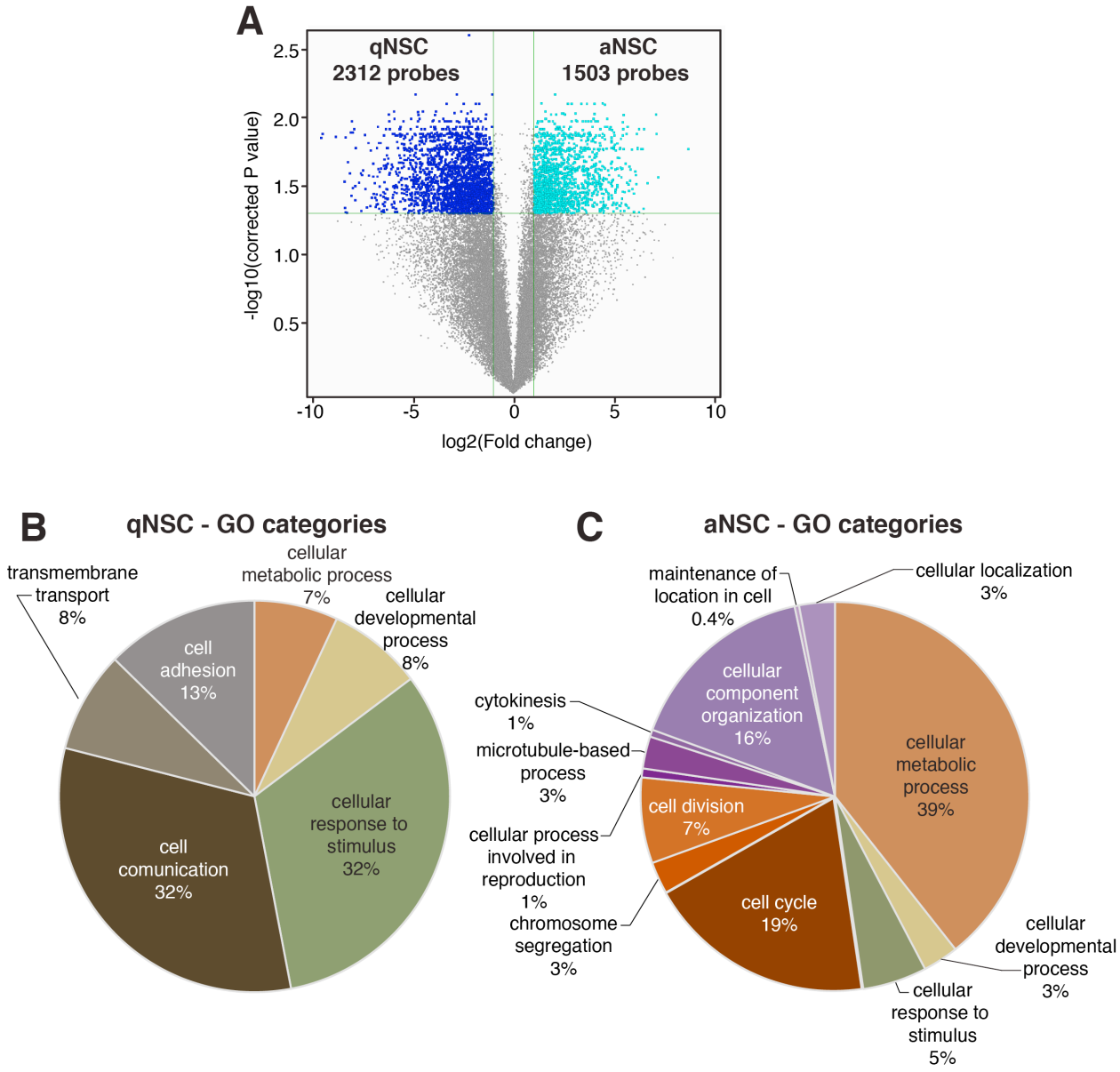

Figure 2.3 Gene Expression Analysis of qNSCs and aNSCs Reveals Distinct Molecular Signatures

(A) Volcano plot of differentially expressed probesets in qNSCs and aNSCs. Probes have at least 2-fold change in expression and a corrected p value < 0.05. (B and C) Pie charts showing representative GO categories for differentially expressed probesets in (B) qNSCs and (C) aNSCs, as determined in (A).

The GO analysis gives only a glimpse into the differences between qNSCs and aNSCs, as it only considers a small fraction of genes expressed by each population. To explore the transcriptomes in greater depth, I turned to Gene Set Enrichment Analysis (GSEA) (Subramanian et al., 2005). GSEA analyzes the entire transcriptome, and instead of looking for single genes with large fold changes (greater than 2-fold), this method identifies sets of genes that exhibit an accumulation of enough small fold changes (less than 2-fold) in the same direction to be considered significant. These gene sets are defined from the literature and correspond to biological pathways, changes in response to drugs, or genes regulated by the same transcription factors. GSEA may therefore find biologically relevant changes to the transcriptome that might be overlooked by other methods.

GSEA revealed that qNSCs and aNSCs have distinct molecular features and confirmed the functional differences observed *in vivo* (Figure 2.4A–C, Figure 2.2). GSEA again highlighted the actively dividing state of aNSCs; their transcriptome was enriched in genes involved in the cell cycle, transcription and translation, and DNA repair (Figure 2.4A cyan bars; Table S2; full GSEA categories in Table S3). The most represented GSEA groups for qNSCs were related to transport, signaling, receptors, cell surface, and extracellular matrix (Figure 2.4A royal blue bars; Table S3), again relating to and underscoring the quiescent cells' interaction with the niche and reliance on extrinsic signals to actively maintain their quiescent state.

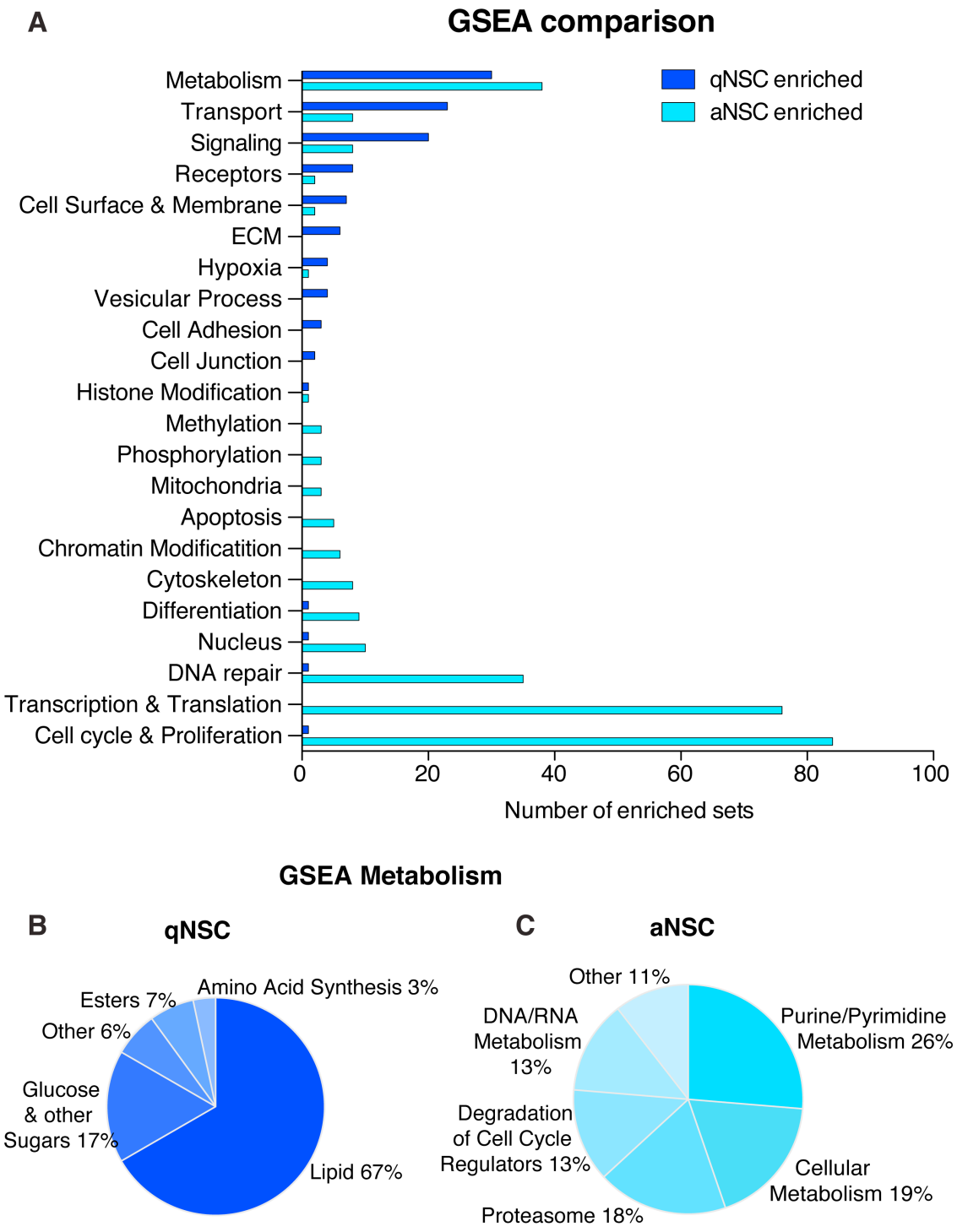

Figure 2.4 Gene Set Enrichment Analysis gives insight into overall transcriptional changes between qNSCs and aNSCs

(A) GSEA thematic categories for qNSCs (royal blue bars) versus aNSCs (cyan bars). Sets have a false discovery rate (q value) of <0.05 and are hand curated into thematic categories. (B and C) Specific metabolic pathways enriched (B) in qNSCs or (C) in aNSCs. See Supplemental Table 3 for full list of sets.

Notably, with GSEA analysis we could better appreciate the differences in the types of metabolism enriched in qNSC and aNSC. The majority of the metabolism sets enriched in qNSCs were related to lipids (Figure 2.4B), which are emerging as important signals in NSC (Knobloch et al., 2013). In contrast, and in alignment with an actively dividing state, the metabolism sets enriched in the aNSCs were DNA/RNA-related metabolism. These sets also included proteasome activity related to the degradation of cell-cycle regulators (Figure 2.4C).

Interestingly, qNSCs are uniquely enriched for sets relating to the extracellular matrix and cell adhesion. One such gene is Vcam1, which encodes an adhesion molecule that prevents cells from proliferating and maintains V-SVZ architecture. Indeed, *Vcam1* is expressed in qNSCs at a high level (Figure 2.6A; Kokovay et al., 2012). Other adhesion genes such as *Itga6, Ncam1,* and *Numb,* which have been reported to be expressed in neural stem cells are also enriched in the qNSC population (Table S4; Kazanis et al., 2010; Kokovay et al., 2010; Kuo et al., 2006; Lim et al., 2006), suggesting that maintaining close contact with the niche may be necessary for quiescence.

Analysis of Microarray Data Reveals Bi-Directional Regulation Between qNSCs and aNSCs

From the transcriptional profiles of qNSCs and aNSCs, a very interesting pattern of bidirectional regulation emerged, with one population expressing ligands of one pathway, and the other expressing the receptor. Below, I have outlined a few examples of this in our data, with special focus on factors previously reported to have relevance in the V-SVZ adult neural stem cell niche.

Notch signaling plays an important role in adult V-SVZ biology. Several Notch ligands are enriched in aNSCs, as compared to qNSCs. For example, by microarray and quantitative PCR (qPCR), aNSCs show enrichment of *Delta-like ligand 1* (*Dll1)* (Figure 2.5, Table 2.1,

Figure 2.6B), as has been previously reported (Kawaguchi et al., 2013). *Jagged 1* (*Jag1*) is also enriched in aNSCs and TACs (Figure 2.5, Table 2.1), which is in agreement with its ability to maintain a proliferative state and promote self-renewing divisions (Nyfeler et al., 2005; Andreu-Agulló et al., 2009). While Jag1 is known to be expressed in opposition to cells expressing Notch1 (Nyfeler et al., 2005), as discussed below, *Notch1* is also enriched in aNSCs. In contrast, *Delta-like 1 homolog* (*Dlk1*) expression is significantly enriched in the qNSCs and was previously shown to be important for V-SVZ stem cell self-renewal (Figure 2.5, Table 2.1, Ferrón et al., 2012).

My analysis showed that *Notch1* is expressed in aNSCs, in accordance with the finding that Notch1 deletion selectively reduces aNSC number (Figure 2.5, Table 2.1; Basak et al., 2012). Conversely, *Notch 2* and *3* are enriched in the qNSCs (Figure 2.5, Table 2.1). These receptors have previously been found on $GFAP^+$ V-SVZ cells, although Notch2 is also present on neuroblasts (Basak et al., 2012). *Rbpj,* the immediate downstream transcription factor for the intercellular domain of Notch, is enriched in aNSCs (Figure 2.5, Table 2.1). RBPJ expression is sufficient to convert neural progenitors into neural stem cells in embryonic brain development (Mizutani et al., 2007) and to maintain stemness and self-renewing division in the adult SGZ (Ehm et al., 2010).

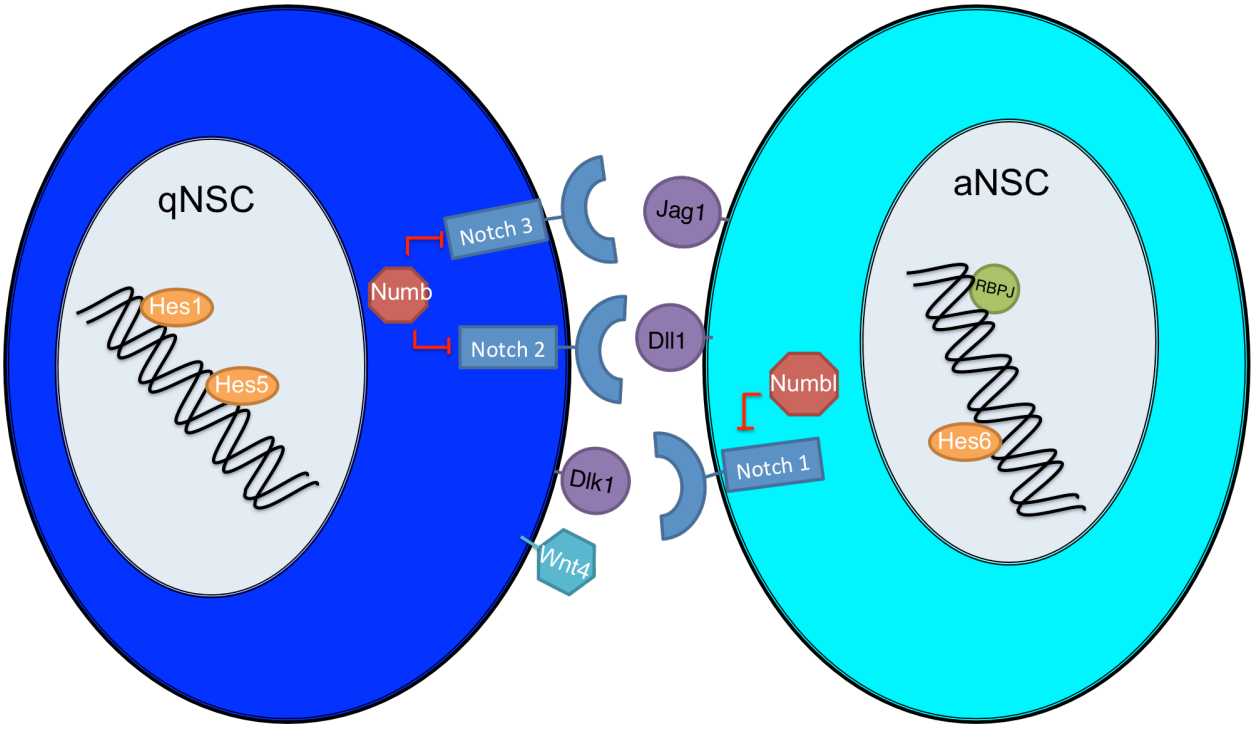

Figure 2.5 Schema of distribution of components of Notch signaling pathway by microarray expression.

There are several Notch-effector transcription factors, three of which show a differential expression pattern in our dataset: *Hes1, Hes5,* and *Hes6*. In accordance with its ability to suppress proliferation (Shimojo et al., 2008), *Hes1* is enriched in qNSCs (Figure 2.5, Table 2.1). Hes1 is also known to suppress *Ascl1* expression (Bae et al., 2000), and indeed *Ascl1* expression is restricted to the aNSCs (Figure 2.6C). Excitingly, *Hes6*, a known antagonist of Hes1, is also enriched in the aNSCs (Figure 2.5, Table 2.1), indicating a potential regulatory loop between the two stem cell populations (Bae et al., 2000; Gratton et al., 2003). *Hes5* is also enriched in the qNSC population (Figure 2.5, Table 2.1), and has been shown to mark a slowly dividing population in the V-SVZ (Giachino et al., 2014). Hes5, together with Hes1, is known to downregulate Dll1 expression (reviewed in Salomoni & Calegari, 2010).

The inhibitors of Notch, Numb and Numb-like (Numbl), are expressed in the qNSCs and aNSCs, respectively (Figure 2.5, Table 2.1). The selective postnatal loss of Numb and Numbl from both V-SVZ stem cells and ependymal cells causes a failure of adult neural stem cells to stay in the more quiescent niche, directly in contact with the ventricular lumen, as their ability to connect with ependymal cells is lost and the quiescent niche is compromised (Kuo et al., 2006, niche reviewed in Fuentealba et al., 2012 and Kokovay et al., 2012).

Interestingly, Wnt4 expression has been reported to be activated by Notch1-Jag1 co-expression (Wang et al., 2013). Wnt4 is also upregulated after Notch2 expression, which leads to G1-stage arrest and reduced proliferation (Fujimura et al., 2010). In our system, *Wnt4* is expressed by the qNSCs (Figure 2.5, Table 2.1). *Sox5* is similarly present in our qNSCs (Table 2.1), and is another activator of Wnt4 expression. As with Notch2, expression of Sox5 results in reduced proliferation (Martinez-Morales et al., 2010). *BLBP,* a marker of stem cell astrocytes, has been shown to be a direct target of Notch in the CNS and is expressed in the qNSCs (reviewed in Louvi & Artavanis-Tsakonas, 2006). *Egfr* (Andreu-Agulló et al., 2009, discussed below) and *Sox2* (Table S4, Ehm et al., 2010, discussed below) are also direct targets and are regulated via RBPJ.

Probe Set ID	Gene Title	Gene Symbol	Fold Change	Examinations of function in adult brain
1418633_at	Notch gene homolog 1	Notch1	1.299	Basak et al., 2012; Ables et al., 2010; Imayoshi et al., 2010; Andreu-Agullo et al., 2009
1418634_at			1.005	
1451889_at	Notch gene homolog 2	Notch2	-1.711	Basak et al., 2012
1455556_at			-2.78	
1421964_at	Notch gene homolog 3	Notch3	-9.633	Basak et al., 2012
1421965_s_at			-4.649	
1419204_at	delta-like 1 (Drosophila)	Dll1	15.73	Kawaguchi et al., 2010
1449939_s_at	delta-like 1 homolog	Dlk1	-17.071	Ferron et al., 2011
1442724_at			-4.167	
1418102_at	hairy and enhancer of split 1	Hes1	-1.166	Andreu-Agullo et al., 2009
1423146_at	hairy and enhancer of split 5	Hes5	-2.698	Lugert et al., 2010; Giachino et al., 2013
1456010_x_at			-2.957	
1436050_x_at	hairy and enhancer of split 6	Hes6	14.964	Lugert et al., 2010; Giachino et al., 2013
1452021_a_at			22.392	
1421105_at	jagged 1	Jag1	2.411	Nyfeler et al., 2005
1421106_at			2.74	
1434070_at			2.725	
1416891_at	numb gene homolog	Numb	-3.17	Kuo et al., 2006
1425368_a_at			1.04	
1416491_at	numb-like	Numbl	1.095	Kuo et al., 2006
1418114_at	recombination signal binding protein for immunoglobulin kappa J region	Rbpj	1.317	Ehm et al., 2010
1448957_at			3.221	
1454896_at			1.945	
1450782_at	wingless-related MMTV integration site 4	Wnt4	-1.643	Beckervordersandforth, 2010

Table 2.1 Notch Pathway components and their enrichment in V-SVZ stem cells

Less reliable probesets are italicized (for reference, _a_ denotes detection of a gene family, _s_ hybridizes to multiple transcript variants, while _x_ hybridizes to multiple genes. Direction of fold change is denoted by highlight color where deeper reds indicate fold change enrichment in aNSCs and deeper green indicates fold change enrichment for qNSCs.

Kokovay et al. identified the CXCR4-CXCL12 (SDF-1) axis as important for proper homing of $CXCR4^+$ adult neural progenitor cells to the blood vessels, a largely proliferative niche (Tavazoie et al., 2008; Shen et al., 2008). Additionally, Kokovay et al., find that CXCl12 is expressed by ependymal cells. In our data set, I find that aNSCs express *Cxcr4,* while *Cxcl12* is expressed by qNSCs (Table S4). It would be interesting to explore the function of this signaling axis within the more quiescent niche near the ventricular lumen.

The quiescent stem cells of the V-SVZ express high levels of *Lrig1* (Figure 2.6C), which is a known marker of stem cell quiescence in the skin and the intestine (Jensen & Watt, 2006; Jensen et al., 2009; Powell et al., 2012). Previous work has shown that Lrig1 targets EGFR protein for degradation from the membrane, thereby downregulating EGFR signaling (Gur et al., 2004). There is little to no *Egfr* expression in our qNSCs (Figure 2.6D), although both *Egfr* and *Lrig1* are expressed in aNSCs, where *Lrig1* could have a tuning effect on the amount of EGFR protein expressed.

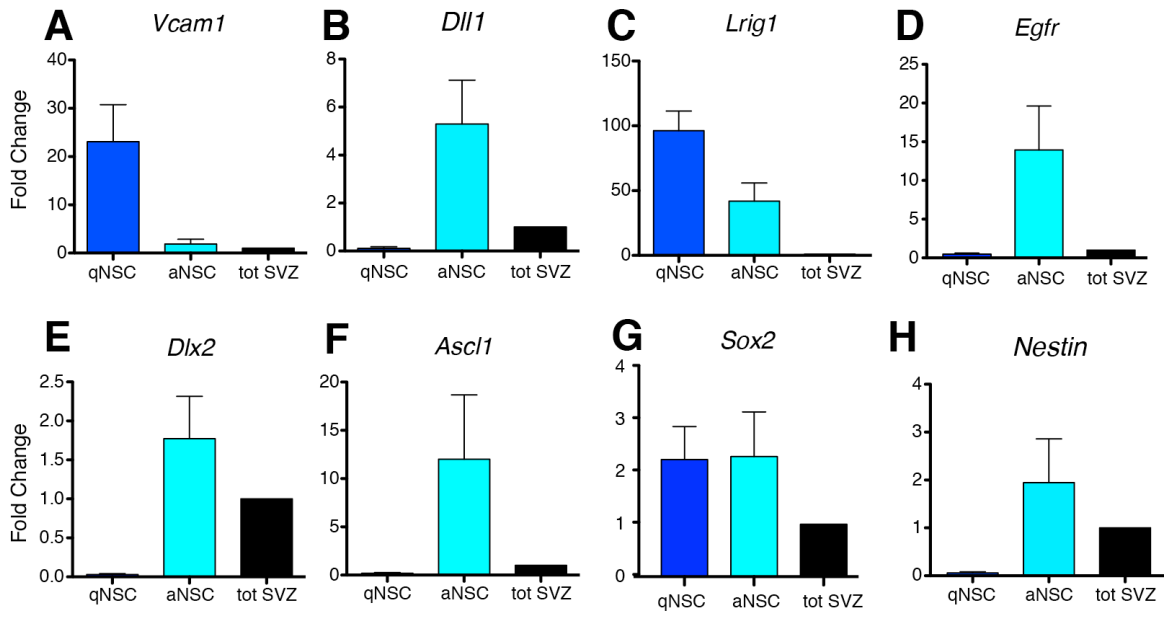

Figure 2.6 qPCR validation of genes enriched in the V-SVZ stem cells

(A-H) mRNA expression levels in the qNSCs and aNSCs as normalized to total SVZ. (A) Vcam1 (B) Dll1 (C) Lrig1 (D) Egfr (E) Dlx2 (F) Ascl1 (G) Sox2 and (H) Nestin.

Transcription Factors Associated with NSCs Are Differentially Expressed in qNSCs and aNSCs

As cells progress down the V-SVZ stem cell lineage to differentiate into neurons, they upregulate different pro-neural and neurogenic transcription factors, a list of which may be found in Table S4. One such example is Dlx2, which is known to be expressed at the protein level by V-SVZ transit amplifying cells and neuroblasts (Doetsch et al., 2002) but not in aNSCs or qNSCs. Interestingly, the expression of *Dlx2* mRNA was found by qPCR to be present in aNSCs at a 2-fold increase over the total V-SVZ (Figure 2.6E). This pattern of mRNA and protein expression suggests that aNSCs may be primed for Dlx2 protein expression or that there could be post-transcriptional regulation of this transcript. Another transcription factor, Ascl1, is expressed at the protein level by approximately 50% of aNSCs (Codega et al., 2014). *Ascl1* is strongly expressed at the mRNA level by aNSCs, but not by qNSCs (Figure 2.6F). Sox2 is considered a neural stem cell transcription factor and is often used as a marker for the identification of stem

cell astrocytes both in the adult and embryonic brain (Lendahl et al., 1990; Graham et al., 2003; Kazanis et al., 2010; Imayoshi et al., 2011; Marqués-Torrejón et al., 2013). Interestingly, while *Sox2* mRNA is enriched in both qNSCs and aNSCs (Figure 2.6G), and more than 90% of qNSCs and aNSCs expressed Sox2, protein expression was stronger among the aNSC population (Codega et al., 2014). The fact that Sox2 is more highly enriched in aNSCs lends weight to the idea that high Sox2 levels may be related to a more proliferative state (Marqués-Torrejón et al., 2013). Remarkably, all three of these transcription factors have mRNA expression that does not match their protein expression, suggesting that in some cases post-transcriptional regulation may be important to restricting protein expression.

Importantly, Nestin, an intermediate filament protein widely considered a hallmark of NSCs both during development and in the adult (Lendahl et al., 1990; Imayoshi et al., 2011), was not expressed in qNSCs. Both microarray and qPCR analysis showed that qNSCs express very low to no levels of *Nestin* mRNA in contrast to aNSCs, in which *Nestin* mRNA is highly expressed (Figure 2.6H). Further functional experiments showed that Nestin is upregulated as qNSCs become activated (Codega et al., 2014). As such, Nestin cannot be used to detect qNSCs.

Comparison of our Neural Stem Cell Populations to Others Previously Identified

We directly compared our transcriptional profiles with those Beckervordersandforth et al. generated from FACS-purified $CD133^+$ GFAP::GFP^+ cells. By comparing their GFAP::GFP^+CD133^+ cells to $CD133^+$ or $GFAP^+$ only V-SVZ cells as well as diencephalic astrocytes (which are $GFAP^+$ but post-mitotic and non-neurogenic), Beckervordersandforth et al. proposed sets of genes that are adult neural stem cell specific (Figure 2.7A and B). When we examined the expression of these genes in our qNSCs and aNSCs, we found that we could resolve two distinct subsets of NSCs with different molecular and functional properties from the

single population collected by Beckervordersandforth et al. (Figure 2.7A and B; Table S7). Importantly, we found that neurogenic transcription factors such as *Dlx1*, *Dlx2*, *Sox4*, *Sox11*, and *Ascl1*, which were proposed to be lineage priming and hallmarks of the GFAP::GFP^{+}CD133^{+} NSCs (Beckervordersandforth et al., 2010), were in fact primarily expressed by or restricted to aNSCs (Table S4, Figure 2.6E and F).

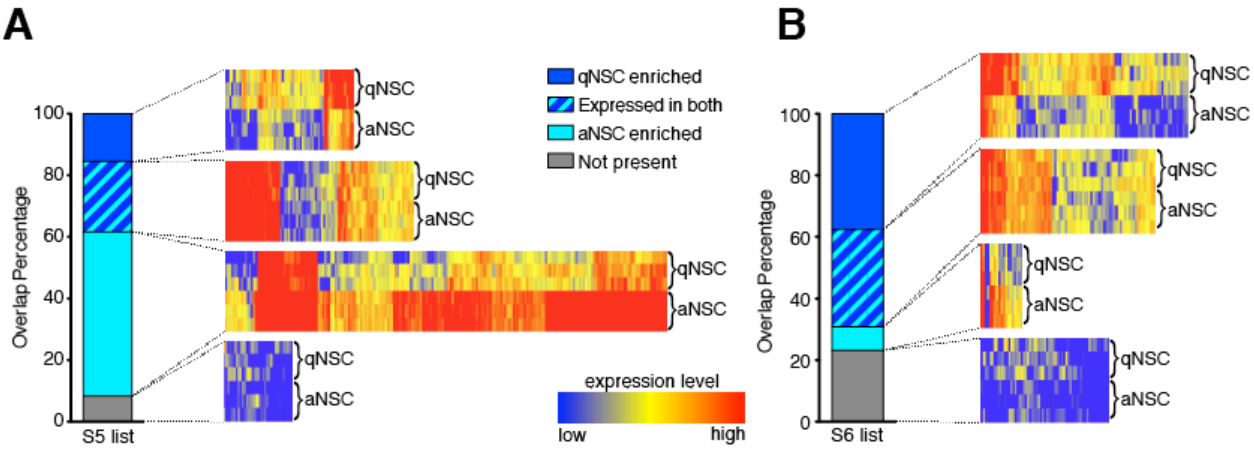

Figure 2.7 Gene Expression Profiling Compared to Beckervordersandforth et al., 2010

(A-B) Comparison of our microarray data with those of Beckervordersandforth et al. 2010. The expression of genes present in "genes enriched in adult NSCs in comparison to diencephalic astrocytes" (A) (corresponding to Table S5 from Beckervordersandforth et al., 2010) and "adult NSC-enriched genes" (B) (corresponding to Table S6 from Beckervordersandforth et al., 2010) lists was analyzed and genes subcategorized by enrichment in qNSCs and aNSCs, expression in both or not present (as defined by expression in raw data < 50 for no expression). Gene lists are in Supplementary Table S7

Features of Quiescence or Activation are Shared Across Adult Tissue Compartments

Populations of quiescent and activated stem cells have been identified in other tissue compartments. To investigate whether qNSCs and aNSCs from the adult brain shared transcriptional features with their counterparts in other organs, I used Genespring to compare our data sets with published lists from hematopoietic, muscle, skin, and intestinal stem cells (Ivanova et al., 2002; Venezia et al., 2004; Forsberg et al., 2010; Pallafacchina et al., 2010; Powell et al., 2012; Blanpain et al., 2004; Fukada et al., 2007; Cheung & Rando, 2013). The genes in each list

were categorized by fold change analysis as being qNSC enriched, aNSC enriched, expressed in both, or not expressed if their expression in the raw data was less than 50. Indeed, those genes published in the short-term/proliferative stem cell lists from other tissues were up-regulated in our activated population, and the majority of these genes are involved in the cell cycle and cell division (Figure 2.8B; Table S5). Interestingly, the majority of genes in long-term/quiescent populations were also upregulated in our quiescent V-SVZ stem cells (Figure 2.8A; Table S5). Gene Ontology analysis of the list of genes expressed by at least two quiescent stem cell types shows that they commonly upregulate lipid metabolism, cell signaling pathways, and adhesion molecule binding (i.e. ECM) (Table S5). Together, these data suggest that common transcriptional programs for quiescence or activation are shared between stem cells in different tissues.

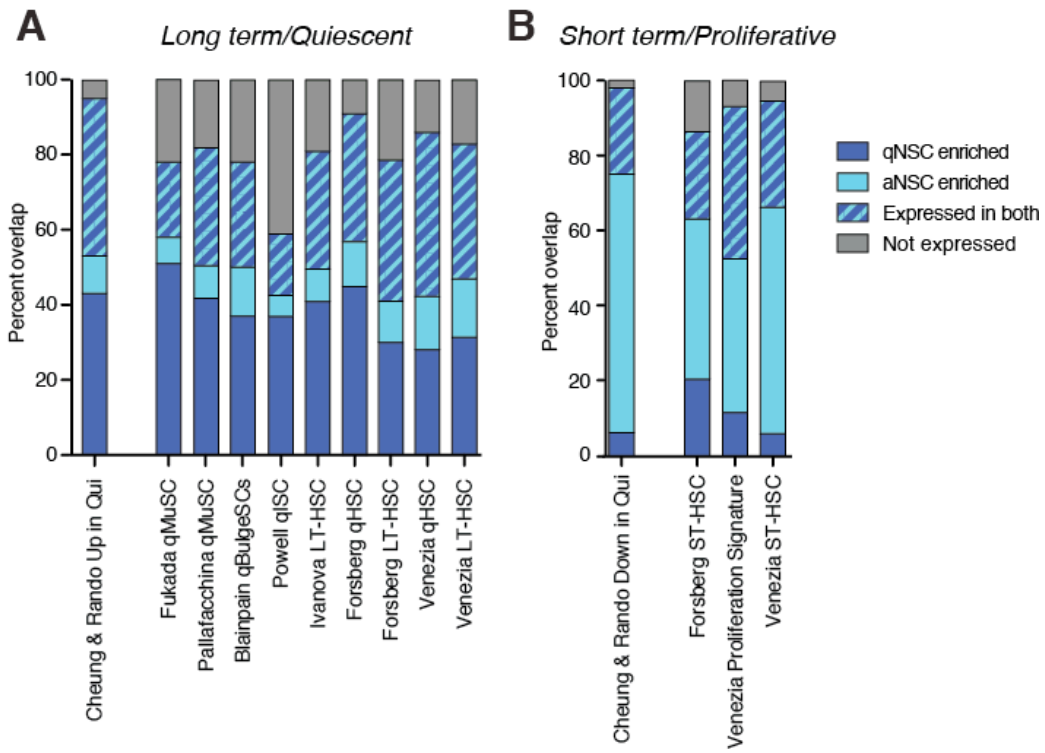

Figure 2.8 Quiescence or Activation Gene Expression overlap with stem cells of other tissues

(A-B) Percentage of overlap with signatures of quiescent and dividing stem cells from other organs: (E) long-term (LT)/quiescent signatures and (F) short-term (ST)/proliferative signatures as determined by fold-change analysis of published lists compared to qNSC and aNSC populations. Qui, quiescent; HSC, hematopoietic stem cells; qMuSC, quiescent muscle stem cells; qBulgeSC, quiescent bulge stem cells; qISC, quiescent intestinal stem cells. G-H) in both or not present (as defined by expression in raw data < 50 for no expression). Gene lists are in Supplementary Table S5

Signaling Pathways, Including G-Protein Coupled Receptors, Modulate Activation and Proliferation

To gain insight into signaling pathways that modulate quiescence or activation, we mined our transcriptome data using GSEA (Figure 2.9A and B). Notably, not only is EGFR enriched in aNSCs at both the mRNA and protein levels, but components of the EGFR signaling pathway are also enriched in these cells. Therefore, EGFR may not only be a marker of, but be functionally involved in the activated stem cell identity (Figure 2.9B, Doetsch et al., 2002).

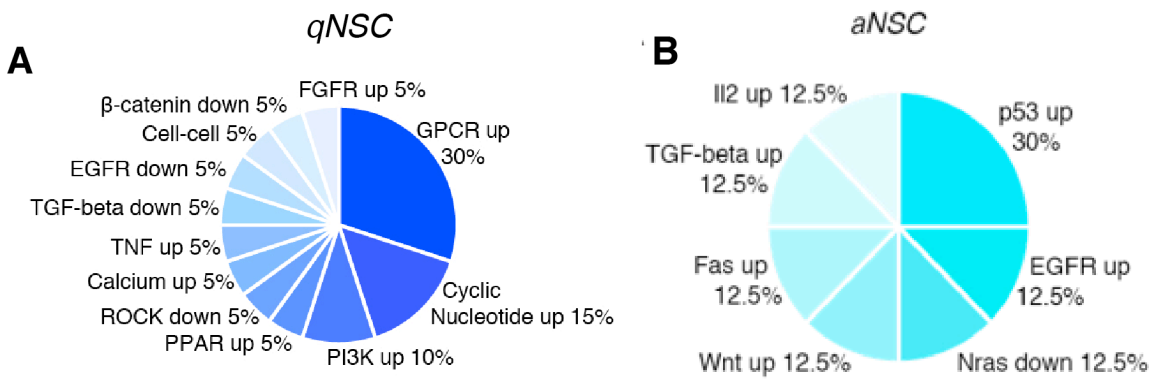

Figure 2.9 GSEA reveals differences in signaling between q and aNSCs

(A) Types of signaling sets enriched in qNSCs (B) Types of signaling sets enriched in aNSC

Interestingly, quiescent stem cells also show a significant enrichment for signaling pathways, the largest of which is G protein-coupled receptor (GPCR) signaling (30% of all GSEA qNSC signaling sets; Figure 2.9A, Table S3). To assess the role of GPCR-signaling on the regulation of qNSCs, we selected 25 GPCRs that were more than 10-fold enriched in qNSCs over aNSCs as a basis for a functional screen (Table 2.2, full list in Table S6).

Table 2.2 GPCRs assayed and their enrichment in aNSCs

Gene Title	Symbol	Targeting compound	Fold Change (qNSC vs. aNSC)
sphingosine-1-phosphate receptor 5	S1pr5	Sphingosine-1-phosphate	53.72806
lysophosphatidic acid receptor 1	Lpar1	1-Oleoyl lysophosphatidic acid sodium salt	46.594353
sphingosine-1-phosphate receptor 3	S1pr3	Sphingosine-1-phosphate	39.406864
adenosine A2b receptor	Adora2b	Adenosine	31.048176
neuropeptide Y receptor Y1	Npy1r	Neuropeptide Y	29.172924
histamine receptor H1	Hrh1	Histamine dihydrochloride	27.785969
endothelin receptor type A	Ednra	Endothelin 1	26.673853
adenosine A2b receptor	Adora2b	Adenosine	25.13803
G protein-coupled receptor 17	Gpr17	Leukotriene D4	24.492632
adrenergic receptor, alpha 2a	Adra2a	(-)-Epinephrine / (-)-Norepinephrine	20.029146
endothelin receptor type A	Ednra	Endothelin 1	19.084913
calcitonin receptor-like	Calcrl	Amylin	18.947807
lysophosphatidic acid receptor 1	Lpar1	1-Oleoyl lysophosphatidic acid sodium salt	18.843597
adrenergic receptor, alpha 1a	Adra1a	(-)-Epinephrine / (-)-Norepinephrine	18.837431
glutamate receptor, metabotropic 3	Grm3	L-CCG-I	17.349558
adenosine A2b receptor	Adora2b	Adenosine	16.695187
neurotensin receptor 1	Ntsr1	Neurotensin	16.52517
adenosine A2b receptor	Adora2b	Adenosine	16.485117
leucine-rich repeat-containing G protein-coupled receptor 4	Lgr4	R-spondin1	13.53013
latrophilin 3	Lphn3	α-Latrotoxin	13.519957
G protein-coupled receptor 146	Gpr146	Proinsulin C-Peptide	13.392646
lysophosphatidic acid receptor 1	Lpar1	1-Oleoyl lysophosphatidic acid sodium salt	12.428424
endothelin receptor type A	Ednra	Endothelin 1	12.049671
adrenergic receptor, alpha 2a	Adra2a	(-)-Epinephrine / (-)-Norepinephrine	11.954656
hypocretin (orexin) receptor 2	Hcrtr2	Orexin A	11.6158285
sphingosine-1-phosphate receptor 1	S1pr1	Sphingosine-1-phosphate	11.028068
tachykinin receptor 2	Tacr2	Neurokinin A	10.985823
G protein-coupled receptor 37	Gpr37	Prosaptide	10.867761
5-hydroxytryptamine (serotonin) receptor 6	Htr6	Serotonin Hydrochloride	10.586905
adenosine A1 receptor	Adora1	Adenosine	10.397678
growth hormone releasing hormone receptor	Ghrhr	GRF	10.390047
secretin receptor	Sctr	Secretin	10.334803
leucine-rich repeat-containing G protein-coupled receptor 4	Lgr4	R-spondin1	10.199413
prostaglandin F receptor	Ptgfr	Prostaglandin D2	10.063209
prostaglandin D receptor	Ptgdr	Prostaglandin D2	10.0564

This screen revealed that both Sphingosine 1 Phosphate (S1P) and prostaglandin D2 reduced the activation of qNSCs by about one half, with S1P selectively acting on qNSCs but not aNSCs (Codega et al., 2014, Figure 2.10A). S1P also decreased the proliferation of activated qNSCs by approximately 50% (Figure 2.10B). Together, these functional data suggest that the adult NSC quiescent state is actively maintained, and that the GPCR ligand S1P is an important ligand for stem cell quiescence.

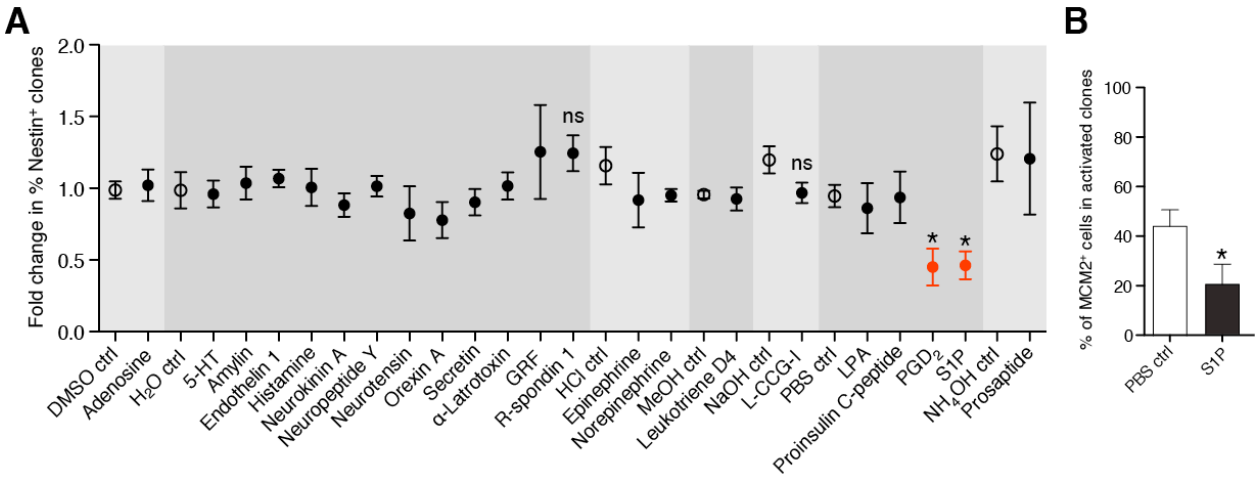

Figure 2.10 GPCR modulation screen

(A) Plot of the fold change of qNSC activated Nestin$^+$ clones. Compounds that were statistically significant are in red (n=3, mean ± SEM, *p<0.05, unpaired Student's t-test). Different shades of grey demarcate compounds in the same diluent, and open circles are controls. (B) Quantification of percentage of MCM2$^+$ cells within activated Nestin$^+$ clones in qNSC.

Conclusions

Here, we prospectively identified and isolated quiescent adult NSCs by defining a combination of markers (CD133, GFAP, and EGFR) that allows the simultaneous purification of quiescent and activated populations of stem cell astrocytes from the V-SVZ niche.

The bioinformatic analyses I have performed, including Differential expression, Gene Ontology, and Gene Set Enrichment, highlight that qNSCs and aNSCs have very different transcriptomes. Processes related to cell cycling and the concomitant DNA/protein metabolism

required to support active cycling dominate the aNSC transcriptome. Conversely, qNSCs show enrichment for lipid metabolism and adhesion.

GSEA revealed that both qNSCs and aNSCs are enriched for signaling pathways, indicating that signals from the outside may be important to the maintenance of quiescence. GPCR signaling is especially enriched in qNSCs. While GPCRs modulate many different facets of adult neurogenesis (Doze & Perez, 2013), our findings highlight that they are also key regulators of qNSCs. Strikingly, the S1P ligand, as well as Prostaglandin D2, which we identify in our GPCR screen, inhibits the activation of qNSCs, suggesting that stem cell quiescence is an actively maintained state.

Investigation of genes previously associated with NSCs shows that many are differentially expressed by qNSCs and aNSCs. In fact, exploration of ligand and receptor binding patterns show that qNSCs and aNSCs are engaged in bi-directional regulation. Exploration of important pro-neural and neurogenic V-SVZ transcription factors shows a similar pattern of differential expression between the two newly defined stem cell populations, including *Dlx2,* and *Ascl1*. Furthermore, we find that Nestin, which is frequently used as a pan-NSC marker, is restricted to aNSCs. Finally, adhesion molecules show enriched expression in qNSCs, further highlighting that interaction with and maintenance of niche architecture may be essential for quiescence.

This work reveals important molecular features of activated and quiescent NSCs, which importantly highlight overarching biology common to each state and provides a platform to dissect the essential pathways of each. Future functional experiments that manipulate

differentially expressed genes and pathways will be important to fully understand the gene regulatory networks underlying qNSCs and aNSCs.

Methods

FACS Purification Strategy

The SVZs from 2-3 month old heterozygous GFAP::GFP mice (The Jackson Laboratory), which express GFP under the control of the human GFAP (glial fibrillary acidic protein) promoter (Zhuo, 1997), and wild-type CD-1 mice (Charles River Laboratories) were dissected, digested with papain (Worthington, 1,200 units per 5 mice, 10 min at 37ºC) in PIPES solution (120 mM NaCl, 5 mM KCl, 50 mM PIPES (SIGMA), 0.6% glucose, 1x Pen/Strep (Gibco) in water, pH adjusted to 7.6) and mechanically dissociated to single cells after adding ovomucoid (Worthington, 0.7 mg per 5 mice) and DNAse (Worthington, 1,000 units per 5 mice). Cells were centrifuged for 10 min at 4ºC without brakes in 22% Percoll (SIGMA) to remove myelin and incubated for 15 min with PE-conjugated rat anti-mCD24 (1:1000; BD Pharmingen), A647-complexed EGF (1:300; Molecular Probes) and biotinylated rat anti-mCD133 (1:300, clone 13A4, eBioscience), washed by centrifugation and incubated for 15 min with PE-Cy7-conjugated streptavidin (1:1000; eBioscience). All stainings and washes were carried out on ice in 1% BSA, 0.1% Glucose HBSS solution. To avoid clumping, cells were passed through a 40-µm filter. To assess cell viability, 4',6-diamidino-2-phenylindole (DAPI; 1:1000; SIGMA) was added to the cells before sorting. All cell populations were isolated in a single sort using a Becton Dickinson FACS Aria II using 13 psi pressure and 100-μm nozzle aperture. Cells were collected in neurosphere medium (details below) without growth factors. Gates were set manually by using control samples (see appendix). Data was analyzed with FlowJo 9.3 data analysis software and displayed using biexponential scaling.

qPCR Analysis

RNA was purified from FACS sorted populations by the miRNeasy kit, which allows the extraction of both large RNA and enriches for smaller RNAs such as miRs (Qiagen). cDNA

was generated using WT- Ovation Pico System (NuGEN). The total SVZ sample consisted of all live cells (all cells shown in Figure 2.1). For qRT-PCR, all reactions were carried out in duplicate on 4 biological replicates using Brilliant III Ultra Fast SYBR Green QPCR Master Mix (Agilent) in a Stratagene Mx3000P machine with an annealing temperature of 60ºC. Data was normalized to GAPDH expression and analyzed by the $2^{-\Delta\Delta Ct}$ method which normalizes expression to both a control sample (here, total SVZ) and a reference gene (GAPDH) (Livak & Schmittgen, 2001). All primers used for qPCR are in Table 2.3.

Table 2.3 qPCR primers used

Gene name	Forward primer	Reverse Primer
Ascl1 (Mash1)	ATGCAGCTACTGTCCAAACG	AACAGTAAGGGGTGGGTGTG
Dll1	CTACTACGGAGAAGGTTG	GTATCCATGTTGGTCATC
Dlx2	GTTGTGAAAGCTGCGACGTA	ACCCCCAAATACCTTGCATT
EGFR	AGGCCGTGAACCACGTCTGC	CACGCACTCCCTGCCTCTGC
GFAP	CTCCGCCAAGCCAAGCACGA	GCGCAGGGACTCCAGATCGC
GFP	TGGCGATGGCCCTGTCCTTTT	AAGGGCAGATTGTGTGGACAGGT
Gapdh	AACTTTGGCATTGTGGAAGG	ACACATTGGGGGTAGGAACA
Lrig1	TGCCAGAGCAAGCACGCTGA	GCCTCTCAGAAGCAGCAAATTCACA
Nestin	GGGCCCAGAGCTTTCCCACG	GGGCATGCACCAGACCCTGTG
Prom1	GCCTCTACCCTGGAAGCAAA	GATGCTGGTGGATGGCTCTT
Sox2	CCCCCTTTTATTTTCCGTAGTT	TCTCAAACTGTGCATAATGGAGT
Vcam-1	AAGAGAACCCAGGTGGAGGT	TCTGCTAATTCCAGCCTCGT

Microarrays

RNA was purified from FACS-sorted populations with the miRNeasy kit (QIAGEN) from three biological replicates. cDNA was synthesized with the NuGen Pico amplification kit and hybridized to Affymetrix MOE430.2 chips by the Collaborative Science Genome Technology Center of New York University Langone Medical Center.

Bioinformatic Analysis of Microarray Data

Normalization, quality control, differential expression, and gene ontology analysis were carried out using Genespring GX 11.

Pre-Analysis Processing

Once all chips were hybridized, raw image data was loaded into Genespring GX 11. The files were then collectively normalized using the MAS5 method, which takes into account miss-matched probes, and has been shown to outperform other methods (Lim et al., 2007). No baseline normalization was taken. Quality control was performed using Principle Component Analysis (PCA). Biological replicates were examined for spatial and regression correlation by this method. All were found to have an r^2 value greater than 0.87 and clustered tightly.

Differential Expression Analysis and Gene Ontology (GO)

Differentially expressed probesets were filtered by average expression level greater than 50 in at least 1 population in the raw data, at least 2-fold differential expression, and corrected p-value less than 0.05 by Benjamini-Hochberg multiple testing correction. GO categories were obtained with p-value less than 0.05.

Gene Set Enrichment Analysis (GSEA)

GSEA sets with FDR (q value) < 0.05 were hand-curated into thematic categories to highlight transcriptional differences between populations. This analysis was carried out with GSEA software from the Broad Institute, using MSigDB v3.0.

Identification of Conserved Transcriptome Features

Gene lists of published quiescence or activation stem cell signatures from other adult tissue compartments were downloaded and then imported into Genespring GX 11. The expression of genes in these lists was then determined for our system using our microarray data.

GPCR screen

FACS-purified qNSCs were plated at 100 cells per well on adherent substrates in the presence of EGF and different GPCR ligands or vehicles for 4 days. At 4 days, their activation as measured by number of $Nestin^+$ clones was quantified.

Chapter 3 miR-17~92 Regulation of Adult Neural Stem Cells

Introduction

In the previous chapter, I showed that the transcriptional states of qNSCs and aNSCs are strikingly different and reflect their differing behaviors. Interestingly, this analysis showed that for some factors, RNA expression precedes protein expression suggesting post-transcriptional regulation (Codega et al., 2014). I hypothesized that microRNAs (miRs) might be a key regulatory step in modulating the transition from quiescence to activation in the V-SVZ. Currently, little is known about how stem cells transition from the quiescent to active state, especially in the adult neural stem cell niche.

miRNAs (miRs) are small non-coding RNAs capable of rapidly modulating cell states through their ability to target hundreds of mRNAs simultaneously at the post-transcriptional level. Recent work has demonstrated the importance of microRNAs in stem cell differentiation and self-renewal, as well as stem cell quiescence (Brett et al., 2011; Zhao et al., 2009; Cheung et al., 2013). However, the role of miRNAs in regulating the transition from quiescence to activation in neural stem cells has not been explored.

In this chapter, I analyze microRNA expression in FACS-purified qNSCs and aNSCs. I identify the miR-17~92 cluster as significantly enriched in aNSCs over qNSCs. I then investigate the functional effect of miR-17~92 in the V-SVZ by conditionally deleting the miR-17~92 cluster *in vitro* and *in vivo*, thereby testing my hypothesis that this miRNA cluster is necessary for activation and proliferation of adult neural stem cells.

Results

microRNA Profiling of Quiescent and Activated Adult Neural Stem Cells

Using the FACS purification strategy outlined in Chapter 2, Codega et al., 2014, and Pastrana et al., 2009, I collected quiescent and activated adult neural stem cells, as well as other astrocytes, transit amplifying cells, and neuroblasts from the V-SVZ (Figure 2.1). RNA containing both mRNA and miRNA fractions was extracted from the purified populations. cDNA libraries made from the resulting RNA were applied to Taqman low-density arrays (TLDAs) in order to survey 384 miRs in parallel (Figure 3.1 top). TLDA expression data was normalized in the Statminer software package. These results were then loaded into the Genespring GX11 analysis suite software (Agilent).

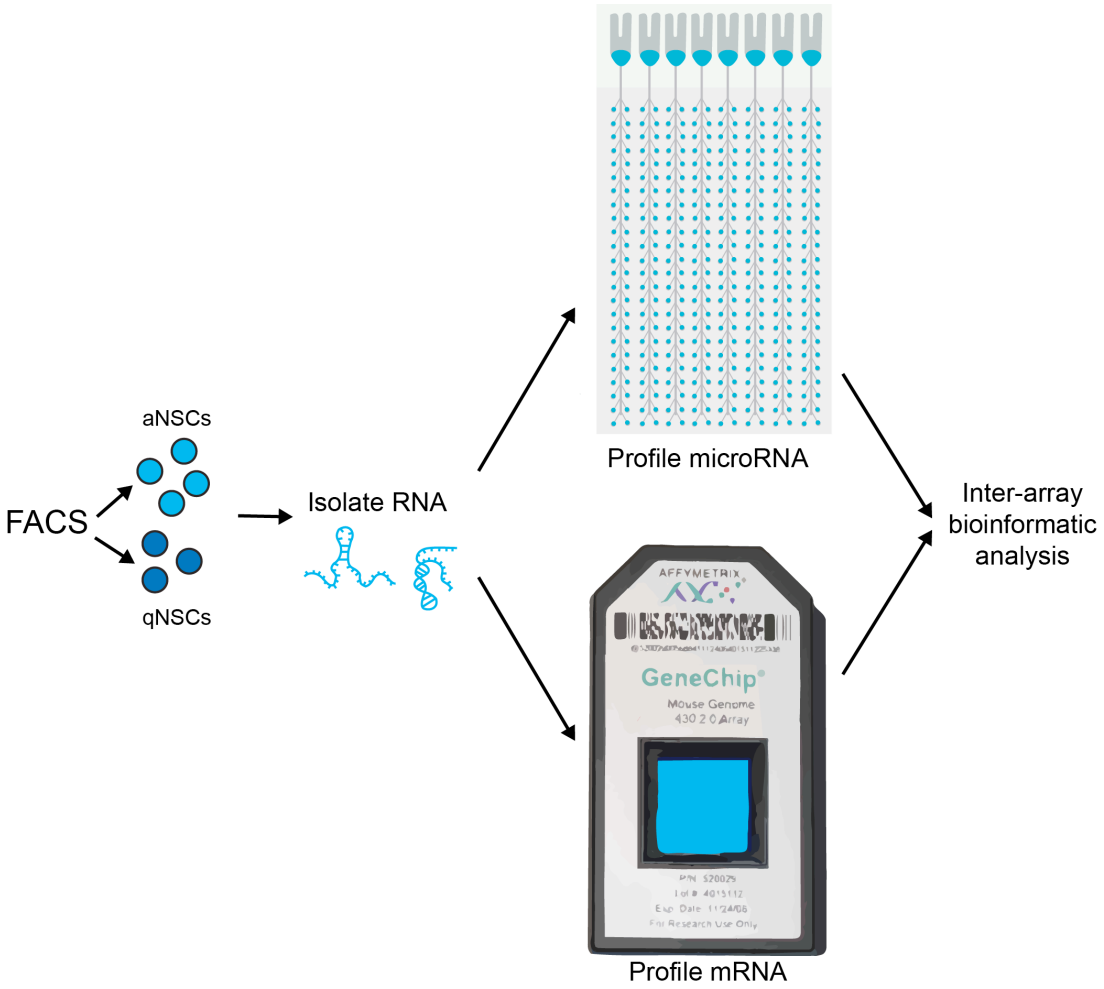

Figure 3.1 ANOVA of miRNA expression and Schematic of the miR-17~92 cluster and paralogs

(A) Schema of experimental paradigm. FACS was used to purify qNSCs and aNSCs. RNA retaining both mRNAs and microRNAs was then isolated. For microRNA profiling, half of the RNA sample underwent a single round of amplification for the TLDA. For mRNA profiling, cDNA was synthesized from the other half of the RNA sample and then hybridized to Affymetrix microarray chips. Splitting the sample in this way allows for the simultaneous analysis of microRNA and mRNA expression.

Using analysis of variance (ANOVA) within the Genespring software, I identified a cohort of miRs with enriched expression in aNSCs (Figure 3.2A) and a second cohort enriched in the qNSCs (Supplemental Figure 1). Interestingly, among the cohort enriched in the aNSCs were four out of the six members of the miR-17~92 cluster, as well as members from the paralogs of miR-17~92; the 106a~363 and 106b~25 clusters (Figure 3.2A-C). To confirm the TLDA

profiles, I performed qPCR for members of the miR-17~92 cluster in V-SVZ cells. In agreement with the arrays, expression of members of the miR-17~92 cluster are enriched in aNSCs and TACs over qNSCs (Figure 3.2D).

The presence of members of the miR-17~92 cluster is exciting, as this cluster is known to play an essential role in promoting proliferation and survival during embryonic development (Ventura et al., 2008). Furthermore, the miR-17~92 cluster is often over- or mis- expressed in malignancies, where these same qualities, so essential for development, enhance tumor progression and growth (Reviewed in Olive et al., 2010; Mogilyansky & Rigoutsos, 2013). Therefore, I chose to focus my work on understanding the role of the miR-17~92 cluster in the adult neural stem cells of the V-SVZ.

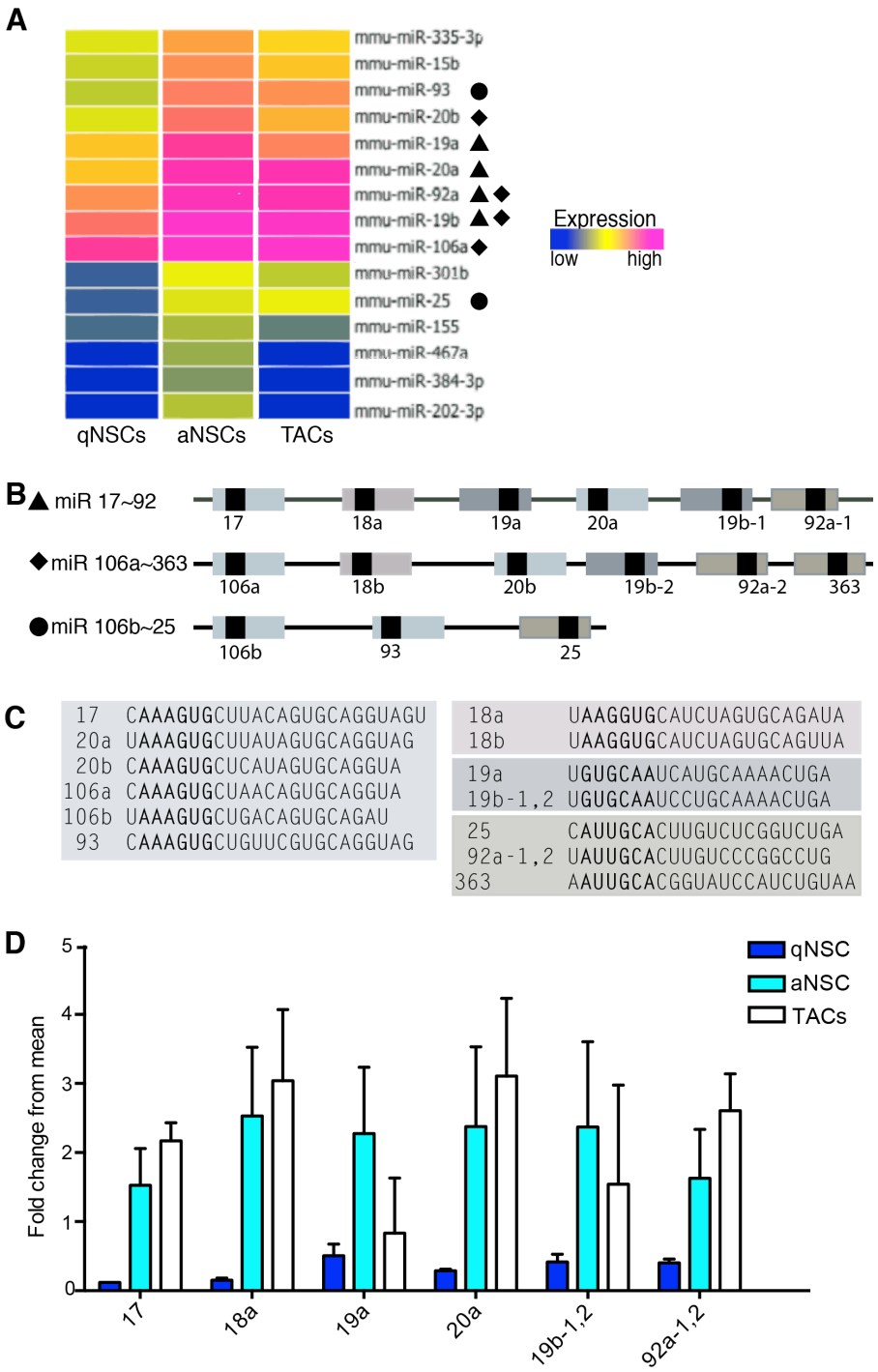

Figure 3.2 The miR-17~92 cluster shows enrichment in aNSCs by qPCR

(A) Analysis of Variance identifies a cohort of miRs enriched in aNSCs. Among these are members of the miR-17~92 cluster (indicated with black triangles) and its paralogs mir-106a~363 (black diamonds) and miR-106b-25 (black circles). The three clusters share a similar order of miRs (B) and sequence homology among the individual miRs (C). Seed sequence conservation is used to group miRs into families, and those miRs encoded in the miR-17~92 cluster and paralogs fall into four families represented but the gray boxes (seed sequence bold) (D) Relative expression of miR-17~92 cluster members normalized to global mean expression.

Development of Tools to Investigate the Role of miR-17~92 in the Adult V-SVZ

To directly probe the role of miR-17~92 in adult neural stem cells, I wanted to combine the powerful ability to purify cells directly from their niche by FACS, with the ability to conditionally manipulate expression levels of miR-17~92 using transgenic mouse lines.

Transgenic Mouse Line

Several conditional mouse lines have been generated that allow the genetic manipulation of miR-17~92 cluster (Ventura et al., 2008; Chen et al., 2013; Feuermann et al., 2012; Marrone et al., 2014; Mu et al., 2009). To be able to investigate the role of the miR-17~92 cluster in adult FACS-purified V-SVZ stem cells, I generated CAGG-CreERT2$^{+/-}$; miR-17~92$^{fl/fl}$; ROSA $^{(ACTB\text{-}tdTomato,\text{-}EGFP+/+)}$ mice by breeding CAGG-CreERT2$^{+/-}$; miR-17~92$^{fl/fl}$ (Ventura et al., 2008) with ROSA $^{(ACTB\text{-}tdTomato,\text{-}EGFP+/+)}$ mice (Muzumdar et al., 2007). Upon the addition of hydroxytamoxifen (4OHT), a ubiquitously expressed CreERT2 induces deletion of the miR-17~92 cluster, as well as causing the reporter locus to switch from expression of the tdTomato reporter to eGFP (enhanced GFP, Figure 3.3) allowing cells that have undergone recombination to be readily identified.

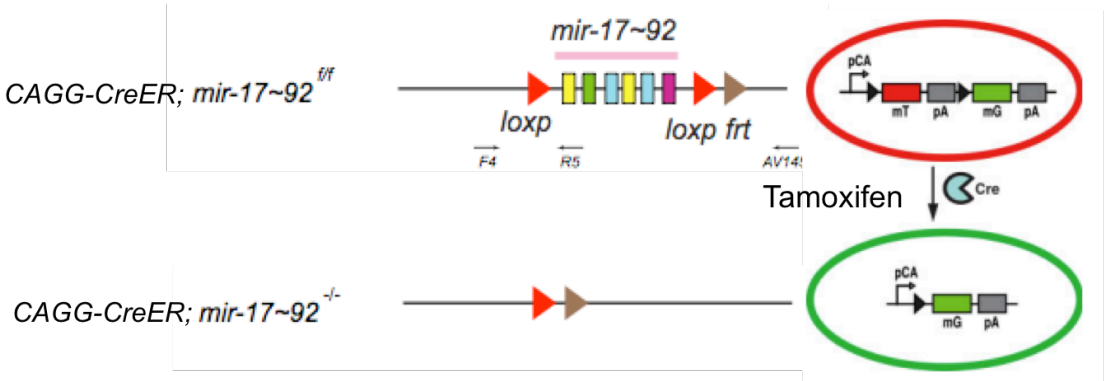

Figure 3.3 Recombination system for miR-17~92 *in vitro* functional analysis

Schema adapted from Ventura et al., 2008 and Muzumdar et al., 2007 showing genetic loci before Cre-mediated recombination (top) and after Cre-recombination (bottom).

FACS Strategy

In order to purify qNSCs and aNSCs from the CAGG-CreERT2$^{+/-}$; miR-17~92$^{fl/fl}$; ROSA$^{(ACTB\text{-}tdTomato,\text{-}EGFP+/+)}$ mice, I first adapted the sorting strategy described in Chapter 2 and (Codega et al., 2014) (hereafter referred to as the "Astro-sort"), which relies on the presence of the GFAP::GFP locus. The new strategy used hereafter will be referred to as the "Wild-type sort".

For the wild-type sort strategy, CD24-FITC, EGF ligand-Alexa647, and CD133-PE-Cy7 antibodies were used. Forward and side scatter were used to exclude cellular debris (Figure 3.4A), and then doublets were excluded (Figure 3.4B). To exclude any dead cells, only DAPI-negative single cells were collected (Figure 3.4C). Next, tdTomato^{+} cells were selected (Figure 3.4D) to ensure that only cells expressing the reporter locus were collected, thereby allowing tracking of recombination in downstream applications. From tdTomato^{+} cells, two gates were defined for aNSCs and qNSCs, both of which exclude FITC positive cells (Figure 3.4E). The FITC-exclusion serves two purposes: first, as eGFP expression occurs after recombination, removing FITC^{+} cells ensures that none of the cells collected have already recombined, a possibility due to the fact that even when present only as a single copy, CAGG-CreERT2 can sometimes activate aberrantly (Figure 3.4G and H). Secondly, CD24^{+} cells were also FITC labeled, and so neuroblasts and ependymal cells were excluded (Calaora et al., 1996). To isolate an aNSC-like population (hereafter referred to aNSC+ due to the possible inclusion of some TACs) that were used for all experiments, FITC^{-}EGF-Alexa647^{+} cells (Figure 3.4E) were gated on EGF-Alexa647 and CD133-PE-Cy7 expression to define the FITC^{-}EGF-Alexa647^{+}CD133-PE-Cy7^{+} population (Figure 3.4I). To isolate a qNSC-like population, FITC^{-}EGF-Alexa647^{-} cells were selected (Figure 3.4E) and then gated based on expression of CD133-PE-Cy7 to define a population of FITC^{-}EGF-Alexa647^{-}CD133^{+} cells (Figure 3.4F). In all experiments, the CreERT2^{-}

population was used for control due to the leaky nature of CreERT2 activation, an example of which can be seen in Figure 3.4G and H.

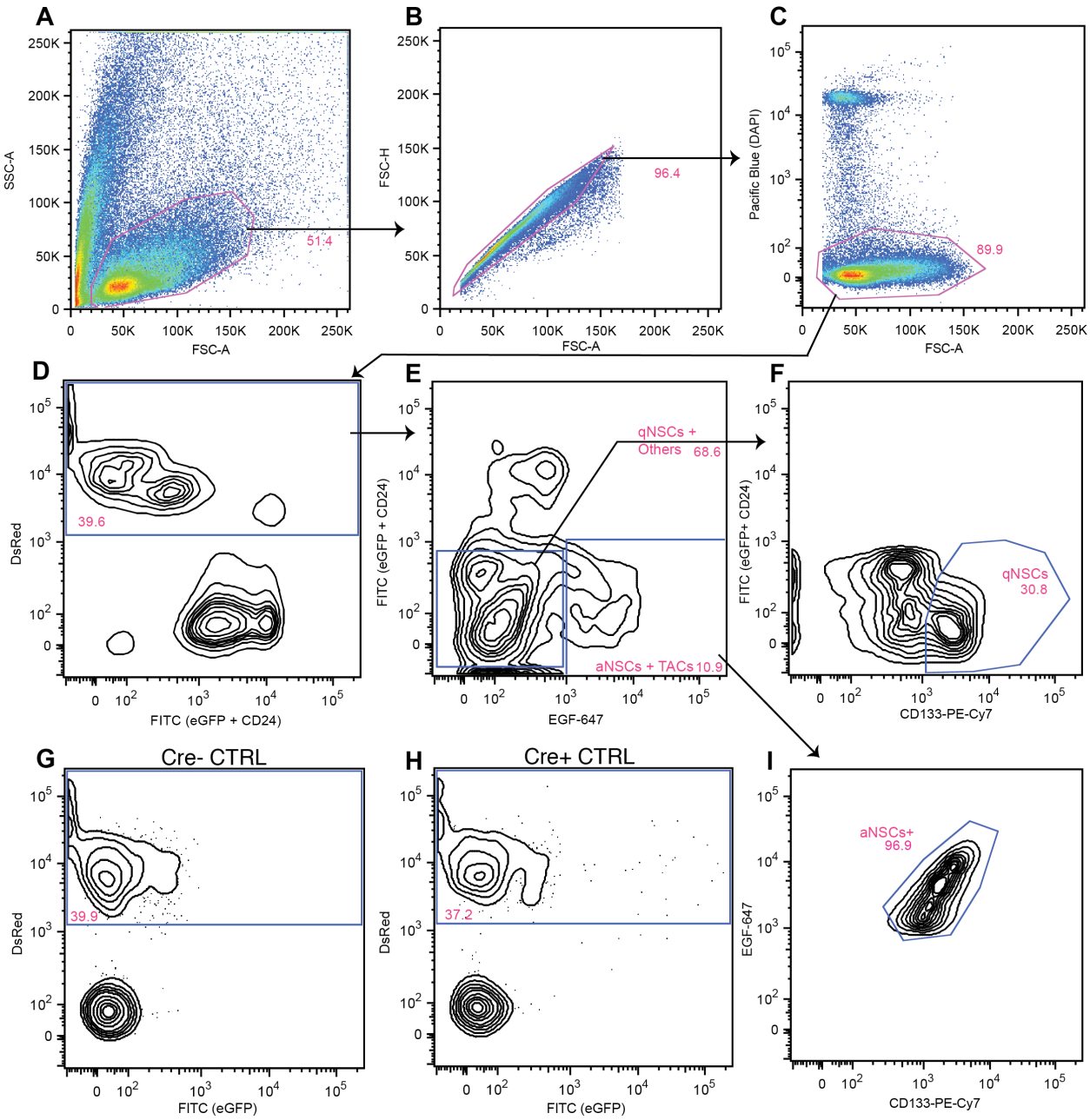

Figure 3.4 Wild-type Sort gating strategy

(A-I) FACS plot flow chart of the 5 color strategy used for sorting and analyzing V-SVZ astrocyte subpopulations using DAPI, CD24-FITC, EGF-A647 and CD133-PE-Cy7 in CAGG-CreERT2$^{+/-}$ or $^{-/-}$; miR-17~92$^{fl/fl}$; ROSA (ACTB-tdTomato,-EGFP$^{+/+}$) mice. (A) Exclusion of cell debris (A), (B) gating to exclude doublets and (C) gating for live DAPI negative single cells. (D) Gating on Tomato expression (E) Gating on FITC expression to exclude already recombined cells and neuroblasts. From this population, two sub-populations could be derived (F) FITC^{-} EGF^{-}CD133^{+} and (I) FITC^{-}EGF^{+}CD133^{+}. (G) CreERT2^{-} control (H) CreERT2^{+} control. Percentages and Astro-sort population being captured are labeled in pink.

Comparison of the neurosphere formation rates for the aNSC+ population collected from the wild-type and the aNSCs from Astro-sort (reviewed in Pastrana et al., 2011) showed no significant differences (Figure 3.5). This sorting strategy therefore provides an aNSC+ population from mice that do not express GFAP::GFP, and can be used for experiments in which the miR-17~92 locus can be inducibly deleted.

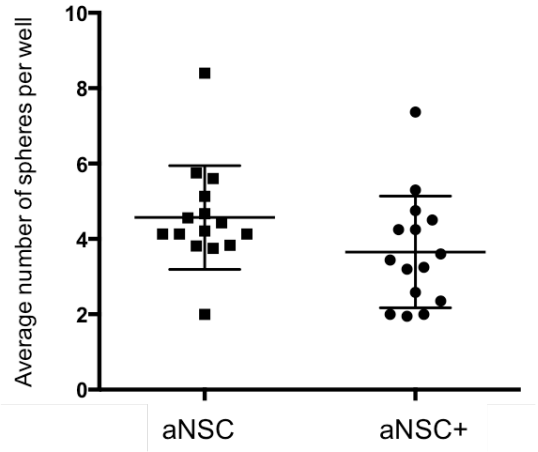

Figure 3.5 Comparison of Neurosphere formation by activated neural stem cells cells from Astro- or wild type sorts

(Left) Sphere formation for aNSCs purified by the Astro-sort method; rate is 4.57% ± 1.38. (Right) Sphere formation for aNSCs+ isolated by the Wild-type sort method; rate is 3.65 ± 1.48. No significant change is observed. $p = 0.55$ $N \geq 14$ from 4 biological replicates.

Validation of miR-17~92 Deletion

Although miR-17~92 is efficiently deleted after addition of tamoxifen in CAGG-CreERT2$^{+/-}$; miR-17~92$^{fl/fl}$ mice (Ventura et al., 2008; Chen et al., 2011), I wanted to confirm that aNSC+ cells were able to delete miR-17~92 with the added ROSA $^{(ACTB\text{-}tdTomato,\text{-}EGFP+/+)}$ reporter.

FACS-purified aNSC+ cells were expanded in EGF for 5 days before recombination was induced with the addition of 4OHT, in order to have enough material to test deletion efficiency (Figure 3.6A). After tamoxifen treatment, cells were cultured for an additional 5 days.

At 5 days after tamoxifen treatment, cells were FACS-purified to separate non-recombined cells (tomato$^+$ only) from recombined cells (either GFP$^+$ only [both reporter loci recombined] or GFP$^+$Tomato$^+$ [only one reporter locus recombined, appear yellow]) (Figure 3.6A). Recombination of the miR-17~92 locus was then assessed at the genomic level as well as for loss of mature miRs after deletion. Preliminary assays for genetic recombination revealed that the miR-17~92 locus was more efficiently recombined than the ROSA$^{(ACTB\text{-}tdTomato,\text{-}EGFP+/+)}$ reporter, as recombined cells, which included cells in which only one reporter allele recombined, were completely negative for the miR-17~92 locus (Figure 3.6B).

To assess microRNA levels after genetic recombination of the miR-17~92 locus, qPCR was used to determine miR-17 expression as a proxy for the expression of other cluster members (Figure 3.6A). Preliminary data shows that recombined cells exhibited a significant reduction in miR-17 expression (Figure 3.6C, green and yellow striped bar) as compared to non-recombined cells that were either CreERT2$^-$ or CreERT2$^+$ (Figure 3.6C, dark red and red bar respectively). As above, more efficient recombination was observed for miR-17~92 than for the reporter locus, as Cre$^+$Tomato$^+$ cells had lower levels of miR-17 than Cre$^-$Tomato$^+$ control cells. Therefore, for all subsequent experiments, Cre$^-$ populations were used as controls.

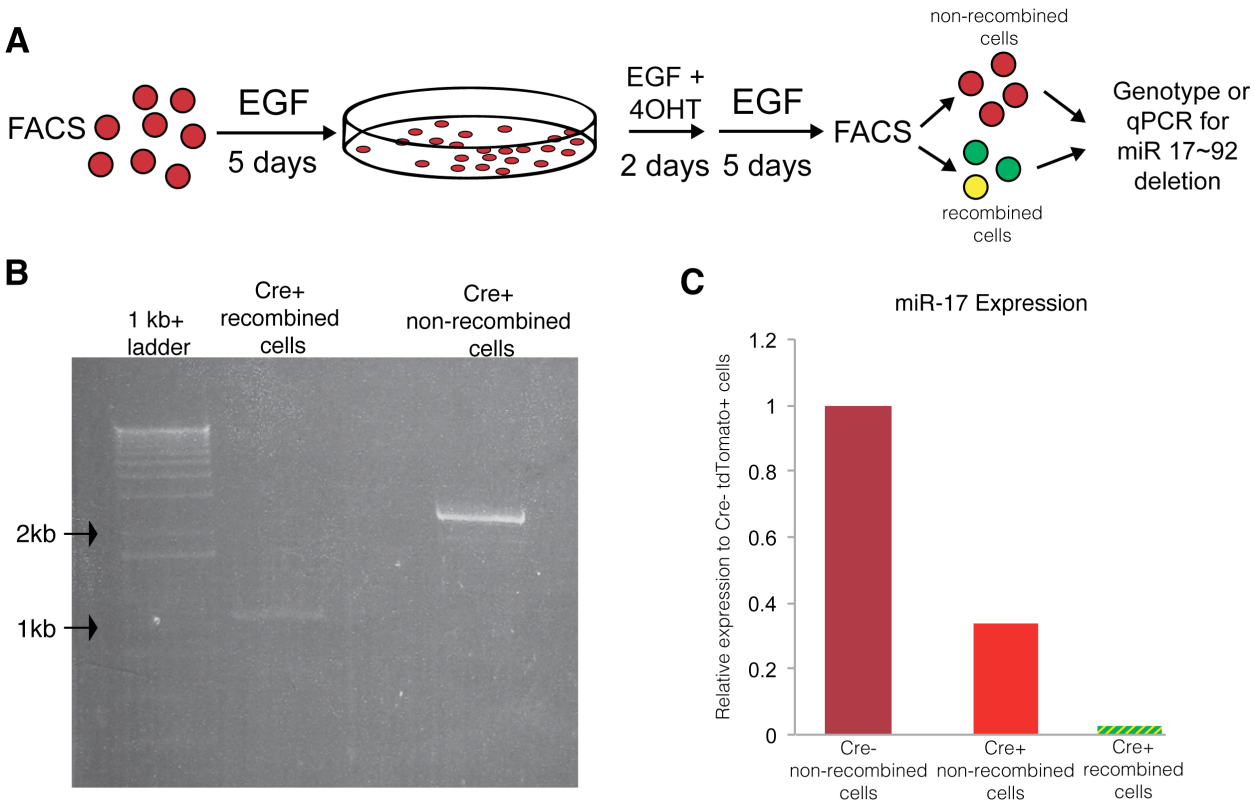

Figure 3.6 Verification of miR-17~92 deletion by PCR and qPCR

(A) Schema of miR-17~92 deletion verification assays. Red cells indicate that no recombination at the reporter locus has occurred (non-recombined), while yellow indicates that a single reporter locus has recombined and cells are expressing both tomato and eGFP protein. Both yellow cells and GFP+ cells were collected as recombined cells. (B) PCR results from genetic deletion assay. A band of 2.5kb indicates an intact miR-17~92 locus, while a band of 1.2kb indicates that the miR-17~92 locus has been deleted (n=1). (C) qPCR results showing relative abundance of miR-17 in non-recombined Cre- (dark red) and Cre+ (red) or recombined cells (green and yellow striped bar) (n=1).

miR-17~92 Deletion *In Vitro*

miR-17~92 Deletion Impairs Adult NSC Activation, Proliferation, and Self-Renewal

To assess the functional effect of deleting miR-17~92 in aNSCs, I first used *in vitro* assays where I could directly quantify the effect on activation, proliferation and self-renewal. I first tested the ability of FACS-purified aNSCs to give rise to neurospheres upon deletion of miR-17~92. FACS-purified aNSCs+ were plated in EGF, EGF and 4OHT, or EGF and vehicle

(ethanol, EtOH) for 24 hours to induce recombination. Five days after recombination, the number of neurospheres that formed was quantified (Figure 3.7A).

Strikingly, miR-17~92 deletion had a dramatic effect on the ability of activated adult neural stem cells to form neurospheres; only 27% as many neurospheres were formed when miR-17~92 was deleted (Figure 3.7E, $p < 0.025$), and those spheres were visibly smaller than their wild-type counter parts (Figure 3.7B-D). Therefore, miR-17~92 deletion reduces recruitment of aNSCs to form neurospheres, and reduces their ability to proliferate.

To test the self-renewal capacity of these cells *in vitro,* I performed sphere passaging by enzymatic and physical dissociation of existing spheres into a single cell suspension, which was then re-plated to assess the cells' continuing ability to form spheres. Notably, the cells from miR-17~92 deleted spheres were never able to form secondary spheres, whereas their counterparts with wild-type miR-17~92 expression always did (data not shown).

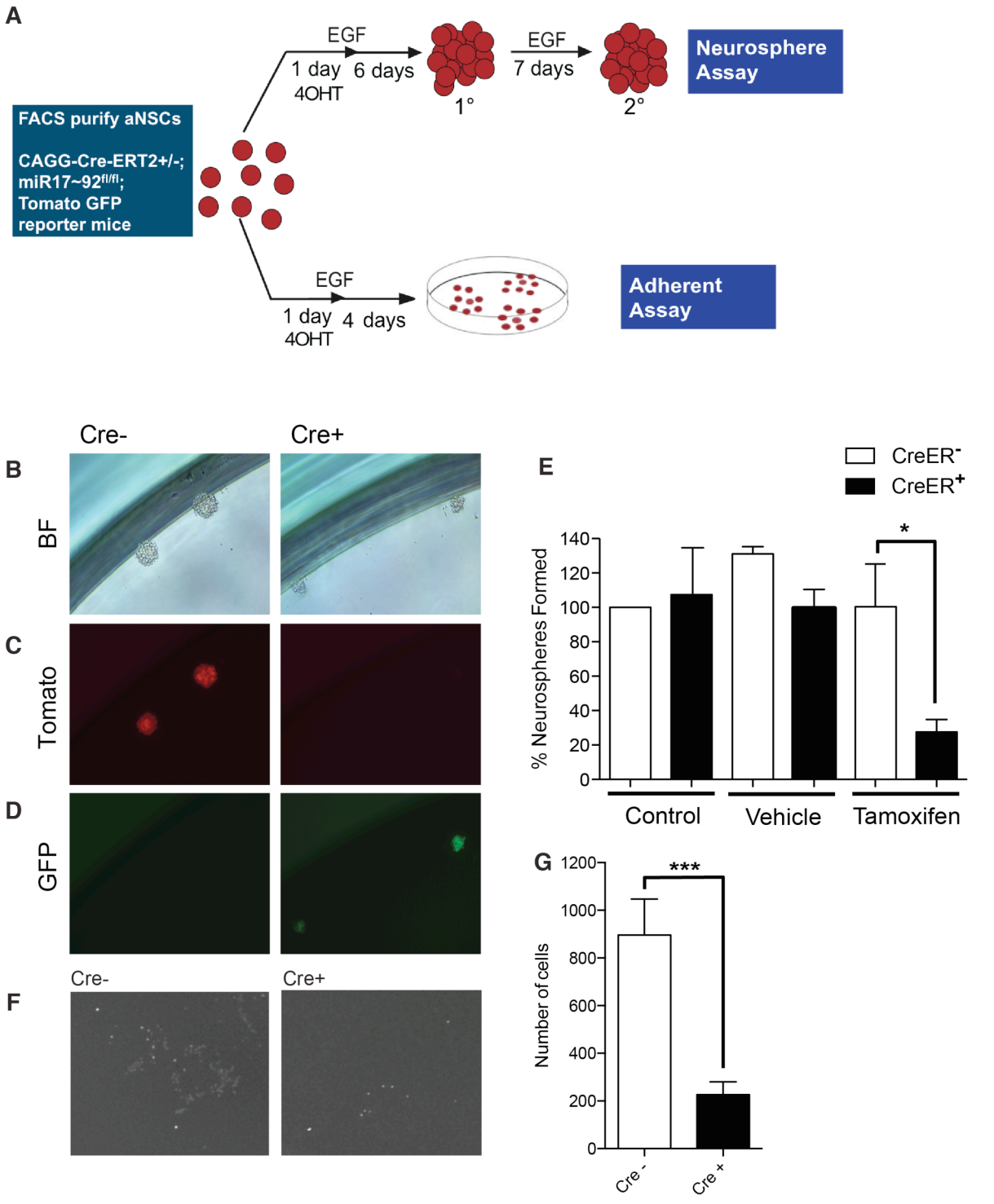

Figure 3.7 Assessing the effects of 17~92 deletion *in vitro*

(A) Schematic of Neurosphere and adherent assays (B-D) Sphere formation for CreERT2$^-$ (Cre$^-$) miR-17~92$^+$ cells (left column) and Cre$^+$ miR-17~92$^-$ cells (right column) (B) bright field (C) Tomato (D) GFP (E) Quantification of neurospheres formed, *$p < 0.025$. (F) Colonies formed in adherent conditions by Cre$^-$ miR-17~92$^+$ cells (left) and by Cre$^+$ miR-17~92 deleted cells (right). (G) Quantification of total cells in each condition at day 5, ***$p < 0.005$.

To more accurately assess the effect of miR-17~92 deletion on aNSC+ proliferation, I used adherent assays. This assay uses adherent substrates to cause cells to grow as a monolayer, which greatly facilitates their quantification (Figure 3.7F). In the adherent condition, cells continued to show a deficit in proliferation when miR-17~92 was deleted; only 25% as many cells were present five days after plating (Figure 3.7G, $p < 0.01$).

miR 17~92 and Survival

The miR 17~92 cluster is known to promote cell survival via suppression of pro-apoptotic factors such as Bim and Pten (Ventura et al., 2008; Xiao et al., 2008; Koralov et al., 2008; Olive et al., 2009; Tung et al., 2015). To determine whether at least part of the activation and proliferation effects shown above might be due to a deficit in cell survival of aNSCs, cells were plated under adherent conditions. Unlike the above assays, after recombination cells were incubated in media without EGF in order to minimize the effects of activation and proliferation.

To visualize changes in survival, cells were stained with Annexin V conjugated to Alexa647, which binds to phosphatidylserine, allowing visualization of apoptotic cells from the earliest to latest stages of apoptosis (vanEngeland et al., 1996). Cells were then fixed and stained with DAPI to visualize intact nuclei (Figure 3.8A). I then counted $DAPI^+$ cells and recorded their co-expression of Tomato, eGFP, and Annexin V. Despite only being exposed to EGF for 24 hours, there were differences in the sizes of colonies formed by $CreER^-$ and $CreER^+$ cells. Regardless of size, colonies were always Annexin V^-. Therefore, I counted each colony as a single clone rather than counting all of the individual cells within it, allowing me to assess survival independent of differences in proliferative capacity.

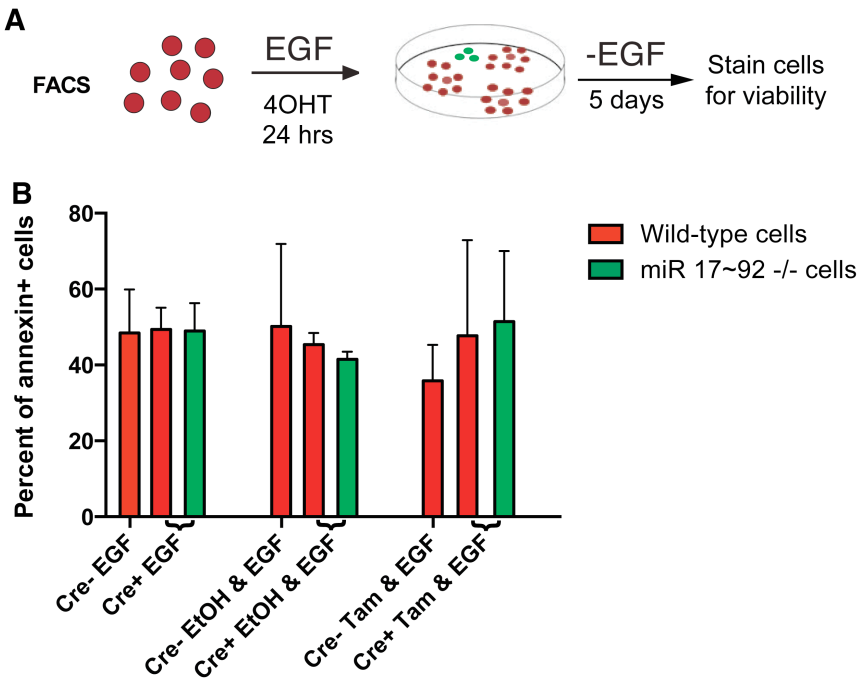

Figure 3.8 miR-17~92 and survival

(A) Schema of survival assay. (B) Normalized percentages of cells positive for annexin V- Alexa647. First bar (red) is the normalized percentage of Cre^{-}miR-17~92^{+}AnnexinV^{+} cells, second bar (red) is normalized percent of Cre^{+}miR-17~92^{+}Annexin V^{+} cells, third bar (green) is normalized percentage of Cre^{+}miR-17~92^{-}Annexin V^{+} cells. (N=2).

Although the pro-survival properties of the miR-17~92 cluster have been demonstrated for other systems, in V-SVZ stem cells, miR-17~92 does not have a significant effect on cell survival for the first five days after the cluster is deleted (Figure 3.8B, $p < 0.6$, n=2). However, this finding does not preclude the possibility that miR-17~92 loss may affect survival of neural stem cells or their progeny at other stages.

miR-17~92 is Necessary for Robust Neurogenesis

The role of miR-17~92 in differentiation is beginning to be understood; several studies have reported that miR-17~92 is down-regulated during the differentiation process for many cell and cancer types (Beveridge et al., 2009; Westermark et al. 2011; Mogilyansky & Rigoutsos, 2013). Recent work has shown that expression of the miR-17~92 cluster promotes neurogenesis

in embryonic stem cells, and that overexpression delays the temporal switch to gliogenic competence (Naka-Kaneda et al., 2014). The ability to promote neurogenesis in adult neural progenitors has also been shown for the miR-17~92 paralog, miR 106b~25 (Brett et al., 2011).

To establish the effect of miR-17~92 deletion on differentiation, FACS-purified aNSCs+ were first plated and expanded in EGF alone for five days to circumvent the effect of miR-17~92 on activation and proliferation described above. At five days, 4OHT was added for 48 hours to induce recombination. Following recombination, cells were allowed to differentiate for 7 days in the absence of EGF, following which differentiation into neurons, astrocytes, and oligodendrocytes was quantified. All conditions were stained with DAPI to visualize nuclei. I stained the cells with O4 (a marker of oligodendrocytes), GFAP (a marker of astrocytes), or TuJ1 (a marker of neurons). I then quantified $DAPI^+$ cells for expression of tdTomato, eGFP, and either GFAP, O4, or TuJ1 (Figure 3.9A).

Strikingly, miR-17~$92^{-/-}$ cells ($CreERT2^+eGFP^+$) only generated about 25% as many neurons as their miR-17~92^+ counterparts ($CreERT2^-tdTomato^+$ cells) (Figure 3.9H-J, $p < 0.039$), while astrocyte and oligodendrocyte formation was not significantly affected (Figure 3.9B-G). Therefore, miR-17~92 cluster deletion selectively decreases the amount of neurogenesis *in vitro,* but does not affect astrocyte or oligodendrocyte formation, although these studies do not rule out a selective effect of miR-17~92 on neuronal survival.

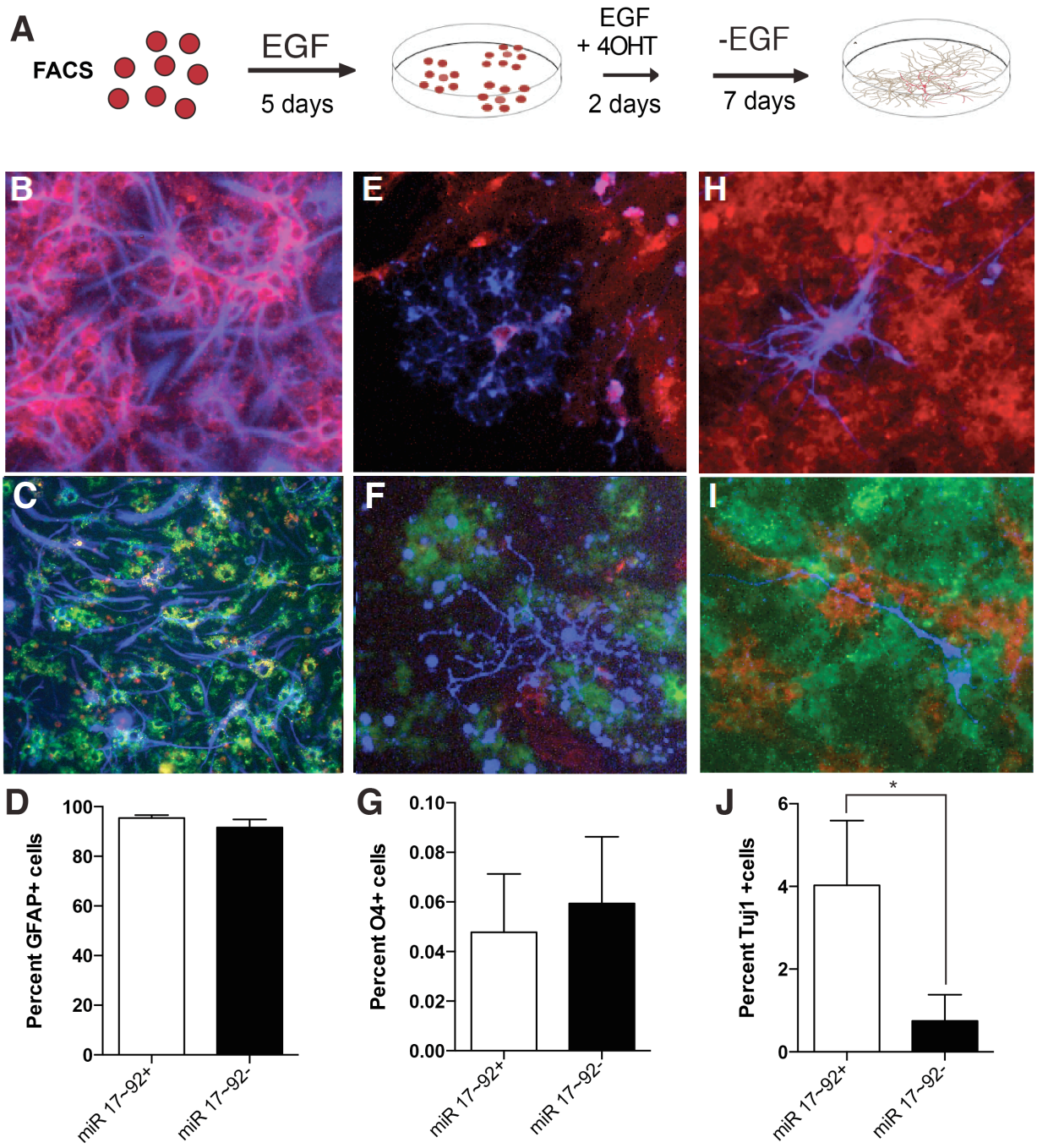

Figure 3.9 miR-17~92 deletion alters neurogenesis *in vitro*

(A) Schema of differentiation experiment timeline. Seven days after recombination, (B –C) GFAP$^+$ astrocytes (blue) are made by both miR-17~92 $^+$ (B, red) and miR-17~92$^-$ (C, green) cells and the amount of astrocytes made by each is the same (D). (E-F) O4$^+$ oligodendrocytes (blue) are made by both miR-17~92$^+$ (E, red) and miR-17~92$^-$ (F, green) cells and the amount of oligodendrocytes made by each is the same (G). TuJ1$^+$ neurons (blue) are made by both miR-17~92$^+$ (H, red) and miR-17~92$^-$ (I, green) cells, although the amount of neurons made are reduced when miR-17~92 is deleted (J, n=3, $p < 0.039$).

miR-17~92 Deletion *In Vivo*

In the first part of this chapter, I found that loss of the miR-17~92 cluster results in a lack of activation, proliferation, and neurogenesis *in vitro*. I then wanted to understand whether the same effects would occur when miR-17~92 was deleted *in vivo*. In order to selectively look at the effect of miR 17~92 cluster deletion on V-SVZ stem cells, which are GFAP^{+}, I generated a new line of mice in which GFAP-CreERT2 is used to drive recombination. The mice possess miR-17~92 $^{+/+}$ or $^{fl/fl}$ loci and the R26R lslTomato$^{+/+}$ reporter. In these mice, tamoxifen treatment induces Cre activity only in cells expressing GFAP. These cells then either have no change to the miR-17~92 locus, or homozygously delete it. In all mice, CreERT2 expression drives expression of the Tomato protein by removal of a stop codon, which allows tracking of cells in which recombination has occurred (Figure 3.10).

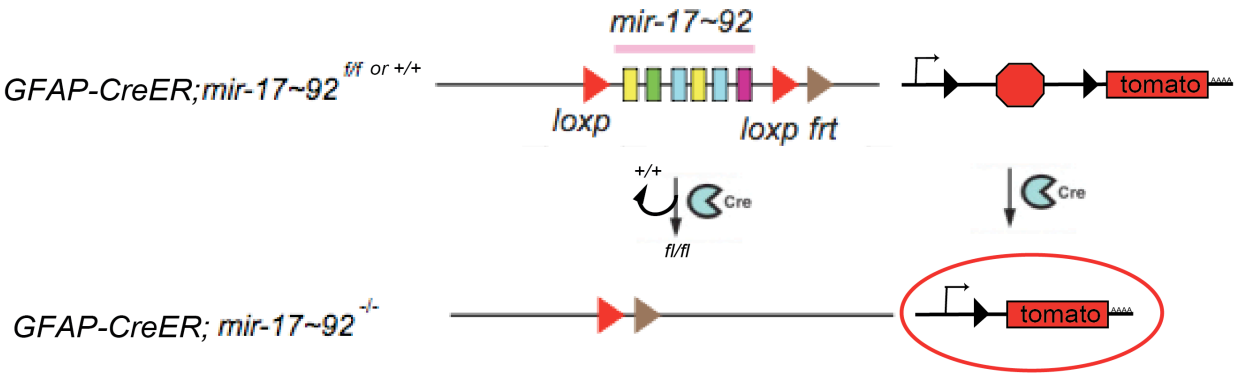

Figure 3.10 Schema of miR-17~92 recombination strategy in vivo

Top- miR-17~92 $^{fl/fl}$ mice and $^{+/+}$ mice before recombination by GFAP-driven CreERT2. After recombination, $^{+/+}$ retain the miR-17~92 locus, while the $^{fl/fl}$ mice lose it (Bottom). Both types of mice recombine out the stop codon encoded before the Tomato protein and become Tomato positive (Bottom right).

Young adult mice aged 2-4 months, were interperotineally injected with tamoxifen once a day for three days to induce recombination. Thirty days after induction of recombination, brains were sectioned and immunostained with GFAP (a marker of V-SVZ astrocytes), mini-

chromosome maintenance protein 2 (MCM2, a marker of dividing cells), or Doublecortin (DCX, a marker of neuroblasts and newly generated neurons) (Figure 3.12A). To quantify changes in marker expression among recombined cells, the V-SVZ was imaged in z-stacks at 4 positions; the outermost lateral edge (OE), central wedge (W), most ventral edge (B), and halfway between the ventral edge and central wedge (C) (Figure 3.11).

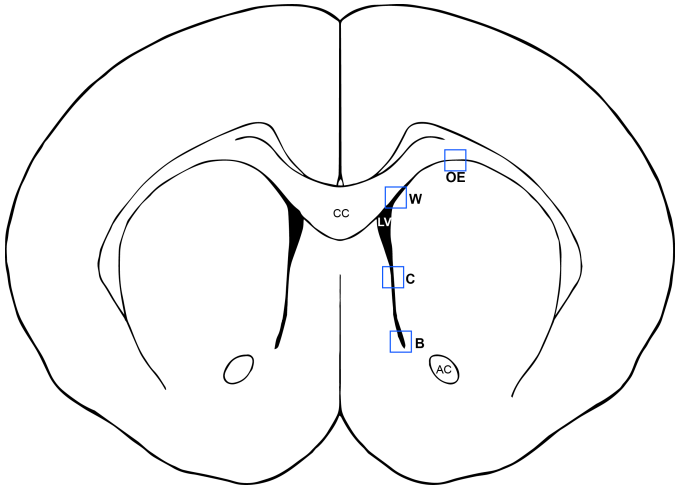

Figure 3.11 Schema of *in vivo* imaging

Anatomy: CC- corpus callosum, LV – lateral ventricle AC—anterior commissure. Imaging areas indicated by blue boxes: OE – outer lateral edge of the V-SVZ. W– the wedge of the V-SVZ where the dorsal and lateral walls meet. C – Center of the dorsal ventral axis of the V-SVZ. B – the bottom of the V-SVZ or most ventral edge.

I counted Tomato$^+$ cells and their co-expression with GFAP (Figure 3.12B-C, green), MCM2 (Figure 3.12B-C, blue), or DCX (Figure 3.12G-H, blue). Interestingly, there is a 32% increase in the proportion of Tomato$^+$GFAP$^+$ cells (Figure 3.12B-C, yellow) in mice that have lost the miR-17~92 locus (Figure 3.12D, $p < 0.008$), and a concomitant 60% decrease in the proportion of Tomato$^+$MCM2$^+$ (Figure 3.12B-C and E, purple, $p < 0.0125$). Importantly, the proportion of Tomato$^+$DCX$^+$ cells was reduced by almost 50% when miR-17~92 was deleted (Figure 3.12F-H, purple, $p < 0.0001$). Together, these data indicate that loss of miR-17~92 leads to a decrease in proliferation in GFAP-derived cells, and furthermore significantly reduces neurogenesis *in vivo*.

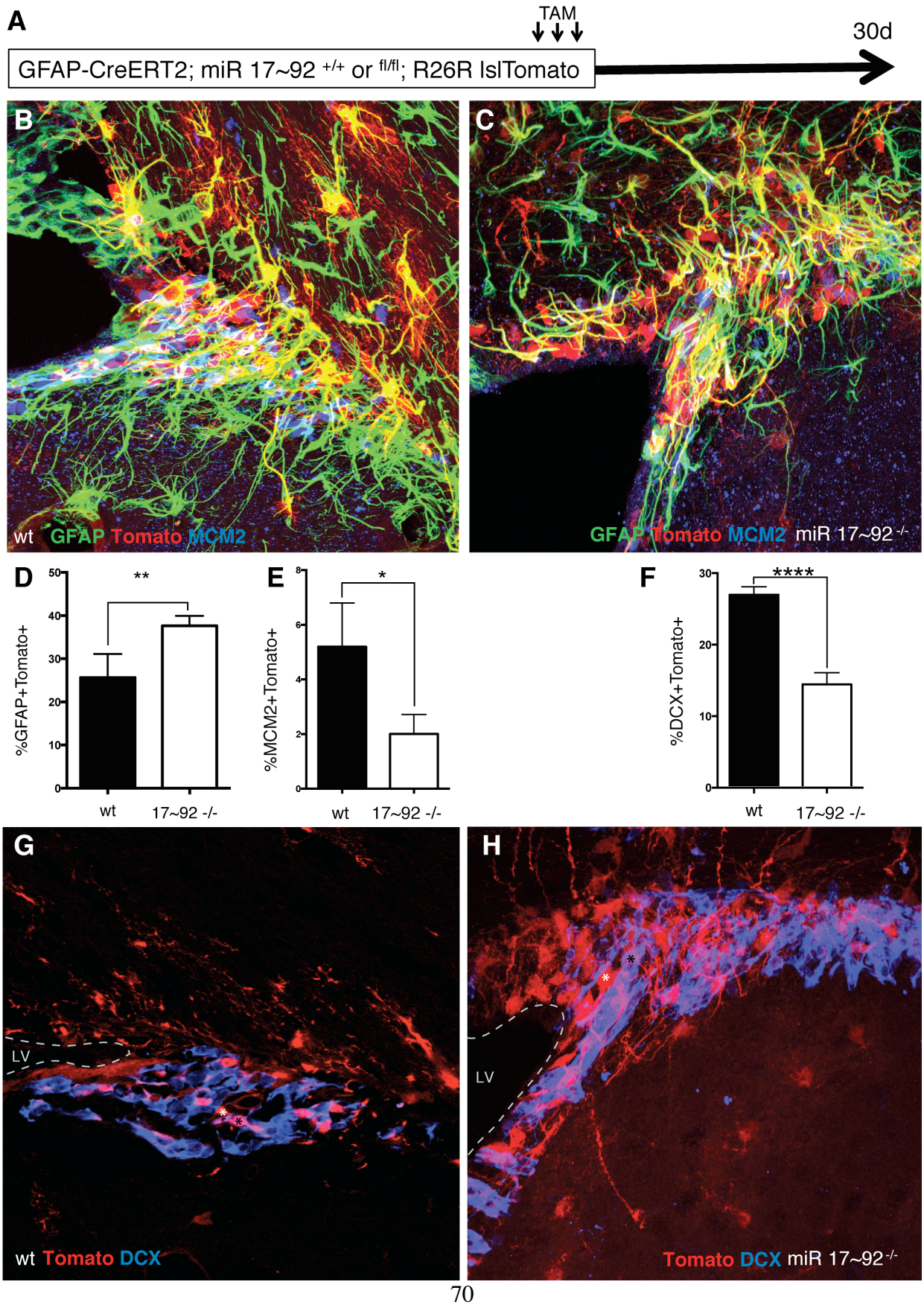
A
TAM
30d
GFAP-CreERT2; miR 17~92 +/+ or fl/fl; R26R lslTomato
B
wt GFAP Tomato MCM2
C
GFAP Tomato MCM2 miR 17~92 -/-
D
%GFAP+Tomato+
**
wt
17~92 -/-
E
%MCM2+Tomato+
*
wt
17~92 -/-
F
%DCX+Tomato+
****
wt
17~92 -/-
G
LV
wt Tomato DCX
H
LV
Tomato DCX miR 17~92 -/-

Figure 3.12 Effects of miR 17~92 deletion *in vivo*

(A) Schema of miR 17~92 deletion in vivo. (B) Wild-type coronal section stained for GFAP (green) and MCM2 (blue). (C) miR-17~92$^{-/-}$ brain section stained with GFAP (green) and MCM2 (blue). (D) Quantification of Tomato^{+}GFAP^{+} cells. (E) Quantification of Tomato^{+}MCM2^{+} cells. (F) Quantification of Tomato^{+}DCX^{+} cells. (G) Wedge area of wild-type brain section stained for DCX (blue). (H) Wedge area of miR-17~92$^{-/-}$ brain section stained for DCX (blue). White asterisks indicate DCX^{-} cells, while black asterisks indicate DCX^{+} cells. For all images, recombined cells are Tomato^{+}.

Conclusions

In this chapter, I have shown that miR-17~92 is enriched in aNSCs. By FACS purifying aNSCs from conditional miR-17~92 deletion mice, I have demonstrated that this cluster is responsible for most of the *in vitro* activation and proliferation activity exhibited by aNSCs. Importantly, my work shows, for the first time, that this miR cluster is involved in proliferation and activation at the stem cell level in the adult brain. Notably, this model showed that the miR-17~92 cluster is not involved in aNSC survival at early time points after deletion. Finally, loss of the miR-17~92 cluster leads to a decrease in neurogenesis, but does not affect astrocyte or oligodendrocyte generation *in vitro*.

After selective deletion of miR-17~92 in GFAP^{+} V-SVZ stem cells *in vivo*, there was a notable increase in the proportion of GFAP^{+} cells while there was a concomitant decrease in the number of MCM2^{+} cells, indicating that there is an increase in the number of non-dividing GFAP^{+} V-SVZ astrocytes. Furthermore, I showed that miR-17~92 also leads to decreased levels of neurogenesis. I will follow up these studies with immunostaining for mature neuron markers in the olfactory bulb to confirm that fewer neurons are made *in vivo*. Further studies are needed to determine if miR-17~92$^{-/-}$ cells are largely quiescent or differentiating prematurely into astrocytes via immunostaining with S100β, a marker of mature astrocytes. Given the continued radial morphology of cells in which miR-17~92 has been deleted, I predict that there will be no

change in the number of S100β positive cells, and that instead the proportion of quiescent stem cells will have increased.

In the next chapter, I will explore potential targets of the miR-17~92 cluster that may mediate quiescence and have to be downregulated in order for miR-17~92 to have its pro-activation and proliferation effects.

Methods

RNA Collection for Profiling and Validation Experiments

qNSCs, aNSCs and transit amplifying cells were purified from GFAP::GFP mice and processed into cDNA as outlined in Chapter 2 and Codega et al., 2014.

miRNA Profiling

RNA was extracted using the miRNeasy kit (Qiagen). cDNA was synthesized using the WT-Ovation Pico System (NuGEN). cDNA was applied to Taqman low-density arrays as specified by the manufacturer at the Collaborative Science Genome Technology Center of New York University Langone Medical Center.

Raw data from at least three replicates per cell type was then loaded into the Statminer program where several control RNAs were identified and used to normalize the dataset. Genespring GX 11 was used to analyze the normalized dataset and identify differentially expressed miRs by analysis of variance (ANOVA).

qPCR Validation

RNA from FACS-purified populations was extracted for a miR-rich fragment using the miRNeasy kit as described in Codega et al., 2014. miR-rich cDNA was then created using the Exiqon miRCURY LNA Universal RT microRNA kit. qPCR for the six members of the miR-17~92 cluster was then run using Exiqon miRCURY LNA probes for the mature forms of the miRs, in accordance with the LNA probes.

Mice Breeding and Usage for miR-17~92 *In Vitro* Deletion Experiments

CAGG-CreERT2$^{+/-}$; miR-17~92$^{fl/fl}$ mice were a generous gift from Jun-An Chen of the Wichterle lab. These were then bred to ROSA $^{(ACTB\text{-}tdTomato,\text{-}EGFP+/+)}$ mice to generate CAGG-CreERT2$^{+/-}$ or $^{-/-}$;

miR-17~92$^{fl/fl}$; ROSA $^{(ACTB\text{-}tdTomato,\text{-}EGFP+/+)}$ mice. These mice express tdTomato before recombination, and eGFP afterwards, allowing tracking of recombination.

Sort Strategy and *in vitro* assays

CAGG-CreERT2$^{+/-}$ or $^{-/-}$; miR-17~92$^{fl/fl}$; ROSA $^{(ACTB\text{-}tdTomato,\text{-}EGFP+/+)}$ mice were processed for FACs as in Codega et al. and stained with CD24-FITC (1:1000; BD Pharmingen), EGF-Alexa647 (1:300; Molecular Probes), and biotinylated rat anti-mCD133 (1:300, clone 13A4, eBioscience), which was followed by secondary staining with PE-Cy7-conjugated streptavidin (1:1000; eBioscience).

For all *in vitro* assays, FACS-purified aNSC+ cells were purified from young adult mice aged 2-4 months.

Neurosphere Assay

For the neurosphere assay, aNSC+ cells were plated at a density of 100 cells per well in 96-well low-attachment plates (Costar). Cells were grown in Neurosphere medium (NSM), composed of DMEM/F12 (Life Technologies) supplemented with 0.6% Glucose (Sigma), 1x Hepes (Life Technologies), 1x Insulin-Selenium-Transferrin (Life Technologies), N-2 (Life Technologies), and B-27 supplement (Life Technologies) in the presence of 20 ng/ml EGF (Upstate). For the first 24 hours immediately after plating, cells were also treated with 500nM hydroxytamoxifen (4OHT, Sigma) or vehicle (500nM ethanol, EtOH). At 24 hours, half of the media was replaced with NSM & EGF to reduce toxicity. The cells were then monitored every 2 days for sphere formation and recombination.

Neurosphere Passaging

At 7 days post-plating, the total content of each well was collected and dissociated with 3 mg (600 units) of papain for 10 min at 37°C. The reaction was stopped by adding ovomucoid

inhibitor (Worthington, 0.7 mg). DNAse (Worthington, 0.5 mg) was added and cells dissociated to single cells by pipetting. The resulting cells were then re-plated at a density of 100 live cells per well (as determined by trypan blue staining). This plating was then monitored for the formation of secondary spheres every two days.

Adherent Assay

This assay was used to monitor activation, proliferation, survival, deletion, and differentiation. 96-well plates were coated with poly-D-lysine (Sigma, 10 µg/ml) and Fibronectin (Sigma, 2 µg/ml). Cells were then plated at a density of 100 cells per well. For activation/proliferation during the first 24 hours after plating, cells were treated with NSM & EGF, NSM & EGF & 250nM 4OHT, or NSM & EGF & 250nM vehicle (EtOH). At 24 hours, the entire media was replaced with NSM & EGF to prevent toxicity. Wells were imaged at 5 days post plating with DAPI to visualize cells present and recombination rates as shown by tdTomato or eGFP positivity.

Survival Assay

For survival assays, during the first 24 hours after plating, cells in NSM were treated with NSM & EGF, NSM & EGF & 250nM 4OHT, or NSM & EGF & 250nM vehicle (EtOH). At 24 hours the media was replaced with NSM alone for 5 days, at which point cells were stained with Annexin V-Alexa647 (1:500, Life Technologies), fixed for 30 minutes with 3.2% PFA, and stained for DAPI (1:1000, SIGMA). The wells were imaged on the ZEISS Observer 7.1 at 5x. $DAPI^{+}$ cells were quantified for co-expression with Tomato, eGFP, and Annexin V using the cell counter plugin for FIJI.

Deletion Assay

To confirm deletion of the miR-17~92 cluster, after plating cells were grown in NSM & EGF for five days, then the entire media was replaced with NSM & EGF, NSM & EGF & 250nM 4OHT,

or NSM & EGF & 250nM vehicle (EtOH) for two days to induce recombination. At 7 days post-plating, cells were given NSM & EGF for 5 days to allow recombined cells to further expand. At 5 days post-recombination, cells were collected for sorting; they were first treated with Trypsin for 5 minutes at 37°C, then treated with NSM to stop the trypsin reaction. The cells were then dissociated into single cells by pipetting and passed through a 40-μm filter. DAPI was added prior to FACS to remove dead cells. Cells were then gated by their expression of tdTomato and eGFP. DNA was extracted using a specialized digestion buffer, provided by Chyuan-Sheng (Victor) Lin of the Columbia University Transgenic Core Facility. Deletion of the miR-17~92 locus was verified using the primers in Table 3.1

Table 3.1 miR-17~92 deletion primers

17~92 deletion forward	17~92 deletion reverse
TCGAGTATCTGACAATGTGG	TAGCCAGAAGTTCCAAATTGG

A band of ~2kb indicates an intact locus, whereas a band of ~1kb indicates deletion of miR-17~92. To verify the loss of mature miR expression, RNA was extracted from sorted cells using the Exiqon miRCURY RNA extraction kit, and expression of mature miRs assayed by qPCR using the Exiqon probe for miR-17 as described above.

Differentiation Assay

For differentiation assays, after the initial five-day expansion with EGF and two days of recombination as performed for the deletion assay, cells were cultured with NSM only for 7 days to induce differentiation. Cells were then live stained with mouse IgM anti-O4 (1:500, Chemicon) for 30 minutes, fixed as above, and stained overnight with rat anti-GFAP (1:500,

Invitrogen) or mouse anti-βIII Tubulin (TuJ1, 1:500, Covance). All post-fix staining was performed in PBS with 10% normal goat or donkey serum and 0.5% Triton X-100. Secondary antibodies were used at 1:500 (Alexa fluor-conjugated, Molecular Probes). Prior to imaging cells were incubated for 5 minutes in DAPI. Images were then hand counted for the co-expression of DAPI with tdTomato, eGFP, and either O4, GFAP, or TuJ1.

Mice Breeding and Usage for miR-17~92 Deletion *In Vivo*

CAGG-CreERT2$^{-/-}$; miR-17~92$^{fl/fl}$; ROSA $^{(ACTB\text{-}tdTomato,\text{-}EGFP\ -/-)}$ mice were then crossed to GFAP-CreERT2$^{+/-}$ mice and R26R lslTomato$^{+/+}$ mice to generate GFAP-CreERT2$^{+/-}$; miR-17~92$^{+/+}$ or $^{fl/fl}$; R26R lslTomato$^{+/+}$ mice.

Experimental Paradigm for In Vivo miR-17~92 Deletion

To induce deletion of the miR-17~92 cluster, young adult GFAP-CreERT2$^{+/-}$; miR-17~92$^{+/+}$ or $^{fl/fl}$; R26R lslTomato$^{+/+}$ mice aged 2-4 months were intraperitoneally injected once every 24 hours over the course of three days with 0.1 mL of 30uM tamoxifen (Tam) in 90% sunflower seed oil, 10% EtOH. After a 30-day chase, mice were transcardially perfused with saline and 3.2% PFA. Brains were then removed and placed in 3.2% PFA overnight at 4°C. 30-50μM thick sections were cut using a vibratome (Leica) and immunostained as previously described (Doetsch et al., 2002; Doetsch & Alvarez-Buylla, 1996). Sections were then stained as described above with rat anti-GFAP (1:500, Invitrogen), goat anti-MCM2 (1:100, Santa Cruz Biotechnology), and guinea pig anti-DCX (1:1000, Millipore).

The V-SVZ was imaged on a Zeiss 500 or 800 LSM confocal microscope in z-stacks at 4 positions; the outermost lateral edge, central wedge, most ventral edge, and halfway between the ventral edge and central wedge. Images were quantified in FIJI using the Cell Counter plug-in to count each stack continuously.

Chapter 4 mRNA Targets of the miR-17~92 Cluster

Introduction

In Chapter 3, I show that the miR-17~92 cluster is important for adult neural stem cell activation, proliferation, and neurogenesis. The function and mode of action for microRNAs is largely dependent on the mRNAs available for targeting, i.e. the context of their expression. To identify potential targets of miR-17~92, I used databases of computationally predicted miRNA targets in combination with the high dimensional data sets for mRNAs and miRNAs (described in Chapter 2 and Chapter 3). I identified three interesting potential targets: Mycn, Lrig1 and S1pr1. In this chapter, I perform expression analyses to show that *Mycn, Lrig1,* and *S1pr1* are expressed in V-SVZ stem cells, and focus on the functional interaction between miR-17~92 and S1PR1 in the adult V-SVZ.

Results

Computational Identification of miR-17~92 mRNA Targets, Including S1PR1

microRNAs repress gene expression at a post-transcriptional level through two mechanisms: translational repression or mRNA decay, with mRNA decay being the dominant mode in mammals (reviewed in Li & Rana, 2014). In the mRNA decay mechanism, not only is there a reduction in the final gene product, i.e. protein, but there is also a measureable decrease in the mRNA present. Therefore, in my search for miR 17~92 cluster targets, I used our microarray data to look for genes which had enriched expression in qNSCs.

First, I identified genes that were common targets for multiple members of the miR-17~92 cluster. To do so, I obtained a list of predicted mRNA targets for each individual member of the 17~92 cluster (miR-17, 18a, 19a, 29a, 19b, and 92a) from the TargetScan 5.2 database (Lewis et al., 2005). I then cross-referenced these lists to find genes that were targeted by two or more miRs.

Interestingly, one of the common targets of all six members of the miR-17~92 cluster is *Mycn*/N-myc, which is a known activator of miR-17~92 transcription (Fontana et al., 2008; Schulte et al., 2008). By microarray and qPCR, *Mycn* expression is restricted to the aNSCs (Figure 4.1, green line), while the miR-17~92 cluster continues to be expressed in TACs (Figure 4.1, royal blue lines). This expression pattern suggests that after being activated by N-myc in aNSCs, the miR-17~92 cluster forms a negative feedback loop by suppressing *Mycn,* the results of which may be the observed reduced expression of *Mycn* in TACs. Indeed Cloonan et al. showed that *Mycn* is a direct target of miR-17. Furthermore, N-myc is an immediate-early gene (Kenney et al., 2003), which suggests that N-myc expression induction may be a rapidly-induced first step towards an activated state for aNSCs.

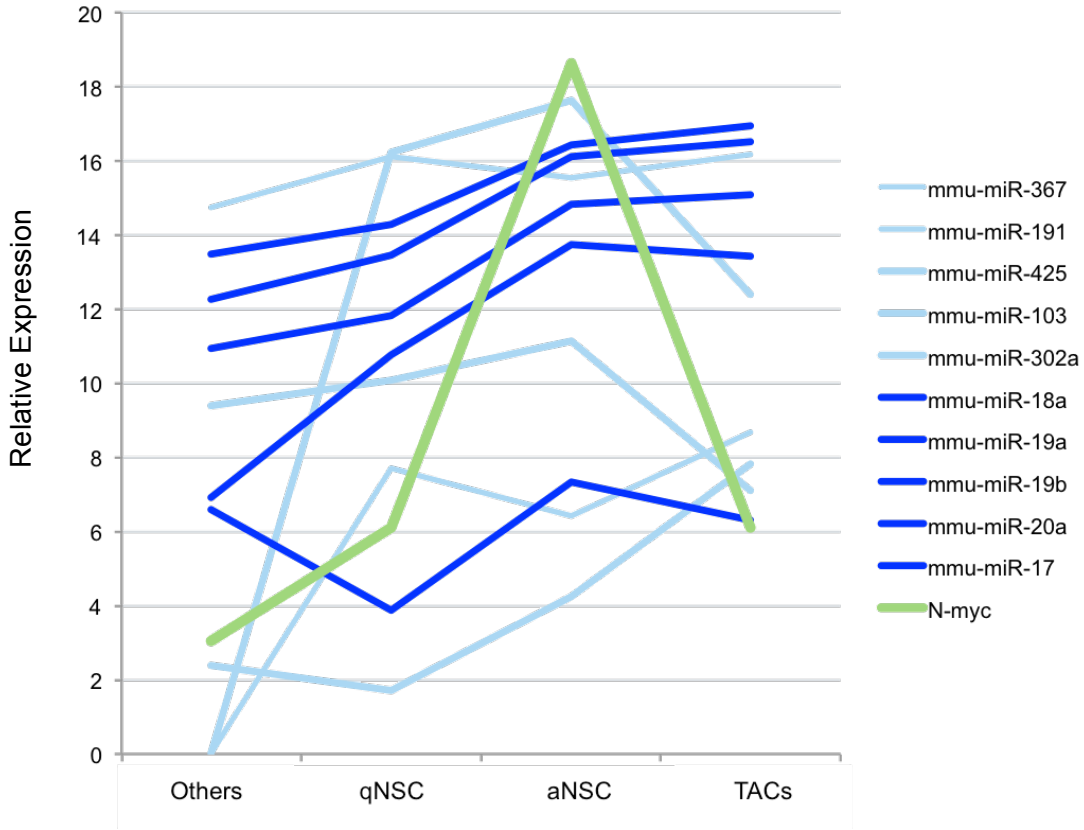

Figure 4.1 Expression of N-myc and its targeting miRNAs

Green- *Mycn* qPCR expression. Royal blue – expression of miR-17~92 cluster members that target *Mycn* by TLDA. All cluster members except for miR-92a are predicted to target *Mycn*. Light blue- expression of other miRs that target *Mycn* by TLDA. N=3.

I next focused my analysis on identifying genes that were targeted by multiple members of the miR-17~92 cluster and showed mRNA enrichment in the qNSCs over aNSCs, as downregulation of these targets might be relevant to achieving an activated or proliferative state. To find such genes, I used Genespring to generate a list of all genes that were targeted by at least two miR-17~92 cluster members and at least two-fold enriched in our qNSC population.

From this analysis, I identified Lrig1, which I had already verified as expressed in our qNSCs by qPCR (Figure 2.6G, Figure 4.2, magenta line). TargetScan predicts it to be targeted by members of the miR-17/20 seed sequence family, as well as by the miR-19 family (Figure 4.2,

royal blue lines). As discussed in Chapter 2, Lrig1 functions to degrade EGFR protein, thereby preventing the cell from receiving EGF signaling (Gur et al., 2004). Therefore, downregulation of Lrig1 expression by the miR-17~92 cluster could be important for activation of qNSCs, as it would allow perdurance of EGFR proteins at the cell surface, and hence increased EGFR signaling. This hypothesis is supported by the fact that EGFR signaling is enriched in aNSCs and is important for maintaining proliferation in the V-SVZ (Figure 2.6, Doetsch et al., 2002). Notably, when I reversed this analysis and examined the expression of miRs predicted to target Lrig1 by our TLDA data, approximately 75% of these miRs are greater than 1.5-fold enriched in aNSCs over qNSCs (Figure 4.2, blue lines). This finding further highlights Lrig1's potential importance to quiescence.

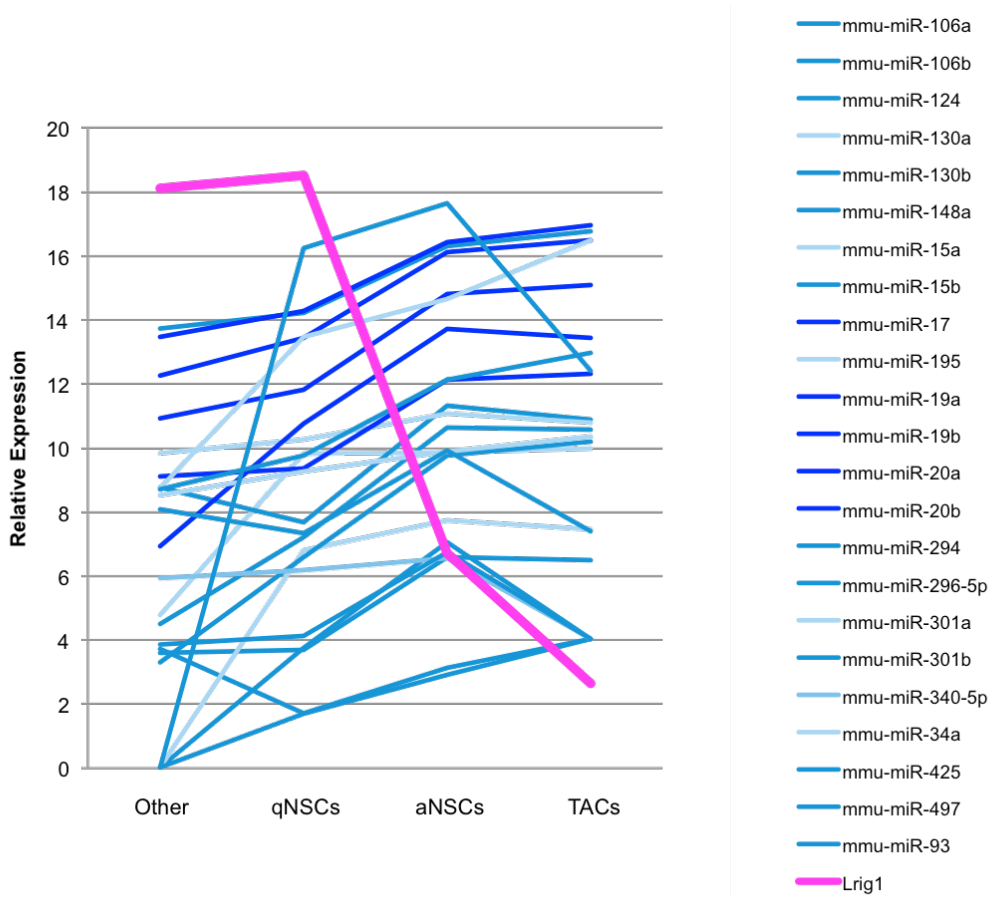

Figure 4.2 Expression of Lrig1 and its targeting miRNAs

Magenta line- Lrig1 expression by qPCR. Royal Blue lines- expression of members of the miR-17~92 cluster predicted to target Lrig1 by TLDA. Medium Blue- miRs with at least 1.5x fold enrichment in aNSCs over qNSCs by TLDA. Light Blue Lines- expression of remaining miRs predicted to target Lrig1 by TLDA. N=3.

The gene set enrichment analysis outlined in Chapter 2 showed that approximately 30% of the sets enriched for signaling in the qNSCs were involved in G-protein coupled receptor signaling, and that some of these had functional effects on the behavior of qNSCs (see Figure 2.10). I was curious as to whether any of the genes identified in these sets were also targets of the miR 17~92 cluster. To determine whether there was overlap between GPCR genes and predicted 17~92 targets, I downloaded individual target lists for each member of the 17~92 cluster (miR-17, 18a, 19a, 29a, 19b, and 92a) from StarBase 2.0 (Yang et al., 2010; Li et al., 2013). I then cross-referenced these lists to the list of GPCR genes upregulated in qNSCs over aNSCs (Table

2.2). Of these, S1pr1 was the top candidate as it had the most miR-17~92 cluster members computationally predicted to target it, and had an 11-fold increase in expression in qNSCs over aNSCs by microarray analysis (Table 4.1). S1PR1 is an especially interesting candidate as treatment of qNSCs with its ligand, S1P, decreased their activation and proliferation (Figure 2.10).

Gene Name	Gene Symbol	Fold Change from aNSC	Targeting 17~92 members
Frizzled 6	Fzd6	18.597136	17, 20
		14.635587	
		11.8910055	
Sphingosine 1 phosphate receptor 1	S1pr1	11.028068	17, 19a, 19b, 20, 92a
Opiate receptor-like 1	Oprl1	7.331031	19a, 19b
G-protein coupled receptor 146	Gpr146	6.4464536	17, 20
		-1.1891292	
Calcitonin receptor-like	Calcrl	18.947807	17, 20
		2.610176	
		-1.5489525	
G-protein coupled receptor 174	Gpr174	1.2402235	17, 20
		-1.520696	

Table 4.1 Identification of potential targets of the 17~92 cluster from among genes involved in G-protein coupled receptors

Shading in the column "Fold change from aNSC" relates to the magnitude of fold change with dark red corresponding to high enrichment in qNSCs and blues indicating enrichment in aNSCs

Although there are five S1P receptors, S1pr1 and S1pr5 are the only members of the family expressed in the qNSC population. Of the two, *S1pr1* has a much higher level of expression in qNSCs than *S1pr5*, suggesting that the effects observed from treatment of qNSCs

with S1P in Chapter 2 might be due almost entirely to S1PR1-mediated signaling (Figure 4.3, fuchsia line vs. dark blue line).

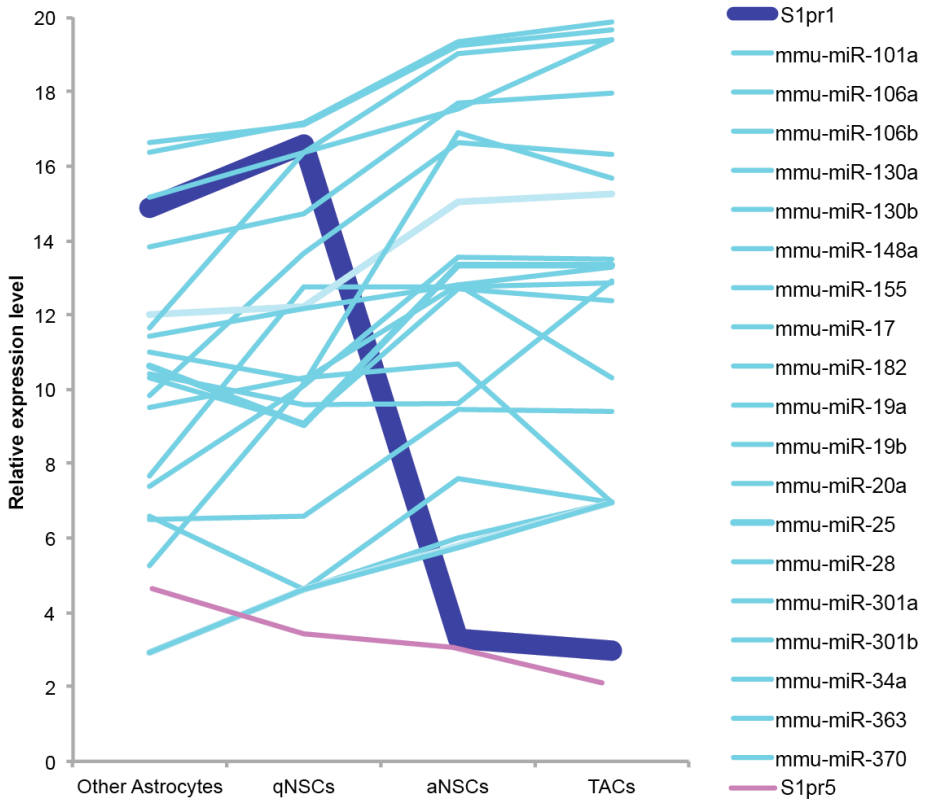

Figure 4.3 microRNAs predicted to target *S1pr1* are upregulated in aNSCs

Dark Blue – microarray expression of S1pr1. Light blue- Expression of miRs predicted to target s1pr1 and also enriched in aNSCs by TLDA. Over 70% of the miRs predicted to target S1pr1 are enriched in aNSCs Pink- Expression of S1pr5 by microarray.

As with Lrig1, I was interested in the expression pattern of other potential miR regulators of S1pr1. Interestingly, over 70% of the miRs computationally predicted to target S1pr1 were upregulated in aNSCs over the qNSCs (Figure 4.3, light blue lines), further highlighting the potential importance of S1pr1 in maintaining quiescence of qNSCs. This possible involvement of S1PR1 in maintaining quiescence suggests a regulatory role for miR-17~92 in mediating the

transition from quiescence to activation by repressing S1PR1 expression. I therefore focused on this miR-17~92 target for further functional studies.

S1pr1 mRNA and Protein Expression in the V-SVZ

I first verified S1pr1 mRNA expression in V-SVZ stem cells by performing qPCR in FACS-purified populations. S1pr1 expression was enriched in qNSCs over aNSCs (Figure 4.4).

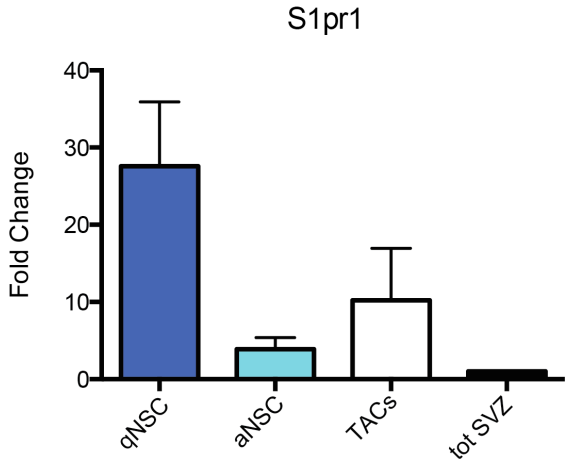

Figure 4.4 S1pr1 mRNA expression by qPCR

S1pr1 mRNA expression was analyzed in indicated cells types by qPCR. Y axis is logarithmic fold change from total SVZ sample, calculated by the $2^{\wedge-\Delta\Delta Ct}$ method. N=3.

I then performed immunostaining for S1PR1 protein in coronal sections of the adult V-SVZ of CD-1 ("wild-type") mice for GFAP, MCM2, and S1PR1, using the same S1PR1 antibody as characterized in Nishimura et al., 2010 and Akiyama et al., 2008. I found that V-SVZ astrocytes, as well as those in the striatum, are S1PR1 positive, which is in accordance with the distribution observed by Akiyama et al., 2008 and Nishimura et al., 2010 (Figure 4.5A-D). Although GFAP co-immunostaining is difficult to quantify, most GFAP-positive cells were also S1PR1$^+$. The vast majority of S1PR1$^+$GFAP$^+$ cells were negative for MCM2 (Figure 4.5E). Moreover, S1PR1 expression regardless of GFAP was largely restricted to non-dividing cells, as

only 1% of all S1PR1 positive cells were also MCM2 positive (Figure 4.5F). Conversely, less than 5% of total $MCM2^+$ cells in the V-SVZ were $S1PR1^+$ (Figure 4.5G).

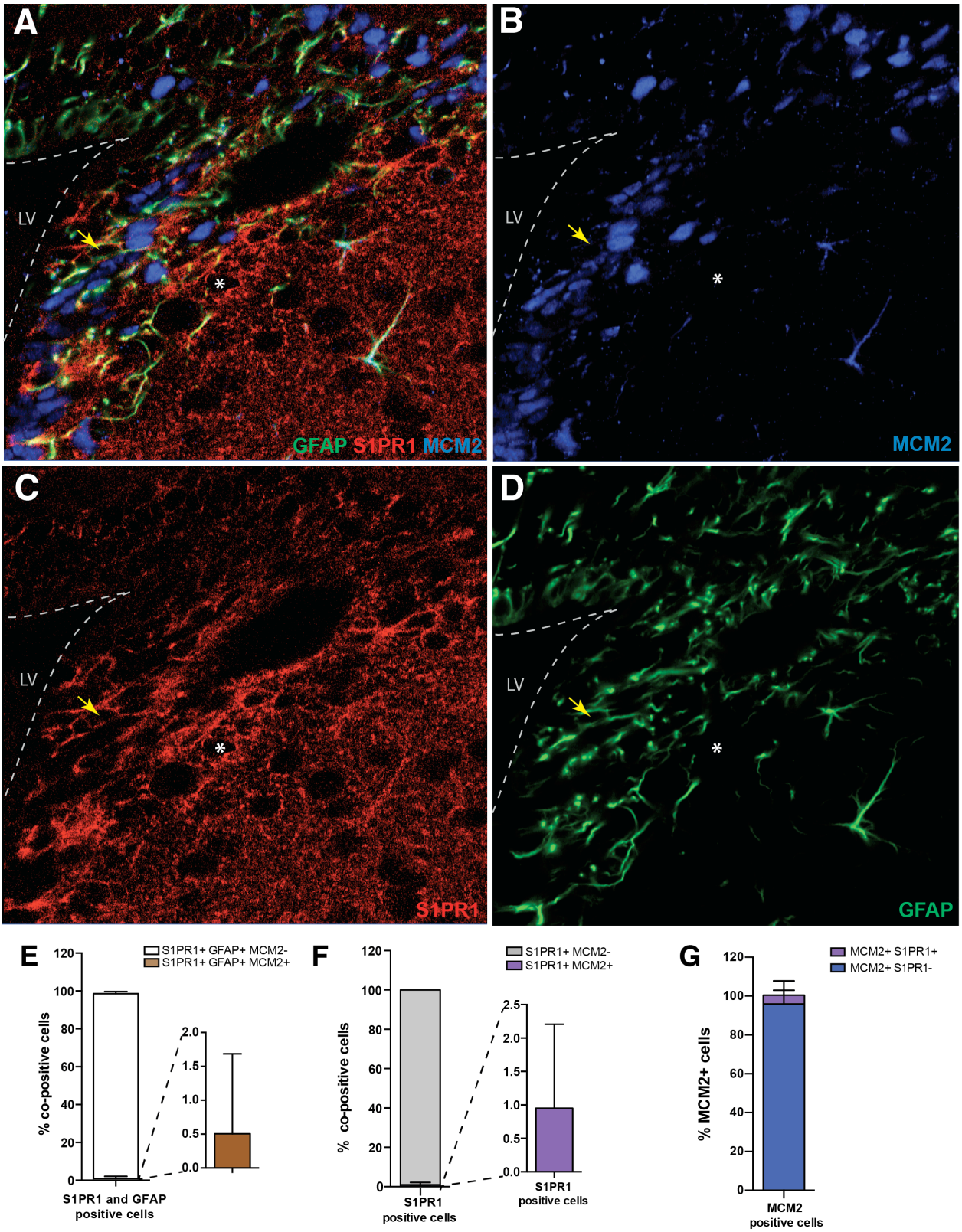
A
LV
*
GFAP S1PR1 MCM2
B
LV
*
MCM2
C
LV
*
S1PR1
D
LV
*
GFAP
E
S1PR1+ GFAP+ MCM2-
S1PR1+ GFAP+ MCM2+
% co-positive cells
120
100
80
60
40
20
0
2.0
1.5
1.0
0.5
0.0
S1PR1 and GFAP
positive cells
F
S1PR1+ MCM2-
S1PR1+ MCM2+
% co-positive cells
120
100
80
60
40
20
0
2.5
2.0
1.5
1.0
0.5
0.0
S1PR1
positive cells
S1PR1
positive cells
G
MCM2+ S1PR1+
MCM2+ S1PR1-
% MCM2+ cells
120
100
80
60
40
20
0
MCM2
positive cells

Figure 4.5 S1PR1 expression in the adult V-SVZ

(A-D) The wedge of the V-SVZ showing expression of MCM2 (blue, B), S1PR1 (Red, C) and GFAP (green, D). merge (A) Yellow arrowheads indicate an example of a double positive cell, white asterisk shows an example of a cell expressing S1PR1 only. (E) Percentage of $GFAP^+$ cells that are S1PR1 positive from all areas. (F) Percentage of S1PR1 positive cells that are $MCM2^+$ (purple) or $MCM2^+$ and $GFAP^+$ (gray). (G) Percentage of $MCM2^+$ cells that are $S1PR1^+$ or $MCM2^+$ only.

To investigate whether S1PR1 was a functional target of miR-17~92, I assessed changes in S1PR1 expression after deletion of miR-17~92 in GFAP-$CreERT2^{+/-}$; miR-17~$92^{+/+}$ or $^{fl/fl}$; R26R $lslTomato^{+/+}$ mice (described in Chapter 3). If S1PR1 is a target of miR-17~92, loss of this cluster should lead to an increase in $MCM2^+$ cells expressing S1PR1 protein. To explore this possibility, mice received interperotineal injections of tamoxifen once a day for three days, followed by a 30-day chase. Brains were then immunostained for S1PR1 (Figure 4.6A and B green), and MCM2 (Figure 4.6A and B, blue). Tomato expression was used to track recombined cells (Figure 4.6A and B, red).

When miR-17~92 was deleted, a greater proportion of $Tomato^+$ cells expressed S1PR1 than their wild-type counterparts (Figure 4.6C, $p < 0.005$). In agreement with earlier MCM2 immunostaining data, in this instance I also observed fewer $Tomato^+MCM2^+$ cells when miR-17~92 was deleted (Figure 4.6D). Strikingly, despite the overall decrease in $Tomato^+MCM2^+$ cells, there was an increase in $Tomato^+MCM2^+S1PR1^+$ cells in the mutant mice, confirming that S1PR1 is normally targeted by miR-17~92 in these cells (Figure 4.6E)

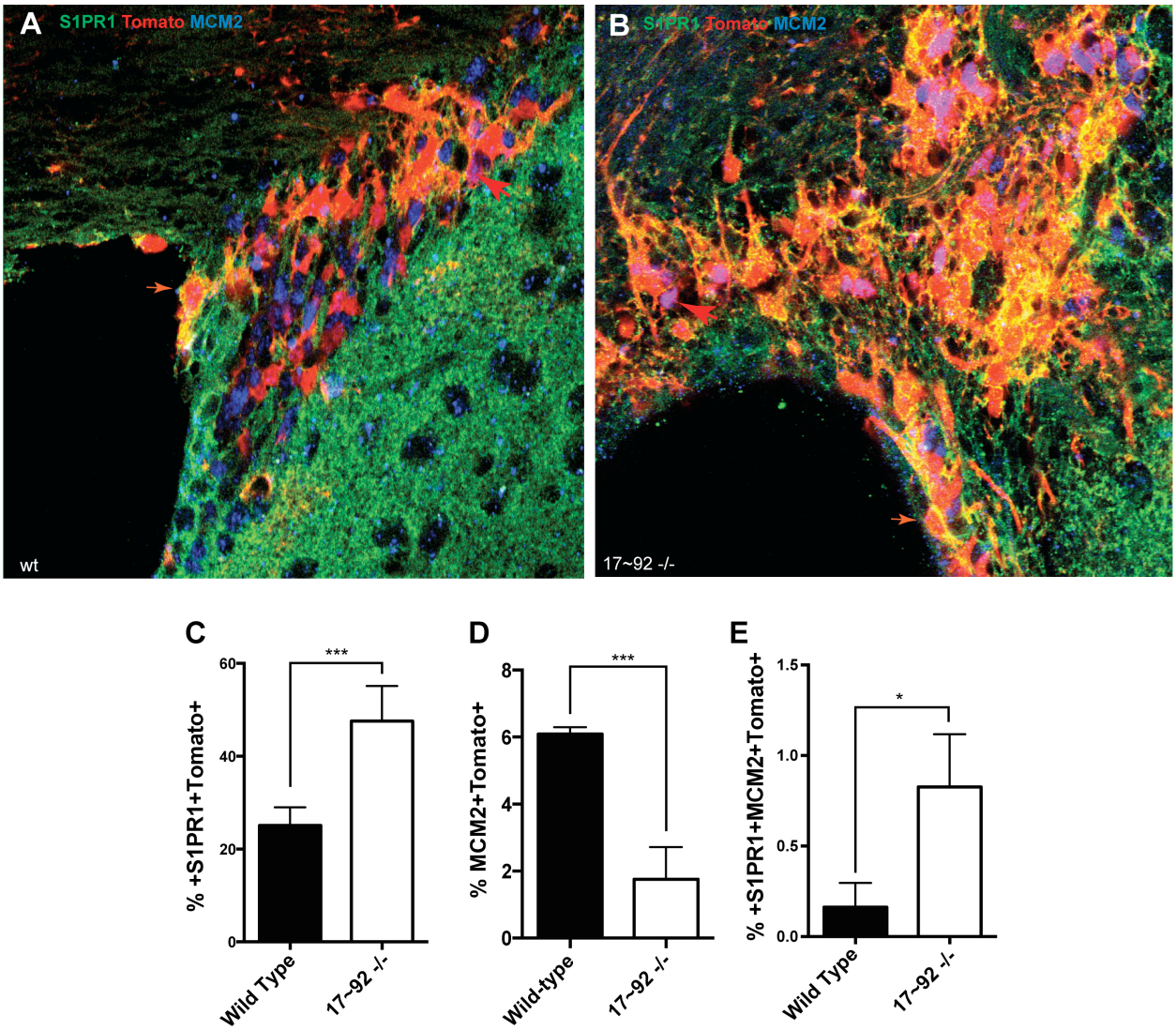

Figure 4.6 S1PR1^{+} cells increase in number when miR-17~92 is deleted

(A) Merge of wedge region of wild-type mouse in which recombined cells are Tomato^{+} (red) sections stained for S1PR1 (green) and MCM2 (blue). Orange arrow indicates a Tomato^{+}S1PR1^{+} cell. Red arrow indicates Tomato^{+}MCM2^{+} (B) Merge of wedge region from miR-17~92$^{-/-}$ mouse recombined cells are Tomato^{+} (red) sections stained for S1PR1 (green) and MCM2. (blue). Orange arrow indicates a Tomato^{+}S1PR1^{+} cell. Red arrow indicates Tomato^{+}MCM2^{+}. (C) Quantification of S1PR1^{+}Tomato^{+} cells. (D) Quantification of MCM2^{+}Tomato^{+} cells. (E) Quantification of S1PR1^{+}MCM2^{+}Tomato^{+}. ***$p < 0.005$. *$p < 0.05$.

Conclusions

In this chapter, I have identified *Mycn, Lrig1,* and *S1pr1* as potential targets of miR-17~92 mediated repression and examined the functional consequences of miR-17~92 on S1PR1. S1pr1 is largely expressed, at both the RNA and protein levels, by non-dividing GFAP$^+$ V-SVZ astrocytes.

In the future, it will be important to establish whether S1PR1 expression is restricted to qNSCs or simply non-dividing astrocytes in both homeostatic and miR-17~92 deleted conditions. Co-immunostaining with S100β will determine whether S1PR1 is expressed by mature astrocytes. Nestin is a marker of aNSCs (Codega et al., 2014), therefore, co-staining with S1PR1 will further resolve whether S1PR1 is expressed in these cells. Interestingly, induction of S1PR1 signaling in angiogenic cells stops them from making new sprouts, but inhibition allows new vessels to grow ectopically (Gaengel et al., 2012). It could be that similar mechanisms are at work in regulating the behavior of angiogenic cells as well as neurogenic cells of the V-SVZ.

The expression of S1pr1 in qNSCs in combination with the strong effect on blocking activation and proliferation that S1P treatment has on these cells (Figure 2.10), suggests that S1PR1 may be playing an important role in the active maintenance of the quiescent stem cell state. Furthermore, *S1pr1* mRNA, but not protein, is expressed in aNSCs, and S1PR1 protein is upregulated upon miR-17~92 deletion *in vivo*, showing that *S1pr1* is targeted by miR-17~92. Together, these findings suggest that in the adult V-SVZ, S1PR1 signaling works to maintain stem cell quiescence and needs to be downregulated in order for activation to take place (summarized in Figure 4.7).

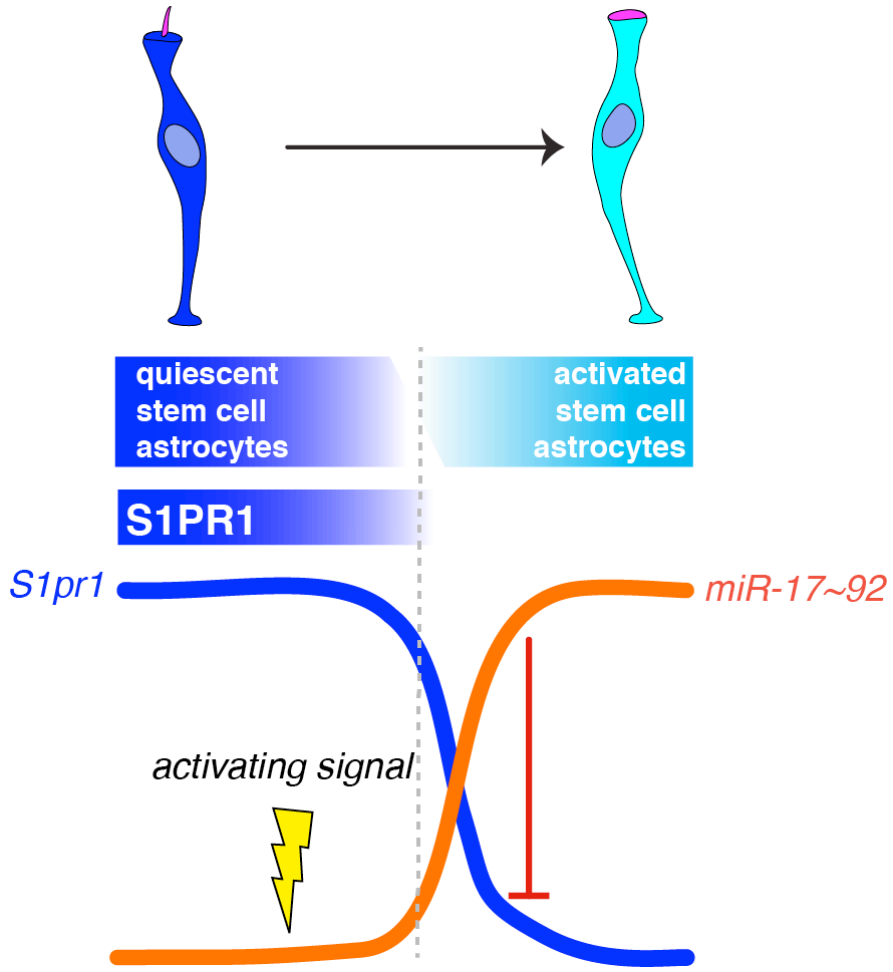

Figure 4.7 Model of miR-17~92 mediated stem cell activation via repression of S1pr1

Stem cell activation events proceed from left to right. miRNA suppression indicated by '⊣'

Methods

Bioinformatic Analysis of miRNA and mRNA Interactions within V-SVZ Lineage Cells

A list of genes involved in GPCR signaling was compiled from the GSEA enrichment results generated in Chapter 2. This list was then imported into Genespring where fold change for the probes for each gene were added to the table. In parallel, computationally predicted targets for the individual members of the miR-17~92 cluster, miR-17, 18a, 19a, 20a, 19b and 92a were downloaded from StarBase 2.0 (Li et al., 2013; Yang et al., 2010). The miR lists and GPCR lists were compared to find overlap. Those miRs that contained a given GPCR gene were then recorded into the GPCR table.

To determine which miRs target S1pr1, a list of its computationally predicted targeting miRs was downloaded from StarBase 2.0 and imported into Genespring. Fold change analysis was then run on the expression of those miRs in aNSCs as compared to qNSCs.

qPCR for S1PR1

RNA was purified from FACS sorted populations by the miRNeasy kit (Qiagen) and cDNA was generated using WT- Ovation Pico System (NuGEN). The total SVZ sample consisted of all live cells (all cells in Figure 2.1A). For qRT-PCR, all reactions were carried out in triplicate on 3 biological replicates using Brilliant III Ultra Fast SYBR Green QPCR Master Mix (Agilent) in a Stratagene Mx3000P machine with an annealing temperature of 60ºC. Data was normalized to GAPDH expression and analyzed by the $2^{-\Delta\Delta CT}$ method (Livak & Schmittgen, 2001). Primers used are in Table 4.2.

Table 4.2 Primers used for the detection of S1pr1

Gene name	Forward primer	Reverse Primer
S1pr1	ACAGCACCTTTGGCACTTTT	TCTCCCCCAGTTGGTTGAAAT

S1PR1 Expression in Wild-Type V-SVZ

Young adult 2-3 month old CD-1 mice (Jackson Laboratories) were sacrificed and transcardially perfused to with saline and 3.2% PFA. Brains were then removed and placed in 3.2% PFA overnight at 4°C. Brains were then made into 50 μm sections using a vibratome (Leica) as previously described (Doetsch et al., 2002; Doetsch & Alvarez-Buylla, 1996). These sections were then stained for rabbit anti-S1PR1 (1:50, Santa Cruz Biotechnology), rat ant-GFAP (1:1000, Invitrogen), and goat anti-MCM2 (1:100, Santa Cruz Biotechnology). Sections were imaged on Zeiss 500 and 800 Confocals in four areas per section: the outermost lateral edge, central wedge, most ventral edge, and halfway between the ventral edge and central wedge. Staining was quantified in FIJI using the Cell Counter plug-in to count each stack continuously. For MCM2, only those cells showing a solid nucleus were counted as MCM2-positive, regardless of their size.

S1PR1 Expression After miR-17~92 Deletion

Young adult GFAP-CreERT2$^{+/-}$; miR-17~92 $^{+/+}$ or $^{fl/fl}$; R26R lslTomato$^{+/+}$ mice aged 2-4 months were intraperitoneally injected once every 24 hours over the course of three days with 0.1 mL of 30uM tamoxifen (Tam) in 90% sunflower seed oil, 10% EtOH. After a 30-day chase, mice were sacrificed and their brains sectioned. Sections were then immunostained with rabbit anti-S1PR1 (1:50, Santa Cruz Biotechnology) and goat anti-MCM2 (1:100, Santa Cruz Biotechnology) and quantified as described above.

Chapter 5 Discussion and Future Directions

Over the course of this dissertation, I have shown that the transcriptomes of quiescent and activated adult neural stem cells are significantly different, and share features with quiescent or activated stem cells of other tissue compartments. I identified the miR-17~92 cluster as significantly enriched in activated neural stem cells, and determined that it plays an important role in stem cell activation, proliferation, and neuronal differentiation. Finally, I identified S1PR1 as potential mediator of quiescence. S1PR1 expression increases when miR-17~92 is lost *in vivo* and therefore is a functional target of this cluster.

Quiescent and Activated States are Transcriptionally Distinct and Actively Maintained

Bioinformatic analysis shows that qNSC and aNSC populations possess strikingly and significantly different gene expression. aNSC transcriptomes are dominated by expression of genes related to cell cycling and the concomitant DNA/protein metabolism required to support this, a finding which has recently been confirmed (Llorens-Bobadilla et al., 2015). qNSCs show an enrichment for lipid metabolism, a feature found in the other quiescent cell types examined above, and is important for normal neurogenesis (Knobloch et al., 2013). Lipid metabolism as well as glucose metabolism were both confirmed to correlate with more quiescent adult neural stem cell populations both in the V-SVZ and SGZ (Llorens-Bobadilla et al., 2015; Shin et al., 2015).Quiescent stem cells additionally expressed markers in common; for example, Lrig1 is common to the V-SVZ, intestine, and skin stem cells (Codega et al., 2014; Jensen & Watt, 2006; Jensen et al., 2009; Powell et al., 2012).

Both quiescent and activated neural stem cells show enrichment in diverse signaling pathways. aNSCs not only express EGFR but are also enriched for components of the EGFR signaling pathway. qNSCs are enriched for several types of cell signaling, the largest of which is

GPCR mediated signaling. It will be important to functionally explore the signaling pathways active in qNSCs to determine which are important for maintaining quiescence, and how qNSCs integrate information from the niche to determine whether to become activated.

A promising candidate for further investigation into quiescence and activation mediation is the Lrig1-EGFR signaling axis. *Lrig1* has high expression among the qNSCs, while EGFR is highly expressed by the aNSCs. Previous work has shown that Lrig1 targets EGFR for degradation from the membrane, thereby downregulating EGFR signaling (Gur et al., 2004). Interestingly, loss of Lrig1 function causes hyperplasias in skin (Gur et al., 2004). Lrig1 is a predicted target of the miR-17~92 cluster, as well as many other miRs expressed in aNSCs. Therefore, Lrig1 expression in the qNSCs may maintain their quiescent state by degrading EGFR, thereby preventing premature activation by downregulating the cell's ability to respond to EGFR signaling. Lrig1's repression of this pathway must be downregulated in order for cells to have sustained EGFR expression and become activated. Greater understanding of the normal function of Lrig1 may be pivotal to developing cancer treatments, as Lrig1 was recently identified as one of four genes with prognostic impact in glioma (reviewed in Simion et al., 2014).

Of the signaling pathways enriched in qNSCs, the best-represented family is GPCRs. While GPCRs modulate many different facets of adult neurogenesis (reviewed in Doze & Perez, 2013), for instance the CXCR4 mediated homing of aNSCs in the V-SVZ to blood vessels (Kokovay et al., 2010), our findings highlight that GPCRs are also key regulators of qNSCs. In particular, we show that S1P inhibits the activation of qNSCs, lending weight to the idea that stem cell quiescence is an actively maintained state (Codega et al., 2014).

This idea was confirmed by Llorens-Bobadilla et al. who show that inhibition of the Notch receptors is sufficient to activate quiescent stem cells. Interestingly, upon ischemic injury, Llorens-Bobadilla et al. show that qNSCs are more capable of responding than aNSCs, and that qNSCs recruitment is dependent on interferon-γ signaling. Llorens-Bobadilla et al. further confirm our finding that qNSCs are enriched for many receptors. Together with their functional data on Notch and interferon- γ, it is now established that qNSCs are especially attuned to environmental cues, and that these signals can be used to both reinforce a quiescent state and recruit quiescent stem cells to activate.

S1P is present in the CSF (Sato et al., 2007), which is emerging as a reservoir of factors important for stem cell regulation in both the embryo and the adult (Silva-Vargas et al., 2013). Furthermore, microarray analysis of the lateral ventricle choroid plexus (CP), a mini-organ located within the ventricles that produces the CSF, revealed that this organ expresses several genes involved in S1P metabolism and export (Table 5.1, CP expression is unpublished data from Violeta Silva-Vargas). Strikingly, many of the same genes are enriched in qNSCs over aNSCs (Table 5.1). In fact, S1P can act in an autocrine and paracrine manner in many tissues, including during angiogenesis (reviewed in Maceyka et al., 2012). Therefore, in the V-SVZ, both the CP and qNSCs may produce S1P in order to mediate quiescence. As such, the CSF, CP, and qNSCs may together act as key niche components mediating quiescence in the adult V-SVZ.

Probe Set ID	Gene Title	Gene Symbol	Expression in Choroid plexus	qNSC average expression	aNSC average expression
1421839_at	ATP-binding cassette, sub-family A (ABC1), member 1	Abca1	+	1605.413833	562.3829267
1421840_at			+++++	7125.9598	2478.051867
1450392_at			No information	4313.761967	1255.742033
1421378_s_at	ATP-binding cassette, sub-family C (CFTR/MRP), member 1	Abcc1	No information	724.84283	291.1922367
1452233_at			No information	488.38209	430.0338433
1451601_a_at	spinster homolog 2 (Drosophila)	Spns2	+	203.0812567	104.382625
1451596_a_at	sphingosine kinase 1	Sphk1	--	6.499328967	14.954722
1417431_a_at	sphingosine kinase 2	Sphk2	+	552.66867	505.7168133
1426230_at			++	4125.5728	371.5279733
1416735_at	N-acylsphingosine amidohydrolase 1	Asah1	++++	4755.463333	2000.9459
1425994_a_at	N-acylsphingosine amidohydrolase 2	Asah2	+	98.998609	19.8882152
1450726_at			No information	205.5453933	13.1566699
1458849_at			--	75.68537167	5.707459667
1450825_at	alkaline ceramidase 1	Acer1	--	8.482901533	5.2214446
1439183_at			--	12.26565573	9.265371367
1421496_at	alkaline ceramidase 2	Acer2	+	666.9655433	284.8136767
1451355_at			+	190.1910633	42.403121
1429520_a_at	alkaline ceramidase 3	Acer3	+	359.5338	96.31067333
1438435_at			+	209.51215	73.9261998
1453179_at			+	103.3996717	31.70996767
1459771_x_at			+	51.15177567	25.89181567

Table 5.1 Genes involved in S1P metabolism and transport

Probeset IDs for less than optimal probes have been italicized. Expression in choroid plexus, qNSCs and aNSCs has been color coded: no information is white, not present (expression under 50) is gray, expression greater than 50 is colored with increasingly intense shades of orange as level of expression increases.

Another key component of the niche in mediating quiescence is adhesion, especially to the extra-cellular matrix. Bioinformatic analysis shows that genes involved in cell adhesion such as *Vcam1*, *Ncam1*, and *Inta6* are upregulated in the qNSC population of the V-SVZ, as well as

being up regulated in other quiescent stem cells (Table S4). Given the current data, adhesion for these cells enhances the reception of quiescence maintenance signals, which may only be present in certain restricted domains within the V-SVZ niche, as for example, S1P in CSF.

As additional anatomical and cellular features of the V-SVZ stem cell niche are uncovered, the transcriptome data I present in this thesis will be a tremendous resource to define specific molecular candidates. In addition, it will illuminate the gene regulatory networks that functionally mediate stem cell quiescence and activation in the adult V-SVZ.

V-SVZ Stem Cell Heterogeneity

Recent work has shown that stem cells within the V-SVZ exhibit regional heterogeneity in terms of transcription factor expression, and type of olfactory bulb interneuron they generate (Merkle et al., 2014; Jhaveri et al., 2015; Ravi et al., 2015; reviewed in Lim & Alvarez-Buylla, 2014 and Bayraktar et al., 2014). Regional differences in response to injury or diffusible signals have also been observed (Lopez-Juarez et al., 2013; Jhaveri et al., 2015). A very recent paper performing single cell analysis of adult NSC FACS-purified using GLAST and CD133 have begun to dissect the heterogeneity of these cells (Llorens-Bobadilla et al., 2015). Notably, this study revealed that qNSCs and aNSCs can be subdivided into four classes; dormant qNSCs, primed qNSCs, aNSCs, and dividing aNSCs. Broadly speaking, these cells correspond well with molecular features we defined for our qNSCs and aNSCs purified using GFAP::GFP, EGF, and CD133. They confirm the expression of *Id2* and *3, Hes5, Notch2, Blbp, Bmpr1a, Aldh1l1,* and *Glast* in quiescent stem cells, while showing that *Sox11 and 4, Ascl1, Dlx1* and *2,* as well as *Dll1* are enriched in aNSCs (Table S4).

In terms of pathway analysis, Llorens-Bobadilla et al. find that lipid metabolism genes are expressed in both qNSCs and aNSCs, but are more highly expressed in qNSCs. Furthermore,

they find that glycolysis is enriched in qNSCs, which we also found via GSEA (Figure 2.9A, Table S3). In accordance with our findings, Llorens-Bobadilla et al. also find that protein metabolism correlates activation (Figure 2.9B, Table S3), and can use the amount of protein synthesis to differentiate between dormant and primed qNSCs.

miR-17~92 Mediates Activation and Proliferation of aNSCs

During my thesis work, I focused on miRs enriched in aNSCs. My bioinformatic analysis identified members of the miR-17~92 cluster as highly enriched in aNSCs, as compared to qNSCs, In the course of this work, I also identified miRNAs that are enriched in qNSCs, which will be very interesting to examine in the future.

In vitro studies in which miR-17~92 was conditionally deleted suggest that this cluster is important to activation of V-SVZ stem cells. Furthermore, those cells that did manage to activate proliferated less, suggesting that this cluster is also important to support proliferation. I confirmed this finding *in vivo,* where deletion of the miR-17~92 locus results in reduced expression of MCM2 (Figure 5.1, blue group), as well as in decreased neurogenesis.

Although miR-17~92 has been found to act in a pro-survival manner in the hematopoietic system as well as in cancers (summarized in Figure 5.1, Gray group, reviewed in Concepcion et al., 2012), there was no effect on apoptosis for aNSCs within the first five days of culturing. A lack of survival defects has also been observed in other systems (Bian et al., 2013; Chen et al., 2013). However, it is possible that miR-17~92 is important for survival at later stages in the V-SVZ lineage, such as in newly generated neurons. Indeed, the reduction in neurogenesis I observed could be due to fewer stem cells becoming activated and progressing down the lineage, as well as to selective survival defects in neurons. Distinguishing between these two possibilities

is important in determining which mRNAs are being targeted by miR-17~92 in order to drive neurogenesis (Figure 5.1 red and gray groups).

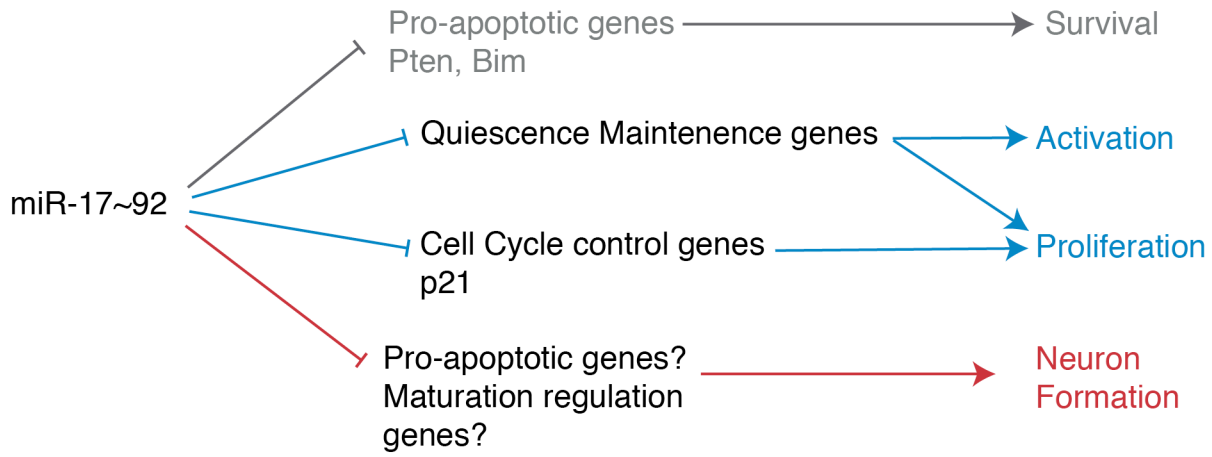

Figure 5.1 Model of miR-17~92 functions relevant to the V-SVZ niche based on downstream gene repression

(Gray) miR-17~92 is known to suppress Pten and Bim, thereby evading apoptosis and mediating cell survival (Blue) In our study, we find that miR-17~92 expression is important for normal levels of activation. This could be achieved through the repression of genes important to maintain a quiescent state. Previous studies and the work herein have shown that miR-17~92 promotes a proliferative state. This is achieved in part through the suppression of p21, a cell cycle regulatory gene. (Red) miR-17~92 expression is needed for neurogenesis, however it is unclear from our studies whether this is achieved through miR-17~92 mediated survival, or failure to repress programs for maturation of a different cell type.

In neural stem cells in the embryo, miR-17~92 regulates a temporal switch from neurogenesis to gliogenesis, and specifically keeps cells in a neuro-competent state (Naka-Kaneda et al., 2014). Loss of miR-17~92 in this context causes an increase in the generation of $GFAP^+$ cells (Naka-Kaneda et al., 2014). Although a switch to gliogenic competence is an intriguing possibility for adult NSCs that have lost miR-17~92 expression, there was no increase in $GFAP^+$ cells concomitant with the loss of neurons in my differentiation experiments. This disparity may be due to differences between stem cells in the embryo and in the adult.

Conditional miR-17~92 Overexpression Studies

In addition to conditional deletion of miR-17~92, the effect of ectopic miR-17~92 overexpression has been well studied. Previous research has found that overexpression of miR-17~92 leads to marked increase in proliferation of cells in many systems (Olive et al., 2013a; Yang et al., 2013; Carraro et al., 2009; Lu et al., 2007; Chen et al., 2013; Li et al., 2012; Liu et al., 2013; Trompeter et al., 2011; Venturini et al., 2007; Meenhuis et al., 2011). Confoundingly, some studies have found that the forced overexpression of miR-17~92 leads to a concomitant increase in apoptosis (Olive et al., 2013a), while others have seen no difference (Liu et al., 2013, work done on ischemic V-SVZ and progenitors), or found a protective effect (Tung et al., 2015). Additionally, it has been shown that ectopic miR-17~92 overexpression leads to a delay in neuronal differentiation (Naka-Kaneda et al., 2014; Lu et al., 2007).

It would be interesting to overexpress miR-17~92 in the V-SVZ using conditionally inducible mice, and to assess the functional consequences on proliferation and neuronal production. It would also be exciting to determine if miR-17~92 overexpression induces astrocytes in non-neurogenic brain regions to become actively dividing and neurogenic, especially as qNSCs have a very similar transcriptome to cortical astrocytes.

Dissection of the Role of Individual Members of miR-17~92 Cluster

In the future, it will also be important to dissect which miRNA(s) in the miR-17~92 cluster contribute to the functional effects described in this thesis. For example, miRs 19a and 92a are thought to sometimes act antagonistically (Olive et al., 2013b). Understanding which components of the miR-17~92 cluster are responsible for which aspects of the phenotypes described above could prove essential for fine-tuning V-SVZ stem cell behavior. To dissect the effects of each miR or seed sequence family, individual members or small cohorts sharing seed

sequences (e.g. 17 and 20a) could be overexpressed in cells to determine their effects on behavior. Conversely, it might be more advantageous to knock down all but one miR-17~92 cluster member or seed sequence family. This could be achieved via nucleofection or viral delivery of a microRNA sponge vector, i.e. a sequence(s) of DNA designed to be anti-sense to the miRNA(s) of interest. A sponge could be designed to be anti-sense to all but one member of the miR-17~92 cluster, thereby inhibiting the activity of all but one of the miR-17~92 members by out-competing potential mRNA targets for miRNA binding (Ebert & Sharp, 2010; Ebert et al., 2007), and revealing the function of the non-blocked microRNA.

Regulation of miR 17~92 Expression

miR-17~92 is highly expressed in aNSCs, but not in qNSCs— yet a direct driver for this change in expression is unknown. N-myc is a transcription factor, and an "immediate early" gene which "respond[s] rapidly to growth factors in the absence of protein synthesis" (Lau & Nathans, 1987) and drives cell cycling. Both N-myc and its closely related family member C-myc are known to drive miR-17~92 expression (Fontana et al., 2008). N-myc overexpression has been observed in 20% of neuroblastomas, where it correlates with higher glade tumors and poor prognosis due to the rapid progression of such tumors, and is furthermore known to drive expression of miR-17~92 in this context (reviewed in Buechner & Einvik, 2012). For N-myc, two induction factors have been identified so far; sonic hedgehog (Shh, Kenney et al., 2003) and estrogen (Murphy et al., 1987). Indeed, by qPCR I find that *Mycn* expression spikes in the aNSCs (Figure 4.1). Interestingly, the miR-17~92 cluster also targets *Mycn* mRNA, and reflecting this, *Mycn* expression rapidly declines as cells become TACs (Figure 4.1) suggesting an auto-regulatory loop, which may function to prevent overexpression of either the transcription factor or the cluster (Figure 5.2, Buechner & Einvik, 2012).

Taking all of these ideas into account, I propose that N-myc, via a yet to be determined exogenous signal, is rapidly expressed by aNSCs and translated into protein. N-myc then activates transcription of the miR-17~92 cluster, which down regulates mediators of quiescence, such as S1PR1. At the same time, N-myc activates transcription of cell cycle and DNA/RNA metabolism genes important for activation and proliferation. These genes, unlike the miR-17~92 cluster, are protein encoding and thus, must be translated in order to have an effect. The time delay caused by translation may be helpful to the transition from quiescence to activation as some activation-important genes, like EGFR, seem to be actively targeted by genes expressed in the qNSCs, like Lrig1 (Perini et al., 2005; Gur et al., 2004). In turn, miR-17~92 downregulates *Mycn* expression, thereby tightly regulating the expression of the "activation/proliferation" factors, as well as its own transcription, which likely acts to prevent overproliferation and possibly cancer formation (Summarized in Figure 5.2).

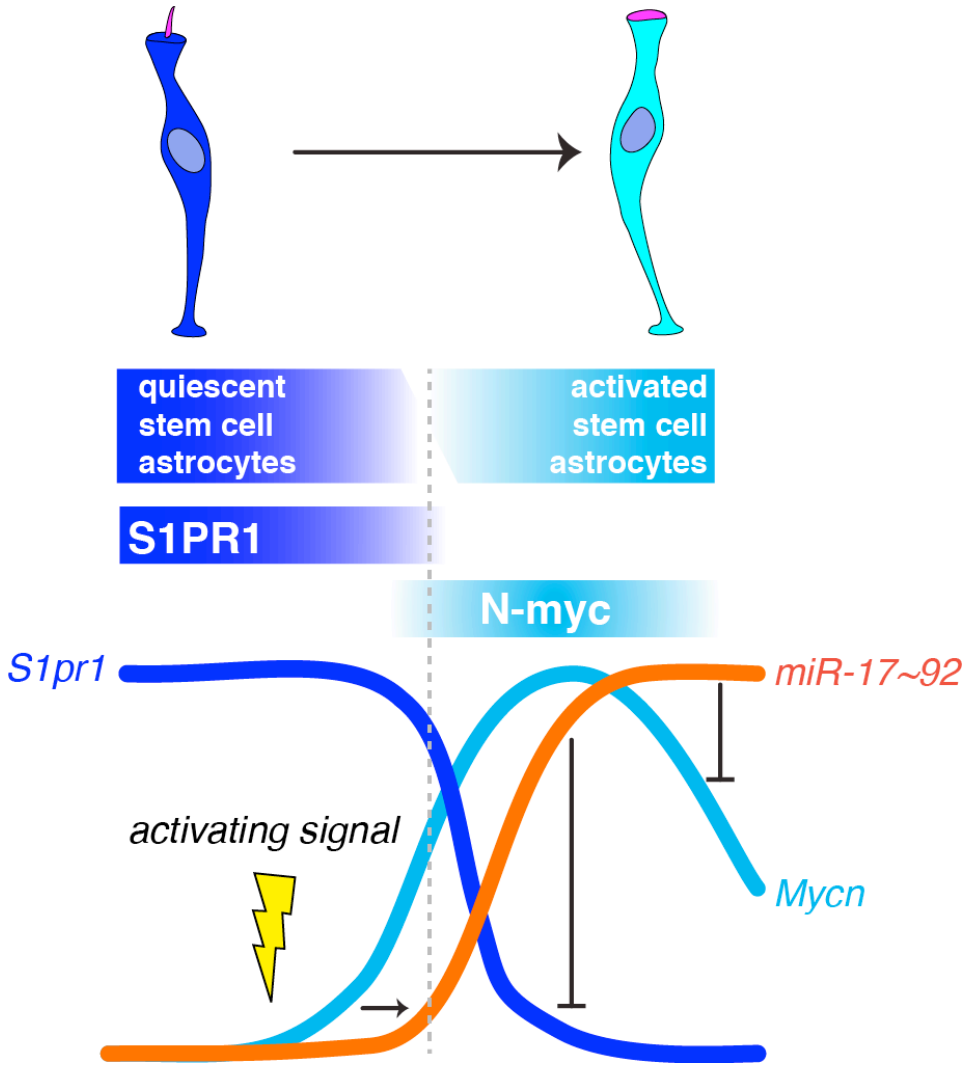

Figure 5.2 Model of how activation occurs over the S1pr1-miR-17~92 axis including regulation by Mycn

Activation process proceeds from left to right. Transcriptional activation indicated by '→', while miRNA inhibition is indicated by '⊣'

Further studies should be done on the expression of N-myc protein in the adult V-SVZ stem cells, and what signals coming from the niche might be inducing *Mycn* expression in these aNSCs, as this could reveal a "prime mover" for activation in this system. Interestingly, while the majority of Feingold syndrome cases are caused by mutations in the *MYCN* gene (van Bokhoven et al., 2005), a subset of the cases have been found to be caused by mutations in *MIR17HG*-- the host gene of the miR-17~92 cluster (Concepcion et al., 2012; de Pontual et al.,

2011; Tassano et al., 2013). In patients with the miR-17~92 mutation cases, fewer of the clinical features of Feingold syndrome are apparent than patients harboring Mycn mutations. These findings suggest that the activation of miR-17~92 by N-myc is important for normal brain development.

S1pr1 Expressed in qNSCs and is a Target of miR-17~92

S1pr1 is highly enriched in qNSCs, and S1PR1 highly expressed by $GFAP^+$ cells, while having little co-expression with MCM2. Treatment of qNSCs with S1PR1 ligand S1P reduces their activation and proliferation, and S1PR1 is the most expressed S1PR family member among the qNSCs. Together, this data suggests that S1P acts through S1PR1 to induce or reinforce a quiescent state. To more directly probe the function of S1PR1 in mediating quiescence, it will be important to manipulate S1PR1 signaling via different routes, either pharmacologically, or with viral approaches. It will also be interesting to overexpress S1PR1 in aNSCs to determine if this is sufficient to induce quiescence.

Potential miR-17~92 Targeting of *S1pr1*

Bioinformatic analysis shows that S1PR1 is a computationally predicted target of members of the miR-17~92 cluster, which is highly enriched in the aNSCs, suggesting that suppression of S1PR1 signaling may be important to achieving an active state. When miR-17~92 is deleted *in vivo*, S1PR1 expression increases, even on MCM2-positive cells, further supporting the idea that miR-17~92 targets this mRNA.

Recent work has shown that the 3' UTR of *S1pr1* is directly targeted by miR-363, a microRNA which shares its seed sequence with miR-17, -20a and -20b (Zhou et al., 2014). Other recent studies have shown that overexpression of miR-92a, a member of the miR-17~92 cluster, is sufficient to reduce levels of *S1pr1* mRNA and protein in an angiogenesis model (Bonauer et

al., 2009; Ando et al., 2013). However, direct interaction of miR-92a and *S1pr1* by luciferase assay was not shown. These findings support the idea that miR-17~92 regulation of *S1pr1* may proceed via the mRNA degradation route, the mechanism most common in mammals. To date, no one has shown direct regulation of *S1pr1* by any members of the miR-17~92 cluster. Ongoing studies in the lab are aimed at determining whether direct interaction between miR-17~92 and the 3' UTR of *S1pr1* occurs.

S1PR1 Function in Humans and in Disease

S1pr1 has been found to promote tumor growth or cell proliferation in some contexts. Elevated expression of S1pr1 has been found in tumor-derived myeloid cells (Lee et al., 2010), and correlates with poor prognosis in glioblastoma multiforme (Marfia et al., 2014), as well as directly driving proliferation in hepatocellular carcinoma (Zhou et al., 2014) and in diffuse large B-cell lymphoma (Liu et al., 2012). However, these effects may be explained, in part, by the known pro-survival effect of S1pr1 (reviewed in Blaho & Hla, 2014) working in the context of malignancy.

Fingolimod, an immunomodulatory drug approved by the Food and Drug Administration for the treatment of multiple sclerosis (Kappos et al., 2006), acts on S1P receptors, primarily through S1PR1 (Chun & Hartung, 2010). Recent studies have shown that fingolimod also acts on multiple CNS cell types (Groves et al., 2013), including astrocytes. Our identification of S1P as a regulator of stem cell quiescence and S1PR1 expression in the V-SVZ suggests that this drug may have additional effects on stem cells in the adult brain.

Final Conclusions

I have shown that quiescent and activated adult neural stem cells have very different transcriptomes, especially in areas of signaling and metabolism. In depth analysis of these

transcriptomes revealed potential bi-directional regulation between these cells. Comparison of these transcriptomes with quiescent or activated counterparts from other tissues revealed that features of these states are conserved. I found that miR-17~92 is upregulated in aNSCs, and that it is needed for normal activation, proliferation and neurogenesis both *in vitro* and *in vivo*. Finally, I explored a few potential miR-17~92 targets, and found that S1pr1 is an excellent candidate for direct targeting by miR-17~92, and potentially mediates quiescence. Indeed, the response of qNSCs to S1PR1's ligand, S1P, and its increased expression after miR-17~92 deletion, even in dividing cells, highlight its functional importance in quiescent neural stem cells residing in the V-SVZ.

In conclusion, this data provides the first evidence that miRs are involved in the transition from neural stem cell quiescence to activation and could provide a powerful approach to harness adult neural stem cells for brain repair after injury, stroke, or onset of neurodegenerative disorder. Moreover, miRNAs have altered expression patterns in many cancers, and play a role in the development of many cancer types (reviewed in Ha, 2011). Therefore, this work will also have important implications for cancer, providing mechanistic insight into pathways that may become misregulated and revealing which cells in the V-SVZ may be capable of giving rise to tumors. Finally, S1pr1 is emerging as a target of miR-17~92 that may have an integral role in mediation of quiescence. Having the ability to suppress or induce quiescence will be pivotal for upregulating stem cell activity in the context of brain repair, or downregulating it in the context of cancer.

References:

Akiyama, T., Sadahira, Y., Matsubara, K., Mori, M., & Igarashi, Y. (2008). Immunohistochemical detection of sphingosine-1-phosphate receptor 1 in vascular and lymphatic endothelial cells. *Journal of Molecular Histology*, *39*(5), 527–533. http://doi.org/10.1007/s10735-008-9193-y

Alfonso, J., Le Magueresse, C., Zuccotti, A., Khodosevich, K., & Monyer, H. (2012). Diazepam Binding Inhibitor Promotes Progenitor Proliferation in the Postnatal SVZ by Reducing GABA Signaling. *Stem Cell*, *10*(1), 76–87. http://doi.org/10.1016/j.stem.2011.11.011

Allen, E. (1912). The cessation of mitosis in the central nervous system of the albino rat, 1–31.

Altman, J. (1962a). Are New Neurons Formed in the Brains of Adult Mammals? *Science*, *135*(3509), 1127–1128. http://doi.org/10.1126/science.135.3509.1127

Altman, J. (1962b). Autoradiographic study of degenerative and regenerative proliferation of neuroglia cells with tritiated thymidine. *Experimental Neurology*, *6*(2), 142–151. http://doi.org/10.1016/0014-4886(62)90084-5

Altman, J. (1963). Autoradiographic investigation of cell proliferation in the brains of rats and cats. *The Anatomical Record*, *145*, 573–591.

Altman, J. (1969). Autoradiographic and histological studies of postnatal neurogenesis. IV. Cell proliferation and migration in the anterior forebrain, with special reference to persisting neurogenesis in the olfactory bulb. *The Journal of Comparative Neurology*, *137*(4), 433–457. http://doi.org/10.1002/cne.901370404

Altman, J., & Chorover, S. L. (1963). Autoradiographic investigation of the distribution and utilization of intraventricularly injected adenine-3h, uracil-3h and thymidine-3h in the brains of cats. *The Journal of Physiology*, *169*(4), 770–779. http://doi.org/10.1111/(ISSN)1469-7793

Altman, J., & Das, G. D. (1965). Autoradiographic and histological evidence of postnatal hippocampal neurogenesis in rats. *The Journal of Comparative Neurology*.

Altman, J., & Das, G. D. (1966). Autoradiographic and histological studies of postnatal neurogenesis. I. A longitudinal investigation of the kinetics, migration and transformation of cells incorporating tritiated thymidine in neonate rats, with special reference to postnatal neurogenesis in some brain regions. *The Journal of Comparative Neurology*, *126*(3), 337–389. http://doi.org/10.1002/cne.901260302

Ando, H., Okamoto, A., Yokota, M., Shimizu, K., Asai, T., Dewa, T., & Oku, N. (2013). Development of a miR-92a delivery system for anti-angiogenesis-based cancer therapy. *The Journal of Gene Medicine*, *15*(1), 20–27. http://doi.org/10.1002/jgm.2690

Andreu-Agulló, C., Andreu-Agulló, C., Morante-Redolat, J. M., Morante-Redolat, J. M., Delgado, A. C., & Fariñas, I. (2009). Vascular niche factor PEDF modulates Notch-dependent stemness in the adult subependymal zone. *Nature Neuroscience*, *12*(12), 1514–1523. http://doi.org/10.1038/nn.2437

Ashburner, M., Ball, C. A., Blake, J. A., Botstein, D., Butler, H., Cherry, J. M., et al. (2000). Gene Ontology: tool for the unification of biology. *Nature Genetics*, *25*(1), 25–29. http://doi.org/10.1038/75556

Bae, S., Bessho, Y., Hojo, M., & Kageyama, R. (2000). The bHLH gene Hes6, an inhibitor of Hes1, promotes neuronal differentiation. *Development*, *127*(13), 2933–2943.

Barraud, P., Thompson, L., Kirik, D., Björklund, A., & Parmar, M. (2005). Isolation and characterization of neural precursor cells from the Sox1-GFP reporter mouse. *European Journal of Neuroscience*, *22*(7), 1555–1569. http://doi.org/10.1111/j.1460-

9568.2005.04352.x
Basak, O., Giachino, C., Fiorini, E., MacDonald, H. R., & Taylor, V. (2012). Neurogenic Subventricular Zone Stem/Progenitor Cells Are Notch1-Dependent in Their Active But Not Quiescent State. *Journal of Neuroscience*, *32*(16), 5654–5666. http://doi.org/10.1523/JNEUROSCI.0455-12.2012
Bayraktar, O. A., Fuentealba, L. C., Alvarez-Buylla, A., & Rowitch, D. H. (2014). Astrocyte Development and Heterogeneity. *Cold Spring Harbor Perspectives in Biology*, a020362. http://doi.org/10.1101/cshperspect.a020362
Beckervordersandforth, R., Tripathi, P., Ninkovic, J., Bayam, E., Lepier, A., Stempfhuber, B., et al. (2010). SUPPLEMENTAL In Vivo Fate Mapping and Expression Analysis Reveals Molecular Hallmarks of Prospectively Isolated Adult Neural Stem Cells. *Cell Stem Cell*, *7*(6), 744–758. http://doi.org/10.1016/j.stem.2010.11.017
Bergmann, O., Liebl, J., Bernard, S., Alkass, K., Yeung, M. S. Y., Steier, P., et al. (2012). The Age of Olfactory Bulb Neurons in Humans. *Neuron*, *74*(4), 634–639. http://doi.org/10.1016/j.neuron.2012.03.030
Beveridge, N. J., Tooney, P. A., Carroll, A. P., Tran, N., & Cairns, M. J. (2009). Down-regulation of miR-17 family expression in response to retinoic acid induced neuronal differentiation. *Cellular Signalling*, *21*(12), 1837–1845. http://doi.org/10.1016/j.cellsig.2009.07.019
Bian, S., & Sun, T. (2011). Functions of Noncoding RNAs in Neural Development and Neurological Diseases. *Molecular Neurobiology*, *44*(3), 359–373. http://doi.org/10.1007/s12035-011-8211-3
Bian, S., Hong, J., Li, Q., Schebelle, L., Pollock, A., Knauss, J. L., et al. (2013). MicroRNA Cluster miR-17-92 Regulates Neural Stem Cell Expansion and Transition to Intermediate Progenitors in the Developing Mouse Neocortex. *Cell Reports*, *3*(5), 1398–1406. http://doi.org/10.1016/j.celrep.2013.03.037
Blaho, V. A., & Hla, T. (2014). An update on the biology of sphingosine 1-phosphate receptors. *The Journal of Lipid Research*, *55*(8), 1596–1608. http://doi.org/10.1194/jlr.R046300
Blanpain, C., Lowry, W. E., Geoghegan, A., Polak, L., & Fuchs, E. (2004). Self-renewal, multipotency, and the existence of two cell populations within an epithelial stem cell niche. *Cell*, *118*(5), 635–648. http://doi.org/10.1016/j.cell.2004.08.012
Bonauer, A., Carmona, G., Iwasaki, M., Mione, M., Koyanagi, M., Fischer, A., et al. (2009). MicroRNA-92a controls angiogenesis and functional recovery of ischemic tissues in mice. *Science*, *324*(5935), 1710–1713. http://doi.org/10.1126/science.1174381
Brett, J. O., Renault, V. M., Rafalski, V. A., & Webb, A. E. (2011). The microRNA cluster miR-106b~ 25 regulates adult neural stem/progenitor cell proliferation and neuronal differentiation. *Aging (Albany NY)*.
Brümmer, A., & Hausser, J. (2014). MicroRNA binding sites in the coding region of mRNAs: Extending the repertoire of post-transcriptional gene regulation. *BioEssays*, *36*(6), 617–626. http://doi.org/10.1002/bies.201300104
Buechner, J., & Einvik, C. (2012). N-myc and noncoding RNAs in neuroblastoma. *Molecular Cancer Research : MCR*, *10*(10), 1243–1253. http://doi.org/10.1158/1541-7786.MCR-12-0244
Cajal, S. R. Y., & May, R. M. (1991). Résumé of the Structure of the Normal Medullated Nerve. (J. DeFelipe & E. G. Jones, Eds.) (pp. 1–26). Oxford University Press. http://doi.org/10.1093/acprof:oso/9780195065169.001.0001

Calaora, V., Chazal, G., Nielsen, P. J., Rougon, G., & Moreau, H. (1996). mCD24 expression in the developing mouse brain and in zones of secondary neurogenesis in the adult. *Nsc*, *73*(2), 581–594.

Capela, A., & Temple, S. (2002). LeX/ssea-1 is expressed by adult mouse CNS stem cells, identifying them as nonependymal. *Neuron*, *35*(5), 865–875.

Carraro, G., El-Hashash, A., Guidolin, D., Tiozzo, C., Turcatel, G., Young, B. M., et al. (2009). miR-17 family of microRNAs controls FGF10-mediated embryonic lung epithelial branching morphogenesis through MAPK14 and STAT3 regulation of E-Cadherin distribution. *Developmental Biology*, *333*(2), 238–250. http://doi.org/10.1016/j.ydbio.2009.06.020

Chen, J., Huang, Z. P., Seok, H. Y., Ding, J., Kataoka, M., Zhang, Z., et al. (2013). mir-17-92 Cluster Is Required for and Sufficient to Induce Cardiomyocyte Proliferation in Postnatal and Adult Hearts. *Circulation Research*, *112*(12), 1557–1566. http://doi.org/10.1161/CIRCRESAHA.112.300658

Chen, J.-A., Huang, Y.-P., Mazzoni, E. O., Tan, G. C., Zavadil, J., & Wichterle, H. (2011). Mir-17-3p controls spinal neural progenitor patterning by regulating Olig2/Irx3 cross-repressive loop. *Neuron*, *69*(4), 721–735. http://doi.org/10.1016/j.neuron.2011.01.014

Chen, L., Cui, J., Hou, J., Long, J., Li, C., & Liu, L. (2014). A Novel Negative Regulator of Adipogenesis: MicroRNA-363. *Stem Cells*, *32*(2), 510–520. http://doi.org/10.1002/stem.1549

Cheng, L.-C., Pastrana, E., Tavazoie, M., & Doetsch, F. (2009). miR-124 regulates adult neurogenesis in the subventricular zone stem cell niche. *Nature Neuroscience*, *12*(4), 399–408. http://doi.org/10.1038/nn.2294

Cheung, T. H., & Rando, T. A. (2013). Molecular regulation of stem cell quiescence. *Nature Reviews Molecular Cell Biology*, *14*(6), 329–340. http://doi.org/10.1038/nrm3591

Cheung, T. H., Quach, N. L., Charville, G. W., Liu, L., Park, L., Edalati, A., et al. (2013). Maintenance of muscle stem-cell quiescence by microRNA-489. *Nature*, *482*(7386), 524–528. http://doi.org/10.1038/nature10834

Chun, J., & Hartung, H.-P. (2010). Mechanism of Action of Oral Fingolimod (FTY720) in Multiple Sclerosis. *Clinical Neuropharmacology*, *33*(2), 91–101. http://doi.org/10.1097/WNF.0b013e3181cbf825

Ciccolini, F., Mandl, C., Hölzl-Wenig, G., Kehlenbach, A., & Hellwig, A. (2005). Prospective isolation of late development multipotent precursors whose migration is promoted by EGFR. *Developmental Biology*, *284*(1), 112–125. http://doi.org/10.1016/j.ydbio.2005.05.007

Cloonan, N., Brown, M. K., Steptoe, A. L., Wani, S., Chan, W. L., Forrest, A. R. R., et al. (2008). The miR-17-5p microRNA is a key regulator of the G1/S phase cell cycle transition. *Genome Biology*, *9*(8), R127. http://doi.org/10.1186/gb-2008-9-8-r127

Codega, P., Silva-Vargas, V., Paul, A., Maldonado-Soto, A. R., DeLeo, A. M., Pastrana, E., & Doetsch, F. (2014). Prospective Identification and Purification of Quiescent Adult Neural Stem Cells from Their In Vivo Niche. *Neuron*, *82*(3), 545–559. http://doi.org/10.1016/j.neuron.2014.02.039

Concepcion, C. P., Bonetti, C., & Ventura, A. (2012). The MicroRNA-17-92 Family of MicroRNA Clusters in Development and Disease. *The Cancer Journal*, *18*(3), 262–267. http://doi.org/10.1097/PPO.0b013e318258b60a

Coskun, V., Wu, H., Blanchi, B., Tsao, S., Kim, K., Zhao, J., et al. (2008). CD133+ neural stem cells in the ependyma of mammalian postnatal forebrain. *Proceedings of the National*

Academy of Sciences, *105*(3), 1026–1031. http://doi.org/10.1073/pnas.0710000105
Costa, M. R., Ortega, F., Brill, M. S., Beckervordersandforth, R., Petrone, C., Schroeder, T., et al. (2011). Continuous live imaging of adult neural stem cell division and lineage progression in vitro. *Development*, *138*(6), 1057–1068. http://doi.org/10.1242/dev.061663
de Pontual, L., Yao, E., Callier, P., Faivre, L., Drouin, V., Cariou, S., et al. (2011). Germline deletion of the miR-17~92 cluster causes skeletal and growth defects in humans. *Nature Genetics*, *43*(10), 1026–1030. http://doi.org/10.1038/ng.915
Delgado, A. C., Ferrón, S. R., Vicente, D., Porlan, E., Perez-Villalba, A., Trujillo, C. M., et al. (2014). Endothelial NT-3 Delivered by Vasculature and CSF Promotes Quiescence of Subependymal Neural Stem Cells through Nitric Oxide Induction. *Neuron*, *83*(3), 572–585. http://doi.org/10.1016/j.neuron.2014.06.015
Doetsch, F., & Alvarez-Buylla, A. (1996). Network of tangential pathways for neuronal migration in adult mammalian brain. *Proceedings of the National Academy of Sciences of the United States of America*, *93*(25), 14895–14900.
Doetsch, F., Caillé, I., Lim, D. A., García-Verdugo, J. M., & Alvarez-Buylla, A. (1999a). Subventricular zone astrocytes are neural stem cells in the adult mammalian brain. *Cell*, *97*(6), 703–716.
Doetsch, F., García-Verdugo, J. M., & Alvarez-Buylla, A. (1997). Cellular composition and three-dimensional organization of the subventricular germinal zone in the adult mammalian brain. *The Journal of Neuroscience*, *17*(13), 5046–5061.
Doetsch, F., García-Verdugo, J. M., & Alvarez-Buylla, A. (1999b). Regeneration of a germinal layer in the adult mammalian brain. *Proceedings of the National Academy of Sciences of the United States of America*, *96*(20), 11619–11624.
Doetsch, F., Petreanu, L., Caille, I., Garcia-Verdugo, J. M., & Alvarez-Buylla, A. (2002). EGF converts transit-amplifying neurogenic precursors in the adult brain into multipotent stem cells. *Neuron*, *36*(6), 1021–1034.
Ebert, M. S., & Sharp, P. A. (2010). MicroRNA sponges: progress and possibilities. *Rna*, *16*(11), 2043–2050. http://doi.org/10.1261/rna.2414110
Ebert, M. S., Neilson, J. R., & Sharp, P. A. (2007). MicroRNA sponges: competitive inhibitors of small RNAs in mammalian cells. *Nature Methods*, *4*(9), 721–726. http://doi.org/10.1038/nmeth1079
Ehm, O., Goritz, C., Covic, M., Schaffner, I., Schwarz, T. J., Karaca, E., et al. (2010). RBPJ - Dependent Signaling Is Essential for Long-Term Maintenance of Neural Stem Cells in the Adult Hippocampus. *The Journal of Neuroscience*, *30*(41), 13794–13807. http://doi.org/10.1523/JNEUROSCI.1567-10.2010
Ernst, A., Alkass, K., Bernard, S., Salehpour, M., Perl, S., Tisdale, J., et al. (2014). Neurogenesis in the Striatum of the Adult Human Brain. *Cell*, *156*(5), 1072–1083. http://doi.org/10.1016/j.cell.2014.01.044
Ernst, A., Campos, B., Meier, J., Devens, F., Liesenberg, F., Wolter, M., et al. (2010). De-repression of CTGF via the miR-17-92 cluster upon differentiation of human glioblastoma spheroid cultures. *Oncogene*, 1–12. http://doi.org/10.1038/onc.2010.83
Ferrón, S. R., Charalambous, M., Radford, E., McEwen, K., Wildner, H., Hind, E., et al. (2012). Postnatal loss of Dlk1 imprinting in stem cells and niche astrocytes regulates neurogenesis. *Nature*, *475*(7356), 381–385. http://doi.org/10.1038/nature10229
Feuermann, Y., Robinson, G. W., Zhu, B.-M., Kang, K., Raviv, N., Yamaji, D., & Hennighausen, L. (2012). The miR-17/92cluster is targeted by STAT5 but dispensable for

mammary development. *Genesis*, *50*(9), 665–671. http://doi.org/10.1002/dvg.22023
Fontana, L., Fiori, M. E., Albini, S., Cifaldi, L., Giovinazzi, S., Forloni, M., et al. (2008). Antagomir-17-5p Abolishes the Growth of Therapy-Resistant Neuroblastoma through p21 and BIM. *PLoS ONE*, *3*(5), e2236–13. http://doi.org/10.1371/journal.pone.0002236
Forsberg, E. C., Passegué, E., Prohaska, S. S., Wagers, A. J., Koeva, M., Stuart, J. M., & Weissman, I. L. (2010). Molecular Signatures of Quiescent, Mobilized and Leukemia-Initiating Hematopoietic Stem Cells. *PLoS ONE*, *5*(1), e8785. http://doi.org/10.1371/journal.pone.0008785
Fuentealba, L. C., Obernier, K., & Alvarez-Buylla, A. (2012). Adult neural stem cells bridge their niche. *Cell Stem Cell*, *10*(6), 698–708. http://doi.org/10.1016/j.stem.2012.05.012
Fujimura, S., Jiang, Q., Kobayashi, C., & Nishinakamura, R. (2010). Notch2 Activation in the Embryonic Kidney Depletes Nephron Progenitors. *Journal of the American Society of Nephrology : JASN*, *21*(5), 803–810. http://doi.org/10.1681/ASN.2009040353
Fukada, S.-I., Uezumi, A., Ikemoto, M., Masuda, S., Segawa, M., Tanimura, N., et al. (2007). Molecular Signature of Quiescent Satellite Cells in Adult Skeletal Muscle. *Stem Cells*, *25*(10), 2448–2459. http://doi.org/10.1634/stemcells.2007-0019
Gaengel, K., Niaudet, C., Hagikura, K., Laviña, B., Muhl, L., Hofmann, J. J., et al. (2012). The Sphingosine-1-Phosphate Receptor S1PR1 Restricts Sprouting Angiogenesis by Regulating the Interplay between VE-Cadherin and VEGFR2, *23*(3), 587–599. http://doi.org/10.1016/j.devcel.2012.08.005
Gangaraju, V. K., & Lin, H. (2009). MicroRNAs: key regulators of stem cells. *Nature Reviews Molecular Cell Biology*, *10*(2), 116–125. http://doi.org/10.1038/nrm2621
Garcia, A. D. R., Doan, N. B., Imura, T., Bush, T. G., & Sofroniew, M. V. (2004). GFAP-expressing progenitors are the principal source of constitutive neurogenesis in adult mouse forebrain. *Nature Neuroscience*, *7*(11), 1233–1241. http://doi.org/10.1038/nn1340
Garg, N., Po, A., Miele, E., Campese, A. F., Begalli, F., Silvano, M., et al. (2013). microRNA-17-92 cluster is a direct Nanog target and controls neural stem cell through Trp53inp1. *The EMBO Journal*, *32*(21), 2819–2832. http://doi.org/10.1038/emboj.2013.214
Georgantas, R. W., III, Hildreth, R., Morisot, S., Alder, J., Liu, C.-G., Heimfeld, S., et al. (2007). CD34+ hematopoietic stem-progenitor cell microRNA expression and function: A circuit diagram of differentiation control. *Proceedings of the National Academy of Sciences of the United States of America*, *104*(8), 2750–2755. http://doi.org/10.1073/pnas.0610983104
Gheusi, G., Cremer, H., McLean, H., Chazal, G., Vincent, J. D., & Lledo, P. M. (2000). Importance of newly generated neurons in the adult olfactory bulb for odor discrimination. *Proceedings of the National Academy of Sciences of the United States of America*, *97*(4), 1823–1828.
Giachino, C., Basak, O., Lugert, S., Knuckles, P., Obernier, K., Fiorelli, R., et al. (2014). Molecular Diversity Subdivides the Adult Forebrain Neural Stem Cell Population. *Stem Cells*, *32*(1), 70–84. http://doi.org/10.1002/stem.1520
Gleeson, J. G., Lin, P. T., Flanagan, L. A., & Walsh, C. A. (1999). Doublecortin Is a Microtubule-Associated Protein and Is Expressed Widely by Migrating Neurons. *Neuron*, *23*(2), 257–271. http://doi.org/10.1016/s0896-6273(00)80778-3
Globus, J. H., & Kuhlenbeck, H. (1944). The subependymal cell plate (matrix) and its relationship to brain tumors of the ependymal type. *Journal of Neuropathology & …*, *3*(1), 1–35. http://doi.org/10.1097/00005072-194401000-00001
Graham, V., Khudyakov, J., Ellis, P., & Pevny, L. (2003). SOX2 Functions to Maintain Neural

Progenitor Identity. *Neuron*, *39*(5), 749–765. http://doi.org/10.1016/S0896-6273(03)00497-5
Gratton, M.-O., Torban, E., Jasmin, S. B., Theriault, F. M., German, M. S., & Stifani, S. (2003). Hes6 promotes cortical neurogenesis and inhibits Hes1 transcription repression activity by multiple mechanisms. *Molecular and Cellular Biology*, *23*(19), 6922–6935. http://doi.org/10.1128/MCB.23.19.6922-6935.2003
Groves, A., Kihara, Y., & Chun, J. (2013). Journal of the Neurological Sciences. *Journal of the Neurological Sciences*, *328*(1-2), 9–18. http://doi.org/10.1016/j.jns.2013.02.011
Gur, G., Rubin, C., Katz, M., Amit, I., Citri, A., Nilsson, J., et al. (2004). LRIG1 restricts growth factor signaling by enhancing receptor ubiquitylation and degradation. *The EMBO Journal*, *23*(16), 3270–3281. http://doi.org/10.1038/sj.emboj.7600342
Ha, T.-Y. (2011). MicroRNAs in Human Diseases: From Cancer to Cardiovascular Disease. *Immune Network*, *11*(3), 135–154. http://doi.org/10.4110/in.2011.11.3.135
He, L., & Hannon, G. J. (2004). MicroRNAs: small RNAs with a big role in gene regulation. *Nature Reviews. Genetics*, *5*(7), 522–531. http://doi.org/10.1038/nrg1379
He, L., Thomson, J. M., Hemann, M. T., Hernando-Monge, E., Mu, D., Goodson, S., et al. (2005). A microRNA polycistron as a potential human oncogene. *Nature Cell Biology*, *435*(7043), 828–833. http://doi.org/10.1038/nature03552
Herzenberg, L. A., Parks, D., Sahaf, B., Perez, O., Roederer, M., & Herzenberg, L. A. (2002). The history and future of the fluorescence activated cell sorter and flow cytometry: a view from Stanford. *Clinical Chemistry*, *48*(10), 1819–1827.
Hébert, S. S., Papadopoulou, A. S., Smith, P., Galas, M.-C., Planel, E., Silahtaroglu, A. N., et al. (2010). Genetic ablation of Dicer in adult forebrain neurons results in abnormal tau hyperphosphorylation and neurodegeneration., *19*(20), 3959–3969. http://doi.org/10.1093/hmg/ddq311
Imayoshi, I., Sakamoto, M., & Kageyama, R. (2011). Genetic methods to identify and manipulate newly born neurons in the adult brain. *Frontiers in Neuroscience*, *5*, 64. http://doi.org/10.3389/fnins.2011.00064
Imayoshi, I., Sakamoto, M., Ohtsuka, T., Takao, K., Miyakawa, T., Yamaguchi, M., et al. (2008). Roles of continuous neurogenesis in the structural and functional integrity of the adult forebrain. *Nature Neuroscience*, *11*(10), 1153–1161. http://doi.org/10.1038/nn.2185
Ivanova, N. B., Dimos, J. T., Schaniel, C., Hackney, J. A., Moore, K. A., & Lemischka, I. R. (2002). A stem cell molecular signature. *Science*, *298*(5593), 601–604. http://doi.org/10.1126/science.1073823
Jensen, K. B., & Watt, F. M. (2006). Single-cell expression profiling of human epidermal stem and transit-amplifying cells: Lrig1 is a regulator of stem cell quiescence. *Proceedings of the National Academy of Sciences of the United States of America*, *103*(32), 11958–11963. http://doi.org/10.1073/pnas.0601886103
Jensen, K. B., Collins, C. A., Nascimento, E., Tan, D. W., Frye, M., Itami, S., & Watt, F. M. (2009). Lrig1 expression defines a distinct multipotent stem cell population in mammalian epidermis. *Cell Stem Cell*, *4*(5), 427–439. http://doi.org/10.1016/j.stem.2009.04.014
Jhaveri, D. J., O'Keeffe, I., Robinson, G. J., Zhao, Q. Y., Zhang, Z. H., Nink, V., et al. (2015). Purification of Neural Precursor Cells Reveals the Presence of Distinct, Stimulus-Specific Subpopulations of Quiescent Precursors in the Adult Mouse Hippocampus. *Journal of Neuroscience*, *35*(21), 8132–8144. http://doi.org/10.1523/JNEUROSCI.0504-15.2015
Jonas, S., & Izaurralde, E. (2015). Towards a molecular understanding of microRNA-mediated gene silencing. *Nature Publishing Group*, *16*(7), 421–433. http://doi.org/10.1038/nrg3965

Julius, M. H., Masuda, T., & Herzenberg, L. A. (1972). Demonstration that antigen-binding cells are precursors of antibody-producing cells after purification with a fluorescence-activated cell sorter. *Proceedings of the National Academy of Sciences of the United States of America*, *69*(7), 1934–1938.

Kaplan, M. S., McNelly, N. A., & Hinds, J. W. (1985). Population-Dynamics of Adult-Formed Granule Neurons of the Rat Olfactory-Bulb. *The Journal of Comparative Neurology*, *239*(1), 117–125. http://doi.org/10.1002/cne.902390110

Kappos, L., Antel, J., Comi, G., Montalban, X., O'Connor, P., Polman, C. H., et al. (2006). Oral fingolimod (FTY720) for relapsing multiple sclerosis. *The New England Journal of Medicine*, *355*(11), 1124–1140. http://doi.org/10.1056/NEJMoa052643

Kawaguchi, A., Miyata, T., Sawamoto, K., Takashita, N., Murayama, A., Akamatsu, W., et al. (2001). Nestin-EGFP Transgenic Mice: Visualization of the Self-Renewal and Multipotency of CNS Stem Cells. *Molecular and Cellular Neuroscience*, *17*(2), 259–273. http://doi.org/10.1006/mcne.2000.0925

Kawaguchi, D., Furutachi, S., Kawai, H., Hozumi, K., & Gotoh, Y. (2013). Dll1 maintains quiescence of adult neural stem cells and segregates asymmetrically during mitosis. *Nature Communications*, *4*, 1–12. http://doi.org/10.1038/ncomms2895

Kazanis, I., Lathia, J. D., Vadakkan, T. J., Raborn, E., Wan, R., Mughal, M. R., et al. (2010). Quiescence and activation of stem and precursor cell populations in the subependymal zone of the mammalian brain are associated with distinct cellular and extracellular matrix signals. *Journal of Neuroscience*, *30*(29), 9771–9781. http://doi.org/10.1523/JNEUROSCI.0700-10.2010

Kenney, A. M. (2003). Nmyc upregulation by sonic hedgehog signaling promotes proliferation in developing cerebellar granule neuron precursors. *Development*, *130*(1), 15–28. http://doi.org/10.1242/dev.00182

Kershman, J. (1938). The Medulloblast and the Medulloblastoma. *Archives of Neurology & Psychiatry*, *40*(5), 937. http://doi.org/10.1001/archneurpsyc.1938.02270110091007

Kim, E. J., Ables, J. L., Dickel, L. K., Eisch, A. J., & Johnson, J. E. (2011). Ascl1 (Mash1) Defines Cells with Long-Term Neurogenic Potential in Subgranular and Subventricular Zones in Adult Mouse Brain. *PLoS ONE*, *6*(3), e18472. http://doi.org/10.1371/journal.pone.0018472

Kimura, A., Ohmori, T., Ohkawa, R., Madoiwa, S., Mimuro, J., Murakami, T., et al. (2006). Essential Roles of Sphingosine 1-Phosphate/S1P 1Receptor Axis in the Migration of Neural Stem Cells Toward a Site of Spinal Cord Injury. *Stem Cells*, *25*(1), 115–124. http://doi.org/10.1634/stemcells.2006-0223

Knobloch, M., Braun, S. M. G., Zurkirchen, L., Schoultz, von, C., Zamboni, N., Araúzo-Bravo, M. J., et al. (2013). Metabolic control of adult neural stem cell activity by Fasn-dependent lipogenesis. *Nature*, *493*(7431), 226–230. http://doi.org/10.1038/nature11689

Kokovay, E., Goderie, S., Wang, Y., Lotz, S., Lin, G., Sun, Y., et al. (2010). Adult SVZ lineage cells home to and leave the vascular niche via differential responses to SDF1/CXCR4 signaling. *Cell Stem Cell*, *7*(2), 163–173. http://doi.org/10.1016/j.stem.2010.05.019

Kokovay, E., Wang, Y., Kusek, G., Wurster, R., Lederman, P., Lowry, N., et al. (2012). VCAM1 is essential to maintain the structure of the SVZ niche and acts as an environmental sensor to regulate SVZ lineage progression. *Cell Stem Cell*, *11*(2), 220–230. http://doi.org/10.1016/j.stem.2012.06.016

Koralov, S. B., Muljo, S. A., Galler, G. R., Krek, A., Chakraborty, T., Kanellopoulou, C., et al.

(2008). Dicer ablation affects antibody diversity and cell survival in the B lymphocyte lineage. *Cell*, *132*(5), 860–874. http://doi.org/10.1016/j.cell.2008.02.020
Kretzschmar, K., & Watt, F. M. (2012). Lineage Tracing. *Cell*, *148*(1-2), 33–45. http://doi.org/10.1016/j.cell.2012.01.002
Kriegstein, A., & Alvarez-Buylla, A. (2009). The Glial Nature of Embryonic and Adult Neural Stem Cells. *Annual Review of Neuroscience*, *32*(1), 149–184. http://doi.org/10.1146/annurev.neuro.051508.135600
Kuo, C. T., Mirzadeh, Z., Soriano-Navarro, M., Rašin, M., Wang, D., Shen, J., et al. (2006). Postnatal Deletion of Numb/Numblike Reveals Repair and Remodeling Capacity in the Subventricular Neurogenic Niche. *Cell*, *127*(6), 1253–1264. http://doi.org/10.1016/j.cell.2006.10.041
Lau, L. F., & Nathans, D. (1987). Expression of a set of growth-related immediate early genes in BALB/c 3T3 cells: coordinate regulation with c-fos or c-myc. *Proceedings of the National Academy of Sciences of the United States of America*, *84*(5), 1182–1186.
Lee, H., Deng, J., Kujawski, M., Yang, C., Liu, Y., Herrmann, A., et al. (2010). STAT3-induced S1PR1 expression is crucial for persistent STAT3 activation in tumors. *Nature Medicine*, 1–9. http://doi.org/10.1038/nm.2250
Lendahl, U., Zimmerman, L. B., & McKay, R. D. (1990). CNS stem cells express a new class of intermediate filament protein. *Cell*, *60*(4), 585–595.
Lewis, B. P., Burge, C. B., & Bartel, D. P. (2005). Conserved Seed Pairing, Often Flanked by Adenosines, Indicates that Thousands of Human Genes are MicroRNA Targets. *Cell*, *120*(1), 15–20. http://doi.org/10.1016/j.cell.2004.12.035
Li, J. H., Liu, S., Zhou, H., Qu, L. H., & Yang, J. H. (2013). starBase v2.0: decoding miRNA-ceRNA, miRNA-ncRNA and protein-RNA interaction networks from large-scale CLIP-Seq data. *Nucleic Acids Research*, *42*(D1), D92–D97. http://doi.org/10.1093/nar/gkt1248
Li, L., & Clevers, H. (2010). Coexistence of quiescent and active adult stem cells in mammals. *Science*, *327*(5965), 542–545. http://doi.org/10.1126/science.1180794
Li, Y., Vecchiarelli-Federico, L. M., Li, Y. J., Egan, S. E., Spaner, D., Hough, M. R., & Ben-David, Y. (2012). The miR-17-92 cluster expands multipotent hematopoietic progenitors whereas imbalanced expression of its individual oncogenic miRNAs promotes leukemia in mice. *Blood*, *119*(19), 4486–4498. http://doi.org/10.1182/blood-2011-09-378687
Li, Z., & Rana, T. M. (2014). Therapeutic targeting of microRNAs: current status and future challenges. *Nature Publishing Group*, *13*(8), 622–638. http://doi.org/10.1038/nrd4359
Lim, D. A., & Alvarez-Buylla, A. (2014). Adult neural stem cells stake their ground. *Trends in Neurosciences*, *37*(10), 563–571. http://doi.org/10.1016/j.tins.2014.08.006
Lim, D. A., Suárez-Fariñas, M., Naef, F., Hacker, C. R., Menn, B., Takebayashi, H., et al. (2006). In vivo transcriptional profile analysis reveals RNA splicing and chromatin remodeling as prominent processes for adult neurogenesis. *Molecular and Cellular Neurosciences*, *31*(1), 131–148. http://doi.org/10.1016/j.mcn.2005.10.005
Lim, W. K., Wang, K., Lefebvre, C., & Califano, A. (2007). Comparative analysis of microarray normalization procedures: effects on reverse engineering gene networks. *Bioinformatics*. http://doi.org/10.1093/bioinformatics/btm201
Liu, C., Teng, Z.-Q., Santistevan, N. J., Szulwach, K. E., Guo, W., Jin, P., & Zhao, X. (2010). Epigenetic regulation of miR-184 by MBD1 governs neural stem cell proliferation and differentiation. *Cell Stem Cell*, *6*(5), 433–444. http://doi.org/10.1016/j.stem.2010.02.017
Liu, J., Carmell, M. A., Rivas, F. V., Marsden, C. G., Thomson, J. M., Song, J.-J., et al. (2004).

Argonaute2 is the catalytic engine of mammalian RNAi. *Science*, *305*(5689), 1437–1441. http://doi.org/10.1126/science.1102513

Liu, X. S., Chopp, M., Wang, X. L., Zhang, L., Hozeska-Solgot, A., Tang, T., et al. (2013). MicroRNA-17-92 Cluster Mediates the Proliferation and Survival of Neural Progenitor Cells after Stroke. *Journal of Biological Chemistry*, *288*(18), 12478–12488. http://doi.org/10.1074/jbc.M112.449025

Liu, Y., Deng, J., Wang, L., Lee, H., Armstrong, B., Scuto, A., et al. (2012). S1PR1 is an effective target to block STAT3 signaling in activated B cell-like diffuse large B-cell lymphoma. *Blood*, *120*(7), 1458–1465. http://doi.org/10.1182/blood-2011-12-399030

Livak, K. J., & Schmittgen, T. D. (2001). Analysis of Relative Gene Expression Data Using Real-Time Quantitative PCR and the 2−ΔΔCT Method. *Methods*, *25*(4), 402–408. http://doi.org/10.1006/meth.2001.1262

Llorens-Bobadilla, E., Zhao, S., Baser, A., Saiz-Castro, G., Zwadlo, K., & Martin-Villalba, A. (2015). Single-Cell Transcriptomics Reveals a Population of Dormant Neural Stem Cells that Become Activated upon Brain Injury. *Stem Cell*, 1–13. http://doi.org/10.1016/j.stem.2015.07.002

Lois, C., & Alvarez-Buylla, A. (1994). Long-distance neuronal migration in the adult mammalian brain. *Science*, *264*(5162), 1145–1148. http://doi.org/10.1126/science.8178174

Lopez-Juarez, A., Howard, J., Ullom, K., Howard, L., Grande, A., Pardo, A., et al. (2013). Gsx2 controls region-specific activation of neural stem cells and injury-induced neurogenesis in the adult subventricular zone. *Genes & Development*, *27*(11), 1272–1287. http://doi.org/10.1101/gad.217539.113

Louvi, A., & Artavanis-Tsakonas, S. (2006). Notch signalling in vertebrate neural development. *Nature Reviews Neuroscience*, *7*(2), 93–102. http://doi.org/10.1038/nrn1847

Lu, Y., Thomson, J. M., Wong, H. Y. F., Hammond, S. M., & Hogan, B. L. M. (2007). Transgenic over-expression of the microRNA miR-17-92 cluster promotes proliferation and inhibits differentiation of lung epithelial progenitor cells. *Developmental Biology*, *310*(2), 442–453. http://doi.org/10.1016/j.ydbio.2007.08.007

Maceyka, M., Harikumar, K. B., Milstien, S., & Spiegel, S. (2012). Sphingosine-1-phosphate signalingand its role in disease. *Trends in Cell Biology*, *22*(1), 50–60. http://doi.org/10.1016/j.tcb.2011.09.003

Malzkorn, B., Wolter, M., Liesenberg, F., Grzendowski, M., Stühler, K., Meyer, H. E., & Reifenberger, G. (2010). Identification and Functional Characterization of microRNAs Involved in the Malignant Progression of Gliomas. *Brain Pathology*, *20*(3), 539–550. http://doi.org/10.1111/j.1750-3639.2009.00328.x

Mao, S., Li, H., Sun, Q., Zen, K., Zhang, C.-Y., & Li, L. (2014). miR-17 regulates the proliferation and differentiation of the neural precursor cells during mouse corticogenesis. *FEBS Journal*, *281*(4), 1144–1158. http://doi.org/10.1111/febs.12680

Marfia, G., Campanella, R., Navone, S. E., Di Vito, C., Riccitelli, E., Hadi, L. A., et al. (2014). Autocrine/paracrine sphingosine-1-phosphate fuels proliferative and stemness qualities of glioblastoma stem cells. *Glia*, *62*(12), 1968–1981. http://doi.org/10.1002/glia.22718

Marqués-Torrejón, M. Á., Porlan, E., Banito, A., Gómez-Ibarlucea, E., Lopez-Contreras, A. J., Fernández-Capetillo, O., et al. (2013). Cyclin-dependent kinase inhibitor p21 controls adult neural stem cell expansion by regulating Sox2 gene expression. *Cell Stem Cell*, *12*(1), 88–100. http://doi.org/10.1016/j.stem.2012.12.001

Marrone, A. K., Stolz, D. B., Bastacky, S. I., Kostka, D., Bodnar, A. J., & Ho, J. (2014).

MicroRNA-17 92 Is Required for Nephrogenesis and Renal Function. *Journal of the American Society of Nephrology*. http://doi.org/10.1681/ASN.2013040390
Marshall, C. A. G., Novitch, B. G., & Goldman, J. E. (2005). Olig2 directs astrocyte and oligodendrocyte formation in postnatal subventricular zone cells. *Journal of Neuroscience*, *25*(32), 7289–7298. http://doi.org/10.1523/JNEUROSCI.1924-05.2005
Martinez-Morales, P. L., Quiroga, A. C., Barbas, J. A., & Morales, A. V. (2010). SOX5 controls cell cycle progression in neural progenitors by interfering with the WNT–β-catenin pathway. *EMBO Reports*, *11*(6), 466–472. http://doi.org/10.1038/embor.2010.61
Meenhuis, A., van Veelen, P. A., de Looper, H., van Boxtel, N., van den Berge, I. J., Sun, S. M., et al. (2011). MiR-17/20/93/106 promote hematopoietic cell expansion by targeting sequestosome 1-regulated pathways in mice. *Blood*, *118*(4), 916–925. http://doi.org/10.1182/blood-2011-02-336487
Menn, B., Garcia-Verdugo, J. M., Yaschine, C., Gonzalez Perez, O., Rowitch, D., & Alvarez-Buylla, A. (2006). Origin of oligodendrocytes in the subventricular zone of the adult brain. *Journal of Neuroscience*, *26*(30), 7907–7918. http://doi.org/10.1523/JNEUROSCI.1299-06.2006
Merkle, F. T., Fuentealba, L. C., Sanders, T. A., Magno, L., Kessaris, N., & Alvarez-Buylla, A. (2014). Adult neural stem cells in distinct microdomains generate previously unknown interneuron types. *Nature Neuroscience*, *17*(2), 207–214. http://doi.org/10.1038/nn.3610
Mira, H., Andreu, Z., Suh, H., Lie, D. C., Jessberger, S., Consiglio, A., et al. (2010). Signaling through BMPR-IA regulates quiescence and long-term activity of neural stem cells in the adult hippocampus. *Cell Stem Cell*, *7*(1), 78–89. http://doi.org/10.1016/j.stem.2010.04.016
Mirzadeh, Z., Merkle, F. T., Soriano-Navarro, M., Garcia-Verdugo, J. M., & Alvarez-Buylla, A. (2008). Neural stem cells confer unique pinwheel architecture to the ventricular surface in neurogenic regions of the adult brain. *Cell Stem Cell*, *3*(3), 265–278. http://doi.org/10.1016/j.stem.2008.07.004
Mizuno, Y., Yagi, K., Tokuzawa, Y., Kanesaki-Yatsuka, Y., Suda, T., Katagiri, T., et al. (2008). miR-125b inhibits osteoblastic differentiation by down-regulation of cell proliferation. *Biochemical and Biophysical Research Communications*, *368*(2), 267–272. http://doi.org/10.1016/j.bbrc.2008.01.073
Mizutani, K.-I., Yoon, K., Dang, L., & Tokunaga, A. (2007). Differential Notch signalling distinguishes neural stem cells from intermediate progenitors. *Nature*, *449*(7160), 351–355. http://doi.org/10.1038/nature06090
Mogilyansky, E., & Rigoutsos, I. (2013). The miR-17/92 cluster: a comprehensive update on its genomics, genetics, functions and increasingly important and numerous roles in health and disease. *Cell Death and Differentiation*, *20*(12), 1603–1614. http://doi.org/10.1038/cdd.2013.125
Montalbán-Loro, R. (2015). Epigenetic regulation of stemness maintenance in the neurogenic niches. *World Journal of Stem Cells*, *7*(4), 700. http://doi.org/10.4252/wjsc.v7.i4.700
Morrison, S. J., White, P. M., Zock, C., & Anderson, D. J. (1999). Prospective Identification, Isolation by Flow Cytometry, and In Vivo Self-Renewal of Multipotent Mammalian Neural Crest Stem Cells. *Cell*, *96*(5), 737–749. http://doi.org/10.1016/S0092-8674(00)80583-8
Mu, P., Han, Y. C., Betel, D., Yao, E., Squatrito, M., Ogrodowski, P., et al. (2009). Genetic dissection of the miR-17 92 cluster of microRNAs in Myc-induced B-cell lymphomas. *Genes & Development*, *23*(24), 2806–2811. http://doi.org/10.1101/gad.1872909
Mullen, R. J., Buck, C. R., & Smith, A. M. (1992). NeuN, a neuronal specific nuclear protein in

vertebrates. *Development*, *116*(1), 201–211.
Murphy, L. J., Murphy, L. C., & Friesen, H. G. (1987). Estrogen induction of N-myc and c-myc proto-oncogene expression in the rat uterus. *Endocrinology*, *120*(5), 1882–1888. http://doi.org/10.1210/endo-120-5-1882
Muzumdar, M. D., Tasic, B., Miyamichi, K., Li, L., & Luo, L. (2007). A global double-fluorescent Cre reporter mouse. *Genesis*, *45*(9), 593–605. http://doi.org/10.1002/dvg.20335
Nacher, J., Crespo, C., & McEwen, B. S. (2001). Doublecortin expression in the adult rat telencephalon. *European Journal of Neuroscience*, *14*(4), 629–644. http://doi.org/10.1046/j.0953-816x.2001.01683.x
Nait-Oumesmar, B., Decker, L., Lachapelle, F., Avellana-Adalid, V., Bachelin, C., & Baron-Van Evercooren, A. (1999). Progenitor cells of the adult mouse subventricular zone proliferate, migrate and differentiate into oligodendrocytes after demyelination. *The European Journal of Neuroscience*, *11*(12), 4357–4366.
Naka-Kaneda, H., Nakamura, S., Igarashi, M., Aoi, H., Kanki, H., Tsuyama, J., et al. (2014). The miR-17/106-p38 axis is a key regulator of the neurogenic-to-gliogenic transition in developing neural stem/progenitor cells. *Proceedings of the National Academy of Sciences*, *111*(4), 1604–1609. http://doi.org/10.1073/pnas.1315567111
Nicolis, S. K. (2007). Cancer stem cells and "stemness" genes in neuro-oncology. *Neurobiology of Disease*, *25*(2), 217–229. http://doi.org/10.1016/j.nbd.2006.08.022
Nishimura, H., Akiyama, T., Irei, I., Hamazaki, S., & Sadahira, Y. (2010). Cellular Localization of Sphingosine-1-phosphate Receptor 1 Expression in the Human Central Nervous System. *Journal of Histochemistry & Cytochemistry*, *58*(9), 847–856. http://doi.org/10.1369/jhc.2010.956409
Nyfeler, Y., Kirch, R. D., Mantei, N., Leone, D. P., Radtke, F., Suter, U., & Taylor, V. (2005). Jagged1 signals in the postnatal subventricular zone are required for neural stem cell self-renewal. *The EMBO Journal*, *24*(19), 3504–3515. http://doi.org/10.1038/sj.emboj.7600816
Olive, V., Bennett, M. J., Walker, J. C., Ma, C., Jiang, I., Cordon-Cardo, C., et al. (2009). miR-19 is a key oncogenic component of mir-17-92. *Genes & Development*, *23*(24), 2839–2849. http://doi.org/10.1101/gad.1861409
Olive, V., Jiang, I., & He, L. (2010). mir-17-92, a cluster of miRNAs in the midst of the cancer network. *The International Journal of Biochemistry & Cell Biology*, *42*(8), 1348–1354. http://doi.org/10.1016/j.biocel.2010.03.004
Olive, V., Li, Q., & He, L. (2013a). mir-17-92: a polycistronic oncomir with pleiotropic functions. *Immunological Reviews*, *253*(1), 158–166. http://doi.org/10.1111/imr.12054
Olive, V., Sabio, E., Bennett, M. J., De Jong, C. S., Biton, A., McGann, J. C., et al. (2013b). A component of the mir-17-92 polycistronic oncomir promotes oncogene-dependent apoptosis. *eLife*, *2*(0), e00822–e00822. http://doi.org/10.7554/eLife.00822
Pallafacchina, G., François, S., Regnault, B., Czarny, B., Dive, V., Cumano, A., et al. (2010). An adult tissue-specific stem cell in its niche: A gene profiling analysis of in vivo quiescent and activated muscle satellite cells. *Stem Cell Research*, *4*(2), 77–91. http://doi.org/10.1016/j.scr.2009.10.003
Parras, C. M., Galli, R., Britz, O., Soares, S., Galichet, C., Battiste, J., et al. (2004). Mash1 specifies neurons and oligodendrocytes in the postnatal brain. *The EMBO Journal*, *23*(22), 4495–4505. http://doi.org/10.1038/sj.emboj.7600447
Pastrana, E., Cheng, L.-C., & Doetsch, F. (2009). Simultaneous prospective purification of adult subventricular zone neural stem cells and their progeny. *Proceedings of the National*

Academy of Sciences, *106*(15), 6387–6392. http://doi.org/10.1073/pnas.0810407106
Pastrana, E., Silva-Vargas, V., & Doetsch, F. (2011). Protocol Review. *Stem Cell*, *8*(5), 486–498. http://doi.org/10.1016/j.stem.2011.04.007
Perini, G., Diolaiti, D., Porro, A., & Valle, Della, G. (2005). In vivo transcriptional regulation of N-Myc target genes is controlled by E-box methylation. *Proceedings of the National Academy of Sciences of the United States of America*, *102*(34), 12117–12122. http://doi.org/10.1073/pnas.0409097102
Petreanu, L., & Alvarez-Buylla, A. (2002). Maturation and death of adult-born olfactory bulb granule neurons: role of olfaction. *Journal of Neuroscience*, *22*(14), 6106–6113.
Ponti, G., Obernier, K., Guinto, C., Jose, L., Bonfanti, L., & Alvarez-Buylla, A. (2013). Cell cycle and lineage progression of neural progenitors in the ventricular-subventricular zones of adult mice. *Proceedings of the National Academy of Sciences*, *110*(11), E1045–54. http://doi.org/10.1073/pnas.1219563110
Porlan, E., Marti-Prado, B., Morante-Redolat, J. M., Consiglio, A., Delgado, A. C., Kypta, R., et al. (2014). MT5-MMP regulates adult neural stem cell functional quiescence through the cleavage of N-cadherin. *Nature Cell Biology*, *16*(7), 629–638. http://doi.org/10.1038/ncb2993
Porlan, E., Morante-Redolat, J. M., Marqués-Torrejón, M. Á., Andreu-Agulló, C., Carneiro, C., Gómez-Ibarlucea, E., et al. (2013). Transcriptional repression of Bmp2 by p21. *Nature Neuroscience*, *16*(11), 1567–1575. http://doi.org/10.1038/nn.3545
Powell, A. E., Wang, Y., Li, Y., Poulin, E. J., Means, A. L., Washington, M. K., et al. (2012). The Pan-ErbB Negative Regulator Lrig1 Is an Intestinal Stem Cell Markerthat Functions as a Tumor Suppressor. *Cell*, *149*(1), 146–158. http://doi.org/10.1016/j.cell.2012.02.042
Ravi, N., Li, Z., Oettl, L. L., Bartsch, D., Schonig, K., & Kelsch, W. (2015). Postnatal subventricular zone progenitors switch their fate to generate neurons with distinct synaptic input patterns. *Development*, *142*(2), 303–313. http://doi.org/10.1242/dev.110767
Reya, T., Morrison, S. J., Clarke, M. F., & Weissman, I. L. (2001). Stem cells, cancer, and cancer stem cells. *Nature*, *414*(6859), 105–111. http://doi.org/10.1038/35102167
Reynolds, R., & Hardy, R. (1997). Oligodendroglial progenitors labeled with the O4 antibody persist in the adult rat cerebral cortex in vivo. *Journal of Neuroscience Research*, *47*(5), 455–470. http://doi.org/10.1002/(SICI)1097-4547(19970301)47:5<455::AID-JNR1>3.0.CO;2-G
Sakamoto, M., Ieki, N., Miyoshi, G., Mochimaru, D., Miyachi, H., Imura, T., et al. (2014a). Continuous Postnatal Neurogenesis Contributes to Formation of the Olfactory Bulb Neural Circuits and Flexible Olfactory Associative Learning. *Journal of Neuroscience*, *34*(17), 5788–5799. http://doi.org/10.1523/JNEUROSCI.0674-14.2014
Sakamoto, M., Kageyama, R., & Imayoshi, I. (2014b). The functional significance of newly born neurons integrated into olfactory bulb circuits. *Frontiers in Neuroscience*, *8*, 121. http://doi.org/10.3389/fnins.2014.00121
Salomoni, P., & Calegari, F. (2010). Cell cycle control of mammalian neural stem cells: putting a speed limit on G1. *Trends in Cell Biology*, *20*(5), 233–243. http://doi.org/10.1016/j.tcb.2010.01.006
Sanai, N., Alvarez-Buylla, A., & Berger, M. S. (2005). Neural stem cells and the origin of gliomas. *The New England Journal of Medicine*, *353*(8), 811–822. http://doi.org/10.1056/NEJMra043666
Sanai, N., Nguyen, T., Ihrie, R. A., Tsai, H.-H., Wong, M., Gupta, N., et al. (2011). Corridors of

migrating neurons in the human brain and their decline during infancy. *Nature*, *478*(7369), 382–386. http://doi.org/10.1038/nature10487

Sanai, N., Tramontin, A. D., Quiñones Hinojosa, A., Barbaro, N. M., Gupta, N., Kunwar, S., et al. (2004). Unique astrocyte ribbon in adult human brain contains neural stem cells but lacks chain migration. *Nature*, *427*(6976), 740–744. http://doi.org/10.1038/nature02301

Sato, K., Malchinkhuu, E., Horiuchi, Y., Mogi, C., Tomura, H., Tosaka, M., et al. (2007). HDL-like lipoproteins in cerebrospinal fluid affect neural cell activity through lipoprotein-associated sphingosine 1-phosphate. *Biochemical and Biophysical Research Communications*, *359*(3), 649–654. http://doi.org/10.1016/j.bbrc.2007.05.131

Schaper, A. (1897). The earliest differentiation in the central nervous system of Vertebrates. *Science*, *V*(115), 430–431.

Schulte, J. H., Horn, S., Otto, T., Samans, B., Heukamp, L. C., Eilers, U.-C., et al. (2008). MYCN regulates oncogenic MicroRNAs in neuroblastoma. *International Journal of Cancer*, *122*(3), 699–704. http://doi.org/10.1002/ijc.23153

Seri, B., García-Verdugo, J. M., McEwen, B. S., & Alvarez-Buylla, A. (2001). Astrocytes give rise to new neurons in the adult mammalian hippocampus. *The Journal of Neuroscience*, *21*(18), 7153–7160.

Shen, Q., Wang, Y., Kokovay, E., Lin, G., Chuang, S.-M., Goderie, S. K., et al. (2008). Adult SVZ stem cells lie in a vascular niche: a quantitative analysis of niche cell-cell interactions. *Cell Stem Cell*, *3*(3), 289–300. http://doi.org/10.1016/j.stem.2008.07.026

Shi, Y., Zhao, X., Hsieh, J., Wichterle, H., Impey, S., Banerjee, S., et al. (2010). MicroRNA regulation of neural stem cells and neurogenesis. *Journal of Neuroscience*, *30*(45), 14931–14936. http://doi.org/10.1523/JNEUROSCI.4280-10.2010

Shin, J., Berg, D. A., Zhu, Y., Shin, J. Y., Song, J., Bonaguidi, M. A., et al. (2015). Single-Cell RNA-Seq with Waterfall Reveals Molecular Cascades underlying Adult Neurogenesis. *Stem Cell*, 1–14. http://doi.org/10.1016/j.stem.2015.07.013

Shimojo, H., Ohtsuka, T., & Kageyama, R. (2008). Oscillations in notch signaling regulate maintenance of neural progenitors. *Neuron*, *58*(1), 52–64. http://doi.org/10.1016/j.neuron.2008.02.014

Silber, J., Lim, D. A., Petritsch, C., Persson, A. I., Maunakea, A. K., Yu, M., et al. (2008). miR-124 and miR-137 inhibit proliferation of glioblastoma multiforme cells and induce differentiation of brain tumor stem cells. *BMC Medicine*, *6*(1), 14–17. http://doi.org/10.1186/1741-7015-6-14

Silva-Vargas, V., Crouch, E. E., & Doetsch, F. (2013). ScienceDirectAdult neural stem cells and their niche: a dynamic duo during homeostasis, regeneration, and aging. *Current Opinion in Neurobiology*, *23*(6), 935–942. http://doi.org/10.1016/j.conb.2013.09.004

Simion, C., Cedano-Prieto, M. E., & Sweeney, C. (2014). The LRIG family: enigmatic regulators of growth factor receptor signaling. *Endocrine Related Cancer*, *21*(6), R431–R443. http://doi.org/10.1530/ERC-14-0179

Stroynowska-Czerwinska, A., Fiszer, A., & Krzyzosiak, W. J. (2014). The panorama of miRNA-mediated mechanisms in mammalian cells. *Cellular and Molecular Life Sciences : CMLS*, *71*(12), 2253–2270. http://doi.org/10.1007/s00018-013-1551-6

Subramanian, A., Tamayo, P., Mootha, V. K., Mukherjee, S., Ebert, B. L., Gillette, M. A., et al. (2005). Gene set enrichment analysis: a knowledge-based approach for interpreting genome-wide expression profiles. *Proceedings of the National Academy of Sciences of the United States of America*, *102*(43), 15545–15550. http://doi.org/10.1073/pnas.0506580102

Sun, E., & Shi, Y. (2015). MicroRNAs: Small molecules with big roles in neurodevelopment and diseases. *Experimental Neurology*, *268*(C), 46–53. http://doi.org/10.1016/j.expneurol.2014.08.005

Tao, J., Wu, H., Lin, Q., Wei, W., Lu, X.-H., Cantle, J. P., et al. (2011). Deletion of astroglial Dicer causes non-cell-autonomous neuronal dysfunction and degeneration. *Journal of Neuroscience*, *31*(22), 8306–8319. http://doi.org/10.1523/JNEUROSCI.0567-11.2011

Tassano, E., Di Rocco, M., Signa, S., & Gimelli, G. (2013). De novo 13q31.1-q32.1 interstitial deletion encompassing the miR-17-92cluster in a patient with Feingold syndrome-2. *American Journal of Medical Genetics Part A*, *161*(4), 894–896. http://doi.org/10.1002/ajmg.a.35781

Tavazoie, M., Van der Veken, L., Silva-Vargas, V., Louissaint, M., Colonna, L., Zaidi, B., et al. (2008). A specialized vascular niche for adult neural stem cells. *Cell Stem Cell*, *3*(3), 279–288. http://doi.org/10.1016/j.stem.2008.07.025

Trompeter, H.-I., Abbad, H., Iwaniuk, K. M., Hafner, M., Renwick, N., Tuschl, T., et al. (2011). MicroRNAs MiR-17, MiR-20a, and MiR-106b Act in Concert to Modulate E2F Activity on Cell Cycle Arrest during Neuronal Lineage Differentiation of USSC. *PLoS ONE*, *6*(1), e16138. http://doi.org/10.1371/journal.pone.0016138

Tung, Y.-T., Lu, Y.-L., Peng, K.-C., Yen, Y.-P., Chang, M., Li, J., et al. (2015). Mir-17~92 Governs Motor Neuron Subtype Survival by Mediating Nuclear PTEN. *CellReports*, *11*(8), 1305–1318. http://doi.org/10.1016/j.celrep.2015.04.050

Uchida, N., Buck, D. W., He, D., Reitsma, M. J., Masek, M., Phan, T. V., et al. (2000). Direct isolation of human central nervous system stem cells. *Proceedings of the National Academy of Sciences of the United States of America*, *97*(26), 14720–14725. http://doi.org/10.1073/pnas.97.26.14720

Van A Doze, & Perez, D. M. (2013). GPCRs in Stem Cell Function. *Oligomerization and Allosteric Modulation in G-Protein Coupled Receptors* (1st ed., Vol. 115, pp. 175–216). Elsevier Inc. http://doi.org/10.1016/B978-0-12-394587-7.00005-1

van Bokhoven, H., Celli, J., van Reeuwijk, J., Rinne, T., Glaudemans, B., van Beusekom, E., et al. (2005). MYCN haploinsufficiency is associated with reduced brain size and intestinal atresias in Feingold syndrome. *Nature Genetics*, *37*(5), 465–467. http://doi.org/10.1038/ng1546

Van Den Berge, S. A., Middeldorp, J., Zhang, C. E., Curtis, M. A., Leonard, B. W., Mastroeni, D., et al. (2010). Longterm quiescent cells in the aged human subventricular neurogenic system specifically express GFAP-δ. *Aging Cell*, *9*(3), 313–326. http://doi.org/10.1111/j.1474-9726.2010.00556.x

vanEngeland, M., Ramaekers, F., Schutte, B., & Reutelingsperger, C. (1996). A novel assay to measure loss of plasma membrane asymmetry during apoptosis of adherent cells in culture. *Cytometry*, *24*(2), 131–139. http://doi.org/10.1002/(SICI)1097-0320(19960601)24:2<131::AID-CYTO5>3.0.CO;2-M

Venezia, T. A., Merchant, A. A., Ramos, C. A., Whitehouse, N. L., Young, A. S., Shaw, C. A., & Goodell, M. A. (2004). Molecular Signatures of Proliferation and Quiescence in Hematopoietic Stem Cells. *PLoS Biology*, *2*(10), e301. http://doi.org/10.1371/journal.pbio.0020301

Ventura, A., Young, A. G., Winslow, M. M., Lintault, L., Meissner, A., Erkeland, S. J., et al. (2008). Targeted Deletion Reveals Essential and Overlapping Functions of the miR-17~92 Family of miRNA Clusters. *Cell*, *132*(5), 875–886. http://doi.org/10.1016/j.cell.2008.02.019

Venturini, L., Battmer, K., Castoldi, M., Schultheis, B., Hochhaus, A., Muckenthaler, M. U., et al. (2007). Expression of the miR-17-92 polycistron in chronic myeloid leukemia (CML) CD34+ cells. *Blood*, *109*(10), 4399–4405. http://doi.org/10.1182/blood-2006-09-045104

Wang, W., Esbensen, Y., Kunke, D., Suganthan, R., Rachek, L., Bjørås, M., & Eide, L. (2011). Mitochondrial DNA damage level determines neural stem cell differentiation fate. *Journal of Neuroscience*, *31*(26), 9746–9751. http://doi.org/10.1523/JNEUROSCI.0852-11.2011

Wang, Y., Wu, B., Chamberlain, A. A., Lui, W., Koirala, P., Susztak, K., et al. (2013). Endocardial to Myocardial Notch-Wnt-Bmp Axis Regulates Early Heart Valve Development. *PLoS ONE*, *8*(4), e60244–12. http://doi.org/10.1371/journal.pone.0060244

Westermark, U. K., Wilhelm, M., Frenzel, A., & Henriksson, M. A. (2011). The MYCN oncogene and differentiation in neuroblastoma. *Seminars in Cancer Biology*, *21*(4), 256–266. http://doi.org/10.1016/j.semcancer.2011.08.001

Wilczynska, A., & Bushell, M. (2014). The complexity of miRNA-mediated repression, *22*(1), 22–33. http://doi.org/10.1038/cdd.2014.112

Xiao, C., Srinivasan, L., Calado, D. P., Patterson, H. C., Zhang, B., Wang, J., et al. (2008). Lymphoproliferative disease and autoimmunity in mice with increased miR-17-92 expression in lymphocytes. *Nature Immunology*, *9*(4), 405–414. http://doi.org/10.1038/ni1575

Yamadori, T., & Nara, K. (1979). The directions of ciliary beat on the wall of the lateral ventricle and the currents of the cerebrospinal fluid in the brain ventricles. *Scanning Electron Microscopy*, (3), 335–340.

Yang, J. H., Li, J. H., Shao, P., Zhou, H., Chen, Y. Q., & Qu, L. H. (2010). starBase: a database for exploring microRNA-mRNA interaction maps from Argonaute CLIP-Seq and Degradome-Seq data. *Nucleic Acids Research*, *39*(Database), D202–D209. http://doi.org/10.1093/nar/gkq1056

Yang, Y., Ma, W., Ma, W., Wu, D., Wu, D., Huang, Y., et al. (2013). MiR-17 Partly Promotes Hematopoietic Cell Expansion through Augmenting HIF-1α in Osteoblasts. *PLoS ONE*. http://doi.org/10.1371/journal.pone.0070232

Yi, R., Poy, M. N., Stoffel, M., & Fuchs, E. (2008). A skin microRNA promotes differentiation by repressing "stemness." *Nature*, *452*(7184), 225–229. http://doi.org/10.1038/nature06642

Young, S. Z., Taylor, M. M., & Bordey, A. (2011). Neurotransmitters couple brain activity to subventricular zone neurogenesis. *European Journal of Neuroscience*, *33*(6), 1123–1132. http://doi.org/10.1111/j.1460-9568.2011.07611.x

Zhao, C., Sun, G., Li, S., & Shi, Y. (2009). A feedback regulatory loop involving microRNA-9 and nuclear receptor TLX in neural stem cell fate determination. *Nature Structural & Molecular Biology*, *16*(4), 365–371. http://doi.org/10.1038/nsmb.1576

Zhao, C., Sun, G., Li, S., Lang, M.-F., Yang, S., Li, W., & Shi, Y. (2010). MicroRNA let-7b regulates neural stem cell proliferation and differentiation by targeting nuclear receptor TLX signaling. *Proceedings of the National Academy of Sciences*, *107*(5), 1876–1881. http://doi.org/10.1073/pnas.0908750107

Zhou, P., Huang, G., Zhao, Y., Zhong, D., Xu, Z., Zeng, Y., et al. (2014). Cellular Signalling. *Cellular Signalling*, *26*(6), 1347–1354. http://doi.org/10.1016/j.cellsig.2014.02.020

Zhuo, L. E. A. (1997). Live Astrocytes Visualized by Green Fluorescent Protein in Transgenic Mice, 1–7.

Appendix

Neuron
Article

Prospective Identification and Purification of Quiescent Adult Neural Stem Cells from Their In Vivo Niche

Paolo Codega,[1,6] Violeta Silva-Vargas,[1,6] Alex Paul,[4,6] Angel R. Maldonado-Soto,[3,6] Annina M. DeLeo,[1,6] Erika Pastrana,[1,9] and Fiona Doetsch[1,2,3,5,6,7,8,*]
[1]Department of Pathology and Cell Biology
[2]Department of Neurology
[3]Department of Neuroscience
[4]Department of Genetics and Development
[5]Department of Rehabilitation and Regenerative Medicine
[6]Columbia Stem Cell Initiative
[7]Motor Neuron Center
[8]Herbert Irving Comprehensive Cancer Center
Columbia University, New York, NY 10032, USA
[9]Present address: Nature Publishing Group, New York, NY 10013, USA
*Correspondence: fkd2101@cumc.columbia.edu
http://dx.doi.org/10.1016/j.neuron.2014.02.039

SUMMARY

Adult neurogenic niches harbor quiescent neural stem cells; however, their in vivo identity has been elusive. Here, we prospectively isolate GFAP$^+$CD133$^+$ (quiescent neural stem cells [qNSCs]) and GFAP$^+$CD133$^+$EGFR$^+$ (activated neural stem cells [aNSCs]) from the adult ventricular-subventricular zone. aNSCs are rapidly cycling, highly neurogenic in vivo, and enriched in colony-forming cells in vitro. In contrast, qNSCs are largely dormant in vivo, generate olfactory bulb interneurons with slower kinetics, and only rarely form colonies in vitro. Moreover, qNSCs are Nestin negative, a marker widely used for neural stem cells. Upon activation, qNSCs upregulate Nestin and EGFR and become highly proliferative. Notably, qNSCs and aNSCs can interconvert in vitro. Transcriptome analysis reveals that qNSCs share features with quiescent stem cells from other organs. Finally, small-molecule screening identified the GPCR ligands, S1P and PGD_2, as factors that actively maintain the quiescent state of qNSCs.

INTRODUCTION

Quiescent and actively dividing (activated) stem cells coexist in adult stem cell niches (Li and Clevers, 2010). Stem cell quiescence and activation play an essential role in many organs, underlying tissue maintenance, regeneration, function, plasticity, aging, and disease. Quiescent stem cells dynamically integrate extrinsic and intrinsic signals to either actively maintain their dormant state or become activated to divide and give rise to differentiated progeny (Cheung and Rando, 2013). To illuminate their biology and their molecular regulation, it is essential to be able to prospectively identify and purify quiescent stem cells. However, this has been exceedingly difficult in any organ, including the adult brain.

Adult neural stem cells (NSCs) continuously generate neurons throughout life in two brain regions: the subgranular zone (SGZ) of the hippocampus and the ventricular-subventricular zone (V-SVZ), adjacent to the lateral ventricles. The V-SVZ is the largest germinal region in the adult mammalian brain and generates olfactory bulb interneurons and oligodendrocytes. Within the V-SVZ, glial fibrillary acidic protein (GFAP)-positive type B cells with hallmark features of astrocytes are stem cells and have multipotent self-renewing capacity in vitro (Doetsch et al., 1999a; Laywell et al., 2000; Imura et al., 2003; Garcia et al., 2004; Sanai et al., 2004; Ahn and Joyner, 2005; Mirzadeh et al., 2008; Beckervordersandforth et al., 2010; Lee et al., 2012). In vivo, actively dividing V-SVZ stem cells are eliminated by antimitotic treatment (Pastrana et al., 2009). In contrast, slowly dividing astrocytes are label-retaining cells (LRCs), survive treatment with antimitotic drugs and regenerate the V-SVZ, and give rise to neurons under homeostasis (Doetsch et al., 1999a; Ahn and Joyner, 2005; Giachino and Taylor, 2009; Nam and Benezra, 2009; Kazanis et al., 2010; Basak et al., 2012).

Recently, novel features of the anatomical organization of the V-SVZ stem cell niche have been uncovered. GFAP$^+$ type B1 cells have a radial morphology and span different compartments of the stem cell niche (Silva-Vargas et al., 2013). Their apical processes contact the lateral ventricle at the center of pinwheel structures formed by ependymal cells, exhibit a primary cilium, and are exposed to signals in the cerebrospinal fluid (CSF) (Doetsch et al., 1999a, Mirzadeh et al., 2008, Beckervordersandforth et al., 2010, Kokovay et al., 2012). Their basal processes contact blood vessels, which are an important proliferative niche in the adult V-SVZ (Shen et al., 2008; Mirzadeh et al., 2008; Tavazoie et al., 2008; Kazanis et al., 2010; Kokovay et al., 2010, Lacar et al., 2011, 2012).

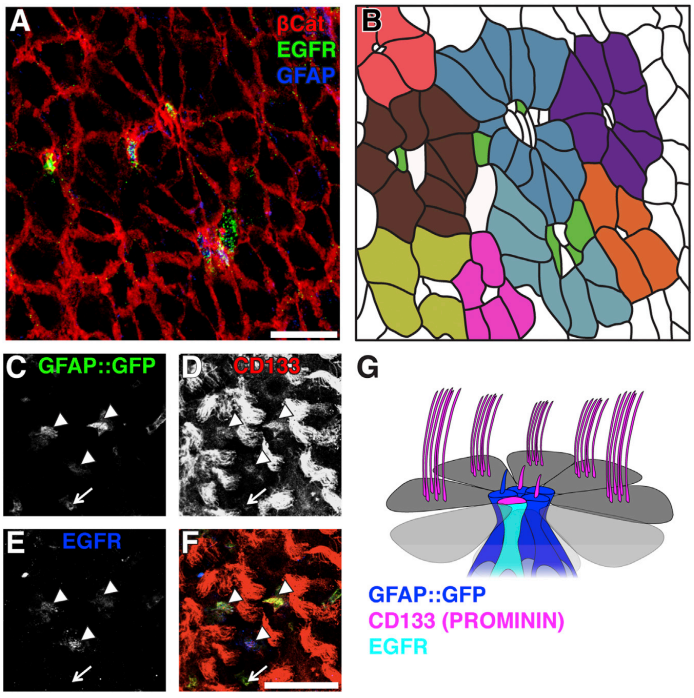

Figure 1. Two Populations of CD133$^+$ V-SVZ Astrocytes Contact the Ventricle

(A and B) A subset of GFAP$^+$ cells at the center of pinwheels express EGFR. (A) Confocal image of a whole mount immunostained for β-catenin ([βCat] red) to visualize pinwheels, GFAP (blue), and EGFR (green). (B) Schematic representation of whole mount shown in (A). Individual pinwheels are highlighted in different colors, and EGFR-expressing cells are green.

(C–F) Optical slice of a confocal z stack at the ventricular surface of a whole mount showing endogenous GFP expression (C) under the control of the human GFAP promoter and immunostained for (D) CD133 and (E) EGFR. (F) Merged image. Note that astrocytes contacting the ventricle with diffuse CD133 staining are EGFR$^+$ (arrowheads), whereas those with CD133 restricted to the primary cilium are EGFR$^-$ (arrow).

(G) Schema showing type B1 astrocytes contacting the ventricle at the center of a pinwheel structure formed by ependymal cells (gray). CD133 (Prominin, magenta) is detected on the cilia of ependymal cells, some primary cilia of some type B1 astrocytes (blue), and is diffusely expressed on the apical surface of EGFR$^+$ type B1 astrocytes (cyan). Scale bars, 30 μm.

See also Figures S1 and S2.

Various molecular markers have been used for the in vivo identification of V-SVZ stem cells and their purification (reviewed in Pastrana et al., 2011). Nestin and Sox2 are widely used as NSC markers in both the embryonic and adult brain (Lendahl et al., 1990; Graham et al., 2003; Kazanis et al., 2010; Imayoshi et al., 2011; Marqués-Torrejón et al., 2013). CD133 (Prominin), a transmembrane glycoprotein expressed on primary cilia of neural progenitors (Uchida et al., 2000; Marzesco et al., 2005; Pinto et al., 2008; Cesetti et al., 2011) has been used to distinguish GFAP$^+$CD133$^+$ stem cells from niche astrocytes (Mirzadeh et al., 2008, Beckervordersandforth et al., 2010). Combinations of markers are beginning to be identified that allow the purification of different subpopulations of V-SVZ cells, in particular of activated stem cells, including epidermal growth factor receptor (EGFR) (Doetsch et al., 2002; Pastrana et al., 2009), and brain lipid binding protein (BLBP) (Giachino et al., 2014). To date, however, combinations of markers have not been identified that allow the prospective isolation of quiescent V-SVZ stem cells. This is crucial to illuminate the functional properties and gene regulatory networks of quiescent adult NSCs.

Herein, we prospectively identify and isolate quiescent adult NSCs from their niche. Our findings reveal that CD133$^+$ astrocytes comprise two functionally distinct populations, quiescent NSCs (qNSCs) and activated NSCs (aNSCs), which differ dramatically in their in vivo cell cycle status and lineage kinetics, their in vitro colony-forming efficiencies, and their molecular signatures. Notably, qNSCs only rarely form colonies in vitro and are natively Nestin negative but upregulate both Nestin and EGFR on activation. qNSCs also share common molecular features with their counterparts in other organs. Finally, we identify GPCR ligands that actively maintain the quiescent state of qNSCs.

RESULTS

Two Populations of CD133$^+$ V-SVZ Astrocytes Contact the Lateral Ventricle

The intermediate filament GFAP is one of the few markers of type B1 astrocytes (Doetsch et al., 1997; Mirzadeh et al., 2008). However, due to its filamentous nature, it is difficult to perform colocalization studies with GFAP, and it cannot be used for live cell sorting. GFAP::GFP mice, in which GFP is expressed under the control of the human GFAP promoter (Zhuo et al., 1997), are a useful tool for visualizing V-SVZ astrocytes in vivo and for their purification by fluorescence-activated cell sorting (FACS) (Tavazoie et al., 2008; Platel et al., 2009, Shen et al., 2008, Pastrana et al., 2009; Beckervordersandforth et al., 2010). Whole-mount preparations allow the pinwheel architecture of the walls of the lateral ventricle to be clearly visualized. We confirmed that, in GFAP::GFP mice, type B1 astrocytes contacting the ventricle at the center of pinwheels were GFP$^+$ and GFAP$^+$, and frequently had a primary cilium, but lacked S100β expression, a marker of mature astrocytes that are found deeper in the tissue at the interface with the striatum (Figures S1A, S1C, and S1D available online).

Notably, a subset of cells localized within individual pinwheels was EGFR$^+$ (11.4% ± 1.3%; n = 129 pinwheels) (Figures 1A and 1B). These ventricle-contacting EGFR$^+$ cells coexpressed

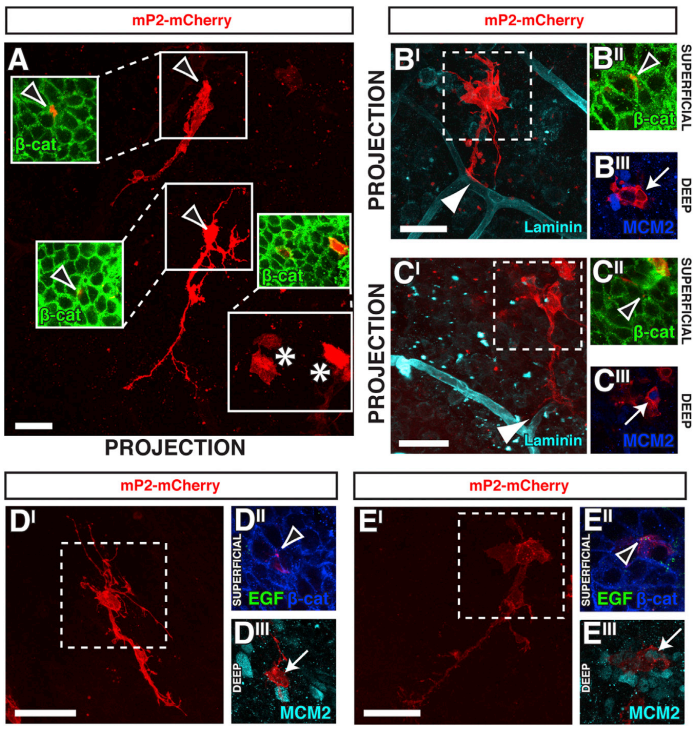

Figure 2. Both Quiescent and Activated CD133$^+$ V-SVZ Astrocytes Have Radial Morphology and Contact the Ventricle and Blood Vessels

(A) Confocal images of whole mounts immunostained with β-catenin ([β-cat] green, superficial optical slice) showing cells labeled by in vivo electroporation of the mP2-mCherry construct (red, z stack projection). Labeled cells are either radial cells that contact the ventricle at the center of pinwheels (open arrowheads in insets) or ependymal cells (asterisks).

(B^I–C^{III}) Confocal images of whole mounts immunostained with Laminin (cyan), β-catenin (green), and MCM2 (blue) showing projections of mP2-mCherry$^+$ cells (B^I and C^I). Insets show superficial (B^{II} and C^{II}) and deep (B^{III} and C^{III}) optical slices. Both MCM2$^-$ and MCM2$^+$ cells contact the ventricle at the center of pinwheels as well as blood vessels.

(D^I–E^{III}) Confocal images of whole mounts immunostained with MCM2 (cyan) and β-catenin (blue) and labeled with EGF-A647 (green) showing projections of mP2-mCherry$^+$ cells (D^I and E^I). Insets show superficial (D^{II} and E^{II}) and deep (D^{III} and E^{III}) optical slices. Note that EGF-negative cells are MCM2$^-$. Scale bars, 30 μm.

See also Figure S3.

both GFAP protein and GFP in GFAP::GFP mice (Figure S1B; Pastrana et al., 2009) and were observed throughout the rostrocaudal axis of the V-SVZ, with 45.7% ± 4.4% of pinwheels containing EGFR$^+$ cells.

To define markers for EGFR-negative type B1 cells contacting the ventricle, we examined the expression of CD133 (Prominin), which is expressed by ependymal cells and on the primary cilium of some type B1 cells (Coskun et al., 2008; Mirzadeh et al., 2008; Beckervordersandforth et al., 2010). We immunostained whole mounts of GFAP::GFP mice for EGFR and CD133 in conjunction with β-catenin (to label pinwheels) or acetylated tubulin (to detect primary cilia). We thereby identified two CD133$^+$ astrocyte populations: GFAP::GFP$^+$CD133$^+$ and GFAP::GFP$^+$CD133$^+$EGFR$^+$ (Figure 1G). GFAP::GFP$^+$CD133$^+$ cells had a primary cilium with CD133 staining localized to its tip (Figures 1C–1F; Figures S2A and S2C). In contrast, GFAP::GFP$^+$CD133$^+$EGFR$^+$ cells exhibited diffuse CD133 staining over their apical surface and lacked a primary cilium (Figures 1C–1F; Figures S2B and S2D). Finally, we also observed GFAP::GFP$^+$ cells contacting the ventricle, which had a primary cilium that was CD133 negative (Figures S2A and S2C).

Visualizing the in vivo morphology of CD133$^+$ type B1 cells is not feasible by immunostaining. To this end, we cloned and electroporated a construct that expresses membrane-targeted mCherry under the control of the mouse minimal P2 (Prominin-1) promoter (mP2-mCherry; Figure S3A) into the lateral ventricle and analyzed whole mounts 2 days later. Both multiciliated flat ependymal cells possessing typical cuboidal morphology and radial cells with B1 morphology were labeled by this construct (Figure 2A), and all coexpressed CD133 protein (23/23 cells; Figures S3B–S3D). Radial mP2-mCherry$^+$ cells expressed CD133 either at the tip of their primary cilium (Figure S3C) or diffusely on their apical surface (Figure S3D) and were GFAP$^+$ (data not shown). To define the cell cycle status and relationship of radial mP2-mCherry$^+$ cells with ependymal cells and blood vessels, electroporated whole mounts were immunostained for combinations of EGF-A647, MCM2, β-catenin, and Laminin to label activated stem cells, dividing cells, pinwheels, and blood vessels, respectively. All radial mP2-mCherry$^+$ cells, regardless of MCM2 expression or epidermal growth factor (EGF)-ligand binding, had a typical B1 morphology with an apical process contacting the ventricle at the center of pinwheels and a long basal process extending away from the surface, which frequently terminated on blood vessels (Figures 2B^I–2B^{III}; Figures 2C^I–2C^{III}; Figures S3E–S3N). Importantly, all MCM2$^+$ radial mP2-mCherry$^+$ astrocytes were colabeled with EGF-ligand (70/70 cells MCM2$^-$ and EGF$^-$; 5/5 cells MCM2$^+$ and EGF$^+$; Figures 2D^I–2D^{III}; Figures 2E^I–2E^{III}).

Prospective Purification of V-SVZ Astrocytes

The aforementioned in vivo characterization suggests that CD133 and EGFR could be used as markers to prospectively purify quiescent and activated NSCs directly from their in vivo

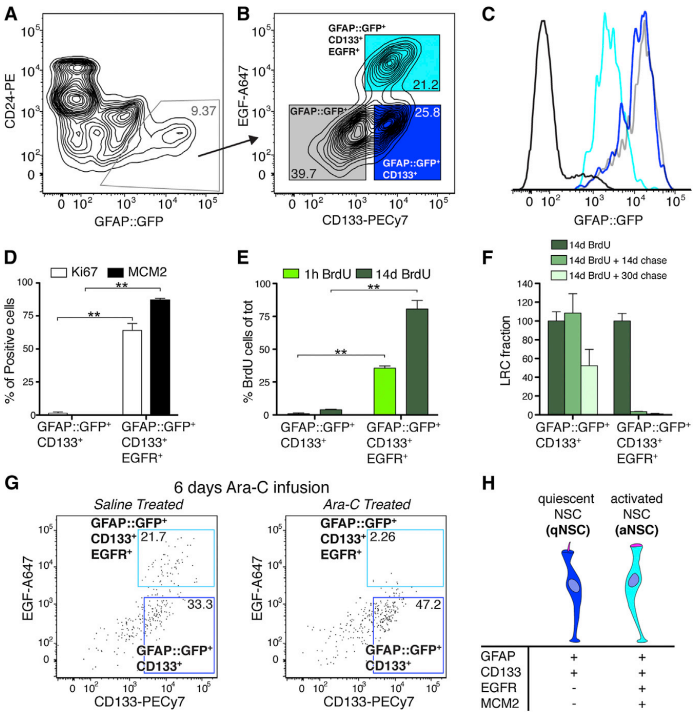

Figure 3. Prospectively Purified CD133$^+$ Astrocyte Subpopulations Exhibit Different Cell Cycle Properties

(A and B) Representative FACS plots showing gating strategy. In (A), the gate used to select GFAP::GFP$^+$CD24$^-$ cells, which are then gated on EGF-A647 and CD133-PE-Cy7. In (B), three populations are clearly defined: GFAP::GFP$^+$ (gray), GFAP::GFP$^+$CD133$^+$ (blue), and GFAP::GFP$^+$CD133$^+$EGFR$^+$ (cyan).

(C) Histogram showing the intensity of GFP signal in GFAP::GFP$^+$, GFAP::GFP$^+$CD133$^+$, and GFAP::GFP$^+$CD133$^+$EGFR$^+$ populations (gray, blue, and cyan, respectively) compared to other V-SVZ cells (GFP$^-$, black). Note that GFAP::GFP$^+$CD133$^+$EGFR$^+$ cells are dimmer than GFAP::GFP$^+$ and GFAP::GFP$^+$CD133$^+$ cells.

(D) Proportion of each CD133$^+$-purified astrocyte subpopulation that expresses Ki67 and MCM2 (n = 3; **p < 0.01, unpaired Student's t test; mean ± SEM).

(E) Proportion of each CD133$^+$-purified astrocyte subpopulation labeled after a single pulse of BrdU (light green) or after 14 days of BrdU in the drinking water (dark green) (n = 3 and n = 4, respectively, **p < 0.01, unpaired Student's t test, mean ± SEM).

(F) LRC fraction in the CD133$^+$-purified astrocyte populations 14 or 30 days after 14 days of BrdU administration (n = 4, mean ± SEM).

(G) Representative FACS plots of CD133$^+$ astrocyte subpopulations from saline- and Ara-C-treated mice.

(H) Summary of markers expressed by CD133$^+$-purified astrocytes.

See also Figures S4 and S6.

niche using FACS. We previously developed a simple strategy to simultaneously isolate activated stem cells (GFAP::GFP$^+$EGFR$^+$), transit-amplifying cells (EGFR$^+$), and neuroblasts (CD24$^+$) by combining EGF-A647 and CD24 in GFAP::GFP mice (Pastrana et al., 2009). By including CD133 in this sorting strategy, we separated two CD133$^+$ astrocyte populations, GFAP::GFP$^+$CD133$^+$ and GFAP::GFP$^+$CD133$^+$EGFR$^+$, from the remaining GFAP::GFP$^+$-only cells (Figures 3A and 3B; Figures S4A–S4I). GFAP::GFP$^+$CD133$^+$ (ranging from 25% to 30% of total GFP$^+$ cells) and GFAP::GFP$^+$CD133$^+$EGFR$^+$ (20%–25% of total GFP$^+$ cells) were both abundant but differed in their GFP brightness (Figure 3C).

We assessed the purity of the sorted populations using qRT-PCR and acute immunostaining. qRT-PCR confirmed that sorted populations were appropriately enriched in *Gfap*, *GFP*, *Prom1*, and *Egfr* expression (Figures S4Q–S4T). Acute immunostaining showed that both GFAP::GFP$^+$CD133$^+$ and GFAP::GFP$^+$CD133$^+$EGFR$^+$ populations were highly enriched in GLAST and GLT1 (Figures S4J and S4K)—glutamate aspartate transporters expressed in astrocytes—as well as BLBP (Figure S4M), that they largely or completely lacked S100β (Figure S4L) and that they were almost completely negative for the neuroblast markers DCX and βIII tubulin (Figures S4O and S4P). Notably, more than 90% of GFAP::GFP$^+$CD133$^+$ and GFAP::GFP$^+$CD133$^+$EGFR$^+$ populations expressed the NSC transcription factor Sox2 (Figures S4N and S4U). High Sox2 levels are related to a more proliferative state (Marqués-Torrejón et al., 2013); of note, 92.8% ± 1.5% of GFAP::GFP$^+$CD133$^+$EGFR$^+$ cells expressed high levels of Sox2 protein, whereas only 38.4% ± 3.5% of GFAP::GFP$^+$CD133$^+$ cells were Sox2 bright, with the remainder being Sox2 dim. In contrast, the GFAP::GFP$^+$-only population was more heterogeneous with significant neuroblast contamination, likely due to perdurance of GFP in neuroblasts (Figures S4O and S4P). We therefore focused our functional analyses below on GFAP::GFP$^+$CD133$^+$ and GFAP::GFP$^+$CD133$^+$EGFR$^+$ populations (all data regarding the GFAP::GFP$^+$-only population are included in Figure S6).

Purified GFAP$^+$CD133$^+$ V-SVZ Cells Have Different Cell Cycle Properties

Quiescent stem cells are largely dormant and lack markers of proliferation such as Ki67 and MCM2 that are expressed in actively dividing cells, but not during the quiescent G_0 state (Maslov et al., 2004). Both markers are expressed during G_1, with MCM2 being expressed earlier than Ki67. Cycling GFAP$^+$ V-SVZ cells in vivo have a fast cell cycle (Ponti et al., 2013). To determine the cell cycle properties of CD133$^+$ astrocyte subpopulations in vivo, we used multiple approaches. First, we determined the instantaneous cell cycle status of FACS-purified cells by acute immunostaining for proliferation-associated markers. GFAP::GFP$^+$CD133$^+$EGFR$^+$ cells were highly enriched in both Ki67 and MCM2 (64% ± 5.2% and 87.3% ± 1.2%,

respectively) whereas these two markers were almost absent in GFAP::GFP$^+$CD133$^+$ cells (1.4% ± 0.9% and 0.0% ± 0.0%, respectively) (Figure 3D). Similar patterns of proliferation were observed after a single in vivo pulse of bromodeoxyuridine (BrdU) 1 hr prior to FACS isolation: 35.5% ± 1.8% of GFAP::GFP$^+$CD133$^+$EGFR$^+$ cells were BrdU$^+$, in contrast to 0.8% ± 0.8% of GFAP::GFP$^+$CD133$^+$ cells (Figure 3E). Thus, at any given moment, the vast majority of GFAP::GFP$^+$CD133$^+$ cells are not proliferating.

LRCs are slowly cycling cells whose DNA remains labeled after prolonged administration of thymidine analogs and a long chase period (Wilson et al., 2008). To label dividing cells and to identify LRCs, we administered BrdU via drinking water for 2 weeks and analyzed the proportion of each population that was BrdU$^+$. Immediately after BrdU treatment, almost all GFAP::GFP$^+$CD133$^+$EGFR$^+$ cells were labeled, whereas only 3.9% ± 0.4% of GFAP::GFP$^+$CD133$^+$ cells had incorporated BrdU, reflecting their much slower rate of division (Figure 3E). Fourteen days after ceasing BrdU treatment, GFAP::GFP$^+$CD133$^+$EGFR$^+$ cells had already almost completely lost BrdU labeling (Figure 3F). In contrast, 52.4% ± 17.3% of GFAP::GFP$^+$CD133$^+$ cells were still BrdU$^+$ 30 days after BrdU withdrawal (Figure 3F).

Finally, we confirmed the different proliferation characteristics of both populations in vivo by infusing cytosine-β-D-arabinofuranoside (Ara-C) directly on the brain surface to eliminate dividing cells (Doetsch et al., 1999b). GFAP::GFP$^+$CD133$^+$ cells survived 6 days of Ara-C treatment, whereas the more rapidly dividing GFAP::GFP$^+$CD133$^+$EGFR$^+$ cells were eliminated (Figure 3G). Thus, although CD133 is regulated in a cell-cycle-dependent manner in dividing neural cell lines (Sun et al., 2009), in the V-SVZ niche, CD133 is expressed in both dividing and nondividing cells in vivo.

Together, these findings reveal that GFAP::GFP$^+$CD133$^+$ cells are largely quiescent in vivo, whereas GFAP::GFP$^+$CD133$^+$EGFR$^+$ cells are actively dividing. Based on their cell cycle properties and the functional studies described below, hereafter we refer to these populations as qNSCs and aNSCs, respectively (Figure 3H).

qNSCs and aNSCs Are Both Neurogenic In Vivo but Differ in Their Kinetics

To assess the in vivo potential of quiescent and activated stem cells, we transplanted purified qNSCs (1 week, n = 8; 1 month, n = 5) and aNSCs (1 week, n = 5; 1 month, n = 11) isolated from GFAP::GFP;β-Actin-PLAP mice (Zhuo et al., 1997; DePrimo et al., 1996) into the SVZ of wild-type recipient mice (Figure 4A). The donor cells were histochemically visualized based on their expression of the reporter human placental alkaline phosphatase (PLAP). In mice transplanted with aNSCs, many migrating neuroblasts were present in the V-SVZ, the rostral migratory stream (RMS), and the olfactory bulb after only 1 week (Figures 4E–4G), confirming their activated state. However, in mice transplanted with qNSCs, no neuroblasts were observed at this time point, and PLAP$^+$ cells were only present in the V-SVZ (Figures 4B–4D). In contrast, after 1 month, both populations generated mature olfactory bulb interneurons (Figures 4J and 4M), and PLAP$^+$ cells were still present in the V-SVZ in all transplants (Figures 4H and 4K). Interestingly, migrating neuroblasts were also present in the RMS in 3 out of 5 qNSC and 3 out of 11 aNSC transplanted brains, demonstrating that both populations continue to generate neurons after 1 month in vivo (Figures 4I and 4L). Oligodendrocytes were also formed by both transplanted populations (data not shown). These data show that both qNSCs and aNSCs can give rise to neurons and retain long-term neurogenic potential in vivo but exhibit very different kinetics of cell generation.

qNSCs and aNSCs Differ in Their In Vitro Behavior and Can Interconvert States

Two in vitro assays are widely used to assess stem cell properties and to enumerate in vivo stem cells: adherent colony formation and neurospheres (Pastrana et al., 2011). With the ability to now prospectively purify qNSCs, we directly tested their in vitro behavior in both assays, as compared to aNSCs.

qNSCs and aNSCs were plated as single cells under adherent conditions in the presence of EGF or EGF/basic fibroblast growth factor (bFGF). Whereas aNSCs were enriched in colony formation (47.9% ± 11.9% in EGF and 41.4% ± 1.8% in EGF/bFGF), in striking contrast, qNSCs only rarely gave rise to colonies (1.2% ± 0.1% in EGF and 0.7% ± 0.2% in EGF/bFGF) (Figure 5A) and did so with much slower growth kinetics than aNSCs. Importantly, although rare, the colonies formed by single qNSCs were large and multipotent, giving rise to neurons, oligodendrocytes, and mature astrocytes (Figures 5B and 5C).

We next compared the ability of qNSCs and aNSCs to form neurospheres and assessed self-renewal by serial passaging. Again, qNSCs only rarely gave rise to neurospheres (0.85% in EGF, 0.82% in EGF/bFGF) in contrast to aNSCs, which robustly generated neurospheres (Figure S5B). Moreover, the proliferation of the qNSC population was delayed by 6 days compared to aNSCs (Figures 5D and S5A). However, once activated, qNSCs exhibited similar rates of division to aNSCs. Neurospheres from both populations could be serially passaged more than three times and were multipotent, giving rise to neurons, astrocytes, and oligodendrocytes (Figures S5B and S5E). Finally, we examined whether more qNSCs were recruited to form neurospheres during in vivo regeneration, at 12 hr post-Ara-C removal when stem cell astrocytes start to divide (Doetsch et al., 1999a, 1999b; Pastrana et al., 2009). Notably, the efficiency of neurosphere formation of qNSCs purified after Ara-C treatment did not increase (Figure 5K). However, as previously shown, total neurosphere formation was almost completely eliminated after Ara-C treatment (Doetsch et al., 2002; Imura et al., 2003; Morshead et al., 2003; Garcia et al., 2004; data not shown), confirming that the vast majority of neurospheres arise from actively dividing cells.

Together, these results reveal that aNSCs are highly enriched in colony formation. In contrast, the qNSC population rarely forms colonies and does so more slowly than aNSCs. However, once activated, qNSCs are highly proliferative and multipotent, almost indistinguishable from aNSCs (Figure S5B). We therefore assessed whether qNSCs and aNSCs can interconvert in vitro by dissociating and analyzing primary spheres by flow cytometry. Intriguingly, the vast majority of cells in neurospheres derived from qNSCs expressed both EGFR and CD133 (Figures 5E

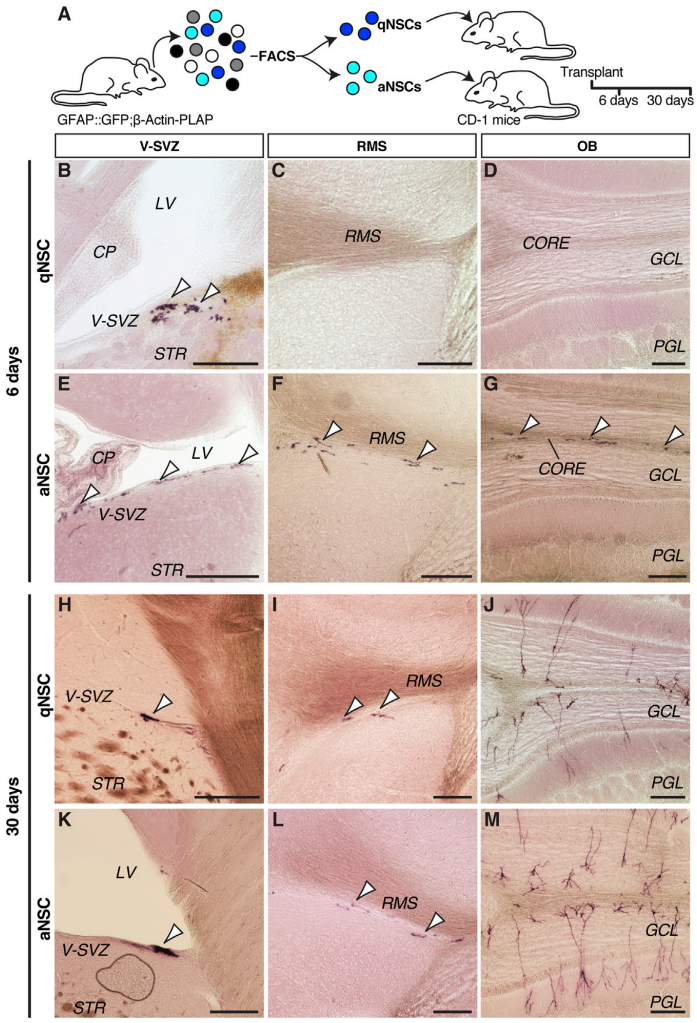

Figure 4. qNSCs and aNSCs Are Neurogenic In Vivo

(A) Schema of experimental design.

(B–G) Horizontal brain sections showing PLAP$^+$ cells (purple, arrowheads) 1 week after transplantation of qNSCs (B–D) and aNSCs (E–G). At this time point, aNSCs generated numerous migrating neuroblasts, whereas no cells were detected in the RMS or in the olfactory bulb of brains transplanted with qNSCs.

(H–M) Horizontal brain sections showing PLAP$^+$ cells (purple, arrowheads) 1 month after transplantation of (H–J) qNSCs and (K–M) aNSCs. In transplants from both populations, cells were present in the V-SVZ and RMS and had generated mature olfactory bulb interneurons. Scale bars, 200 μm. STR, striatum; CP, choroid plexus; LV, lateral ventricle; GCL, granular cell layer; PGL, periglomerular layer.

and 5G), revealing that qNSCs give rise to GFAP::GFP$^+$CD133$^+$EGFR$^+$ cells in vitro. Conversely, aNSCs gave rise to both GFAP::GFP$^+$CD133$^+$ and GFAP::GFP$^+$ populations (Figures 5F and 5H). Moreover, when primary spheres were dissociated and GFAP::GFP$^+$CD133$^+$, GFAP::GFP$^+$CD133$^+$EGFR$^+$, and GFAP::GFP$^+$ cells were reisolated, each population exhibited similar sphere formation efficiencies to primary isolated cells, with the GFAP::GFP$^+$CD133$^+$EGFR$^+$ population being greatly enriched in neurosphere formation compared to GFAP::GFP$^+$CD133$^+$ and GFAP::GFP$^+$ populations (Figures 5I and 5J; Figures S5C and S5D). Therefore, qNSCs and aNSCs can interconvert between more quiescent and activated states, with each population giving rise to all other populations in vitro.

qNSCs Do Not Express Nestin but Upregulate EGFR and Nestin on Activation

Nestin is an intermediate filament protein; its expression is widely considered a hallmark of NSCs, both during development and in the adult (Lendahl et al., 1990; Imayoshi et al., 2011). Unexpectedly, our microarray analysis (see below) suggested that qNSCs express very low to no levels of Nestin mRNA, in contrast to aNSCs, in which Nestin mRNA is highly expressed. We confirmed this observation by qRT-PCR (Figure S8E) as well as by immunostaining of acutely purified cells (Figure 6A). Out of 1,582 plated qNSCs, none were Nestin protein positive. Finally, to assess the Nestin status of NSCs in vivo, we electroporated mice with the mP2-mCherry construct and coimmunostained whole mounts with Nestin and EGF-ligand. In vivo, Nestin is highly expressed by ependymal cells (Doetsch et al., 1997; Figures 6D^{I} and 6E^{I}) as well as SVZ cells (Figures 6D^{II} and 6E^{II}). All radial EGF-ligand-negative mP2-mCherry$^+$ cells were Nestin protein negative (Figures 6D^{I} and 6D^{II}; 0/79 cells in seven whole mounts). In contrast, only EGF-ligand-positive cells coexpressed Nestin protein (Figures 6E^{I} and 6E^{II}; 32/34 cells in seven whole mounts).

To investigate whether qNSCs upregulate Nestin protein on activation, we performed a time-course analysis of qNSCs cultured in adherent conditions and immunostained for Nestin, EGFR, and MCM2 (Figures 6B and 6C). When first isolated and plated, qNSCs were small and round and did not express Nestin, EGFR, or MCM2 (type 1). As qNSCs became activated in vitro, they underwent morphological and molecular changes, enlarging their nuclei and upregulating all three markers

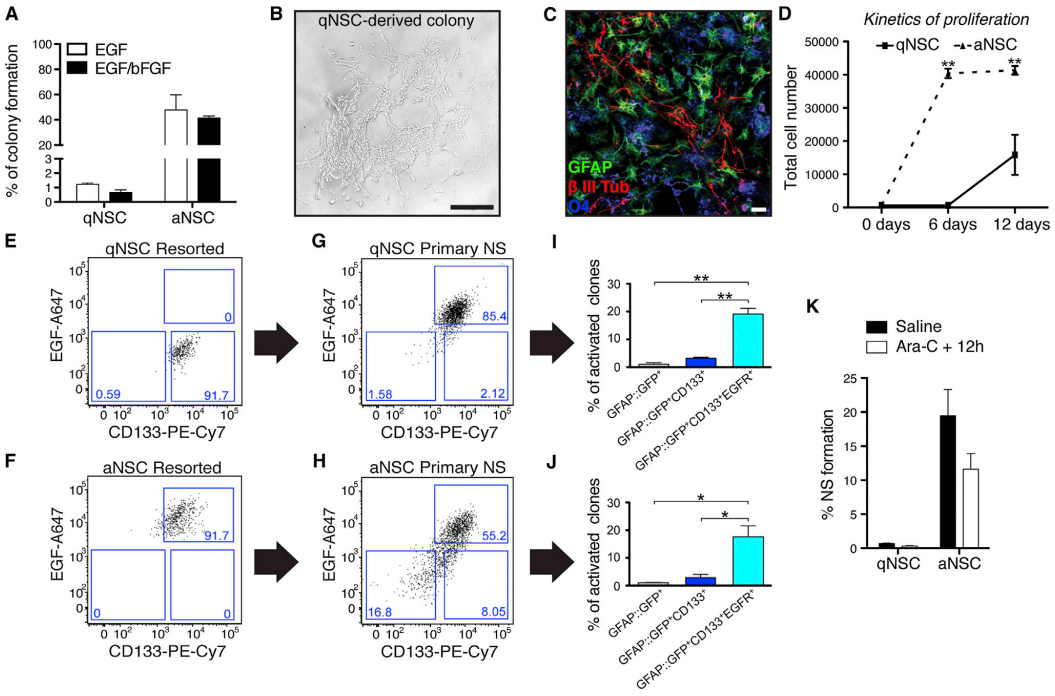

Figure 5. Purified qNSCs and aNSCs Give Rise to Neurospheres with Different Proliferative Properties and Kinetics

(A) Single cell colony formation efficiency of FACS-purified qNSCs and aNSCs in adherent cultures (n = 3, mean ± SEM).

(B) Representative phase contrast image of an adherent colony from a single qNSC after 12 days in the presence of EGF. Scale bar, 100 μm.

(C) Confocal image of neurons (βIII Tubulin [β III Tub], red), astrocytes (GFAP, green) and oligodendrocytes (O4, blue) derived from qNSCs plated under adherent conditions. Scale bar, 10 μm.

(D) Quantification of cell proliferation when plated at 1.4 cells per microliter with EGF under nonadherent conditions after 6 or 12 days (n = 5; $^{**}p < 0.01$ compared to qNSCs at the same time point, unpaired Student's t test, mean ± SEM).

(E–H) Representative FACS plots of, in (E) and (F), purified CD133$^+$ astrocytes immediately resorted after isolation from the brain and, in (G) and (H), of primary neurospheres (NS) derived from each population after 12 days for qNSCs and 6 days for aNSCs cultured in EGF.

(I and J) Clonal activation efficiency of purified GFAP::GFP$^+$, GFAP::GFP$^+$CD133$^+$, and GFAP::GFP$^+$CD133$^+$EGFR$^+$ cells, isolated from primary neurospheres of each population (in EGF, n = 3; $^*p < 0.05$, $^{**}p < 0.01$, unpaired Student's t test; mean ± SEM).

(K) Neurosphere formation 12 hr (12h) after Ara-C treatment as compared to saline-treated controls (n = 6, mean ± SEM).

See also Figures S5 and S6.

(type 2). They then extended processes (type 3) (Figures 6B and 6C) and began to proliferate extensively, closely resembling cultured aNSCs.

To independently confirm the lack of Nestin expression in qNSCs and its upregulation on activation, we used Nestin::Kusabira Orange reporter mice (Kanki et al., 2010; Ishizuka et al., 2011) to FACS-purify CD133$^+$Nes::OR$^-$EGFR$^-$CD24$^-$ (Nestin- and EGFR-negative) cells (Figure S7A). Acutely plated cells all lacked Nestin protein (Figure S7B) and, when cultured, only rarely gave rise to neurospheres (Figures S7C and S7E). Importantly, CD133$^+$Nes::OR$^-$EGFR$^-$CD24$^-$ cells, which originally lacked Nestin::Kusabira Orange reporter expression, upregulated the reporter in all neurospheres that formed (Figure S7C). In contrast, purified CD133$^+$Nes::OR$^+$EGFR$^+$CD24$^-$ cells were very efficient in neurosphere formation (Figures S7D and S7E).

Finally, we examined whether Nestin-negative qNSCs contribute to the lineage during regeneration. At present, it is not feasible to directly trace the lineage of qNSCs in vivo due to the lack of specific markers. We therefore administered tamoxifen to adult GFAP::CreERT2;Rosa26^{tdTomato} mice to induce recombination in GFAP-expressing cells and chased for 10 days after the first injection to allow actively dividing cells to progress down the lineage (Figure S7F). We then infused Ara-C for 6 days to eliminate dividing cells (Figure S7F) and confirmed that all remaining lineage-labeled cells were Nestin negative (0 of 951; Figure S7G) immediately after termination of treatment. Six days after Ara-C removal, tdTomato$^+$Nestin$^+$ cells were present (Figures S7H and S7I), as well as tdTomato$^+$DCX$^+$ neuroblasts (Figure S7I). These data reveal that qNSCs upregulate Nestin, as well as EGFR, during

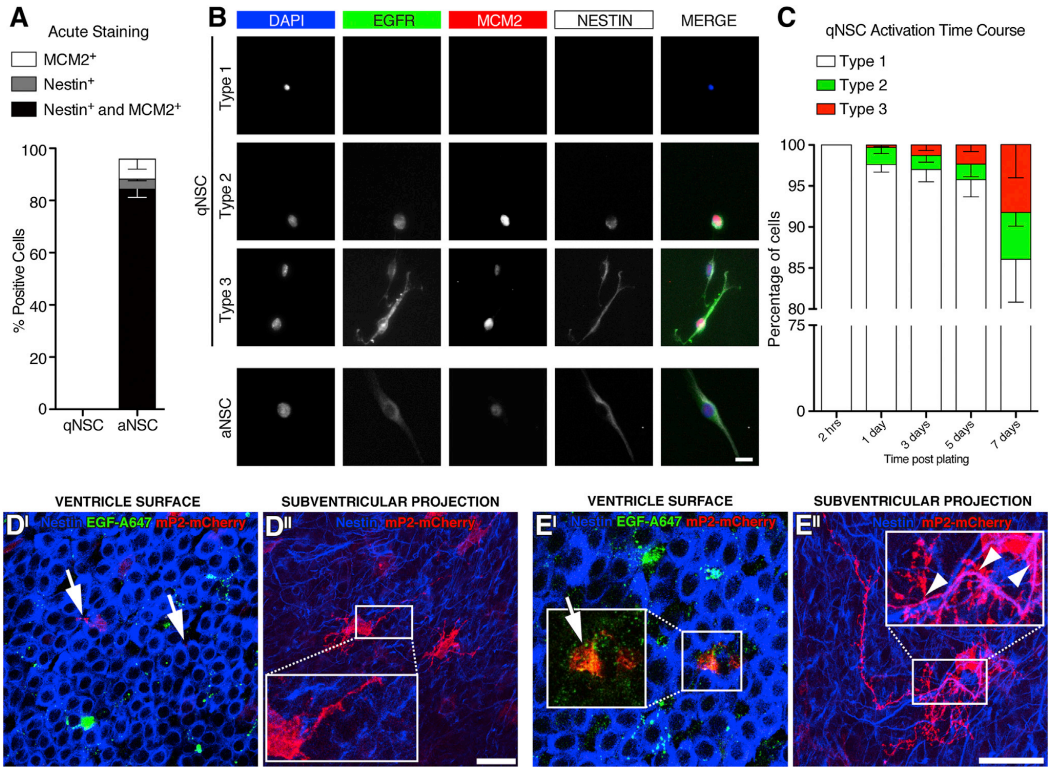

Figure 6. qNSCs Are Nestin Negative

(A) Proportion of acutely plated purified qNSCs and aNSCs immunopositive for MCM2 and Nestin (n = 3, mean ± SEM).

(B) Images of FACS-purified qNSCs cultured in EGF, fixed at different time points, and immunostained with EGFR, MCM2, and Nestin. Three types of cells are present: rounded cells with a condensed nucleus that do not express EGFR, MCM2, or Nestin (type 1); rounded cells with a larger nucleus that express EGFR, MCM2, and Nestin (type 2); and EGFR$^+$MCM2$^+$Nestin$^+$ cells with elongated processes (type 3). Type 3 cells resemble aNSCs after 3 days in culture. Scale bars, 10 μm.

(C) Quantification of activated qNSCs in culture after 2 hr or after 1, 3, 5, or 7 days after plating (n = 4, mean ± SEM).

(D^I–E^{II}) Confocal images showing mP2-mCherry$^+$ cells (red) in whole mount labeled with EGF-A647 (green) and immunostained for Nestin (blue). In (D), two cells contact the ventricle between ependymal cells, do not bind EGF-A647 (D^I, arrows), and are Nestin negative in the subventricular projection (D^{II}). In (E), an EGF-A647-labeled cell (E^I, arrow) is coimmunostained with Nestin in the subventricular projection (E^{II}, arrowheads in inset). Notably, not all processes contained Nestin. Scale bars, 30 μm.

See also Figure S7.

activation and contribute to the lineage during regeneration in vivo.

Gene Expression Analysis of Purified qNSCs and aNSCs Reveals Distinct Molecular Signatures

To gain insight into the biological properties of qNSCs and to define their molecular signatures, we performed microarray analysis on RNA from FACS-purified populations isolated directly from their in vivo niche (Figure 7A; Table S1). Gene ontology (GO) and gene set enrichment analysis (GSEA) (Subramanian et al., 2005) revealed that qNSCs and aNSCs have distinct molecular features (Figures 7B–7D). Confirming the actively dividing state of aNSCs in vivo, their transcriptome was enriched in genes involved in the cell cycle, transcription and translation, and DNA repair (Figures 7C and 7D; Tables S2 and S3). In contrast, qNSCs were enriched in the GO categories of cell communication, response to stimulus, and cell adhesion (Figure 7B; Table S2), underscoring the dynamic regulation of the quiescent state via interaction with the microenvironment. Indeed, the most represented GSEA groups for qNSCs were related to transport, signaling, receptors, cell surface, and extracellular matrix (Figure 7D; Table S3). Notably, qNSCs and aNSCs exhibited different metabolic profiles; the majority of the differentially enriched GSEA metabolism subsets in qNSCs were related

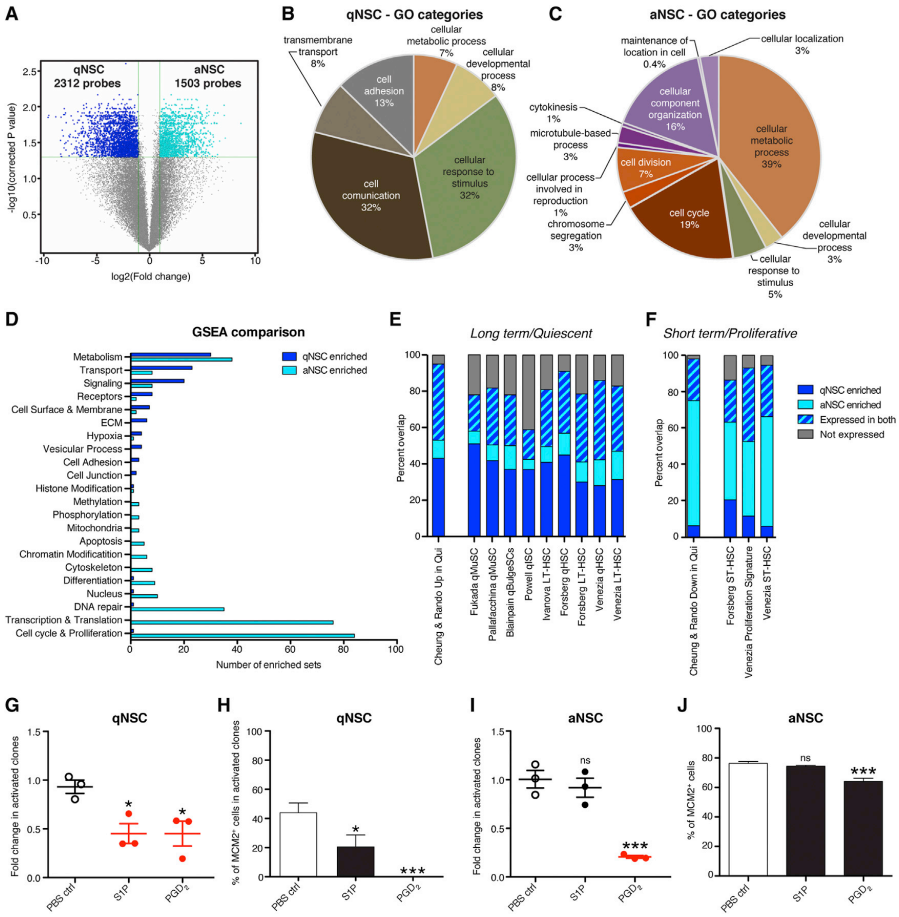

Figure 7. Gene Expression Analysis of qNSCs and aNSCs Reveals Distinct Molecular Signatures

(A) Volcano plot of differentially expressed probesets in qNSCs and aNSCs. Probes have at least 2-fold change in expression and a corrected p value < 0.05.

(B and C) Pie charts showing representative GO categories for differentially expressed probesets in (B) qNSCs and (C) aNSCs, as determined in (A).

(D) GSEA for qNSCs versus aNSCs. Sets have a false discovery rate (q value) <0.05 and are hand curated into thematic categories.

(E and F) Percentage of overlap with signatures of quiescent and dividing stem cells from other organs: (E) long-term (LT)/quiescent signatures and (F) short-term (ST)/proliferative signatures as determined by fold-change analysis of published lists compared to qNSC and aNSC populations. Qui, quiescent; HSC, hematopoietic stem cells; qMuSC, quiescent muscle stem cells; qBulgeSC, quiescent bulge stem cells; qISC, quiescent intestinal stem cells.

(G–J) Targeted GPCR ligand screen. (G) Quantification of qNSC activation (fold change in % Nestin$^+$ clones) as compared to controls (empty dots). (H) Quantification of percentage of MCM2$^+$ cells within activated Nestin$^+$ clones. (I) Quantification of aNSC clones (fold change of percentage of clones that underwent division) as compared to controls (empty dots). (J) Quantification of percentage of MCM2$^+$ aNSCs. Data are represented as means ± SEM.

n = 3. *p < 0.05; ***p < 0.001. ns, not significant.

See also Figure S8 and Tables S1, S2, S3, S4, S5, S6, S7, and S8.

to metabolism of lipids (Figure S8A), which are emerging as important signals in NSC regulation (Knobloch et al., 2013), whereas those in aNSCs were DNA/RNA-related metabolism and proteasome activity (Figure S8B).

Functional studies have implicated numerous genes in the regulation of adult neurogenesis. Many of these were differentially expressed in qNSCs and aNSCs (Table S5). Moreover, direct comparison of qNSC and aNSC transcription profiles with those of purified GFAP::GFP$^+$CD133$^+$ V-SVZ stem cells (Beckervordersandforth et al., 2010) revealed that we have resolved two distinct subsets of NSCs with different molecular and functional properties within their data (Figures S8C and

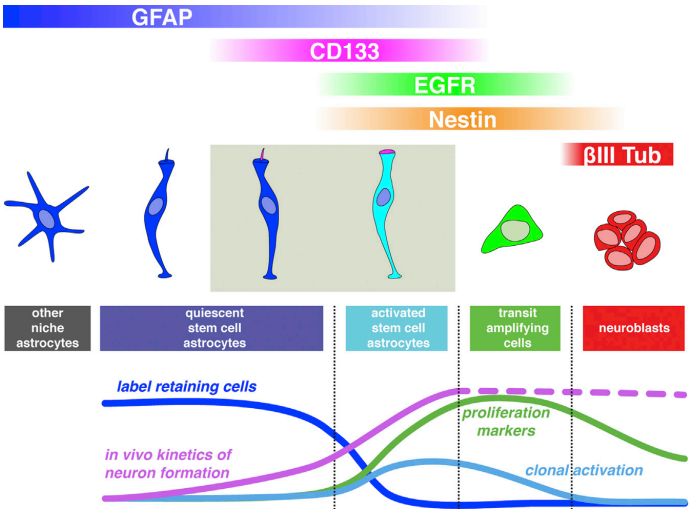

Figure 8. In Vivo and In Vitro Properties of V-SVZ Stem Cells and Their Progeny

Quiescent stem cells (GFAP$^+$CD133$^+$) are Nestin negative, label-retaining (blue line), and neurogenic in vivo (magenta line) but only very rarely give rise to neurospheres and adherent colonies in vitro (light blue line). Activated stem cells (GFAP$^+$CD133$^+$EGFR$^+$) are highly proliferative (green line) and rapidly generate neurons in vivo and are enriched in neurosphere/colony formation. Previous work has shown that EGFR$^+$ transit amplifying cells are also highly proliferative in vivo and give rise to neurospheres. Of note, quiescent stem cells were also present among CD133$^-$ astrocytes. Niche astrocytes have a branched morphology.

S8D; Table S8). Indeed, we found that neurogenic transcription factors such as *Dlx1*, *Dlx2*, *Sox4*, *Sox11*, and *Ascl1*, which were proposed to be hallmarks of NSCs (Beckervordersandforth et al., 2010), were in fact primarily expressed by or restricted to aNSCs (Table S4). We confirmed enrichment of *Dlx2* and *Ascl1* in aNSCs by qRT-PCR (Figures S8F and S8G), as well as enrichment of *Dll1* (Figure S8H), which is expressed in aNSCs (Kawaguchi et al., 2013). In contrast, qNSCs expressed high levels of factors reported to be markers of quiescent stem cells in the adult V-SVZ, such as *Vcam1* (Figure S8I and Table S5; Kokovay et al., 2012), and in other organs, such as *Lrig1* (Figure S8J and Table S1; Jensen and Watt, 2006; Jensen et al., 2009; Powell et al., 2012).

We then performed comparative analysis of our gene expression data with transcriptional signatures from quiescent or proliferative hematopoietic, muscle, skin, and intestinal stem cells (Ivanova et al., 2002; Venezia et al., 2004; Forsberg et al., 2010; Pallafacchina et al., 2010; Powell et al., 2012; Blanpain et al., 2004: Fukada et al., 2007; Cheung and Rando, 2013). The majority of genes in long-term/quiescent populations were upregulated in our quiescent V-SVZ stem cells, whereas those in the short-term/proliferative stem cell lists from other tissues were upregulated in our activated population (Figures 7E and 7F; Table S6). Together, this suggests that common transcriptional programs for quiescence or activation are shared between stem cell lineages in different tissues.

GPCR Signaling Maintains the Quiescent State

To gain insight into signaling pathways that modulate quiescence in qNSCs, we mined our transcriptome data. G protein-coupled receptor (GPCR) signaling was highly enriched in qNSCs (30% of all GSEA signaling sets; Table S3). We selected 25 GPCRs that were more than 10-fold enriched in qNSCs over aNSCs (Table S7) as a basis for a functional screen to assess their role in the regulation of qNSCs. FACS-purified qNSCs were plated under adherent conditions for 4 days in the presence of different ligands, and their activation (number of Nestin$^+$ clones) was quantified (Figure S8K). Two compounds, sphingosine-1-phosphate (S1P) and prostaglandin D_2 (PGD_2), had a significant effect, with both decreasing the activation of qNSCs by approximately one half (Figures 7G and S8L). Both ligands also decreased the number of MCM2$^+$ qNSCs (Figure 7H). PGD_2 exerted a more potent effect, completely abolishing MCM2 expression. To determine whether these compounds act specifically on qNSCs or also affect aNSCs, we plated FACS-purified aNSCs in the presence of S1P or PGD_2 and fixed the cells after 24 hr. This shorter time course is necessary as aNSCs divide very rapidly, making it difficult to distinguish individual clones (Figure S8K). S1P did not alter the number of aNSC clones (Figure 7I) or percentage of MCM2$^+$ cells (Figure 7J). As such, S1P selectively targets qNSCs and appears to act at the level of qNSC recruitment (Figure 7H). In contrast, PGD_2 had a potent inhibitory effect on the number of clones formed by aNSCs (Figure 7I). PGD_2 also reduced the percentage of MCM2$^+$ aNSCs (Figure 7J). As such, PGD_2 acts on both qNSCs and aNSCs. Thus, these GPCR ligands actively maintain the adult NSC quiescent state.

DISCUSSION

Here, we prospectively identified and isolated quiescent adult NSCs by defining a combination of markers (CD133, GFAP, and EGFR) that allows the simultaneous purification of quiescent and activated populations of stem cell astrocytes. Together, our analyses of their cell cycle properties, their morphological and anatomical localization, their in vitro and in vivo functional behavior, and their gene expression profiles highlight the distinct functional and molecular properties of qNSCs and aNSCs (Figure 8). Our functional analyses reveal important features of quiescent NSCs, which affect the interpretation of commonly used in vitro NSC assays and lineage-tracing strategies.

In the adult mouse brain, CD133 was originally proposed to be exclusively expressed by ependymal cells, with FACS-purified CD133$^+$ cells giving rise to neurospheres in vitro and generating neurons in vivo (Coskun et al., 2008). However, CD133 is also expressed by a subset of astrocytes, which behave as NSCs (Mirzadeh et al., 2008; Beckervordersandforth et al., 2010), suggesting that the earlier findings can be attributed to CD133$^+$ astrocytes instead of ependymal cells. Here, we show that CD133 is expressed by both quiescent and activated V-SVZ stem cells.

The neurosphere assay is widely used as a readout of in vivo stem cells (reviewed in Pastrana et al., 2011). Neurospheres were originally proposed to arise from relatively quiescent stem cells in vivo (Morshead et al., 1994). With the ability to prospectively purify cells at different stages of the stem cell lineage, it is now feasible to directly assess the potential of distinct populations to give rise to neurospheres. Here, we show that qNSCs only very rarely give rise to either neurospheres or adherent colonies and do not increase their neurosphere-forming efficiency during regeneration. In contrast, aNSCs are enriched in neurosphere and adherent colony formation. Together, our current findings and previous reports highlight that the major source of neurosphere-initiating cells are actively dividing in vivo, and include both GFAP$^+$ aNSCs and EGFR$^+$GFAP$^-$ transit-amplifying cells (Doetsch et al., 2002, Imura et al., 2003; Morshead et al., 2003; Garcia et al., 2004, Pastrana et al., 2009; data not shown). Thus, the neurosphere assay is a useful tool for assessing the in vitro stem cell potential of proliferative populations but does not allow the identification and enumeration of in vivo quiescent stem cells. This emphasizes the need to develop novel assays, or identify additional niche factors, that allow qNSCs to be expanded in vitro.

Nestin is frequently used both as a marker of NSCs and for their genetic manipulation and lineage tracing in the embryonic (Lendahl et al., 1990; Zimmerman et al., 1994) and adult brain (reviewed in Imayoshi et al., 2011). Nestin$^+$ cells have also been implicated as putative glioblastoma-forming cells (Holland et al., 2000, Chen et al., 2012). Notably, we found that adult V-SVZ qNSCs do not express Nestin but upregulate it on activation in vitro, as well as during regeneration in vivo. These data are consistent with previous observations that Nestin$^-$/CD133$^+$ cells are neurogenic in vivo and give rise to Nestin$^+$ neurospheres in vitro (Coskun et al., 2008). Recently, both Nestin-negative and Nestin-positive radial glia-like stem cells have also been described in the hippocampus (DeCarolis et al., 2013). As we show here in the V-SVZ, in the SGZ, almost all of the dividing radial glia-like stem cells express Nestin (DeCarolis et al., 2013). It is interesting that, in embryonic development, Nestin expression is also regulated in a cell-cycle-dependent manner (Sunabori et al., 2008). Thus, Nestin expression is dynamically regulated in NSCs. Importantly, our study highlights that Nestin immunostaining cannot be used to identify adult qNSCs in vivo. Thus, whether recombination and reporter expression occur in qNSCs needs to be carefully assessed when using Nestin transgenes for in vivo targeting of adult NSCs, V-SVZ lineage tracing, genetic manipulation, or purification. Moreover, interpretation of such assays is further complicated by the high expression of Nestin in ependymal cells, which can lead to nonautonomous effects.

qNSCs are multipotent and self-renewing in vitro. In vivo, qNSCs are long-term neurogenic and exhibit delayed kinetics of neuron formation compared to aNSCs. Interestingly, some aNSC transplants also continue to make neurons 30 days after transplantation. These may arise from a more quiescent subpopulation of aNSCs or from aNSCs that have reverted back to the quiescent state, as occurs in vitro. We also observed oligodendrocyte formation by both transplanted qNSCs and aNSCs (data not shown). In vivo, adult V-SVZ NSCs have regional identity and generate distinct neuronal subtypes, or oligodendrocytes (Merkle et al., 2007; Ventura and Goldman, 2007; Young et al., 2007; Ortega et al., 2013). At present, we cannot distinguish whether neurons and oligodendrocytes arise from regionally distinct subpopulations of NSCs in the transplanted populations or whether some, or all, NSCs are multipotent in vivo. The extent of in vivo V-SVZ stem cell heterogeneity and population dynamics of qNSCs and aNSCs, as well as their lineage relationships and potential under homeostasis and during regeneration, will require the identification of novel markers allowing the specific targeting of qNSCs and aNSCs. Importantly, our present strategy allows qNSCs to be isolated irrespective of their regional origin. Of note, the GFAP::GFP$^+$ CD133$^-$ population also contains quiescent stem cells. By combining different reporter mice, it is emerging that V-SVZ stem cells are molecularly heterogeneous (Giachino et al., 2014). The iterative identification of additional markers that allow subpopulations of NSCs to be isolated and targeted in vivo is a key future step.

Recent findings suggest that quiescent and activated states are differentially regulated at multiple levels, including cell-cell and extracellular matrix interactions, diffusible signals and distinct transcriptional programs coupling cell cycle regulators, quiescence, self-renewal, and differentiation (Kazanis et al., 2010; Young et al., 2011; Le Belle et al., 2011; Alfonso et al., 2012; Basak et al., 2012; Marqués-Torrejón et al., 2013; Kokovay et al., 2012; Porlan et al., 2013; Giachino et al., 2014; Kawaguchi et al., 2013, López-Juárez et al., 2013; Martynoga et al., 2013). Our transcriptome data of qNSCs and aNSCs isolated directly from their in vivo niche provide a platform to functionally assess the gene regulatory networks active in each state. Interestingly, our GSEA analysis reveals that GPCR signaling is specifically enriched in qNSCs. While GPCRs modulate many different facets of adult neurogenesis (Doze and Perez, 2012), our findings highlight that they are also key regulators of qNSCs. Strikingly, both functional ligands we identify in our GPCR screen, S1P and PGD_2, inhibit the activation of qNSCs, suggesting that stem cell quiescence is an actively maintained state. Both S1P and PGD_2 are present in the CSF (Sato et al., 2007; Kondabolu et al., 2011), which is emerging as a reservoir of factors in the embryo and the adult important for stem cell regulation (Silva-Vargas et al., 2013). As such, the CSF may be a key niche compartment mediating quiescence in the adult V-SVZ. Interestingly, PGD_2 has been implicated in promoting the quiescent phase of the hair follicle cycle (Garza et al., 2012), which is consistent with our transcriptome data suggesting that quiescent and activated stem cells in different tissues share common molecular pathways.

As additional mediators of stem cell quiescence and activation are uncovered, it will be important to investigate how clinical drugs targeting these pathways impact NSCs in vivo. For instance, fingolimod, an immunomodulatory drug approved by the Food and Drug Administration for the treatment of multiple sclerosis (Kappos et al., 2006), acts on S1P receptors. Recent studies have shown that fingolimod also acts on multiple CNS cell types (Groves et al., 2013), including astrocytes. Our identification of S1P as a regulator of stem cell quiescence suggests that this drug may have an effect on NSCs in the adult brain.

The ability to purify quiescent NSCs from the adult brain opens new vistas into elucidating the biology of stem cell quiescence, enabling studies in their intrinsic and extrinsic molecular regulation and defining their dynamics during development and aging. V-SVZ GFAP$^+$ stem cells are also present in humans, where they are largely quiescent (Sanai et al., 2004, 2011; van den Berge et al., 2010). Understanding the biology of stem cell quiescence and activation will ultimately lead to insight into how NSCs contribute to brain pathology and can be harnessed for brain repair.

EXPERIMENTAL PROCEDURES

Animal Use

Experiments were performed in accordance with Columbia University institutional and national guidelines for animal use. All mice used were between 2 and 3 months old.

FACS

The FACS strategy was adapted from Pastrana et al. (2009). Briefly, the V-SVZ was microdissected from GFAP::GFP mice and dissociated with papain, the single cell suspension was immunostained, and cell populations were purified by FACS as described in the detailed protocol in Supplemental Experimental Procedures.

Immunostaining

Whole mounts were dissected and processed as described elsewhere (Doetsch et al., 1999b; Tavazoie et al., 2008; Mirzadeh et al., 2010). Briefly, whole mounts were blocked in 10% serum, incubated with primary antibodies for 48 hr at 4°C, revealed with secondary antibodies, and imaged with a Zeiss LSM510 or Leica TCS SP5 II confocal microscope. All immunostainings were performed in triplicate. Immunostaining details for whole mounts and cell cultures are in the Supplemental Experimental Procedures.

In Vitro Assays

For neurosphere assays, FACS-purified cells were collected in neurosphere medium without growth factors and plated at clonal density with EGF (20 ng/ml) or EGF/bFGF (20 ng/ml each). For adherent cultures, purified cells were collected in neurosphere medium and plated on poly-D-lysine and fibronectin-coated 96-well plates as single cells or at clonal density and cultured with EGF or EGF/bFGF. Further details are given in the Supplemental Experimental Procedures.

Ara-C Infusion

A micro-osmotic pump (ALZET, 1007D) filled with 2% Ara-C (Sigma) in 0.9% saline was implanted on to the surface of the brain as described elsewhere (Doetsch et al., 1999b). After 6 days of Ara-C infusion, mice were sacrificed either immediately or 12 hr after pump removal.

Electroporation

One microliter of a solution containing 5 μg/μl of the mP2-mCherry plasmid in 0.9% saline was electroporated according to Barnabé-Heider et al. (2008), using the following coordinates: anterior-posterior (AP), 0.0; lateral (L), 0.85; ventral (V), −2.5 mm relative to bregma. The mP2-mCherry plasmid was made by cloning the mouse P2 element of the Prominin1 promoter into the CherryPicker control vector (Clontech), using the *XhoI* and *AgeI* digestion sites. See the Supplemental Information for details.

Transplants

Three injections of 0.2 μl delivering 1,000–3,000 cells purified from GFAP::GFP/β-actin-PLAP mice were performed in the SVZ of wild-type recipient mice, using the following coordinates: (1) AP, 0.0; L, 1.4; V, −2.1; (2) AP, 0.5; L, 1.1; V, −2.2; (3) AP, 1.0; L, 1.0; V, −2.5 mm relative to bregma. Recipient mice were sacrificed 1 week or 1 month after transplantation. Transplanted cells were revealed by NBT/BCIP staining.

RNA Isolation and Microarray Hybridization

RNA was purified from FACS-sorted populations with the miRNeasy kit (QIAGEN) from three biological replicates. cDNA was synthesized with the Nugen Pico amplification kit and hybridized to Affymetrix MOE430.2 chips. See Supplemental Information for details of the bioinformatic analysis.

qRT-PCR

RNA was purified from FACS-sorted populations with the miRNeasy kit (QIAGEN) and cDNA generated using WT-Ovation Pico System (NuGEN). See Supplemental Information for details on primer sequences.

GPCR Compound Screen

Cells were isolated by FACS and plated on poly-D-lysine- and fibronectin-coated 96-well plates in the presence of EGF. To assay the effect on qNSCs, compounds were added 1 day after plating, and cells were fixed and immunostained at day 4. To assay the effect on aNSCs, cells were plated with compounds and fixed and immunostained 1 day later. Further details are in the Supplemental Experimental Procedures.

ACCESSION NUMBERS

All data are deposited in the National Center for Biotechnology Information Gene Expression Omnibus under accession number GSE54653.

SUPPLEMENTAL INFORMATION

Supplemental Information includes Supplemental Experimental Procedures, eight figures, and eight tables and can be found with this article online at http://dx.doi.org/10.1016/j.neuron.2014.02.039.

ACKNOWLEDGMENTS

Thanks to the F.D. and Wichterle labs for insightful discussion and to Hynek Wichterle and Jun-An Chen for comments. We thank Hideyuki Okano for kindly providing the Nestin::Kusabira Orange and James Stringer for providing the alkaline phosphatase reporter mice; Kristie Gordon and Sandra Tetteh of the Herbert Irving Comprehensive Cancer Center of Columbia University for assistance with FACS and flow cytometry; and Jiri Zavadil and Yutong Zhang of the Office of Collaborative Science Genome Technology Center of New York University Langone Medical Center for microarray processing. This work was supported by the National Institute of Neurological Disorders and Stroke (NINDS) grant NS053884, funding from the NINDS-American Recovery and Reinvestment Act (NS053884-03S109), NINDS grant NS074039, New York State Stem Cell Science contracts C024287 and C026401, funding from The Leona M. and Harry B. Helmsley Charitable Trust, The Irma T. Hirschl Foundation, and The David and Lucile Packard Foundation (to F.D.); a Human Frontiers Scientific Program Long-Term Fellowship (to V.S-V.); NIH grant T32 MH 15174-29 and a fellowship from the Spanish Ministerio de Educación y Ciencia (to E.P.); NINDS grant 1F31NS079057 (to A.R.M.-S.), and NIH grants T32 GM008224, TL1 TR000082 and NINDS grant 1F31NS081990 (to A.M.D.). Work was also supported by the Jerry and Emily Spiegel Laboratory for Cell Replacement Therapies.

Accepted: February 10, 2014
Published: May 7, 2014

REFERENCES

Ahn, S., and Joyner, A.L. (2005). In vivo analysis of quiescent adult neural stem cells responding to Sonic hedgehog. Nature *437*, 894–897.

Alfonso, J., Le Magueresse, C., Zuccotti, A., Khodosevich, K., and Monyer, H. (2012). Diazepam binding inhibitor promotes progenitor proliferation in the postnatal SVZ by reducing GABA signaling. Cell Stem Cell *10*, 76–87.

Barnabé-Heider, F., Meletis, K., Eriksson, M., Bergmann, O., Sabelström, H., Harvey, M.A., Mikkers, H., and Frisén, J. (2008). Genetic manipulation of adult mouse neurogenic niches by in vivo electroporation. Nat. Methods *5*, 189–196.

Basak, O., Giachino, C., Fiorini, E., Macdonald, H.R., and Taylor, V. (2012). Neurogenic subventricular zone stem/progenitor cells are Notch1-dependent in their active but not quiescent state. J. Neurosci. *32*, 5654–5666.

Beckervordersandforth, R., Tripathi, P., Ninkovic, J., Bayam, E., Lepier, A., Stempfhuber, B., Kirchhoff, F., Hirrlinger, J., Haslinger, A., Lie, D.C., et al. (2010). In vivo fate mapping and expression analysis reveals molecular hallmarks of prospectively isolated adult neural stem cells. Cell Stem Cell *7*, 744–758.

Blanpain, C., Lowry, W.E., Geoghegan, A., Polak, L., and Fuchs, E. (2004). Self-renewal, multipotency, and the existence of two cell populations within an epithelial stem cell niche. Cell *118*, 635–648.

Cesetti, T., Fila, T., Obernier, K., Bengtson, C.P., Li, Y., Mandl, C., Hölzl-Wenig, G., and Ciccolini, F. (2011). GABAA receptor signaling induces osmotic swelling and cell cycle activation of neonatal prominin+ precursors. Stem Cells *29*, 307–319.

Chen, J., Li, Y., Yu, T.S., McKay, R.M., Burns, D.K., Kernie, S.G., and Parada, L.F. (2012). A restricted cell population propagates glioblastoma growth after chemotherapy. Nature *488*, 522–526.

Cheung, T.H., and Rando, T.A. (2013). Molecular regulation of stem cell quiescence. Nat. Rev. Mol. Cell Biol. *14*, 329–340.

Coskun, V., Wu, H., Blanchi, B., Tsao, S., Kim, K., Zhao, J., Biancotti, J.C., Hutnick, L., Krueger, R.C., Jr., Fan, G., et al. (2008). CD133+ neural stem cells in the ependyma of mammalian postnatal forebrain. Proc. Natl. Acad. Sci. USA *105*, 1026–1031.

DeCarolis, N.A., Mechanic, M., Petrik, D., Carlton, A., Ables, J.L., Malhotra, S., Bachoo, R., Götz, M., Lagace, D.C., and Eisch, A.J. (2013). In vivo contribution of nestin- and GLAST-lineage cells to adult hippocampal neurogenesis. Hippocampus *23*, 708–719.

DePrimo, S.E., Stambrook, P.J., and Stringer, J.R. (1996). Human placental alkaline phosphatase as a histochemical marker of gene expression in transgenic mice. Transgenic Res. *5*, 459–466.

Doetsch, F., García-Verdugo, J.M., and Alvarez-Buylla, A. (1997). Cellular composition and three-dimensional organization of the subventricular germinal zone in the adult mammalian brain. J. Neurosci. *17*, 5046–5061.

Doetsch, F., Caillé, I., Lim, D.A., García-Verdugo, J.M., and Alvarez-Buylla, A. (1999a). Subventricular zone astrocytes are neural stem cells in the adult mammalian brain. Cell *97*, 703–716.

Doetsch, F., García-Verdugo, J.M., and Alvarez-Buylla, A. (1999b). Regeneration of a germinal layer in the adult mammalian brain. Proc. Natl. Acad. Sci. USA *96*, 11619–11624.

Doetsch, F., Petreanu, L., Caillé, I., Garcia-Verdugo, J.M., and Alvarez-Buylla, A. (2002). EGF converts transit-amplifying neurogenic precursors in the adult brain into multipotent stem cells. Neuron *36*, 1021–1034.

Doze, V.A., and Perez, D.M. (2012). G-protein-coupled receptors in adult neurogenesis. Pharmacol. Rev. *64*, 645–675.

Forsberg, E.C., Passegué, E., Prohaska, S.S., Wagers, A.J., Koeva, M., Stuart, J.M., and Weissman, I.L. (2010). Molecular signatures of quiescent, mobilized and leukemia-initiating hematopoietic stem cells. PLoS ONE *5*, e8785.

Fukada, S., Uezumi, A., Ikemoto, M., Masuda, S., Segawa, M., Tanimura, N., Yamamoto, H., Miyagoe-Suzuki, Y., and Takeda, S. (2007). Molecular signature of quiescent satellite cells in adult skeletal muscle. Stem Cells *25*, 2448–2459.

Garcia, A.D.R., Doan, N.B., Imura, T., Bush, T.G., and Sofroniew, M.V. (2004). GFAP-expressing progenitors are the principal source of constitutive neurogenesis in adult mouse forebrain. Nat. Neurosci. *7*, 1233–1241.

Garza, L.A., Liu, Y., Yang, Z., Alagesan, B., Lawson, J.A., Norberg, S.M., Loy, D.E., Zhao, T., Blatt, H.B., Stanton, D.C., et al. (2012). Prostaglandin D2 inhibits hair growth and is elevated in bald scalp of men with androgenetic alopecia. Sci. Transl. Med. *4*, 126ra34.

Giachino, C., and Taylor, V. (2009). Lineage analysis of quiescent regenerative stem cells in the adult brain by genetic labelling reveals spatially restricted neurogenic niches in the olfactory bulb. Eur. J. Neurosci. *30*, 9–24.

Giachino, C., Basak, O., Lugert, S., Knuckles, P., Obernier, K., Fiorelli, R., Frank, S., Raineteau, O., Alvarez-Buylla, A., and Taylor, V. (2014). Molecular diversity subdivides the adult forebrain neural stem cell population. Stem Cells *32*, 70–84.

Graham, V., Khudyakov, J., Ellis, P., and Pevny, L. (2003). SOX2 functions to maintain neural progenitor identity. Neuron *39*, 749–765.

Groves, A., Kihara, Y., and Chun, J. (2013). Fingolimod: direct CNS effects of sphingosine 1-phosphate (S1P) receptor modulation and implications in multiple sclerosis therapy. J. Neurol. Sci. *328*, 9–18.

Holland, E.C., Celestino, J., Dai, C., Schaefer, L., Sawaya, R.E., and Fuller, G.N. (2000). Combined activation of Ras and Akt in neural progenitors induces glioblastoma formation in mice. Nat. Genet. *25*, 55–57.

Imayoshi, I., Sakamoto, M., and Kageyama, R. (2011). Genetic methods to identify and manipulate newly born neurons in the adult brain. Front. Neurosci. *5*, 64.

Imura, T., Kornblum, H.I., and Sofroniew, M.V. (2003). The predominant neural stem cell isolated from postnatal and adult forebrain but not early embryonic forebrain expresses GFAP. J. Neurosci. *23*, 2824–2832.

Ishizuka, K., Kamiya, A., Oh, E.C., Kanki, H., Seshadri, S., Robinson, J.F., Murdoch, H., Dunlop, A.J., Kubo, K., Furukori, K., et al. (2011). DISC1-dependent switch from progenitor proliferation to migration in the developing cortex. Nature *473*, 92–96.

Ivanova, N.B., Dimos, J.T., Schaniel, C., Hackney, J.A., Moore, K.A., and Lemischka, I.R. (2002). A stem cell molecular signature. Science *298*, 601–604.

Jensen, K.B., and Watt, F.M. (2006). Single-cell expression profiling of human epidermal stem and transit-amplifying cells: Lrig1 is a regulator of stem cell quiescence. Proc. Natl. Acad. Sci. USA *103*, 11958–11963.

Jensen, K.B., Collins, C.A., Nascimento, E., Tan, D.W., Frye, M., Itami, S., and Watt, F.M. (2009). Lrig1 expression defines a distinct multipotent stem cell population in mammalian epidermis. Cell Stem Cell *4*, 427–439.

Kanki, H., Shimabukuro, M.K., Miyawaki, A., and Okano, H. (2010). "Color Timer" mice: visualization of neuronal differentiation with fluorescent proteins. Mol. Brain *3*, 5.

Kappos, L., Antel, J., Comi, G., Montalban, X., O'Connor, P., Polman, C.H., Haas, T., Korn, A.A., Karlsson, G., and Radue, E.W.; FTY720 D2201 Study Group (2006). Oral fingolimod (FTY720) for relapsing multiple sclerosis. N. Engl. J. Med. *355*, 1124–1140.

Kawaguchi, D., Furutachi, S., Kawai, H., Hozumi, K., and Gotoh, Y. (2013). Dll1 maintains quiescence of adult neural stem cells and segregates asymmetrically during mitosis. Nat Commun *4*, 1880.

Kazanis, I., Lathia, J.D., Vadakkan, T.J., Raborn, E., Wan, R., Mughal, M.R., Eckley, D.M., Sasaki, T., Patton, B., Mattson, M.P., et al. (2010). Quiescence and activation of stem and precursor cell populations in the subependymal zone of the mammalian brain are associated with distinct cellular and extracellular matrix signals. J. Neurosci. *30*, 9771–9781.

Knobloch, M., Braun, S.M., Zurkirchen, L., von Schoultz, C., Zamboni, N., Araúzo-Bravo, M.J., Kovacs, W.J., Karalay, O., Suter, U., Machado, R.A., et al. (2013). Metabolic control of adult neural stem cell activity by Fasn-dependent lipogenesis. Nature *493*, 226–230.

Kokovay, E., Goderie, S., Wang, Y., Lotz, S., Lin, G., Sun, Y., Roysam, B., Shen, Q., and Temple, S. (2010). Adult SVZ lineage cells home to and leave

the vascular niche via differential responses to SDF1/CXCR4 signaling. Cell Stem Cell *7*, 163–173.

Kokovay, E., Wang, Y., Kusek, G., Wurster, R., Lederman, P., Lowry, N., Shen, Q., and Temple, S. (2012). VCAM1 is essential to maintain the structure of the SVZ niche and acts as an environmental sensor to regulate SVZ lineage progression. Cell Stem Cell *11*, 220–230.

Kondabolu, S., Adsumelli, R., Schabel, J., Glass, P., and Pentyala, S. (2011). Evaluation of prostaglandin D2 as a CSF leak marker: implications in safe epidural anesthesia. Local Reg. Anesth. *4*, 21–24.

Lacar, B., Young, S.Z., Platel, J.C., and Bordey, A. (2011). Gap junction-mediated calcium waves define communication networks among murine postnatal neural progenitor cells. Eur. J. Neurosci. *34*, 1895–1905.

Lacar, B., Herman, P., Platel, J.C., Kubera, C., Hyder, F., and Bordey, A. (2012). Neural progenitor cells regulate capillary blood flow in the postnatal subventricular zone. J. Neurosci. *32*, 16435–16448.

Laywell, E.D., Rakic, P., Kukekov, V.G., Holland, E.C., and Steindler, D.A. (2000). Identification of a multipotent astrocytic stem cell in the immature and adult mouse brain. Proc. Natl. Acad. Sci. USA *97*, 13883–13888.

Le Belle, J.E., Orozco, N.M., Paucar, A.A., Saxe, J.P., Mottahedeh, J., Pyle, A.D., Wu, H., and Kornblum, H.I. (2011). Proliferative neural stem cells have high endogenous ROS levels that regulate self-renewal and neurogenesis in a PI3K/Akt-dependant manner. Cell Stem Cell *8*, 59–71.

Lee, C., Hu, J., Ralls, S., Kitamura, T., Loh, Y.P., Yang, Y., Mukouyama, Y.S., and Ahn, S. (2012). The molecular profiles of neural stem cell niche in the adult subventricular zone. PLoS ONE *7*, e50501.

Lendahl, U., Zimmerman, L.B., and McKay, R.D. (1990). CNS stem cells express a new class of intermediate filament protein. Cell *60*, 585–595.

Li, L., and Clevers, H. (2010). Coexistence of quiescent and active adult stem cells in mammals. Science *327*, 542–545.

López-Juárez, A., Howard, J., Ullom, K., Howard, L., Grande, A., Pardo, A., Waclaw, R., Sun, Y.Y., Yang, D., Kuan, C.Y., et al. (2013). Gsx2 controls region-specific activation of neural stem cells and injury-induced neurogenesis in the adult subventricular zone. Genes Dev. *27*, 1272–1287.

Marqués-Torrejón, M.Á., Porlan, E., Banito, A., Gómez-Ibarlucea, E., Lopez-Contreras, A.J., Fernández-Capetillo, O., Vidal, A., Gil, J., Torres, J., and Fariñas, I. (2013). Cyclin-dependent kinase inhibitor p21 controls adult neural stem cell expansion by regulating Sox2 gene expression. Cell Stem Cell *12*, 88–100.

Martynoga, B., Mateo, J.L., Zhou, B., Andersen, J., Achimastou, A., Urbán, N., van den Berg, D., Georgopoulou, D., Hadjur, S., Wittbrodt, J., et al. (2013). Epigenomic enhancer annotation reveals a key role for NFIX in neural stem cell quiescence. Genes Dev. *27*, 1769–1786.

Marzesco, A.-M., Janich, P., Wilsch-Bräuninger, M., Dubreuil, V., Langenfeld, K., Corbeil, D., and Huttner, W.B. (2005). Release of extracellular membrane particles carrying the stem cell marker prominin-1 (CD133) from neural progenitors and other epithelial cells. J. Cell Sci. *118*, 2849–2858.

Maslov, A.Y., Barone, T.A., Plunkett, R.J., and Pruitt, S.C. (2004). Neural stem cell detection, characterization, and age-related changes in the subventricular zone of mice. J. Neurosci. *24*, 1726–1733.

Merkle, F.T., Mirzadeh, Z., and Alvarez-Buylla, A. (2007). Mosaic organization of neural stem cells in the adult brain. Science *317*, 381–384.

Mirzadeh, Z., Merkle, F.T., Soriano-Navarro, M., Garcia-Verdugo, J.M., and Alvarez-Buylla, A. (2008). Neural stem cells confer unique pinwheel architecture to the ventricular surface in neurogenic regions of the adult brain. Cell Stem Cell *3*, 265–278.

Mirzadeh, Z., Doetsch, F., Sawamoto, K., Wichterle, H., and Alvarez-Buylla, A. (2010). The subventricular zone en-face: wholemount staining and ependymal flow. J. Vis. Exp. (39) http://dx.doi.org/10.3791/1938.

Morshead, C.M., Reynolds, B.A., Craig, C.G., McBurney, M.W., Staines, W.A., Morassutti, D., Weiss, S., and van der Kooy, D. (1994). Neural stem cells in the adult mammalian forebrain: a relatively quiescent subpopulation of subependymal cells. Neuron *13*, 1071–1082.

Morshead, C.M., Garcia, A.D., Sofroniew, M.V., and van Der Kooy, D. (2003). The ablation of glial fibrillary acidic protein-positive cells from the adult central nervous system results in the loss of forebrain neural stem cells but not retinal stem cells. Eur. J. Neurosci. *18*, 76–84.

Nam, H.-S., and Benezra, R. (2009). High levels of Id1 expression define B1 type adult neural stem cells. Cell Stem Cell *5*, 515–526.

Ortega, F., Gascón, S., Masserdotti, G., Deshpande, A., Simon, C., Fischer, J., Dimou, L., Chichung Lie, D., Schroeder, T., and Berninger, B. (2013). Oligodendrogliogenic and neurogenic adult subependymal zone neural stem cells constitute distinct lineages and exhibit differential responsiveness to Wnt signalling. Nat. Cell Biol. *15*, 602–613.

Pallafacchina, G., François, S., Regnault, B., Czarny, B., Dive, V., Cumano, A., Montarras, D., and Buckingham, M. (2010). An adult tissue-specific stem cell in its niche: a gene profiling analysis of in vivo quiescent and activated muscle satellite cells. Stem Cell Res. (Amst.) *4*, 77–91.

Pastrana, E., Cheng, L.-C., and Doetsch, F. (2009). Simultaneous prospective purification of adult subventricular zone neural stem cells and their progeny. Proc. Natl. Acad. Sci. USA *106*, 6387–6392.

Pastrana, E., Silva-Vargas, V., and Doetsch, F. (2011). Eyes wide open: a critical review of sphere-formation as an assay for stem cells. Cell Stem Cell *8*, 486–498.

Pinto, L., Mader, M.T., Irmler, M., Gentilini, M., Santoni, F., Drechsel, D., Blum, R., Stahl, R., Bulfone, A., Malatesta, P., et al. (2008). Prospective isolation of functionally distinct radial glial subtypes—lineage and transcriptome analysis. Mol. Cell. Neurosci. *38*, 15–42.

Platel, J.C., Gordon, V., Heintz, T., and Bordey, A. (2009). GFAP-GFP neural progenitors are antigenically homogeneous and anchored in their enclosed mosaic niche. Glia *57*, 66–78.

Ponti, G., Obernier, K., Guinto, C., Jose, L., Bonfanti, L., and Alvarez-Buylla, A. (2013). Cell cycle and lineage progression of neural progenitors in the ventricular-subventricular zones of adult mice. Proc. Natl. Acad. Sci. USA *110*, E1045–E1054.

Porlan, E., Morante-Redolat, J.M., Marqués-Torrejón, M.Á., Andreu-Agulló, C., Carneiro, C., Gómez-Ibarlucea, E., Soto, A., Vidal, A., Ferrón, S.R., and Fariñas, I. (2013). Transcriptional repression of Bmp2 by p21(Waf1/Cip1) links quiescence to neural stem cell maintenance. Nat. Neurosci. *16*, 1567–1575.

Powell, A.E., Wang, Y., Li, Y., Poulin, E.J., Means, A.L., Washington, M.K., Higginbotham, J.N., Juchheim, A., Prasad, N., Levy, S.E., et al. (2012). The pan-ErbB negative regulator Lrig1 is an intestinal stem cell marker that functions as a tumor suppressor. Cell *149*, 146–158.

Sanai, N., Tramontin, A.D., Quiñones-Hinojosa, A., Barbaro, N.M., Gupta, N., Kunwar, S., Lawton, M.T., McDermott, M.W., Parsa, A.T., Manuel-García Verdugo, J., et al. (2004). Unique astrocyte ribbon in adult human brain contains neural stem cells but lacks chain migration. Nature *427*, 740–744.

Sanai, N., Nguyen, T., Ihrie, R.A., Mirzadeh, Z., Tsai, H.H., Wong, M., Gupta, N., Berger, M.S., Huang, E., Garcia-Verdugo, J.M., et al. (2011). Corridors of migrating neurons in the human brain and their decline during infancy. Nature *478*, 382–386.

Sato, K., Malchinkhuu, E., Horiuchi, Y., Mogi, C., Tomura, H., Tosaka, M., Yoshimoto, Y., Kuwabara, A., and Okajima, F. (2007). HDL-like lipoproteins in cerebrospinal fluid affect neural cell activity through lipoprotein-associated sphingosine 1-phosphate. Biochem. Biophys. Res. Commun. *359*, 649–654.

Shen, Q., Wang, Y., Kokovay, E., Lin, G., Chuang, S.-M., Goderie, S.K., Roysam, B., and Temple, S. (2008). Adult SVZ stem cells lie in a vascular niche: a quantitative analysis of niche cell-cell interactions. Cell Stem Cell *3*, 289–300.

Silva-Vargas, V., Crouch, E.E., and Doetsch, F. (2013). Adult neural stem cells and their niche: a dynamic duo during homeostasis, regeneration, and aging. Curr. Opin. Neurobiol. *23*, 935–942.

Subramanian, A., Tamayo, P., Mootha, V.K., Mukherjee, S., Ebert, B.L., Gillette, M.A., Paulovich, A., Pomeroy, S.L., Golub, T.R., Lander, E.S., and Mesirov, J.P. (2005). Gene set enrichment analysis: a knowledge-based approach for interpreting genome-wide expression profiles. Proc. Natl. Acad. Sci. USA *102*, 15545–15550.

Sun, Y., Kong, W., Falk, A., Hu, J., Zhou, L., Pollard, S., and Smith, A. (2009). CD133 (Prominin) negative human neural stem cells are clonogenic and tripotent. PLoS ONE *4*, e5498.

Sunabori, T., Tokunaga, A., Nagai, T., Sawamoto, K., Okabe, M., Miyawaki, A., Matsuzaki, Y., Miyata, T., and Okano, H. (2008). Cell-cycle-specific nestin expression coordinates with morphological changes in embryonic cortical neural progenitors. J. Cell Sci. *121*, 1204–1212.

Tavazoie, M., Van der Veken, L., Silva-Vargas, V., Louissaint, M., Colonna, L., Zaidi, B., Garcia-Verdugo, J.M., and Doetsch, F. (2008). A specialized vascular niche for adult neural stem cells. Cell Stem Cell *3*, 279–288.

Uchida, N., Buck, D.W., He, D., Reitsma, M.J., Masek, M., Phan, T.V., Tsukamoto, A.S., Gage, F.H., and Weissman, I.L. (2000). Direct isolation of human central nervous system stem cells. Proc. Natl. Acad. Sci. USA *97*, 14720–14725.

van den Berge, S.A., Middeldorp, J., Zhang, C.E., Curtis, M.A., Leonard, B.W., Mastroeni, D., Voorn, P., van de Berg, W.D., Huitinga, I., and Hol, E.M. (2010). Longterm quiescent cells in the aged human subventricular neurogenic system specifically express GFAP-delta. Aging Cell *9*, 313–326.

Venezia, T.A., Merchant, A.A., Ramos, C.A., Whitehouse, N.L., Young, A.S., Shaw, C.A., and Goodell, M.A. (2004). Molecular signatures of proliferation and quiescence in hematopoietic stem cells. PLoS Biol. *2*, e301.

Ventura, R.E., and Goldman, J.E. (2007). Dorsal radial glia generate olfactory bulb interneurons in the postnatal murine brain. J. Neurosci. *27*, 4297–4302.

Wilson, A., Laurenti, E., Oser, G., van der Wath, R.C., Blanco-Bose, W., Jaworski, M., Offner, S., Dunant, C.F., Eshkind, L., Bockamp, E., et al. (2008). Hematopoietic stem cells reversibly switch from dormancy to self-renewal during homeostasis and repair. Cell *135*, 1118–1129.

Young, K.M., Fogarty, M., Kessaris, N., and Richardson, W.D. (2007). Subventricular zone stem cells are heterogeneous with respect to their embryonic origins and neurogenic fates in the adult olfactory bulb. J. Neurosci. *27*, 8286–8296.

Young, S.Z., Taylor, M.M., and Bordey, A. (2011). Neurotransmitters couple brain activity to subventricular zone neurogenesis. Eur. J. Neurosci. *33*, 1123–1132.

Zhuo, L., Sun, B., Zhang, C.L., Fine, A., Chiu, S.Y., and Messing, A. (1997). Live astrocytes visualized by green fluorescent protein in transgenic mice. Dev. Biol. *187*, 36–42.

Zimmerman, L., Parr, B., Lendahl, U., Cunningham, M., McKay, R., Gavin, B., Mann, J., Vassileva, G., and McMahon, A. (1994). Independent regulatory elements in the nestin gene direct transgene expression to neural stem cells or muscle precursors. Neuron *12*, 11–24.

Neuron, Volume *82*

Supplemental Information

Prospective Identification and Purification of Quiescent Adult Neural Stem Cells from Their In Vivo Niche

Paolo Codega, Violeta Silva-Vargas, Alex Paul, Angel R. Maldonado-Soto, Annina M. DeLeo, Erika Pastrana, and Fiona Doetsch

SUPPLEMENTAL FIGURES

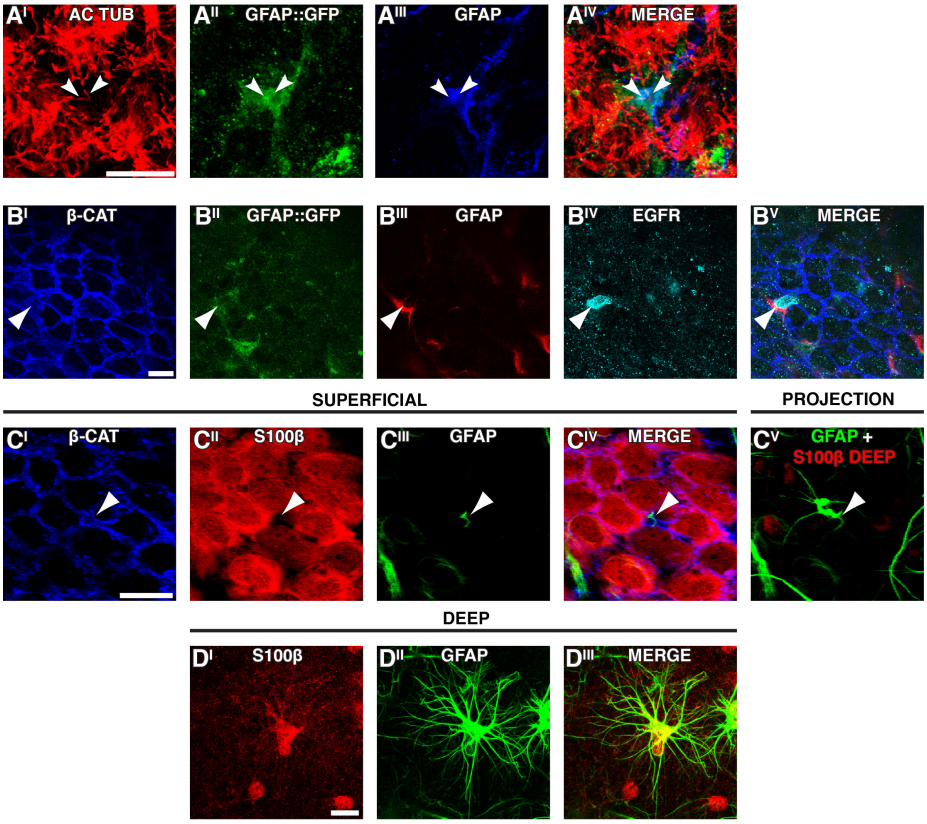

Figure S1. Characterization of V-SVZ astrocytes, related to Figure 1

(A) Confocal images at the ventricular surface of a whole mount preparation showing endogenous expression of GFAP::GFP (A^{II}) and immunostained for Acetylated Tubulin (A^{I}) and GFAP (A^{III}). A^{IV} is a merged image. Some $GFAP^+$ and $GFAP::GFP^+$ cells contact the ventricle and have a single cilium (arrowheads).

(B) Confocal images at the ventricular surface of a whole mount preparation showing endogenous expression of GFAP::GFP (B^{II}) and immunostained for β-Catenin (B^{I}), GFAP (B^{III}) and EGFR (B^{IV}). B^{V} is a merged image. Note that some $GFAP^+$ and $GFAP::GFP^+$ cells are $EGFR^+$ (arrowhead).

(C) Confocal images at the ventricular surface of a whole mount preparation (C^{I}-C^{IV}) immunostained with β-Catenin (C^{I}), S100β (C^{II}) and GFAP (C^{III}). C^{IV} is a merged image. In C^{V}, GFAP and S100β subventricular projection (excluding the ventricular surface) is shown. Note that astrocytes contacting the ventricle are S100β negative.

(D) Confocal subventricular projection for S100β (D^{I}) and GFAP (D^{II}). Large stellate $GFAP^+$ cells, adjacent to the striatum, are S100β positive.

Scale bars: 30 μm.

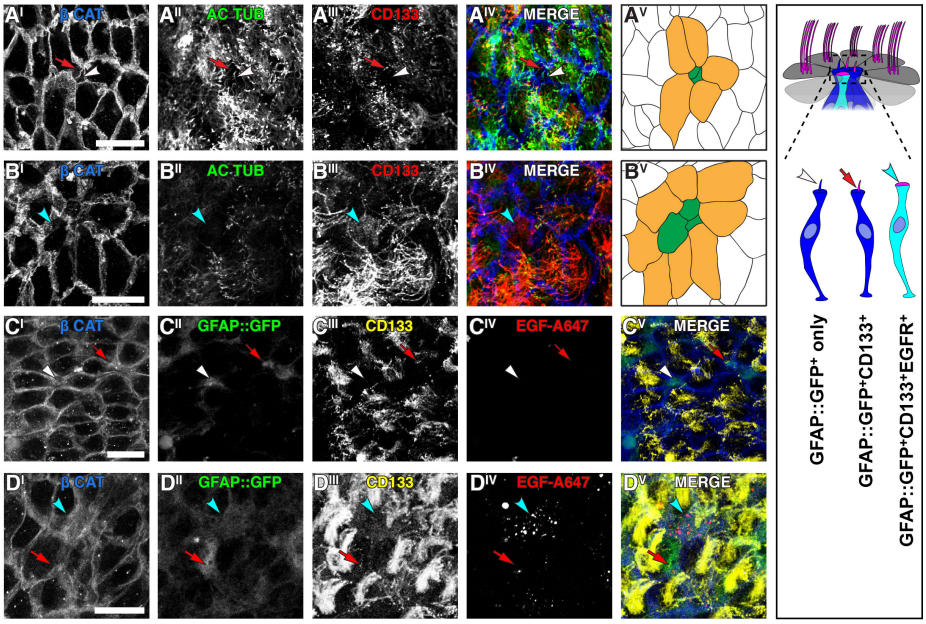

Figure S2. V-SVZ astrocytes contacting the ventricle are heterogeneous, related to Figure 1

(A-B) Confocal images of the ventricular surface of whole mount preparations immunostained for β-Catenin (A^{I} and B^{I}), Acetylated Tubulin (A^{II} and B^{II}) and CD133 (A^{III} and B^{III}). A^{IV} and B^{IV} are merged images. A^{V} and B^{V} are schematic representations of the pinwheels shown in A^{I-IV} and B^{I-IV}. Schema on the right summarizes the profiles of astrocytes contacting the ventricle: red arrows indicate cells contacting the ventricle with a $CD133^{+}$ primary cilium; blue arrowheads indicate cells with diffuse CD133 and lacking a primary cilium; white arrowheads indicate cells contacting the ventricle with a single cilium that is negative for CD133.

(C-D) Confocal images of the ventricular surface of whole mount preparations immunostained for β-Catenin (C^{I} and D^{I}) and CD133 (C^{III} and D^{III}) and showing endogenous expression of GFAP::GFP (C^{II} and D^{II}) and EGF ligand-A647 binding (C^{IV} and D^{IV}). C^{V} and D^{V} are merged images. Examples of $GFAP::GFP^{+}CD133^{+}$ cells that do not bind EGF ligand (red arrows in C and D); GFAP::GFP-dim cells with diffuse CD133 bind EGF ligand (blue arrowhead in D); $GFAP::GFP^{+}$ cells that lack CD133 and EGF ligand (white arrowhead in C).

Scale bars: 30 μm.

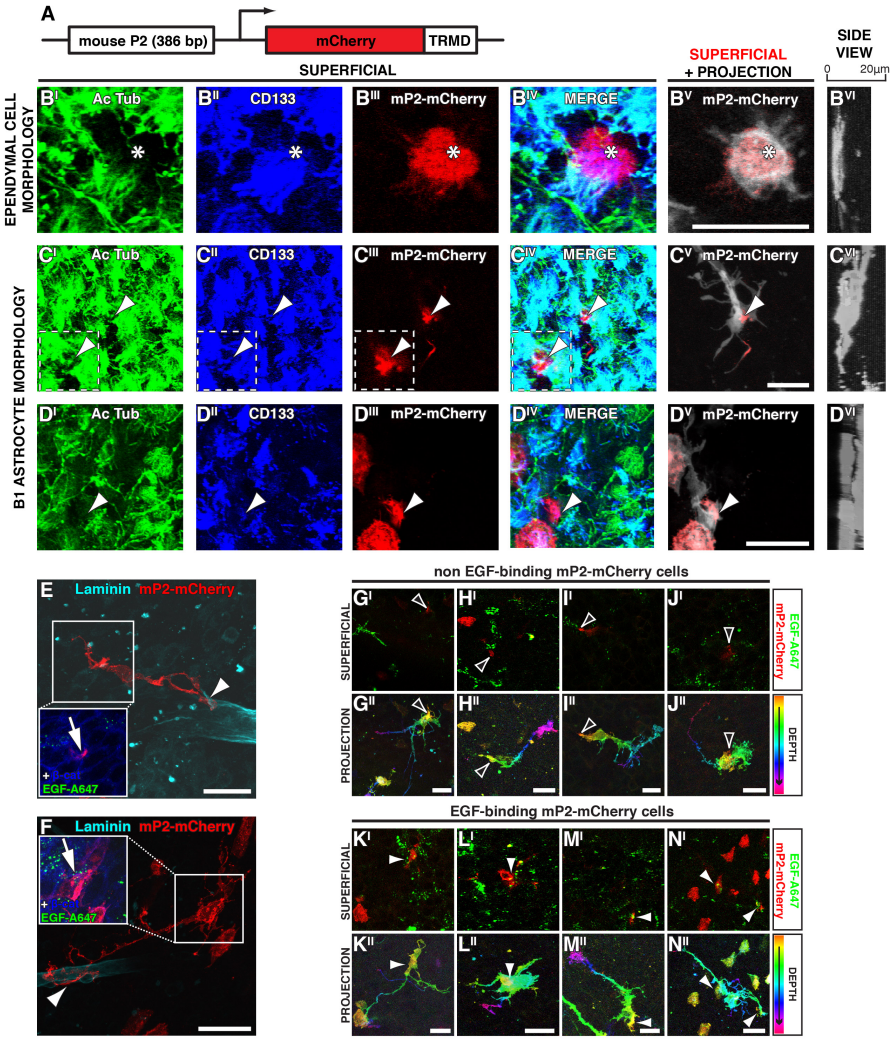

Figure S3. ***In vivo*** **validation of mP2-mCherry transgene and examples of astrocyte morphology, related to Figure 2**

(A) Schema of the transgene used for morphological studies. A plasmid containing an mCherry-transferrin receptor membrane-anchor domain (TRMD) fusion gene under the control of the mouse P2 element of the Prominin1 promoter was electroporated into V-SVZ cells lining the ventricle.

(B-D) Confocal images of the ventricular (superficial) surface of whole mounts immunostained with Acetylated Tubulin (B^{I}, C^{I}, D^{I}) and CD133 (B^{II}, C^{II}, D^{II}), showing mP2-mCherry^{+} cells (B^{III}, C^{III}, D^{III}). B^{IV}, C^{IV} and D^{IV} are merged images. B^{V}, C^{V} and D^{V} are z-stack projections of the same cells through the entire depth of the V-SVZ. B^{VI}, C^{VI} and D^{VI} are side views of the projections. The transgene is expressed in multiciliated CD133^{+} ependymal cells (B, asterisk), CD133^{+} monociliated cells (C, arrowhead and inset) and non-ciliated diffuse CD133^{+} cells (D, arrowhead).

(E-F) Confocal images of whole mounts showing projections of EGF-ligand negative (E) and positive (F) cells labeled by mP2-mCherry transgene (red) and immunostained with laminin (cyan). In the insets, superficial optical slices of the same cells showing EGF-A647 (green) and β-Catenin (blue).

(G-N) Confocal images of whole mounts showing examples of EGF^{-} (G-J) and EGF^{+} (K-N) mP2-mCherry^{+} cells. Upper panels (G^{I}-N^{I}) show EGF-ligand and mP2-mCherry labeling in an optical slice at the ventricular surface. Lower panels (G^{II}-N^{II}) show depth-coded projections of the same mP2-mCherry labeled cells, where orange/yellow is superficial and blue/violet is deep. Scale bars: 30 µm.

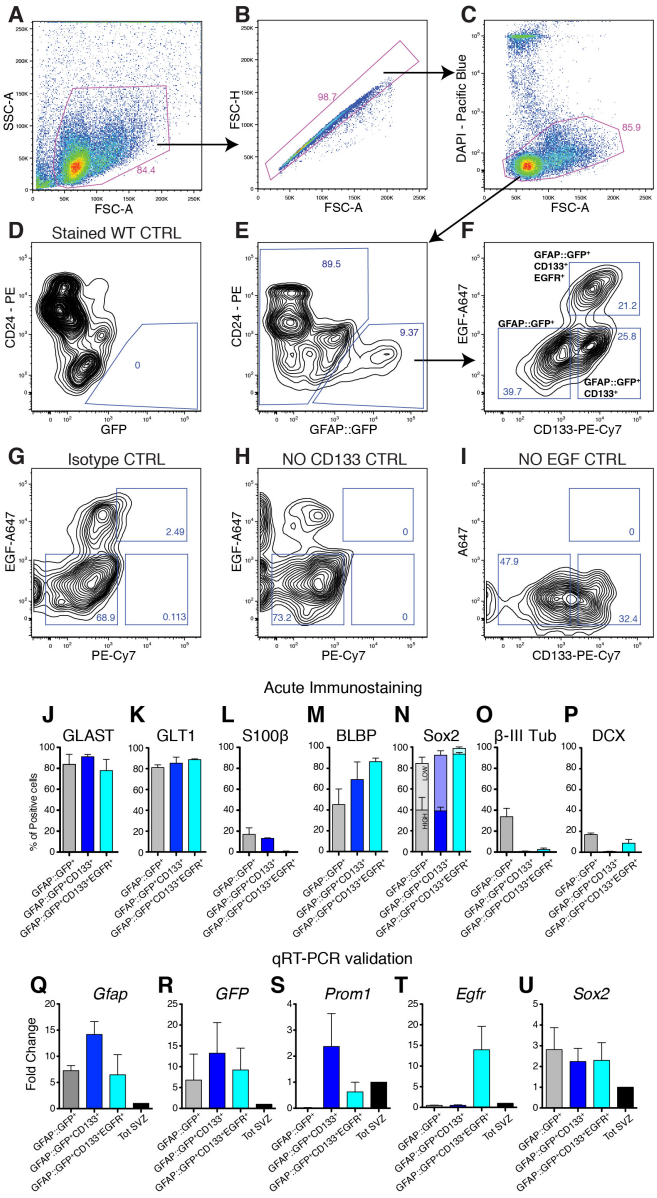

Figure S4. Gating strategy for V-SVZ astrocyte purification by FACS and marker validation of purified populations, related to Figure 3

(A-I) FACS plot flow chart of the 5 color strategy used for sorting and analyzing V-SVZ astrocyte subpopulations using DAPI, CD24-PE, EGF-A647 and CD133-PE-Cy7 in GFAP::GFP mice. After excluding cell debris (A), and gating for single cells (B) and live DAPI negative cells (C), GFP^+CD24^- cells were selected (E) and subsequently three populations were defined (F): $GFAP::GFP^+$, $GFAP::GFP^+CD133^+$ and $GFAP::GFP^+CD133^+EGFR^+$. A wild type (WT) mouse control stained with all the markers was used to set the gate for $GFAP::GFP^+CD24^-$ population (D). The gates for $CD133^+$ astrocytes were set according to the isotype control (G) and the "NO CD133" control (H) in which all markers but CD133 primary antibody were added. Similarly for the "NO EGF" control (I).

(J-P) Proportions of acutely-plated purified cells immunopositive for GLAST (J), GLT1 (K), S100β (L), BLBP (M), Sox2 (HIGH: bright expression darker colors, LOW: dim expression, lighter colors) (N), β-III Tub (O), and DCX (P) (average of 3 independent sorts; mean±SEM).
(Q-U) Gene expression levels of *Gfap* (Q), *GFP* (R), *Prom1* (S), *Egfr* (T), and *Sox2* (U) detected with qRT-PCR in purified populations as compared to sorted total SVZ cells (as gated in S4C) (n=3; mean±SEM). Note that GFAP::GFP^{+}CD133^{+}EGFR^{+} Prom1 gene level is 34 fold enriched over the GFAP::GFP^{+} population, which is CD133^{-}, but does not show enrichment when compared to total SVZ control that also includes ependymal cells, which express very high levels of CD133.

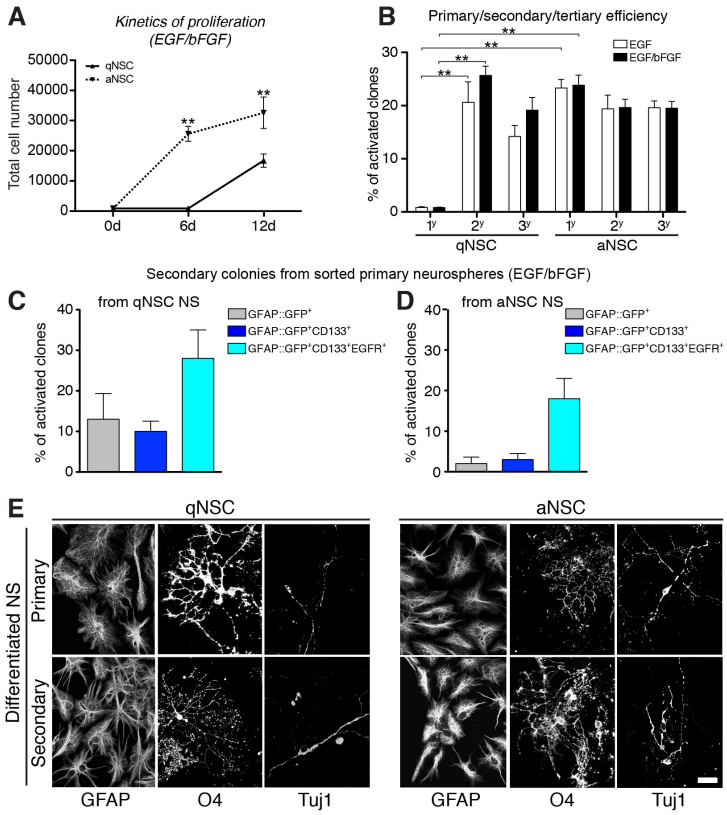

Figure S5. Purified qNSCs and aNSCs exhibit different proliferation kinetics *in vitro*, related to Figure 5

(A) Quantification of cell proliferation when purified cells are plated at clonal density (1.4 cell/µl) in the presence of EGF/bFGF (n=3, mean±SEM, **p<0.01, unpaired Student's t-test).

(B) Percentage of activating clones for primary, secondary and tertiary neurospheres from purified populations cultured in the presence of EGF/bFGF or EGF only (n=5, mean±SEM, **p<0.01, unpaired Student's t-test).

(C-D) Clonal activation efficiency of purified GFAP::GFP$^+$, GFAP::GFP$^+$CD133$^+$ and GFAP::GFP$^+$CD133$^+$EGFR$^+$ cells from primary neurospheres of qNSCs and aNSCs cultured in EGF/bFGF (n=3, mean±SEM, *p<0.05, unpaired Student's t-test).

(E) Confocal images of differentiated primary and secondary neurospheres. All populations give rise to astrocytes (GFAP$^+$), oligodendrocytes (O4$^+$) and neurons (βIII Tubulin$^+$). Scale bar: 10µm.

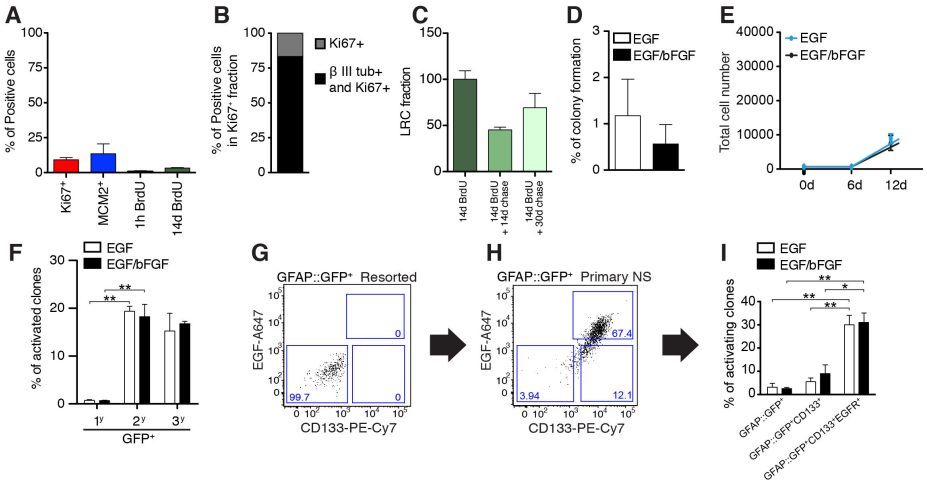

Figure S6. Cell cycle and functional data of GFAP::GFP$^+$only population, related to Figure 3 and Figure 5

(A) Proportion of FACS-purified GFAP::GFP$^+$only population that expresses Ki67 and MCM2 (n=3), and the fraction labeled after a single pulse of BrdU (light green) or after 14 days of BrdU in drinking water (dark green) (n=3 and n=4, respectively) (mean±SEM).

(B) Percentage of βIII Tubulin positive cells in the Ki67$^+$ fraction in GFAP::GFP$^+$only population detected by double acute immunostaining (n=2, mean±SEM).

(C) Label-retaining cell (LRC) fraction in the GFAP::GFP$^+$only population 14 and 30 days of chase after 14 days of BrdU administration (n=4, mean±SEM).

(D) Single cell colony formation efficiency of FACS-purified GFAP::GFP$^+$only population in EGF/bFGF or EGF only in adherent conditions (n=3, mean±SEM).

(E) Quantification of cell proliferation when purified cells are plated at clonal density (1.4 cell/µl) with EGF/bFGF or EGF only in floating conditions (n=5, mean±SEM).

(F) Percentage of activating clones for primary, secondary and tertiary neurospheres from purified GFAP::GFP$^+$only population cultured in the presence of EGF/bFGF or EGF only (n=5, mean±SEM, **p<0.01, unpaired Student's t-test).

(G-H) Representative FACS plots of purified GFAP::GFP$^+$only population resorted immediately after isolation from the brain (G) and of primary neurospheres cultured in EGF for 12 days (H).

(I) Neurosphere formation efficiency of purified GFAP::GFP$^+$, GFAP::GFP$^+$CD133$^+$ and GFAP::GFP$^+$CD133$^+$EGFR$^+$ cells from GFAP::GFP$^+$only population derived primary neurospheres (in EGF/bFGF or EGF only, n=3, mean±SEM, *p<0.05, **p<0.01, unpaired Student's t-test).

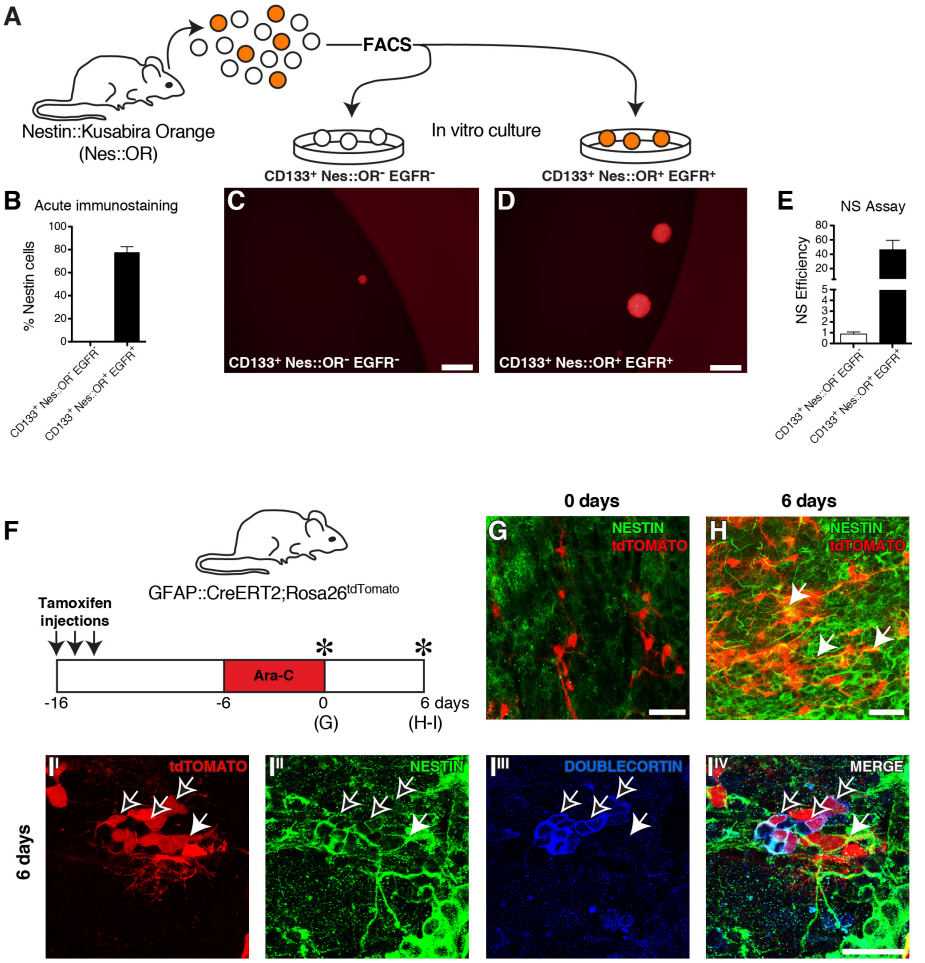

Figure S7. Nestin-negative cells give rise to Nestin-positive cells in vitro and during regeneration in vivo, related to Figure 6

(A-E) In vitro upregulation of Nestin in live cells.

(A) Schema of the experimental design. CD133$^+$Nes::OR$^-$EGFR$^-$CD24$^-$ and CD133$^+$Nes::OR$^+$EGFR$^+$CD24$^-$ cells were isolated from the V-SVZ of adult Nestin::Kusabira Orange (Nes::OR) mice and plated for neurosphere formation.

(B) Quantification of acute immunostaining for Nestin in CD133$^+$Nes::OR$^-$EGFR$^-$ and CD133$^+$Nes::OR$^+$EGFR$^+$ populations (n=3, mean±SEM).

(C-D) Fluorescent images of neurospheres after 6 days in culture from CD133$^+$Nes::OR$^-$EGFR$^-$ (C) and CD133$^+$Nes::OR$^+$EGFR$^+$ (D) populations. All neurospheres were Nestin::Kusabira Orange positive. Note that the sphere from CD133$^+$Nes::OR$^-$EGFR$^-$ cells is much smaller. Scale bar: 200 µm.

(E) Quantification of the efficiency of neurosphere formation from purified populations (n=3, mean±SEM).

(F-I) Nestin-negative cells give rise to the SVZ lineage during regeneration in GFAP::CreERT2;Rosa26^{tdTomato} mice.

(F) Schema of the experimental design. Recombination was induced in adult GFAP::CreERT2;Rosa26^{tdTomato} mice by three tamoxifen injections 10 days before Ara-C treatment. Brains were harvested at day 0 or 6 days after terminating Ara-C treatment (asterisks). Whole mounts were immunostained for Nestin (green) and doublecortin (blue).

(G-H) Confocal images of z-stacks of whole mount preparations at 0 days and 6 days after Ara-C treatment. Radial tdTomato$^+$ cells were all Nestin negative at 0d. Radial tdTomato$^+$Nestin$^+$ cells (white arrows) were detected at 6 days.

(I) Confocal image of a whole mount preparation showing tdTomato expression (I^I, red) and immunostained for Nestin (I^{II}, green) and Doublecortin (I^{III}, blue) showing tdTomato$^+$Nestin$^+$cells (white arrow) and tdTomato$^+$Doublecortin$^+$ (open arrows) at 6 days after Ara-C removal. I^{IV} is a merged image. Scale bar: 30 µm.

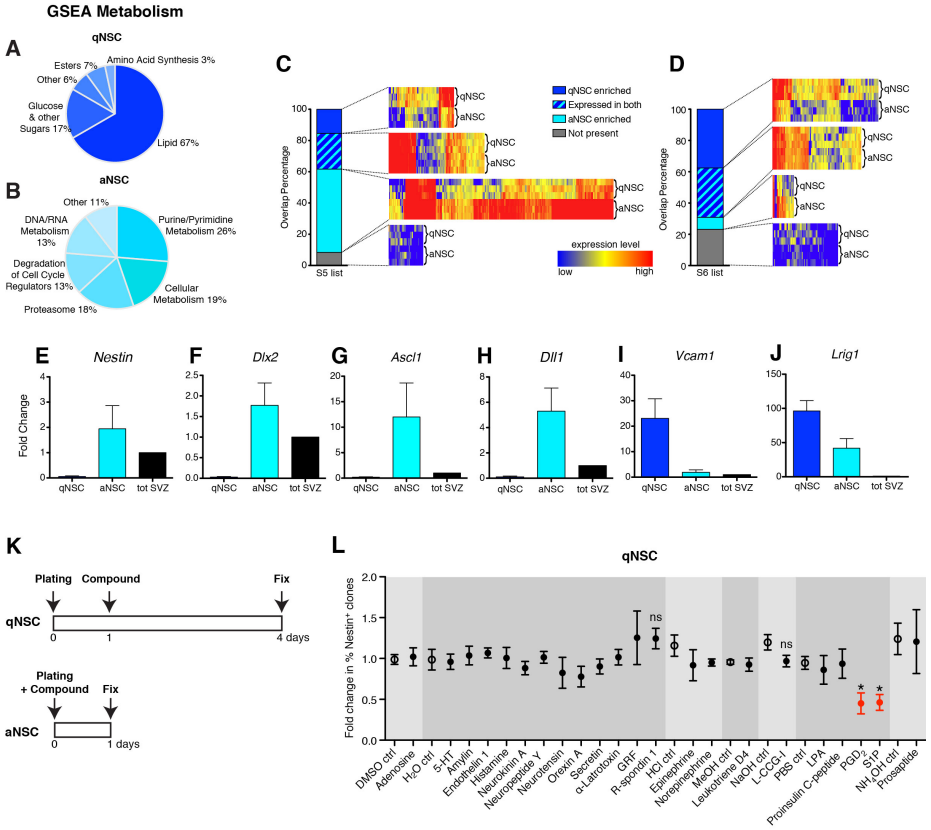

Figure S8. Gene expression profiling and targeted GPCR screen, related to Figure 7

(A-B) Pie charts showing GSEA metabolism subgroups for qNSCs and aNSCs (first bars in Figure 7D)

(C-D) Comparison of our microarray data with those of Beckervordersandforth et al. 2010. The expression of genes present in "genes enriched in adult NSCs in comparison to diencephalic astrocytes" (C) (corresponding to Table S5 from Beckervordersandforth et al., 2010) and "adult NSC-enriched genes" (D) (corresponding to Table S6 from Beckervordersandforth et al., 2010) lists was analyzed and genes subcategorized by enrichment in qNSCs and aNSCs, expression in both or not present (as defined by expression in raw data < 50 for no expression). Gene lists are in Supplementary Table S8.

(E-J) qRT-PCR validation of microarray genes showing fold-change of *Nestin* (E), *Dlx2* (F), *Ascl1* (G), *Dll1* (H), *Vcam1* (I), and *Lrig1* (J) in qNSCs and aNSCs populations relative to sorted total SVZ cells (as gated in S4C) (n=3, mean±SEM).

(K) Schema of experimental design for the qNSC and aNSC GPCR ligand screen.

(L) Plot of the fold change of qNSC activated Nestin$^+$ clones. Compounds that were statistically significant are in red (n=3, mean±SEM, *p<0.05, unpaired Student's t-test). Different shades of grey demarcate compounds in the same diluent, and open circles are controls.

SUPPLEMENTAL TABLE LEGENDS

Table S1, related to Figure 7A
Genes differentially regulated in qNSCs and aNSCs
This table reports the lists of differentially expressed genes in qNSCs and aNSCs.

Table S2, related to Figure 7B-C
Gene Ontology categories for genes differentially regulated in qNSCs and aNSCs
This table reports the lists of genes differentially expressed in qNSCs and aNSCs, grouped by GO categories.

Table S3, related to Figure 7D
GSEA sets for qNSCs and aNSCs
This table reports all the GSEA sets for qNSCs and aNSCs and their link to the Broad Institute Database.

Table S4, related to Figure 7
Expression value and fold change of transcription factors previously reported to be important in neurogenesis
This table reports the mean gene expression values for qNSCs and aNSCs (average of three replicates, ± standard deviation) and the fold change (positive and highlighted in red if upregulated in aNSCs, negative and highlighted in green if upregulated in qNSCs, color intensity indicates magnitude of fold change) for transcription factor genes previously reported to be involved in adult neurogenesis.

Table S5, related to Figure 7
Expression value and fold change of markers and factors previously reported to be important in neurogenesis
This table reports the mean gene expression values for qNSCs and aNSCs (average of three replicates, ± standard deviation) and the fold change (positive and highlighted in red if upregulated in aNSCs, negative and highlighted in green if upregulated in qNSCs, color intensity indicates magnitude of fold change) for markers and factors previously reported to be involved in adult neurogenesis.

Table S6, related to Figure 7E-F
Comparison of qNSC- and aNSC-enriched genes and molecular signatures of long term/quiescent and short term/proliferative stem cells in other organs
Tab1) Genes from the molecular signatures of long term/quiescent stem cells in other organs were included if they were enriched in qNSCs (more than 2-fold expression compared to aNSCs). Annotation is color-coded by the number of lists they were present in (purple=5; blue=4; light blue=3; green=2; black=1).
Tab2) Genes from the molecular signatures of short term/proliferative stem cells in other organs were included if they were enriched in aNSCs (more than 2-fold expression compared to qNSCs). Annotation is color-coded by the number of lists they were present in (blue=4; light blue=3; green=2; black=1).
Data are from the following articles: Ivanova et al., 2002; Venezia et al., 2004; Forsberg et al., 2010; Pallafacchina et al., 2010; Powell et al., 2012; Blanpain et al., 2004: Fukada et al., 2007; Cheung and Rando, 2013.

Table S7, related to Figure 7
Expression levels of GPCRs in qNSCs and aNSCs.
This table reports the expression levels in qNSCs and aNSCs for all the genes encoding G Protein Coupled Receptors. Genes that were enriched more than 10-fold in qNSCs (in bold) were selected for the small molecule screen.

Table S8, related to Figure 7
Comparison of our microarray data with those of Beckervordersandforth et al. (2010)
The expression of genes present in “genes enriched in adult NSCs in comparison to diencephalic astrocytes” (corresponding to Table S5 from Beckervordersandforth et al., 2010) and “adult NSC-enriched genes” (corresponding to Table S6 from Beckervordersandforth et al., 2010) lists was analyzed and genes subcategorized by enrichment in qNSCs and aNSCs, expression in both or not present (as defined by expression in raw data < 50 for no expression).

SUPPLEMENTAL EXPERIMENTAL PROCEDURES

Immunostaining

Whole mounts were fixed overnight in 3.2% paraformaldehyde, washed in PBS, incubated for 2 hrs in blocking solution (10% serum with or without Triton-X), incubated in primary antibodies in blocking solution for 24-48 hrs at 4ºC, washed 6 times and incubated in secondary antibodies overnight. Whole mounts were then further dissected and the SVZ removed, prior to mounting in Aqua Polymount (Polysciences, Inc.), and imaged using a Zeiss LSM 510 or Leica TCS SP5 II confocal microscope. For acute immunostaining, FACS-purified populations were plated without mitogens on poly-D-lysine coated 16-well Lab-Tek chamber slides (Thermo Scientific) for 2 hours, then fixed for 20 min with 3.2% paraformaldehyde. For EGF-ligand labeling, 0.5 µl of a 40 µg/ml of EGF-A647 (Invitrogen) was stereotaxically injected into the ventricle of deeply anesthetized mice 10 minutes before sacrifice as previously described (Pastrana et al., 2009). For BrdU labeling, mice were either injected intraperitoneally with 100 µl of 10mg/ml BrdU 1 hour before sacrificing or given BrdU in the drinking water (0.75% BrdU 1% glucose) for 14 days and sacrificed immediately, 14 or 30 days after stopping BrdU administration. Cells were FACS purified, acutely plated for 2 hours without mitogens and fixed. For BrdU detection, cells were treated with 2N HCl for 20 min at 37ºC, followed by 1 min 0.1M Boric Acid (pH=8.5), then washed in PBS and processed for immunostaining as above.

Antibodies

The following antibodies were used: rabbit anti-GFP (1:500, Invitrogen); sheep anti-GFP (1:200, AbD Serotec); mouse anti-GFAP (1:200, Millipore); rabbit anti-GFAP (1:500, DAKO); rat anti-GFAP (1:500, Invitrogen); rat anti-CD133 (1:100, Chemicon); mouse anti-β-Catenin (1:200, BD Bioscience); sheep anti-EGFR (1:50, Upstate); rabbit anti-EGFR (1:200, Millipore); rabbit anti-Ki67-A555 (1:100, BD Pharmingen); mouse anti-βIII Tubulin (Tuj1,1:500, Covance); rabbit anti-S100β (1:1000, DAKO); guinea pig anti-GLAST (1:1000, Chemicon); guinea pig anti-GLT1 (1:200, Millipore); rabbit anti-BLBP (1:100, Abcam); rat anti-BrdU (1:200, Accurate Chemical); goat anti-MCM2 (1:50, Santa Cruz Biotechnology); rabbit anti-Laminin (1:200, SIGMA); mouse IgM anti-O4 (1:500, Chemicon); mouse anti-Nestin (1:5, rat-401 DSHB); mouse anti-Acetylated Tubulin (1:2000, SIGMA); rabbit anti-Sox2 (1:200, Millipore); guinea pig anti-DCX (1:1000, Millipore). All staining was performed in PBS with 10% normal goat or donkey serum and 0.5% Triton X-100, except for EGFR staining (no Triton X-100). Secondary antibodies were used at 1:500 (Alexa fluor-conjugated, Molecular Probes) or 1:200 (Cy- or DyLight-conjugated, Jackson ImmunoResearch Laboratories).

FACS

The SVZs from 2-3 month old heterozygous GFAP::GFP mice (The Jackson Laboratory), which express GFP under the control of the human GFAP promoter (Zhuo et al., 1997), or wild-type CD-1 mice (Charles River Laboratories) were dissected, digested with papain (Worthington, 1,200 units per 5 mice, 10 min at 37ºC) in PIPES solution (120 mM NaCl, 5 mM KCl, 50 mM PIPES (SIGMA), 0.6% glucose, 1x Pen/Strep (Gibco) in water, pH adjusted to 7.6) and mechanically dissociated to single cells after adding ovomucoid (Worthington, 0.7 mg per 5 mice) and DNAse (Worthington, 1,000 units per 5 mice). Cells were centrifuged for 10 min at 4ºC without brakes in 22% Percoll (SIGMA) to remove myelin and incubated for 15 min with PE-conjugated rat anti-mCD24 (1:1000; BD Pharmingen), A647-complexed EGF (1:300; Molecular Probes) and biotinylated rat anti-mCD133 (1:300, clone 13A4, eBioscience), washed by centrifugation and incubated for 15 min with PE-Cy7-conjugated streptavidin (1:1000; eBioscience). All stainings and washes were carried out on ice in 1% BSA, 0.1% Glucose HBSS solution. To assess cell viability, 4',6-diamidino-2-phenylindole (DAPI; 1:1000; SIGMA) was added to the cells before sorting. All cell populations were isolated in a single sort using a Becton Dickinson FACS Aria II using 13 psi pressure and 100-µm nozzle aperture. Cells were collected in neurosphere medium (details below) without growth factors. Gates were set manually by using control samples (Fig. S2). Data were analyzed with FlowJo 9.3 data analysis software and displayed using biexponential scaling. For the Nestin-Kusabira Orange FACS, isolated cells were processed as described above and purified using the following markers: CD24-FITC (1:500), Nestin-Kusabira Orange, EGF-A647 (1:300), biotinylated CD133 and PE-Cy7 conjugated streptavidin (1:300 and 1:1000, respectively). $CD133^{+}$Nes::$OR^{-}EGFR^{-}$ and $CD133^{+}$Nes::$OR^{+}EGFR^{+}$ were gated from the CD24 negative population.

In vitro assays

For single cell assays, one cell per well of each sorted population was manually plated into 96 well plates previously coated with Poly-D-Lysine (Sigma, 10 µg/ml) and Fibronectin (Sigma, 2 µg/ml). Cells were grown in Neurosphere (NS) medium, composed of DMEM/F12 (Life Technologies) supplemented with 0.6% Glucose (Sigma), 1x Hepes (Life Technologies), 1x Insulin-Selenium-Transferrin (Life Technologies), N-2 (Life Technologies) and B-27 (Life Technologies) supplement in the presence of 20 ng/ml EGF (Upstate) or 20 ng/ml EGF and 20 ng/ml bFGF (Life Technologies). For proliferation assays, each sorted population was centrifuged after FACS for 10 min at 1300 rpm at 4ºC and seeded in NS medium at a density of 700 cells/well in 500 µl of medium (density of 1.4 cell/µl) in 24 well plates. To assess FACS sorting efficiency, cells were counted in a control well and this value was used to normalize cell number across the plate. For quantification of activated clones, cells were counted 2 days after plating and clusters of two or more cells with large, bright, refractant cytoplasm were counted as activated clones. For neurosphere passaging at all cell densities, the total content of each well was collected and dissociated with 3 mg (600 units) of papain for 10 min at 37ºC. The reaction was stopped by adding ovomucoid inhibitor (Worthington, 0.7 mg). DNAse (Worthington, 0.5 mg) was added and cells dissociated to single cells by pipetting. Live dissociated cells were counted incubating with Vybrant dye (Invitrogen, 1:1000) at 37ºC and plated at a density of 700 cells/well in 500 µl (density of 1.4 cell/µl) in 24 well plates for 6 days. For total cell number counts (live and dead), the cell suspension was plated and incubated 30 min at 37ºC with Vibrant Dye and DAPI (both at 1:1000) and total cells were counted. For differentiation assays, neurospheres were plated in adherent conditions in a 16-well chamber coated with poly-D-Lysine (Sigma, 0.01 mg/ml) and Laminin (Invitrogen, 10 µg/ml) with NS medium alone without B-27 supplement and growth factors for 7 days. For flow cytometry of neurospheres,

neurospheres were collected and dissociated with papain, immunostained with antibodies and sorted at the flow cytometer as described in the FACS methods section.

Lineage Tracing

For lineage tracing experiments, GFAP::CreERT2 mice (Ganat et al., 2006, The Jackson Laboratory) were crossed with Rosa26^{tdTomato} mice (Madisen et al., 2010, The Jackson Laboratory) to generate GFAP::CreERT2;Rosa26^{tdTomato} mice. Tamoxifen (10 mg/ml, Sigma) diluted in 90% oil and 10% ethanol was I.P. injected into adult GFAP::CreERT2;Rosa26^{tdTomato} mice (33mg/kg).

Bioinformatic analysis

Normalization, quality control, differential expression, and gene ontology analysis were carried out using Genespring GX 11. Differentially expressed probesets were filtered by average expression level greater than 50 in at least 1 population, at least 2-fold differential expression and corrected p-value less than 0.05 by Benjamini-Hochberg multiple testing correction. GO categories were obtained with p-value less than 0.05. GSEA sets with FDR (q value) < 0.05 were hand-curated into thematic categories to highlight transcriptional differences between populations. Analysis was carried out with GSEA software from the Broad Institute, using MSigDB v3.0.

Cloning

The mP2-mCherry plasmid was generated by cloning the mouse P2 element, homologous to the human P2 element (Shmelkov et al., 2004), of the Prominin1 promoter into the CherryPicker control vector (Clontech), using the *XhoI* and *AgeI* digestion sites. The following primers were used to amplify the mP2 element by PCR from mouse genomic DNA:
FOR: ACTCTCGAGGGTCCAATCAGTGCGCTCAGAC REV: ATGACCGGTCCTCTCCGGTCCAGCTCTCCT

GPCR compounds screen

The following compounds were tested (final concentration is noted):

Sphingosine-1-phosphate	1µM as in Im et al. 2001, reconstituted in PBS, Tocris
1-Oleoyl lysophosphatidic acid sodium salt	100nM as in Hecht et al. 1996, reconstituted in PBS, Tocris
Adenosine	10µM as in Hill et al. 2013, reconstituted in DMSO, Tocris
Neuropeptide Y	1µM as in Weng et al. 1995, reconstituted in water, Tocris
Histamine dihydrochloride	100µM as in Liu et al. 2001, reconstituted in water, Tocris
Endothelin 1	1µM as in Maguire and Davenport 1995, reconstituted in water, Tocris
Leukotriene D4	1µM as in Lynch et al. 1999, reconstituted in MeOH, Sigma
(-)-Epinephrine	10µM as in Shibata et al. 1995, and Jasper et al. 1998, reconstituted in HCl, Sigma
(-)-Norepinephrine	10µM as in Shibata et al. 1995, and Jasper et al. 1998, reconstituted in HCl, Sigma
Amylin	1µM as in Armour et al. 1999, reconstituted in water, Tocris
L-CCG-I	10µM as in Johnson et al. 1999, reconstituted in NaOH, Tocris
Neurotensin	1µM as in Cusack et al. 2000, reconstituted in water, Tocris
R-spondin1	100nM as in Carmon et al. 2011, reconstituted in water, Sigma
α-Latrotoxin	1nM as in Krasnoperov et al. 1997, reconstituted in water, Enzo LifeSci
Proinsulin C-Peptide	1nM as in Yosten et al. 2013, reconstituted in PBS, Sigma
Orexin A	10µM as in Sakurai et al. 1998, reconstituted in water, Sigma
Neurokinin A	1µM as in Gether et al. 1992, reconstituted in water, Tocris
Prosaptide	1µM as in Meyer et al. 2013, reconstituted in 1%NH_4OH, Anaspec Inc
Serotonin Hydrochloride	1µM as in Boess et al. 1997, reconstituted in water, Tocris
GRF	100nM as in Katsushima et al. 2013, reconstituted in water, Sigma
Secretin	100nM as in Ganguli et al. 1998, reconstituted in water, Tocris
Prostaglandin D2	1µM as in Sugimoto et al. 2005, reconstituted in PBS, Sigma

qRT-PCR

RNA was purified from FACS sorted populations by the miRNeasy kit (Qiagen) and cDNA was generated using WT-Ovation Pico System (NuGEN). The total SVZ sample consisted of all live cells (as gated in Figure S3C). For qRT-PCR, all reactions were carried out in duplicate on 4 biological replicates using Brilliant III Ultra Fast SYBR Green QPCR Master Mix (Agilent) in a Stratagene Mx3000P machine with an annealing temperature of 60ºC. Data was normalized to GAPDH expression and analyzed by the $2^{-\Delta\Delta Ct}$ method.
The primers used were:

Gfap-F: CTCCGCCAAGCCAAGCACGA	Dlx2-F: GTTGTGAAAGCTGCGACGTA
Gfap-R: GCGCAGGGACTCCAGATCGC	Dlx2-R: ACCCCCAAATACCTTGCATT
Egfr-F: AGGCCGTGAACCACGTCTGC	Sox2-F: CCCCCTTTTATTTTCCGTAGTT
Egfr-R: CACGCACTCCCTGCCTCTGC	Sox2-R: TCTCAAACTGTGCATAATGGAGT
GFP-F: TGGCGATGGCCCTGTCCTTTT	Nestin-F: GGGCCCAGAGCTTTCCCACG
GFP-R: AAGGGCAGATTGTGTGGACAGGT	Nestin-R: GGGCATGCACCAGACCCTGTG
Prom1-F: GCCTCTACCCTGGAAGCAAA	Vcam1-F: AAGAGAACCCAGGTGGAGGT
Prom1-R: GATGCTGGTGGATGGCTCTT	Vcam1-R: TCTGCTAATTCCAGCCTCGT
Gapdh-F: AACTTTGGCATTGTGGAAGG	Dll1-F: CTACTACGGAGAAGGTTG
Gapdh-R: ACACATTGGGGGTAGGAACA	Dll1-R: GTATCCATGTTGGTCATC
Ascl1-F: ATGCAGCTACTGTCCAAACG	Lrig1-F: TGCCAGAGCAAGCACGCTGA
Ascl1-R: AACAGTAAGGGGTGGGTGTG	Lrig1-R: GCCTCTCAGAAGCAGCAAATTCACA

ADDITIONAL REFERENCES

Ables JL, Decarolis NA, Johnson MA, Rivera PD, Gao Z, Cooper DC, Radtke F, Hsieh J, and Eisch AJ. (2010). Notch1 is required for maintenance of the reservoir of adult hippocampal stem cells. J Neurosci *30*, 10484-92.

Andreu-Agullo C, Maurin T, Thompson CB, and Lai EC. (2011). Ars2 maintains neural stem-cell identity through direct transcriptional activation of Sox2. Nature *481*, 195-8.

Andreu-Agulló C, Morante-Redolat JM, Delgado AC, and Fariñas I. (2009). Vascular niche factor PEDF modulates Notch-dependent stemness in the adult subependymal zone. Nat Neurosci *12*, 1514-23.

Armour SL, Foord S, Kenakin T, and Chen WJ. (1999). Pharmacological characterization of receptor-activity-modifying proteins (RAMPs) and the human calcitonin receptor. J Pharmacol Toxicol Methods *42*, 217-224.

Bauer S, and Patterson PH. (2006). Leukemia inhibitory factor promotes neural stem cell self-renewal in the adult brain. J Neurosci *26*, 12089-99.

Besson V, Smeriglio P, Wegener A, Relaix F, Nait Oumesmar B, Sassoon DA, and Marazzi G. (2011). PW1 gene/paternally expressed gene 3 (PW1/Peg3) identifies multiple adult stem and progenitor cell populations. Proc Natl Acad Sci USA *108*, 11470-5.

Boess FG, Monsma FJ Jr, Carolo C, Meyer V, Rudler A, Zwingelstein C, and Sleight AJ. (1997). Functional and radioligand binding characterization of rat 5-HT6 receptors stably expressed in HEK293 cells. Neuropharmacology *36(4-5)*, 713-20.

Carmon KS, Gong X, Lin Q, Thomas A, and Liu Q. (2011). R-spondins function as ligands of the orphan receptors LGR4 and LGR5 to regulate Wnt/beta-catenin signaling. Proc. Natl. Acad. Sci. U.S.A. *108 (28)*, 11452-7.

Chojnacki A, Shimazaki T, Gregg C, Weinmaster G, and Weiss S. (2003). Glycoprotein 130 signaling regulates Notch1 expression and activation in the self-renewal of mammalian forebrain neural stem cells. J Neurosci *23*, 1730-41.

Chuikov S, Levi BP, Smith ML, and Morrison SJ. (2010). Prdm16 promotes stem cell maintenance in multiple tissues, partly by regulating oxidative stress. Nat Cell Biol *12*, 999-1006.

Corti S, Nizzardo M, Nardini M, Donadoni C, Locatelli F, Papadimitriou D, Salani S, Del Bo R, Ghezzi S, Strazzer S, Bresolin N, and Comi GP. (2007). Isolation and characterization of murine neural stem/progenitor cells based on Prominin-1 expression. Exp Neurol *205*, 547-62.

Cusack B, Jansen K, McCormick DJ, Chou T, Pang Y, and Richelson E. (2000). A single amino acid of the human and rat neurotensin receptors (subtype 1) determining the pharmacological profile of a species-selective neurotensin agonist. Biochem Pharmacol, *60*, 793-801.

Dong Z, Yang N, Yeo SY, Chitnis A, and Guo S. (2012). Intralineage directional Notch signaling regulates self-renewal and differentiation of asymmetrically dividing radial glia. Neuron *74*, 65-78.

Ehm O, Göritz C, Covic M, Schäffner I, Schwarz TJ, Karaca E, Kempkes B, Kremmer E, Pfrieger FW, Espinosa L, Bigas A, Giachino C, Taylor V, Frisén J, and Lie DC. (2010). RBPJkappa-dependent signaling is essential for long-term maintenance of neural stem cells in the adult hippocampus. J Neurosci *30*, 13794-807.

Fasano CA, Phoenix TN, Kokovay E, Lowry N, Elkabetz Y, Dimos JT, Lemischka IR, Studer L, and Temple S. (2009). Bmi-1 cooperates with Foxg1 to maintain neural stem cell self-renewal in the forebrain. Genes Dev *23*, 561-74.

Ferron SR, Pozo N, Laguna A, Aranda S, Porlan E, Moreno M, Fillat C, de la Luna S, Sánchez P, Arbonés ML, and Fariñas I. (2010). Regulated segregation of kinase Dyrk1A during asymmetric neural stem cell division is critical for EGFR-mediated biased signaling. Cell Stem Cell *7*, 367-79.

Ferrón SR, Charalambous M, Radford E, McEwen K, Wildner H, Hind E, Morante-Redolat JM, Laborda J, Guillemot F, Bauer SR, Fariñas I, and Ferguson-Smith AC. (2011). Postnatal loss of Dlk1 imprinting in stem cells and niche astrocytes regulates neurogenesis. Nature *475*, 381-5.

Ganat YM, Silbereis J, Cave C, Ngu H, Anderson GM, Ohkubo Y, Ment LR, and Vaccarino FM. (2006). Early postnatal astroglial cells produce multilineage precursors and neural stem cells in vivo. J Neurosci, *26*, 8609-21.

Ganguli SC, Park CG, Holtmann MH, Hadac EM, Kenakin TP, and Miller LJ. (1998). Protean effects of a natural peptide agonist of the G protein-coupled secretin receptor demonstrated by receptor mutagenesis. J Pharmacol Exp Ther *286*, 593-598.

Gao Z, Ure K, Ding P, Nashaat M, Yuan L, Ma J, Hammer RE, and Hsieh J. (2011). The master negative regulator REST/NRSF controls adult neurogenesis by restraining the neurogenic program in quiescent stem cells. J Neurosci *31*, 9772-86.

Gether U, Marray T, Schwartz TW, and Johansen TE. (1992). Stable expression of high affinity NK1 (substance P) and NK2 (neurokinin A) receptors but low affinity NK3 (neurokinin B) receptors in transfected CHO cells. FEBS Lett *296*, 241-244.

Gil-Perotin S, Marin-Husstege M, Li J, Soriano-Navarro M, Zindy F, Roussel MF, Garcia-Verdugo JM, and Casaccia-Bonnefil P. (2006). Loss of p53 induces changes in the behavior of subventricular zone cells: implication for the genesis of glial tumors. J Neurosci *26*, 1107-16.

Gregorian C, Nakashima J, Le Belle J, Ohab J, Kim R, Liu A, Smith KB, Groszer M, Garcia AD, Sofroniew MV, Carmichael ST, Kornblum HI, Liu X, and Wu H. (2009). Pten deletion in adult neural stem/progenitor cells enhances constitutive neurogenesis. J Neurosci *29*, 1874-86.

Groszer M, Erickson R, Scripture-Adams DD, Dougherty JD, Le Belle J, Zack JA, Geschwind DH, Liu X, Kornblum HI, and Wu H. (2006). PTEN negatively regulates neural stem cell self-renewal by modulating G0-G1 cell cycle entry. Proc Natl Acad Sci USA *103*, 111-6.

He S, Iwashita T, Buchstaller J, Molofsky AV, Thomas D, and Morrison SJ. (2009). Bmi-1 over-expression in neural stem/progenitor cells increases proliferation and neurogenesis in culture but has little effect on these functions in vivo. Dev Biol *328*, 257-72.

Hecht JH, Weiner JA, Post SR, and Chun J. (1996). Ventricular zone gene-1 (vzg-1) encodes a lysophosphatidic acid receptor expressed in neurogenic regions of the developing cerebral cortex. J. Cell Biol. *135 (4)*, 1071-83.

Hill SJ, May LT, Kellam B, and Woolard J. (2013). Allosteric interactions at adenosine A1 and A3 receptors: New insights into the role of small molecules and receptor dimerization. Br J Pharmacol. 2013 Aug 22. doi: 10.1111/bph.12345. [Epub ahead of print]

Im DS, Clemens J, Macdonald TL, and Lynch KR. (2001). Characterization of the human and mouse sphingosine 1-phosphate receptor, S1P5 (Edg-8): structure-activity relationship of sphingosine1-phosphate receptors. Biochemistry *40 (46)*, 14053-60.

Imayoshi I, Sakamoto M, Yamaguchi M, Mori K, and Kageyama R. (2010). Essential roles of Notch signaling in maintenance of neural stem cells in developing and adult brains. J Neurosci *30*, 3489-98.

Jablonska B, Aguirre A, Vandenbosch R, Belachew S, Berthet C, Kaldis P, and Gallo V. (2007). Cdk2 is critical for proliferation and self-renewal of neural progenitor cells in the adult subventricular zone. J Cell Biol *179*, 1231-45.

Jasper JR, Lesnick JD, Chang LK, Yamanishi SS, Chang TK, Hsu SAO, Daunt DA, Bonhaus DW, and Eglen RM. (1998). Ligand efficacy and potency at recombinant alpha 2 adrenergic receptors: agonist-mediated [35S]GTPgammaS binding. Biochem Pharmacol. *55*, 1035-1043.

Johnson BG, Wright RA, Arnold MB, Wheeler WJ, Ornstein PL, and Schoepp DD. (1999). [3H]-LY341495 as a novel antagonist radioligand for group II metabotropic glutamate (mGlu) receptors: characterization of binding to membranes of mGlu receptor subtype expressing cells. Neuropharmacology *38*, 1519- 1529.

Katsushima Y, Sato T, Yamada C, Ito M, Suzuki Y, Ogawa E, Sukegawa I, Sukegawa J, Fukunaga K, and Yanagisawa T. (2013). Interaction of PICK1 with C-terminus of growth hormone-releasing hormone receptor (GHRHR) modulates trafficking and signal transduction of human GHRHR. J Pharmacol Sci. *122(3)*, 193-204.

Kim EJ, Ables JL, Dickel LK, Eisch AJ, and Johnson JE. (2011). Ascl1 (Mash1) defines cells with long-term neurogenic potential in subgranular and subventricular zones in adult mouse brain. PLoS One *6*, e18472.

Krasnoperov VG, Bittner MA, Beavis R, Kuang Y, Salnikow KV, Chepurny OG, Little AR, Plotnikov AN, Wu D, Holz RW and Petrenko AG. (1997). alpha-Latrotoxin stimulates exocytosis by the interaction with a neuronal G-protein-coupled receptor. Neuron *18 (6)*, 925-37.

Kuo CT, Mirzadeh Z, Soriano-Navarro M, Rasin M, Wang D, Shen J, Sestan N, Garcia-Verdugo J, Alvarez-Buylla A, Jan LY, and Jan YN. (2006). Postnatal deletion of Numb/Numblike reveals repair and remodeling capacity in the subventricular neurogenic niche. Cell *127*, 1253-64.

Lacar B, Young SZ, Platel JC, and Bordey A. (2011). Gap junction-mediated calcium waves define communication networks among murine postnatal neural progenitor cells. Eur J Neurosci *34*, 1895-905.

Lim DA, Huang YC, Swigut T, Mirick AL, Garcia-Verdugo JM, Wysocka J, Ernst P, and Alvarez-Buylla A. (2009). Chromatin remodelling factor Mll1 is essential for neurogenesis from postnatal neural stem cells. Nature *458*, 529-33.

Lim DA, Suárez-Fariñas M, Naef F, Hacker CR, Menn B, Takebayashi H, Magnasco M, Patil N, and Alvarez-Buylla A. (2006). In vivo transcriptional profile analysis reveals RNA splicing and chromatin remodeling as prominent processes for adult neurogenesis. Mol Cell Neurosci *31*, 131-48.

Liu C, Wilson SJ, Kuei C, and Lovenberg TW. (2001). Comparison of human, mouse, rat, and guinea pig histamine H4 receptors reveals substantial pharmacological species variation. J Pharmacol Exp Ther *299*, 121-130.

Lynch KR, O'Neill GP, Liu Q, Im DS, Sawyer N, Metters KM, Coulombe N, Abramovitz M, Figueroa DJ, Zeng Z, Connolly BM, Bai C, Austin CP, Chateauneuf A, Stocco R, Greig GM, Kargman S, Hooks SB, Hosfield E, Williams DL Jr, Ford-Hutchinson AW, Caskey CT, and Evans JF. (1999). Characterization of the human cysteinyl leukotriene CysLT1receptor. Nature *399*, 789-793.

Madisen L, Zwingman TA, Sunkin SM, Oh SW, Zariwala HA, Gu H, Ng LL, Palmiter RD, Hawrylycz MJ, Jones AR, et al. (2010). A robust and high-throughput Cre reporting and characterization system for the whole mouse brain. Nat Neurosci, *13*, 133-40.

Maguire JJ, and Davenport AP. (1995). ETA receptor-mediated constrictor responses to endothelin peptides in human blood vessels in vitro. Br. J. Pharmacol. *115*, 191-197.

Mathieu C, Fouchet P, Gauthier LR, Lassalle B, Boussin FD, and Mouthon MA. (2006). Coculture with endothelial cells reduces the population of cycling LeX neural precursors but increases that of quiescent cells with a side population phenotype. Exp Cell Res *312*, 707-18.

Meletis K, Wirta V, Hede SM, Nistér M, Lundeberg J, and Frisén J. (2006). p53 suppresses the self-renewal of adult neural stem cells. Development *133*, 363-9.

Merson TD, Dixon MP, Collin C, Rietze RL, Bartlett PF, Thomas T, and Voss AK. (2006). The transcriptional coactivator Querkopf controls adult neurogenesis. J Neurosci *26*, 11359-70.

Meyer RC, Giddens MM, Schaefer SA, and Hall RA. (2013). GPR37 and GPR37L1 are receptors for the neuroprotective and glioprotective factors prosaptide and prosaposin. Proc. Natl. Acad. Sci. U.S.A. [Epub ahead of print]. [PMID:23690594]

Molofsky AV, Pardal R, Iwashita T, Park IK, Clarke MF, and Morrison SJ. (2003). Bmi-1 dependence distinguishes neural stem cell self-renewal from progenitor proliferation. Nature *425*, 962-7.

Niola F, Zhao X, Singh D, Castano A, Sullivan R, Lauria M, Nam HS, Zhuang Y, Benezra R, Di Bernardo D, Iavarone A, and Lasorella A. (2012). Id proteins synchronize stemness and anchorage to the niche of neural stem cells. Nat Cell Biol *14*, 477-87.

Nishino J, Kim I, Chada K, and Morrison SJ. (2008). Hmga2 promotes neural stem cell self-renewal in young but not old mice by reducing p16Ink4a and p19Arf Expression. Cell *135*, 227-39.

Niu W, Zou Y, Shen C, and Zhang CL. (2011). Activation of postnatal neural stem cells requires nuclear receptor TLX. J Neurosci *31*, 13816-28.

Nomura T, Göritz C, Catchpole T, Henkemeyer M, and Frisén J. (2010). EphB signaling controls lineage plasticity of adult neural stem cell niche cells. Cell Stem Cell *7*, 730-43.

Nyfeler Y, Kirch RD, Mantei N, Leone DP, Radtke F, Suter U, and Taylor V. (2005). Jagged1 signals in the postnatal subventricular zone are required for neural stem cell self-renewal. EMBO J *24*, 3504-15.

Obermair FJ, Fiorelli R, Schroeter A, Beyeler S, Blatti C, Zoerner B, and Thallmair M. (2010). A novel classification of quiescent and transit amplifying adult neural stem cells by surface and metabolic markers permits a defined simultaneous isolation. Stem Cell Res *5*, 131-43.

Obernier K, Simeonova I, Fila T, Mandl C, Hölzl-Wenig G, Monaghan-Nichols P, and Ciccolini F. (2011). Expression of Tlx in both stem cells and transit amplifying progenitors regulates stem cell activation and differentiation in the neonatal lateral subependymal zone. Stem Cells *29*, 1415-26.

Pfenninger CV, Steinhoff C, Hertwig F, and Nuber UA. (2011). Prospectively isolated CD133/CD24-positive ependymal cells from the adult spinal cord and lateral ventricle wall differ in their long-term in vitro self-renewal and in vivo gene expression. Glia *59*, 68-81.

Renault VM, Rafalski VA, Morgan AA, Salih DA, Brett JO, Webb AE, Villeda SA, Thekkat PU, Guillerey C, Denko NC, Palmer TD, Butte AJ, and Brunet A. (2009). FoxO3 regulates neural stem cell homeostasis. Cell Stem Cell *5*, 527-39.

Sakurai T, Amemiya A, Ishii M, Matsuzaki I, Chemelli RM, Tanaka H, Williams SC, Richardson JA, Kozlowski GP, Wilson S, Arch JR, Buckingham RE, Haynes AC, Carr SA, Annan RS, McNulty DE, Liu WS, Terrett JA, Elshourbagy NA, Bergsma DJ, and Yanagisawa M. (1998). Orexins and orexin receptors: a family of hypothalamic neuropeptides and G protein-coupled receptors that regulate feeding behavior. Cell *92*, 573-585.

Schwamborn JC, Berezikov E, and Knoblich JA. (2009). The TRIM-NHL protein TRIM32 activates microRNAs and prevents self-renewal in mouse neural progenitors. Cell *136*, 913-25.

Sheikh BN, Dixon MP, Thomas T, and Voss AK. (2012). Querkopf is a key marker of self-renewal and multipotency of adult neural stem cells. J Cell Sci *125*, 295-309.

Shibata K, Foglar R, Horie K, Obika K, Sakamoto A, Ogawa S, and Tsujimoto G. (1995). KMD-3213, a novel, potent, alpha 1a-adrenoceptor-selective antagonist: characterization using recombinant human alpha 1-adrenoceptors and native tissues. Mol. Pharmacol. *48*, 250-258.

Shmelkov, S.V., Jun, L., St. Clair, R., McGarrigle, D., Derderian, C.A., Usenko, J.K., Costa, C., Zhang, F., Guo, X., and Rafii, S. (2004) Alternative promoters regulate transcription of the gene that encodes stem cell surface protein AC133. Blood *103*, 2055-61.

Sousa-Nunes R, Yee LL, and Gould AP. (2011). Fat cells reactivate quiescent neuroblasts via TOR and glial insulin relays in Drosophila. Nature *471*, 508-12.

Sugimoto H, Shichijo M, Okano M, and Bacon KB. (2005). CRTH2-specific binding characteristics of [3H]ramatroban and its effects on PGD2-, 15-deoxy-Delta12, 14-PGJ2- and indomethacin-induced agonist responses. Eur J Pharmacol *524*, 30-37.

Sun G, Ye P, Murai K, Lang MF, Li S, Zhang H, Li W, Fu C, Yin J, Wang A, Ma X, and Shi Y. (2011). miR-137 forms a regulatory loop with nuclear receptor TLX and LSD1 in neural stem cells. Nat Commun *2*, 529.

Wang J, Zhang H, Young AG, Qiu R, Argalian S, Li X, Wu X, Lemke G, and Lu Q. (2011). Transcriptome analysis of neural progenitor cells by a genetic dual reporter strategy. Stem Cells *29*, 1589-600.

Weng G, Yee F, Michl P, Reis D, and Wahlestedt C. (1995). Studies on neuropeptide Y receptors in a mouse adrenocortical cell line. Mol Pharmacol *48*, 9-14.

Yosten GL, Kolar GR, Redlinger LJ, and Samson WK. (2013). Evidence for an interaction between proinsulin C-peptide and GPR146. J. Endocrinol., [Epub ahead of print]. [PMID:23759446]

Yun SW, Leong C, Zhai D, Tan YL, Lim L, Bi X, Lee JJ, Kim HJ, Kang NY, Ng SH, Stanton LW, and Chang YT. (2012). Neural stem cell specific fluorescent chemical probe binding to FABP7. Proc Natl Acad Sci USA *109*, 10214-7.

Zheng H, Ying H, Yan H, Kimmelman AC, Hiller DJ, Chen AJ, Perry SR, Tonon G, Chu GC, Ding Z, Stommel JM, Dunn KL, Wiedemeyer R, You MJ, Brennan C, Wang YA, Ligon KL, Wong WH, Chin L, and DePinho RA. (2008). p53 and Pten control neural and glioma stem/progenitor cell renewal and differentiation. Nature *455*, 1129-33.

Many supplemental tables are the same as those included in Codega et al., 2014. The links below will automatically download the supplemental tables.

~

Supplemental Table 1 is avaliable for direct download from http://tinyurl.com/AMD-TableS1

~

Supplemental Table 2
http://tinyurl.com/AMD-TableS2

~

Supplemental Table 3
http://tinyurl.com/AMD-TableS3

~

Supplemental Table 4 is included on the subsequent pages.

Expression value and fold change of transcription factors, markers, and other genes previously reported to be important in neurogenesis

	Probe Set ID	Gene Title	Gene Symbol	Fold Change	qNSC (AV)	qNSC (SD)	aNSC (AV)	aNSC (SD)	
Notch pathway members	1418633_at	Notch gene homolog 1	Notch1	1.299	2199	±164	2856	±442	Basak et al., 2012; Ables et al., 2010; Imayoshi et al., 2010; Andreu-Agullo et al., 2009
	1418634_at	Notch gene homolog 1	Notch1	1.005	4301	±1933	4322	±155	
	1451889_at	Notch gene homolog 2	Notch2	-1.711	1210	±317	707	±124	Basak et al., 2012
	1455556_at	Notch gene homolog 2	Notch2	-2.78	11741	±2971	4224	±320	
	1421964_at	Notch gene homolog 3	Notch3	-9.633	578	±153	60	±62	Basak et al., 2012
	1421965_s_at	Notch gene homolog 3	Notch3	-4.649	437	±78	94	±37	
	1449939_s_at	delta-like 1 homolog	Dlk1	-17.071	239	±172	14	±19	Ferron et al., 2011
	1442724_at	delta-like 1 homolog	Dlk1	-4.167	100	±32	24	±14	
	1418102_at	hairy and enhancer of split 1	Hes1	-1.166	176	±61	151	±90	Andreu-Agullo et al., 2009
	1423146_at	hairy and enhancer of split 5	Hes5	-2.698	1686	±807	625	±81	Lugert et al., 2010; Giachino et al., 2013
	1456010_x_at	hairy and enhancer of split 5	Hes5	-2.957	4335	±906	1466	±220	
	1436050_x_at	hairy and enhancer of split 6	Hes6	14.964	550	±143	8230	±239	
	1452021_a_at	hairy and enhancer of split 6	Hes6	22.392	74	±56	1657	±202	
	1421105_at	jagged 1	Jag1	2.411	421	±119	1015	±186	Nyfeler et al., 2005
	1421106_at	jagged 1	Jag1	2.74	581	±323	1592	±200	
	1434070_at	jagged 1	Jag1	2.725	963	±510	2624	±453	
	1418114_at	recombination signal binding protein for immunoglobulin kappa J region	Rbpj	1.317	792	±150	1043	±177	Ehm et al., 2010
	1448957_at	recombination signal binding protein for immunoglobulin kappa J region	Rbpj	3.221	199	±135	641	±153	
	1454896_at	recombination signal binding protein for immunoglobulin kappa J region	Rbpj	1.945	859	±120	1671	±572	
	1450782_at	wingless-related MMTV integration site 4	Wnt4	-1.643	115	±117	70	±24	Beckervodersandforth, 2010
	1416891_at	numb gene homolog	Numb	-3.17	875	±178	276	±65	Kuo et al., 2006
	1425368_a_at	numb gene homolog	Numb	1.04	100	±89	104	±49	
	1416491_at	numb-like	Numbl	1.095	105	±62	115	±7	Kuo et al., 2006
bi-directional regulators	1417574_at	chemokine (C-X-C motif) ligand 12	Cxcl12	-79.267	1189	±834	15	±12	Kokovay et al., 2010
	1448823_at	chemokine (C-X-C motif) ligand 12	Cxcl12	-6.563	105	±31	16	±10	
	1439084_at	chemokine (C-X-C motif) ligand 12	Cxcl12	-64.333	193	±162	3	±1	
	1448710_at	chemokine (C-X-C motif) receptor 4	Cxcr4	1.368	3330	±1297	4554	±540	Kokovay et al., 2010
Transcription factors	1449470_at	distal-less homeobox 1	Dlx1	10.296	685	±329	7053	±659	Beckervodersandforth, 2010; Lim et al, 2006
	1448877_at	distal-less homeobox 2	Dlx2	8.47	1424	±412	12061	±624	Beckervodersandforth, 2010; Obernier et al., 2011
	1449863_a_at	distal-less homeobox 5	Dlx5	17.175	103	±18	1769	±1049	Lim et al., 2006
	1416967_at	SRY-box containing gene 2	Sox2	-1.324	5841	±417	4411	±324	Lendahl, 1990; Graham, 2003; Kazanis, 2010; Imayoshi, 2011; Marques-Torrejon, 2013.
	1419155_a_at	SRY-box containing gene 4	Sox4	21.253	166	±12	3528	±341	Beckervodersandforth, 2010
	1419156_at	SRY-box containing gene 4	Sox4	49.989	174	±45	8698	±2015	
	1419157_at	SRY-box containing gene 4	Sox4	18.574	47	±24	873	±227	
	1433575_at	SRY-box containing gene 4	Sox4	11.347	597	±473	6774	±1016	
	1449370_at	SRY-box containing gene 4	Sox4	12.697	300	±108	3809	±1374	
	1455867_at	SRY-box containing gene 4	Sox4	46.307	127	±51	5881	±984	
	1443778_at	SRY-box containing gene 4	Sox4	-5	5	±5	1	±0	
	1458332_x_at	SRY-box containing gene 4	Sox4	-2	2	±2	1	±1	
	1423500_a_at	SRY-box containing gene 5	Sox5	-1.727	689	±422	399	±127	Martinez-Morales, 2010; Wang et al., 2011
	1432189_a_at	SRY-box containing gene 5	Sox5	-1.027	873	±109	850	±124	
	1432190_at	SRY-box containing gene 5	Sox5	1.722	72	±41	124	±60	
	1452511_at	SRY-box containing gene 5	Sox5	-1.576	843	±315	535	±223	
	1440827_x_at	SRY-box containing gene 5	Sox5	1.238	273	±78	338	±48	
	1459261_at	SRY-box containing gene 5	Sox5	-2.633	337	±28	128	±97	
	1436790_a_at	SRY-box containing gene 11	Sox11	10.262	759	±354	7789	±1737	Beckervodersandforth, 2010
	1429051_s_at	SRY-box containing gene 11	Sox11	19.901	594	±244	11821	±172	
	1429372_at	SRY-box containing gene 11	Sox11	11.764	466	±390	5482	±626	
	1453002_at	SRY-box containing gene 11	Sox11	4.993	1238	±453	6181	±373	
	1453125_at	SRY-box containing gene 11	Sox11	7.736	546	±327	4224	±700	

1420926_at	aristaless related homeobox	Arx	1.482	353	±100	523	±99	Beckervodersandforth, 2010
1450042_at	aristaless related homeobox	Arx	10.228	361	±355	3696	±449	
1441175_at	aristaless related homeobox	Arx	0.932	71	±59	66	±56	
1417129_a_at	Meis homeobox 2	Meis2	1.666	2152	±542	3586	±825	Beckervodersandforth, 2010
1440091_at	Meis homeobox 2	Meis2	-1.323	512	±206	387	±132	
1447861_x_at	Meis homeobox 2	Meis2	1.433	217	±69	311	±122	
1457632_s_at	Meis homeobox 2	Meis2	1.406	1328	±829	1867	±294	
1450164_at	achaete-scute complex homolog 1	Ascl1	27.331	142	±59	3881	±623	Kim et al., 2011
1437086_at	achaete-scute complex homolog 1	Ascl1	8.927	803	±603	7168	±581	
1419271_at	paired box gene 6	Pax6	-1.497	1475	±378	985	±188	Wang et al., 2011 Beckervodersandforth, 2010
1425960_s_at	paired box gene 6	Pax6	1.425	120	±30	171	±108	
1437816_at	paired box gene 6	Pax6	-2.246	894	±401	398	±137	
1452526_a_at	paired box gene 6	Pax6	-1.472	2808	±1103	1908	±389	
1456342_at	paired box gene 6	Pax6	-2.232	125	±101	56	±55	
1417655_a_at	serrate RNA effector molecule	Srrt	1.726	2164	±71	3734	±773	Andreu-Agullo et al., 2011
1418357_at	forkhead box G1	Foxg1	1.32	4654	±358	6141	±303	Fasano et al., 2009
1425291_at	forkhead box J1	Foxj1	-6.032	187	±84	31	±28	Pfenninger et al., 2011
1434831_a_at	forkhead box O3	Foxo3	1.052	1773	±751	1865	±249	Renault et al., 2009
1434832_at	forkhead box O3	Foxo3	-1.09	1810	±333	1661	±235	
1450236_at	forkhead box O3	Foxo3	1.551	1627	±796	2524	±775	
1444226_at	forkhead box O3	Foxo3	-1.03	104	±35	101	±103	
1449058_at	GLI-Kruppel family member GLI1	Gli1	1.2	414	±309	497	±89	Ahn and Joyner, 2005
1446086_s_at	GLI-Kruppel family member GLI2	Gli2	-1.2308	1287	±244	1046	±139	Petrova et al., 2013
1459211_at	GLI-Kruppel family member GLI2	Gli2	1.4642	1356	±202	1986	±219	
1450525_at	GLI-Kruppel family member GLI3	Gli3	-2.0093	1163	±673	579	±163	Petrova et al., 2013
1455154_at	GLI-Kruppel family member GLI3	Gli3	-2.8287	2962	±430	1047	±19	
1456067_at	GLI-Kruppel family member GLI3	Gli3	-2.7208	846	±137	311	±104	
1425895_a_at	inhibitor of DNA binding 1	Id1	1.925	227	±95	437	±121	Nam and Benezra, 2009; Niola et al., 2012
1422537_a_at	inhibitor of DNA binding 2	Id2	-6.668	2227	±1580	334	±82	Niola et al., 2012
1435176_a_at	inhibitor of DNA binding 2	Id2	-13.353	3218	±821	241	±24	
1453596_at	inhibitor of DNA binding 2	Id2	-14.286	300	±78	21	±21	
1416630_at	inhibitor of DNA binding 3	Id3	-5.933	3014	±373	508	±134	Niola et al., 2012
1427283_at	myeloid/lymphoid or mixed-lineage leukemia 1	Mll1	2.459	810	±306	1992	±300	Lim et al., 2009
1452377_at	myeloid/lymphoid or mixed-lineage leukemia 1	Mll1	1.027	900	±314	924	±174	
1421317_x_at	myeloblastosis oncogene	Myb	16.566	129	±97	2137	±325	
1422734_a_at	myeloblastosis oncogene	Myb	28.733	15	±12	431	±82	
1450194_a_at	myeloblastosis oncogene	Myb	15.919	62	±64	987	±47	
1424942_a_at	myelocytomatosis oncogene	Myc	1.388	294	±177	408	±217	Schwamborn et al., 2009
1434921_at	nuclear receptor subfamily 2, group E, member 1	Nr2e1	-1.505	8727	±1855	5799	±304	Obernier et al., 2011; Sun et al., 2011; Niu et al., 2011
1457289_at	nuclear receptor subfamily 2, group E, member 1	Nr2e1	1.167	2521	±1604	2941	±29	
1429308_at	PR domain containing 16	Prdm16	-1.558	433	±153	278	±65	Chuikov et al., 2010
1429309_at	PR domain containing 16	Prdm16	-2.765	1095	±175	396	±34	
1440745_at	PR domain containing 16	Prdm16	-3.459	1266	±631	366	±59	
1440870_at	PR domain containing 16	Prdm16	-3.013	5526	±1133	1834	±256	
1434336_s_at	REST corepressor 1	Rcor1	2.19	399	±152	874	±243	Gao et al., 2011
1437545_at	REST corepressor 1	Rcor1	1.042	307	±136	320	±119	
1454932_at	REST corepressor 1	Rcor1	4.361	72	±82	314	±139	
1425564_at	RE1-silencing transcription factor	Rest	-1.597	123	±119	77	±18	Gao et al., 2011
1425565_at	RE1-silencing transcription factor	Rest	-3.281	479	±141	146	±37	
1425566_at	RE1-silencing transcription factor	Rest	-3.778	102	±28	27	±19	
1428227_at	RE1-silencing transcription factor	Rest	-3.895	1523	±431	391	±75	
1419101_at	transcriptional regulator, SIN3A	Sin3a	1.14	1852	±1268	2111	±53	Gao et al., 2011
1419102_at	transcriptional regulator, SIN3A	Sin3a	2.35	297	±60	698	±35	
1449343_s_at	transcriptional regulator, SIN3A	Sin3a	1.463	787	±216	1151	±274	
1422485_at	MAD homolog 4	Smad4	1.239	1050	±211	1301	±328	Mira et al., 2010
1422486_a_at	MAD homolog 4	Smad4	-1.028	2817	±1034	2739	±845	
1422487_at	MAD homolog 4	Smad4	1.353	2991	±542	4048	±656	

	1426538_a_at	transformation related protein 53	Trp53	3.715	330	±156	1226	±96	Zheng et al., 2008; Gil-Perotin et al., 2006; Meletis et al., 2006
	1427739_a_at	transformation related protein 53	Trp53	3.378	555	±99	1875	±87	
	1438808_at	transformation related protein 53	Trp53	1.653	98	±35	162	±6	
	1438542_at	transformation related protein 53	Trp53	-1.83	820	±456	448	±156	
	1457623_x_at	transformation related protein 53	Trp53	-2.2	44	±13	20	±8	
	1459780_at	transformation related protein 53	Trp53	5	2	±1	10	±15	
	1459781_x_at	transformation related protein 53	Trp53	2.2	5	±3	11	±15	
Other factors									
	1421679_a_at	cyclin-dependent kinase inhibitor 1A (P21)	Cdkn1a	3.017	115	±77	347	±83	Marques-Torrejon et al., 2013
	1424638_at	cyclin-dependent kinase inhibitor 1A (P21)	Cdkn1a	1.011	562	±760	568	±57	
	1421857_at	a disintegrin and metallopeptidase domain 17	Adam17	-1.329	388	±112	292	±79	Chojnacki et al., 2003
	1421858_at	a disintegrin and metallopeptidase domain 17	Adam17	1.043	795	±46	829	±441	
	1421859_at	a disintegrin and metallopeptidase domain 17	Adam17	-1.902	835	±230	439	±29	
	1424401_at	aldehyde dehydrogenase 1 family, member L1	Aldh1l1	-56	112	±90	2	±0	Obermair et al., 2010
	1423586_at	AXL receptor tyrosine kinase	Axl	-2.584	3139	±756	1215	±489	Wang et al., 2011
	1438621_x_at	AXL receptor tyrosine kinase	Axl	-1.333	8	±11	6	±4	
	1417493_at	Bmi1 polycomb ring finger oncogene	Bmi1	4.159	716	±209	2978	±268	He et al., 2009; Molofosky et al., 2003
	1448733_at	Bmi1 polycomb ring finger oncogene	Bmi1	2.924	381	±145	1114	±51	
	1425491_at	bone morphogenetic protein receptor, type 1A	Bmpr1a	-1.59	6309	±1429	3968	±56	Mira et al., 2010
	1425492_at	bone morphogenetic protein receptor, type 1A	Bmpr1a	-1.579	1528	±275	968	±99	
	1425493_at	bone morphogenetic protein receptor, type 1A	Bmpr1a	-1.755	4484	±819	2555	±117	
	1425494_s_at	bone morphogenetic protein receptor, type 1A	Bmpr1a	-1.042	1617	±566	1552	±191	
	1451729_at	bone morphogenetic protein receptor, type 1A	Bmpr1a	-1.514	162	±49	107	±15	
	1445413_at	bone morphogenetic protein receptor, type 1A	Bmpr1a	-1.5	33	±32	22	±26	
	1422872_at	bone morphogenetic protein receptor, type 1B	Bmpr1b	-5.4	1637	±140	303	±100	Cesetti et al., 2011
	1437312_at	bone morphogenetic protein receptor, type 1B	Bmpr1b	-11.791	3806	±856	323	±120	
	1443720_s_at	bone morphogenetic protein receptor, type 1B	Bmpr1b	-7.045	1608	±388	228	±50	
	1417419_at	cyclin D1	Ccnd1	5.786	56	±52	324	±139	
	1417420_at	cyclin D1	Ccnd1	5.991	112	±31	671	±206	
	1448698_at	cyclin D1	Ccnd1	3.004	272	±32	817	±157	
	1416122_at	cyclin D2	Ccnd2	15.213	704	±346	10710	±1421	Lim et al., 2006
	1416123_at	cyclin D2	Ccnd2	6.225	2225	±1673	13851	±1411	
	1416124_at	cyclin D2	Ccnd2	3.718	3404	±2731	12657	±1095	
	1430127_a_at	cyclin D2	Ccnd2	7.733	1316	±890	10177	±1076	
	1434745_at	cyclin D2	Ccnd2	9.158	1590	±1288	14562	±1274	
	1448229_s_at	cyclin D2	Ccnd2	8.632	1205	±777	10402	±361	
	1455956_x_at	cyclin D2	Ccnd2	8.431	1332	±633	11230	±975	
	1416873_a_at	cyclin-dependent kinase 2	Cdk2	6.674	190	±49	1268	±102	Jablonska et al., 2007
	1447617_at	cyclin-dependent kinase 2	Cdk2	-2.5	15	±14	6	±2	
	1422439_a_at	cyclin-dependent kinase 4	Cdk4	7.423	1037	±106	7698	±56	Jablonska et al., 2007
	1422440_at	cyclin-dependent kinase 4	Cdk4	15.053	190	±63	2860	±413	
	1422441_x_at	cyclin-dependent kinase 4	Cdk4	8.967	1074	±377	9631	±169	
	1423341_at	chondroitin sulfate proteoglycan 4	Cspg4	-5.323	330	±240	62	±53	Jablonska et al., 2007
	1450944_at	chondroitin sulfate proteoglycan 4	Cspg4	-2.111	76	±38	36	±19	
	1417312_at	dickkopf homolog 3	Dkk3	-6.632	18027	±5812	2718	±539	
	1448669_at	dickkopf homolog 3	Dkk3	-8.297	6339	±2272	764	±221	
	1426226_at	dual-specificity tyrosine-(Y)-phosphorylation regulated kinase 1a	Dyrk1a	1.589	710	±109	1128	±160	Ferron et al., 2010
	1428299_at	dual-specificity tyrosine-(Y)-phosphorylation regulated kinase 1a	Dyrk1a	-1.133	2335	±780	2060	±320	
	1451977_at	dual-specificity tyrosine-(Y)-phosphorylation regulated kinase 1a	Dyrk1a	2.438	568	±531	1385	±121	
	1420557_at	Eph receptor A5	Epha5	-8.377	1089	±625	130	±18	Beckervodersandforth, 2010
	1437920_at	Eph receptor A5	Epha5	-4.222	152	±26	36	±17	
	1435286_at	Eph receptor A5	Epha5	-8.75	315	±76	36	±8	
	1444690_at	Eph receptor A5	Epha5	-2.867	238	±119	83	±48	
	1425015_at	Eph receptor B2	Ephb2	6.844	179	±48	1225	±622	Nomura et al., 2010
	1425016_at	Eph receptor B2	Ephb2	3.454	348	±92	1202	±953	
	1454022_at	Eph receptor B2	Ephb2	-1.052	81	±33	77	±43	

1450779_at	fatty acid binding protein 7, brain	Fabp7	1.266	8293	±3860	10497	±814	Platel et a., 2009; Obermair et al., 2010; Mathieu et al., 2006; Yun et al., 2012; Giachino et al., 2013
1415800_at	gap junction protein, alpha 1	Gja1	-7.647	31460	±7224	4114	±147	Lacar et al., 2011
1415801_at	gap junction protein, alpha 1	Gja1	-7.227	12091	±2390	1673	±379	
1437992_x_at	gap junction protein, alpha 1	Gja1	-7.45	40797	±16021	5476	±741	
1438650_x_at	gap junction protein, alpha 1	Gja1	-7.494	34969	±12338	4666	±467	
1438945_x_at	gap junction protein, alpha 1	Gja1	-7.374	26995	±7622	3661	±225	
1438973_x_at	gap junction protein, alpha 1	Gja1	-6.999	5508	±727	787	±61	
1436517_at	H1 histone family, member X	H1fx	3.611	149	±38	538	±80	Beckervodersandforth, 2010
1428029_a_at	H2A histone family, member V	H2afv	7.258	1337	±739	9704	±480	Beckervodersandforth, 2010
1436596_at	H2A histone family, member V	H2afv	1.435	1456	±192	2089	±136	
1416746_at	H2A histone family, member X	H2afx	11.974	605	±267	7244	±1335	Beckervodersandforth, 2010
1416415_a_at	H2A histone family, member Z	H2afz	4.01	4477	±1702	17954	±777	Lim et al., 2006
1438092_x_at	H2A histone family, member Z	H2afz	4.216	2719	±1414	11464	±1639	
1438091_a_at	H2A histone family, member Z	H2afz	3.743	3837	±2220	14361	±1011	
1420376_a_at	H3 histone, family 3B	H3f3b	2.217	3238	±981	7178	±947	Lim et al., 2006
1455725_a_at	H3 histone, family 3B	H3f3b	5.82	2345	±166	13647	±1169	
1430357_at	H3 histone, family 3B	H3f3b	3.617	115	±52	416	±123	
1416184_s_at	high mobility group AT-hook 1	Hmga1	4.019	700	±194	2813	±1060	Nishino et al., 2008
1416176_at	high mobility group box 1	Hmgb1	2.01	2970	±457	5970	±419	
1425048_a_at	high mobility group box 1	Hmgb1	1.307	7340	±1718	9595	±1128	
1435324_x_at	high mobility group box 1	Hmgb1	2.028	8475	±2187	17188	±1516	
1437313_x_at	high mobility group box 2	Hmgb2	4.675	1967	±1036	9195	±816	
1452534_a_at	high mobility group box 2	Hmgb2	10.811	1451	±208	15687	±2118	
1438307_at	high mobility group box 2	Hmgb2	11.283	60	±39	677	±213	
1423377_at	insulin-like growth factor binding protein-like 1	Igfbpl1	10.094	64	±42	646	±48	Lim et al., 2006
1450960_at	insulin-like growth factor binding protein-like 1	Igfbpl1	9.469	64	±17	606	±38	
1425107_a_at	leukemia inhibitory factor receptor	Lifr	-6.59	402	±246	61	±31	Bauer and Patterson, 2006
1450207_at	leukemia inhibitory factor receptor	Lifr	-8.486	628	±100	74	±28	
1454984_at	leukemia inhibitory factor receptor	Lifr	-9.507	1293	±466	136	±76	
1421239_at	interleukin 6 signal transducer	Il6st	-4.376	3041	±2093	695	±127	Chojnacki et al., 2003
1452843_at	interleukin 6 signal transducer	Il6st	-2.762	2149	±450	778	±153	
1460295_s_at	interleukin 6 signal transducer	Il6st	-2.934	1417	±328	483	±163	
1437303_at	interleukin 6 signal transducer	Il6st	-2.873	744	±269	259	±67	
1417756_a_at	lymphocyte specific 1	Lsp1	-2.2	121	±40	55	±18	Sun et al., 2011
1434079_s_at	minichromosome maintenance deficient 2 mitotin	Mcm2	19.267	191	±142	3680	±468	Beckervodersandforth, 2010
1448777_at	minichromosome maintenance deficient 2 mitotin	Mcm2	28.603	141	±90	4033	±1226	
1420028_s_at	minichromosome maintenance deficient 3	Mcm3	14.309	444	±83	6353	±477	Lim et al., 2006
1420029_at	minichromosome maintenance deficient 3	Mcm3	18.901	111	±96	2098	±174	
1426652_at	minichromosome maintenance deficient 3	Mcm3	25.4	75	±107	1905	±537	
1426653_at	minichromosome maintenance deficient 3	Mcm3	13.626	123	±107	1676	±285	
1449705_x_at	minichromosome maintenance deficient 3	Mcm3	26.27	126	±135	3310	±728	
1416214_at	minichromosome maintenance deficient 4	Mcm4	6.18	488	±144	3016	±394	Beckervodersandforth, 2010
1436708_x_at	minichromosome maintenance deficient 4	Mcm4	4.573	895	±303	4093	±241	
1415945_at	minichromosome maintenance deficient 5, cell division cycle 46	Mcm5	39.701	77	±104	3057	±861	Beckervodersandforth, 2010
1436808_x_at	minichromosome maintenance deficient 5, cell division cycle 46	Mcm5	16.203	468	±448	7583	±60	
1459658_at	minichromosome maintenance deficient 5, cell division cycle 46	Mcm5	3.329	73	±71	243	±105	
1422869_at	c-mer proto-oncogene tyrosine kinase	Mertk	-23.441	3985	±1528	170	±47	Wang et al., 2011
1451818_at	mindbomb homolog 1	Mib1	1.359	1007	±205	1369	±874	Dong et al., 2012
1433853_at	mindbomb homolog 1	Mib1	-1.927	237	±159	123	±50	
1454740_at	mindbomb homolog 1	Mib1	1.156	1933	±224	2235	±472	
1421409_at	Musashi homolog 1	Msi1	3.53	1228	±519	4335	±528	Corti et al., 2007
1452287_at	Musashi homolog 1	Msi1	1.454	3800	±223	5524	±210	
1444306_at	Musashi homolog 1	Msi1	-2.519	728	±316	289	±61	
1417592_at	mechanistic target of rapamycin (serine/threonine kinase)	Mtor	-1.3	1974	±230	1519	±38	Sousa-Nunes et al., 2011
1436267_a_at	mechanistic target of rapamycin (serine/threonine kinase)	Mtor	-1.329	291	±29	219	±70	
1446185_at	mechanistic target of rapamycin (serine/threonine kinase)	Mtor	-3.03	100	±21	33	±49	

	1423508_at	MYST histone acetyltransferase monocytic leukemia 4	Myst4	1.36	547	±11	744	±164	Sheikh et al., 2012; Merson et al., 2006
	1446189_at	MYST histone acetyltransferase monocytic leukemia 4	Myst4	-2.805	373	±154	133	±31	
	1447758_x_at	MYST histone acetyltransferase monocytic leukemia 4	Myst4	-1.063	34	±14	32	±7	
	1420391_at	par-3 (partitioning defective 3) homolog	Pard3	1.333	78	±54	104	±12	Dong et al., 2012
	1434775_at	par-3 (partitioning defective 3) homolog	Pard3	-1.061	693	±131	653	±53	
	1436764_at	par-3 (partitioning defective 3) homolog	Pard3	-1.116	173	±29	155	±48	
	1436765_at	par-3 (partitioning defective 3) homolog	Pard3	1.786	42	±46	75	±29	
	1417355_at	paternally expressed 3	Peg3	1.046	1533	±596	1604	±185	Besson et al., 2011
	1417356_at	paternally expressed 3	Peg3	-2.7	5545	±2364	2054	±92	
	1433924_at	paternally expressed 3	Peg3	-1.921	6332	±2249	3297	±323	
	1447731_at	paternally expressed 3	Peg3	2.5	2	±1	5	±3	
	1447732_x_at	paternally expressed 3	Peg3	-2	14	±15	7	±5	
	1428143_a_at	patatin-like phospholipase domain containing 2	Pnpla2	-1.513	711	±145	470	±95	
	1428591_at	patatin-like phospholipase domain containing 2	Pnpla2	1	59	±44	59	±44	
	1422553_at	phosphatase and tensin homolog	Pten	1.429	938	±555	1340	±218	Cesetti et al., 2011; Bonaguidi et al., 2011; Gregorian et al., 2009; Zheng et al., 2008; Groszer et al., 2006
	1450655_at	phosphatase and tensin homolog	Pten	1.087	934	±80	1015	±149	
	1454722_at	phosphatase and tensin homolog	Pten	1.216	1204	±238	1464	±135	
	1438454_at	phosphatase and tensin homolog	Pten	1.08	500	±358	540	±176	
	1455728_at	phosphatase and tensin homolog	Pten	-1.091	1058	±413	970	±199	
	1457493_at	phosphatase and tensin homolog	Pten	-2.039	634	±157	311	±26	
	1421546_a_at	Rac GTPase-activating protein 1	Racgap1	41.444	72	±73	2984	±202	Lim et al., 2006
	1451358_a_at	Rac GTPase-activating protein 1	Racgap1	34.612	103	±84	3565	±305	
	1441889_x_at	Rac GTPase-activating protein 1	Racgap1	-1.188	19	±19	16	±1	
	1428443_a_at	Rap1 GTPase-activating protein	Rap1gap	-2.117	631	±415	298	±103	Niola et al., 2012
	1415943_at	syndecan 1	Sdc1	5.139	166	±84	853	±121	Kazanis et al., 2010; Beckervodersandforth, 2010
	1415944_at	syndecan 1	Sdc1	-1.16	87	±45	75	±14	
	1437279_x_at	syndecan 1	Sdc1	11.253	95	±85	1069	±170	
	1448158_at	syndecan 1	Sdc1	13.563	16	±10	217	±50	
	1426340_at	solute carrier family 1 (GLAST), member 3	Slc1a3	-5.006	14753	±580	2947	±1014	Platel et al., 2009
	1426341_at	solute carrier family 1 (GLAST), member 3	Slc1a3	-4.057	12897	±2795	3179	±518	
	1452031_at	solute carrier family 1 (GLAST), member 3	Slc1a3	-6.083	28425	±13335	4673	±719	
	1439072_at	solute carrier family 1 (GLAST), member 3	Slc1a3	-4.157	2615	±2455	629	±290	
	1440491_at	solute carrier family 1 (GLAST), member 3	Slc1a3	-4.629	3009	±1151	650	±297	
	1443749_x_at	solute carrier family 1 (GLAST), member 3	Slc1a3	-5.174	3808	±1814	736	±9	
	1421656_at	sprouty homolog 2	Spry2	1.091	1793	±1215	1956	±425	Ferron et al., 2010
	1436584_at	sprouty homolog 2	Spry2	-1.019	2893	±179	2838	±213	
	1427476_a_at	tripartite motif-containing 32	Trim32	-1.1	1056	±286	960	±57	Schwamborn et al., 2009
	1425248_a_at	TYRO3 protein tyrosine kinase 3	Tyro3	1.076	909	±408	978	±117	Wang et al., 2011
	1425249_a_at	TYRO3 protein tyrosine kinase 3	Tyro3	1.256	164	±122	206	±47	
Adhesion molecules									
	1422444_at	integrin alpha 6	Itga6	-5.194	1309	±310	252	±102	Kokovay et al., 2010; Kazanis et al., 2010
	1422445_at	integrin alpha 6	Itga6	-11.506	1910	±591	166	±66	
	1422444_at	integrin alpha 6	Itga6	-5.194	1309	±310	252	±102	
	1422445_at	integrin alpha 6	Itga6	-11.506	1910	±591	166	±66	
	1426918_at	integrin beta 1	Itgb1	1.727	773	±287	1336	±426	Kazanis et al., 2010
	1426919_at	integrin beta 1	Itgb1	-1.068	61	±19	57	±41	
	1426920_x_at	integrin beta 1	Itgb1	1.642	57	±32	94	±65	
	1427771_x_at	integrin beta 1	Itgb1	1.28	220	±105	282	±87	
	1438119_at	Integrin beta 1	Itgb1	-4.857	10	±15	2	±2	
	1452545_a_at	integrin beta 1	Itgb1	-1.023	827	±204	808	±165	
	1421966_at	neural cell adhesion molecule 1	Ncam1	-32.212	3640	±2300	113	±51	Lim et al., 2006
	1425126_at	neural cell adhesion molecule 1	Ncam1	-4.11	1426	±583	347	±67	
	1426864_a_at	neural cell adhesion molecule 1	Ncam1	1.125	2649	±1019	2979	±768	
	1426865_a_at	neural cell adhesion molecule 1	Ncam1	-1.306	5673	±2049	4345	±1162	
	1450437_a_at	neural cell adhesion molecule 1	Ncam1	-3.367	3943	±110	1171	±131	
	1450438_at	neural cell adhesion molecule 1	Ncam1	-2.266	213	±101	94	±19	

1439556_at	neural cell adhesion molecule 1	Ncam1	**-6.833**	**615**	±225	**90**	±8	
1415989_at	vascular cell adhesion molecule 1	Vcam1	**-11.215**	**3241**	±720	**289**	±17	Kokovay et al., 2012
1448162_at	vascular cell adhesion molecule 1	Vcam1	**-5.831**	**6892**	±1533	**1182**	±113	
1451314_a_at	vascular cell adhesion molecule 1	Vcam1	**-5.543**	**521**	±100	**94**	±29	
1436003_at	vascular cell adhesion molecule 1	Vcam1	**-4.7**	**94**	±40	**20**	±9	

Further supplemental tables:

~

Supplemental Table 5 is available on dropbox as it contains additional information from Codega et al.: http://tinyurl.c

~

Supplemental Table 6 is available for direct download from: http://tinyurl.com/AMD-TableS6

~

Supplemental Table 7 is available for direct download from http://tinyurl.com/AMD-TableS7

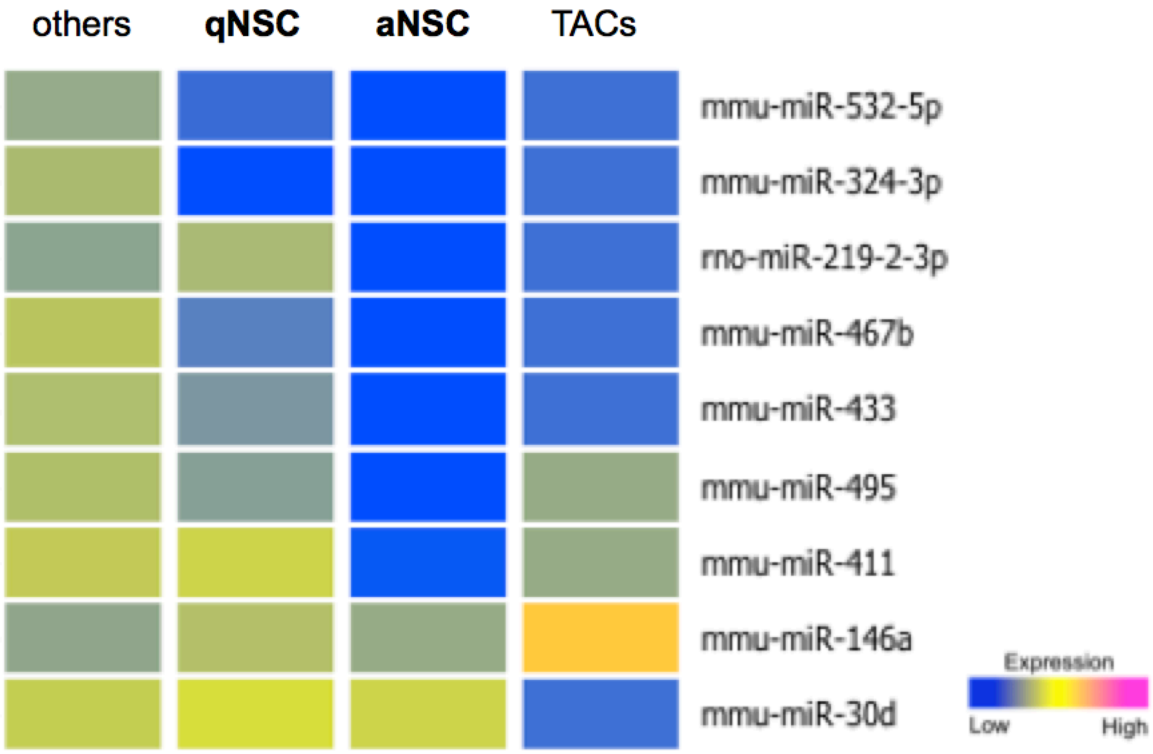

Supplemental Figure 1 miRs enriched in qNSCs
Analysis of Variance Identified a cohort of miRs enriched in qNSCs. Blue indicates low expression, yellow medium expression, and pink high expression.